APPLICATION OF GRAPH THEORY TO INTENTIONAL CONTROLLED ISLANDING FOR BLACKOUT PREVENTION AND SYSTEM SECTIONALISING FOR PARALLEL RESTORATION

A Thesis submitted to The University of Manchester for the degree of

Doctor of Philosophy

In the Faculty of Engineering and Physical Sciences

2014

by

Jairo H. Quirós-Tortós

School of Electrical and Electronic Engineering

Electrical Energy and Power Systems Group

List of Content

Final count: 55 342 words.

List of Figures

List of Tables

Nomenclature

List of Symbols

$\mathbf{0}$	Column vector with all entries equal to zero
$\mathbf{1}$	Column vector with all entries equal to one
b_{ij}	Susceptance between buses *i* and *j*
$\overline{b}_{ij}$	Boolean variable
bou (·)	The value of a boundary of a subgraph
c	The number of connected components
cut (·)	The value of a cut in a graph
d	Degree of the node
d^+, d^-	Out-degree and In-degree
e_{ij}	Edge joining nodes v_i and v_j
$\overline{e}_{ij}$	Arc joining the nodes v_i and v_j from v_i to v_j
e_k , $\overline{e}_k$	The k^{th} edge and k^{th} arc
f (·), *g* (·)	A function
l	The number of branches of the power system
m	The number of generators of the power system
n	The number of buses of the power system
p	The length of a path
q	The number of cutsets
r	The number of islands
s (·)	Similarity measure between points in Euclidean space
u	Node weight
u, w, x	Vectors
v	Node of the graph *G* or digraph *H*
vol (·)	The value of the volume of a subgraph
w	Edge weight
wei (·)	The value of the weight of a subgraph
y	A normalised vector
$\overline{\mathbf{A}}$	System state matrix
A	Adjacency matrix of a graph *G*
$\mathbf{A_H}$	Adjacency matrix of a digraph *H*
$\mathbf{A}^*$	Reachability matrix of a graph
B	Susceptance matrix
C	Indicator matrix
D	Diagonal matrix with degree in the main diagonal
E	Set of edges of the graph *G*

E_i	Subset of edges of the subgraph G_i
$\overline{E}$	Set of arcs of the digraph H
$\overline{E}_i$	Subset of arcs of the digraph H_i
$E_S, \overline{E}_S$	A cutset
G	Undirected graph
G_i	The i^{th} subgraph
H	Directed graph or digraph
H_i	The i^{th} digraph
$\mathbf{I}$	Identity matrix of applicable size
$\mathbf{J_A}, \mathbf{J_B}, \mathbf{J_C}, \mathbf{J_D}$	Jacobian matrices
$\mathbf{L}, \mathbf{L_N}$	Unnormalised and normalised Laplacian matrices
$\mathbf{M}$	Incidence matrix of G
$\mathbf{M_I}, \mathbf{M_G}$	Diagonal matrices involving the machine inertia constants
$\mathbf{M_H}$	Incidence matrix of H
N	Number of components of the system
N_L	Set of boundary nodes
P	A path
P_{ij}	Active power flow in the branch from bus i to bus j
$\mathbf{P}$	Projection matrix
Q	Cutset in the cutset matrix
$\mathbf{Q}$	Cutset matrix of the graph G
$\mathbf{Q_H}$	Cutset matrix of the digraph H
R_{ij}	Resistance between buses i and j
S	Dominating set
$\mathbf{S}$	A similarity matrix containing similarity measures
$\mathbf{S_L}$	A sensitivity matrix
T	A tree
V	A set of nodes of the graph G or the digraph H
V_i	A subset of nodes of the subgraph G_i or digraph H_i
$\overline{V}_i$	The complement of the node set V_i
$\tilde{V}$	A voltage phasor
$\mathbf{V}$	$2n$-vector of bus voltage angles and magnitudes
$\mathbf{W}$	Weighted adjacency matrix of G
$\mathbf{W_H}$	Weighted adjacency matrix of H
$\mathbf{X}$	A matrix with eigenvectors placed as columns
X_{ij}	Reactance between buses i and j
$\mathbf{Y}$	A matrix with normalised vectors
$\mathbf{Y_{BUS}}$	Admittance matrix
Y_{ij}	Admittance between buses i and j
α	Percentage of load to be restored

β	Threshold indicating the power imbalance in OBDD-based methods
$\gamma(\cdot)$	Domination number of a graph
δ	Generator rotor angle
ε	Threshold to defined the weak areas
ζ	Number of possible combinations using the free nodes
$\eta(\cdot)$	Quality of a subgraph
θ	Voltage phase angle
κ	Number of blackstart units
λ	Eigenvalue of the matrix $\mathbf{L}$
$\boldsymbol{\mu}$	A centroid
ν	Eigenvalue of the matrix $\mathbf{L_N}$
$\rho(\cdot)$	Function that assign edge weights
$\sigma(\cdot)$	Function that assign node weights
$\boldsymbol{\varphi}$	Eigenvector of the matrix $\mathbf{L}$
$\phi(\cdot)$	Expansion of a subgraph
χ	Number of free nodes
$\boldsymbol{\psi}$	Eigenvector of the matrix $\mathbf{L_N}$
ω	Nominal system frequency
$\boldsymbol{\Omega}$	Incidence function
$\{\}$	A collection of elements
$\cap, \cup$	Intersection and union
$\subseteq, \subset$	Subset and proper subset
$\not\subset$	Not subset
$\leq$	Less than or equal to
$\geq$	Larger than or equal to
$\setminus$	Set-theoretic difference
$\in$	Belongs to
$\notin$	Not belong to
$\times$	Cartesian product
$\lvert\cdot\rvert$	Cardinality
$\lVert\cdot\rVert$	Norm
$\langle\cdot,\cdot\rangle$	Standard inner product
$\forall$	For all
$\otimes, \oplus$	Boolean multiplication and addition operators
$\varnothing$	Empty set
$\mathbb{R}$	Real number set
$\mathbb{R}^n$	n-dimensional Euclidean space
$\mathbb{S}^{n-1}$	Unit (n–1)-dimensional sphere

Subscripts

0	Initial values/equilibrium point
d	*d*-axis (machine reference frame)
i	Index value, where *i* = 1, 2, 3…
j	Index value, where *j* = 1, 2, 3…
k	Index value, where *k* = 1, 2, 3…
B	Blackstart
CLD	Critical load
GN	Generator
LD	Load
RED	Reduced

Superscripts

max	Maximum limit
min	Minimum limit
GN	Generator
LD	Load
T	Transpose
¨	Double derivative
′	Transient

Acronyms

BFS	Breath-First Search
CL	Cannot-Link
CPU	Central Processing Unit
CSC	Constrained Spectral Clustering
DFS	Depth-First Search
EPSRC	Engineering and Physical Science Research Council
FACTS	Flexible AC Transmission System
GPS	Global Positioning System
HVDC	High Voltage Direct Current
ICI	Intentional Controlled Islanding
IEEE	Institute of Electrical and Electronic Engineers
MCC	Minimal Cutset Constraint
MDS	Minimum Dominating Set
ML	Must-Link
NP	Non-deterministic Polynomial-time
OBDD	Ordered Binary Decision Diagram

PBC	Power Balance Constraint
PC	Personal Computer
PMU	Phasor Measurement Unit
PPSR	Parallel Power System Restoration
PSR	Power System Restoration
RAM	Random Access Memory
RAS	Remedial Action Scheme
SC	Spectral Clustering
SCCI	Spectral Clustering Controlled Islanding
SIPS	System Integrity Protection Scheme
SPS	Special Protection Scheme
SSC	Separation and Synchronization Constraint
TSO	Transmission System Operators
UCR	University of Costa Rica
UCTE	Union for the Coordination of Transmission of Electricity (Europe)
UK	United Kingdom
USA	United States of America
WAMS	Wide Area Measurement System

Abstract

Application of Graph Theory to Intentional Controlled Islanding for Blackout Prevention and System Sectionalising for Parallel Restoration

Mr Jairo Quirós-Tortós, The University of Manchester, February 2014.

This thesis investigates the application of graph theory to Intentional Controlled Islanding (ICI) for blackout prevention and system sectionalising for Parallel Power System Restoration (PPSR). The outcomes of the thesis are the development of more efficient and more accurate methodologies to partition the power system in a controlled manner for blackout prevention, and the development of methodologies to systematically determine suitable system sectionalising strategies for the purpose of reliable parallel restoration.

This research has been conducted as the number and the impact of large-area power system blackouts have considerably increased worldwide over the last two decades, affecting hundreds of millions of people. In this context, ICI has been proposed as an effective corrective control strategy that can be used to minimise and limit the impact of cascading outages leading to large-area blackouts by separating, in a controlled manner, the power system into multiple sustainable and stable islands.

Moreover, the duration of these catastrophic and expensive events has lasted for several hours and even weeks in numerous cases. Therefore, PPSR has been suggested as an effective and efficient restoration strategy. This approach sectionalises the entire blackout area into multiple islands and restores the created islands in parallel using their own resources, considerably accelerating the restoration process of large-scale power systems affected by complete blackouts.

In the context of ICI, this thesis presents new graph theory-based methodologies to determine islanding solutions. The methodologies developed in this thesis for islanding are computationally more efficient and more accurate compared to existing methods. This thesis also explores the dynamic performance of the electrical network, and introduces the concept of weak areas. These weak areas are defined as the zones where, based on the dynamic coupling between the system buses, network splitting is more likely to occur.

In the context of PPSR, this thesis introduces new methodologies that systematically determine suitable system sectionalising strategies for PPSR. These strategies accelerate the restoration process by enabling system operators to simultaneously restore more elements of the electrical network, as the restoration of each island is performed independently. Moreover, they help maintain the steady-state stability of the created islands, as multiple constraints are taken into account during the sectionalising strategies design.

All formulations presented in this thesis are validated in different IEEE test systems.

Declaration

No portion of the work referred to in the thesis has been submitted in support of an application for another degree or qualification of this or any other university or other institute of learning.

Copyright Statement

[1] See: http://www.campus.manchester.ac.uk/medialibrary/policies/intellectual-property.pdf

[2] See: http://www.manchester.ac.uk/library/aboutus/regulations

Acknowledgements

I would like to express my sincere gratitude to my supervisor Prof. Vladimir Terzija for his constant support, guidance and motivation during my PhD studies.

A special acknowledgement must also go to the Office of International Affairs and External Cooperation at the University of Costa Rica (UCR) and the Engineering and Physical Science Research Council (EPSRC) in the UK who have sponsored this project.

I want to express my gratitude to Dr Mathaios Panteli, Dr Robin Preece, Dr Rubén Sánchez-García, Dr Gustavo Valverde, Dr Gary Preston, Dr Peter Wall, Dr Elias Kyriakides, Dr Lei Ding and Prof. Janusz Bialek for their help during my research work.

I also wish to thank all my friends and family in Costa Rica for their support, particularly to Jeffrey, Eddie, Jacob, Rebeca (I am deeply grateful with you for receiving me in Manchester) and my uncles Marvin, Alexis and Eduardo for helping me all the time.

Special thanks to all my colleagues and friends in Manchester for making my life easier and funnier, particularly to Mathaios, Elina, Jaime, Valentina, Alban, Claire, Robin (I am indebted with you for all the help), Gary, Manuel, Alex, Carlos, Feras, Adrien, Jonathan (both), Chomba, Tee, Jiashen, Yutian, Shantanu, Melios, Yuhang, Vedran, Alejandro, Antonios, Roger, Nela, Edmond, Deyu, Peter, Pawel, Angel, Nando and Helge.

I am wholly indebted to my parents Juan Quirós and Guisselle Tortós, and my brothers and sisters Christian, Alonso, Nabyl and Esdras for their unconditional love, support and comprehension throughout my life. You helped me make my dream come true and I am sure you are very proud about it.

Finally, I want to express my gratitude to my beloved future wife *Jessica* for being there always next to me. Thanks for your comprehension and support during stressful moments of my studies. I have no way to pay you back all the love I received in the last years. I am sure this is just the starting point of a long way beside you.

To Jessica, and my family

Chapter 1. Introduction

Chapter 1 introduces fundamental concepts of power system stability and security. A review of the major power system blackouts that have taken place over the last decades is then conducted, and the importance to develop effective and efficient Intentional Controlled Islanding (ICI) strategies for blackout prevention and system sectionalising strategies for Parallel Power System Restoration (PPSR) is discussed. This chapter provides a thorough review of the current methods for ICI and system sectionalising strategies for PPSR to highlight the significance to advance existing ICI and sectionalising methods. A brief introduction to the basis of graph theory is then provided. This chapter finally presents the research aims, objectives and main contributions of this thesis.

Power systems are prone to cascading outages leading to large-area blackouts, and ICI has been proposed as an effective corrective control strategy to mitigate cascading events. ICI can be used as a last resort to optimally separate the power system into electrically isolated and stable islands. However, this adaptive control strategy may not always mitigate blackouts due to the inherent complexity of cascading outages. Hence, Power System Restoration (PSR), which aims to re-energise the network affected by partial or complete blackouts as quickly and safely as possible, must be undertaken to re-establish the blackout area. In this context, PPSR, which sectionalises the entire blackout area into multiple islands using a suitable sectionalising strategy and restores the created islands in parallel, is commonly adopted by utilities as it considerably accelerates the restoration process.

1.1. Power System Stability

Power system stability describes the ability of the electrical power system to maintain stable operation during normal conditions and to reach an acceptable stable operating point after being subjected to a physical disturbance [1]. Interconnected power systems are prone to instabilities, as they are increasingly being operated close to the stability limits in order to meet the growing demand and increasing penetration of renewable energy resources, as

well as to respond to the economic pressure from electricity markets and to satisfy environmental constraints [2]. These factors impose additional stress on the transmission system and significantly increase the probability of cascading outages [2-4].

Cascading outages are defined as a sequence of dependent failures of individual power system components that successively weaken the network and frequently lead to the loss of part or the entire power system [2, 3]. Cascading outages may be initiated by relatively small disturbance such as the contact between an overloaded line and vegetation. When this happens, the overloaded line is automatically disconnected, and adjacent components may subsequently be overloaded. If control actions are not timely implemented by operators, the new overloaded line may be automatically disconnected by its own protections, and this will trigger the cascading overloading and tripping of more elements, which eventually weaken the entire system and commonly cause large-area blackouts [3, 4].

1.1.1. Stability Issues

Power system stability issues can be broadly classified into three main categories. These categories and their subcategories are shown in Figure 1.1 and explained below [1, 5, 6].

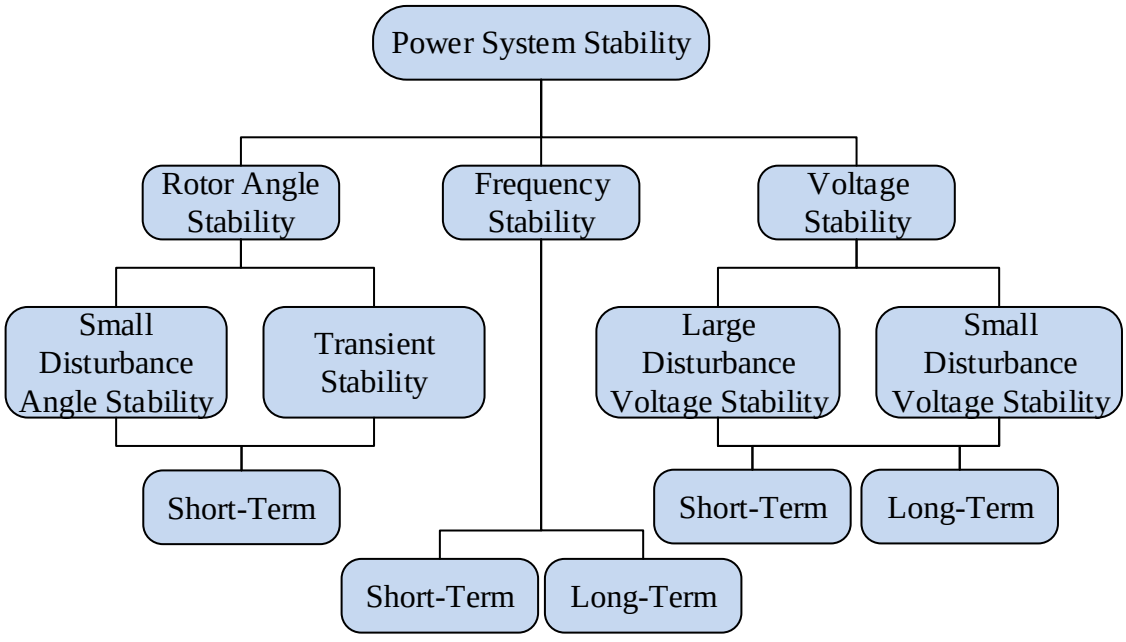

Figure 1.1: Classification of power system stability [5]

Rotor Angle Stability refers to the ability of the interconnected generators within the power system to maintain synchronous operation at the same rotational speed after being subjected to a disturbance [1]. Rotor angle stability can be further divided into small-signal and large-signal rotor angle stability, depending on the severity of the disturbance. While the former concerns the ability of the generators to retain synchronism after small disturbances (small variations in loads and generation), the latter – usually referred to as transient stability – studies the synchronism between machines following a severe disturbance (short-circuits) [6]. Small system disturbances may cause the rotor of the synchronous machines to oscillate, and these power oscillations are usually damped by the power swing damping controllers [1]. However, if the disturbance is severe enough, the machines may ultimately lose synchronism. The loss of synchronism in a multi-machine power system creates coherent groups of generators [5]. The loss of synchronism can occur between one generator and the other machines in the system, or between groups of generators [5], and it may lead to cascading outages that end in blackouts [7].

Frequency Stability refers to the ability of the power system to maintain the frequency within acceptable limits [1]. Frequency problems occur when the active power balance between the generation and the demand is not satisfied, and they can occur in the entire power system, or in electrically isolated islands [5].

Voltage Stability refers to the ability of the system to maintain acceptable voltages at all system buses [1]. A power system can be considered to be voltage unstable if an increase in reactive power injection at any system bus yields a drop in the voltage at the same bus [6].

1.1.2. Definitions

Islanding is an effective corrective control strategy to mitigate cascading events. It refers to the controlled separation of the transmission system after instabilities have been detected, but before the system becomes uncontrollable [8, 9], to limit the impact of cascading outages leading to blackouts.

Blackout (power system blackout) refers to the complete disconnection of part or the entire network [2-4]. A blackout can significantly affect the global economic and social life of

millions of people [10-12]. Defined as high-impact and low-probability events [10], blackouts are the most severe disturbance in the system. They can occur when the stability limits of the system are violated and cascading outages result in customer disconnection, degrading thus the system security and affecting the reliable operation of the system.

1.2. Power System Security

Power system security is related to the robustness of the network to withstand imminent disturbances [5]. It describes the ability of the power system to continue the power supply to customers even after imminent contingencies [5, 6]. The system security depends on the power system operating state – described below – as well as the probability of disturbances at that state [6]. In practice, power system security is associated with the operation of the network in a preventive mode, which ensures the withstanding of a set of contingencies likely to occur and referred to as "normal contingencies" in the network. This is usually referred to as the $N-1$ security criterion [6] because it examines the behaviour of a power system with N components following the loss of any of its major components.

1.2.1. Power System Operating States

Power system security describes the operation of the network by five operating states, as depicted in Figure 1.2 [1, 5]. These states are also used to indicate the severity of a disturbance, to analyse system security and to design the most appropriate control actions to assist operators in restoring the power system to a normal state [1, 4]. Table 1.1 shows numerous control actions available in the control centres to overcome problems during each operating state [4]. As noted, the control action to be used at each operating state depends on the level of security at which the power system is being operated. Furthermore, it should be noticed that the lower the security level, the more radical the control action.

The power system is in the **normal** state when all electrical variables are within the normal range, and no equipment is being overloaded. In this state, the system operates securely and can withstand any single contingency, without constraint violations [1, 4].

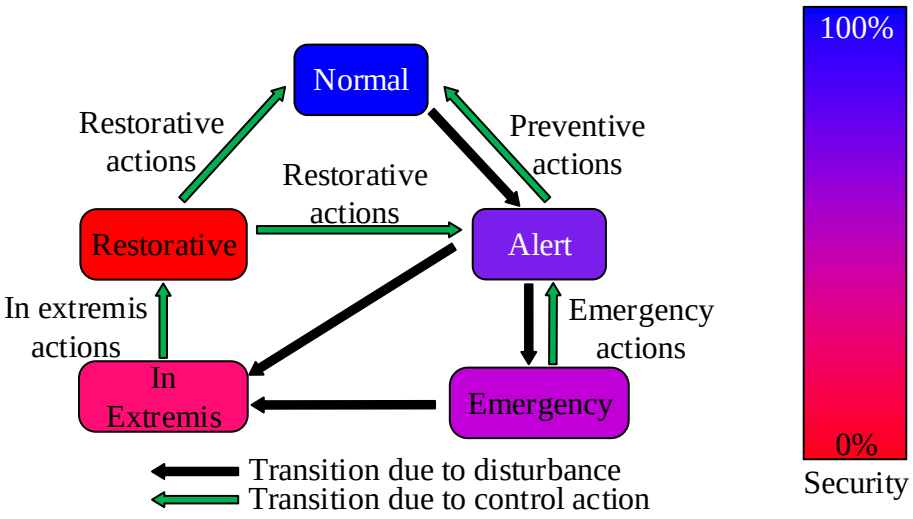

Figure 1.2: Power system operating states [5]

Table 1.1: Examples of available control actions in each power system operating state

Operating State	Examples
Alert	Generation rescheduling, start-up of generation units, tie-line rescheduling, change of substation configuration, change of reference points of controllable devices
Emergency	All preventive actions, plus fault clearing, excitation control, fast-valving, capacitor switching, fast HVDC power transfer control, ICI, controlled opening of interconnection to neighbouring systems, blocking of tap changer of transformers
In extremis	All actions mentioned above, plus load shedding (involving underfrequency and under-voltage protection schemes)
Restorative	Unit restarting and synchronisation, sectionalising strategies, load restoration, resynchronisation of areas

The system enters the **alert** state if the security level falls below a certain limit of adequacy, or if the probability of disturbance increases [4]. In this state, all electrical variables are within the normal range and all constraints are satisfied, but a single contingency may result in limit violations. Preventive actions can restore the system to the normal state [1].

If a severe disturbance occurs before preventive control actions are implemented, the system can either enter the **emergency** or the ***in extremis*** state, depending on the severity of the perturbation [1]. In the former, system voltages may be considerably low, equipment may be overloaded and security levels are very low. The effective and timely implementation of emergency actions can restore the system to at least the alert state. If

these actions are not implemented in a timely manner or are ineffective, the system enters the ***in extremis*** state. This transition results in rapid cascading outages, increasing the probability of partial or large-area blackouts and significantly reducing the security levels.

The **restorative** state represents a condition in which restorative actions are implemented to reconnect generators, to restore system load, and to resynchronise electrical islands. Either the **alert** or the **normal** state can be achieved, depending on the system conditions.

It is important to mention that ICI is considered to be a corrective control strategy for power systems under emergency and *in extremis* states [3, 4, 7, 13]. Furthermore, system sectionalising for PPSR is considered to be a restoration strategy performed by system operators in power system under the restorative state [14-17].

1.3. Power System Blackouts

This section presents a review of major power system blackouts to highlight the necessity for developing effective and efficient control actions to mitigate blackouts. It also studies the anatomy of the blackout to identify the stages where the control actions are undertaken.

1.3.1. Review of Major Power System Blackouts

A review of major power system blackouts that have taken place over the last decades [11, 12, 18-24] enables a power system blackout to be described in terms of two main characteristics: the **impact** on the system in terms of population affected, and its **duration** [2-4]. Table 1.2 describes the most significant blackouts over the last decades.

A review of these blackouts shows that there are two types of blackout causes [11, 12, 18-24]. Blackouts can be initiated by external causes, such as natural disasters (earthquakes, ice storms, tornadoes, and hurricanes/tropical storms), vandalism, or operator error [25]. Operator errors still remain among the most important causes or contributing factors of power system blackouts [4], despite the increasing use of automation in power systems. Blackouts can also be initiated by a set of electrical events that triggers a sequence of subsequent component outages, i.e., by cascading outages.

Table 1.2: Duration and impact of major power system blackouts

Location	Date	Impact (Million)	Duration
Northeast, USA/Canada	09/11/1965	30	12 h
New York, USA	13-14/07/1977	8	26 h
New Zealand	20/02/1998	0.07	4 weeks
Brazil	11/03/1999	97	5 h
India	02/01/2001	226	12 h
Iran	20/05/2001	30	12 h
USA (North-East)/Canada (Central)	14/08/2003	50	4 days
Italy	27-28/09/2003	56	18 h
Spain	29/11/2004	2	10 days
Indonesia	18/08/2005	100	7 h
UCTE	04/11/2006	15	2 h
Brazil-Paraguay	10/11/2009	87	7 h
Brazil	04/02/2011	53	16 h
India	30-31/07/2012	620	2 days
Queensland, Australia	26-27/01/2013	0.25	10 days

Incorrect system splitting is also a major cause of system blackouts [2-4]. Other causes of blackouts include inadequate understanding of the system, insufficient level of situation awareness and inadequate level of support from the Reliability Coordinator, which result in the configuration of the system in an "$N - 1$" insecure state, increasing the probability of cascading outages and loss of supply following the occurrence of an electrical outage.

As it can be noticed in Table 1.2, the number and the impact of power system blackouts have considerably increased over the last two decades, affecting worldwide hundreds of millions of people [2-4]. In this context, ICI has been proposed as an effective corrective control action that can be used to minimise and limit the impact of cascading outages leading to large-area blackouts [11, 12].

Furthermore, the duration of recent blackouts – associated with the restoration duration – has lasted for several hours or even weeks in numerous cases [11, 12, 18-24]. In this context, PPSR is an effective, reliable, and efficient restoration strategy to accelerate the restoration process of power systems affected by complete blackouts. PPSR requires the definition of a suitable sectionalising strategy to optimally sectionalise the blackout area into multiple islands that are then restored in parallel using their own resources [14-17].

The development of computational efficient and effective methodologies to determine ICI strategies for blackout prevention and system sectionalising strategies for PPSR have taken major attention during the last decades, and represents the main motivation of this research. Studying the past blackouts can help preventing future ones. However, neither studying nor analysing past events can avoid all future blackouts [4, 20, 21]. Thus, research on blackout mitigation seeks to reduce the probability of their occurrence and the extent of their consequences. This would eventually lead to improved system reliability [4].

1.3.2. Anatomy of a Blackout

Two different approaches that capture the blackout progress have been suggested in the literature [20, 21]. Both approaches highlight the importance of power system operators and automatic control actions such as ICI during the development of cascading outages [21], and demonstrate that effective restorative control actions can assist system operators during the restoration of the affected system to a normal state.

The study of major power system blackouts during the last decades reveals that this phenomenon progresses with some similarities in spite of the network. In most of the cases, the sequence of events leading to blackouts can be divided into five common phases shown in Figure 1.3 and identified as: (i) precondition, (ii) initiating events, (iii) cascade events, (iv) final state and (v) restoration [20]. Cascade events – defined as the most important stage of the blackout progression – can be further divided into three phases: (iii-1) steady-state progression, (iii-2) triggering events and (iii-3) high-speed cascade. These phases are used to identify the role of operators and the moment of undertaking control actions (Table 1.1). They also reveal that system blackouts are not caused only by a single event, but by a combination of several deficiencies – initiating events plus triggering events [23].

The study of major blackouts demonstrate that the system condition prior the initiating events (**precondition**) can significantly affect the evolution and the severity of a blackout [4]. High power demand (summer and winter peaks), inadequate active and reactive power reserves, severe weather condition and equipment unavailability are only some examples of preconditions that can influence the development of a power system blackout.

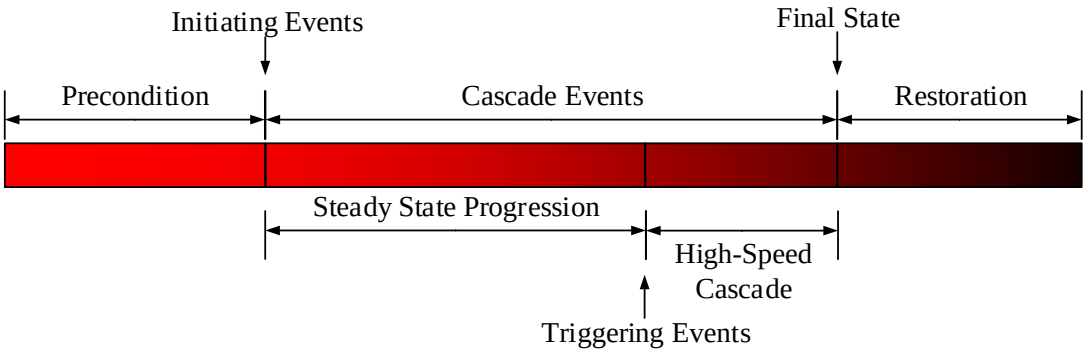

Figure 1.3: Typical phases of power system blackouts [20]

The **initiating events**, following the precondition, can be broad. Short circuits followed by overloads, significant voltage and/or frequency deviations, disconnection of substations and/or generating stations, cascading outages, and incorrect system islanding can significantly deteriorate the system condition [2, 20].

The **steady-state progression** of the cascade events takes place after the initiating events, and is very slow. System operators usually have time to respond and maintain the balance between the generation and the demand. This phase is crucial as the effective and timely implementation of appropriate control actions can stop the spread of the failure before the situation becomes uncontrollable [4].

The **triggering events** stage then occurs, and the power system enters the **high-speed cascade** phase, where maintaining the balance between the generation and demand is usually not possible. Furthermore, system equipment may be rapidly disconnected, and the system blackout can happen in a very short period of time [4]. Consequently, transmission system operators are not able to react, and the system integrity relies on the successful implementation of the automatic control actions described in Table 1.1 [4].

The **final** state is then reached. The system may eventually contain multiple areas in blackout, and restorative control actions – **restoration** stage – are critically important for rapidly restoring the blackout areas to a normal state.

1.4. Wide Area Measurements Systems

The mitigation of large-area power system blackouts and the restoration of large-scale power systems following a major incidence have been largely facilitated in recent years by the development of Wide Area Measurement Systems (WAMS) [26-30].

WAMS can collect synchronised data from various points within a power system to provide fast and accurate observability of the electrical variables. They use Phasor Measurement Units (PMUs), also called synchrophasors, to collect time-stamped phasors of voltages and currents, as well as frequency information at the bus at which the device is located.

PMUs – developed in 1988 and originally used as disturbance recorders – currently use signals from the Global Positioning System (GPS), or any other timing source, in order to achieve a synchronisation accuracy of 1 μs [31]. These devices are used in modern power systems to monitor: system inter-area oscillations [26], frequency and rotor angle oscillations for coherency identification [27, 32], power flows and bus voltages for state estimation [28], power flows for ICI [29], stability of the system during system restoration [30], and others [33].

In 2011, the Institute of Electrical and Electronic Engineers (IEEE) published the Standard C.37.118-2011 to establish the data exchange requirements to create and transmit files by commercially available PMUs [34]. The OpenPMU, open source, platform exists to encourage research into further synchrophasor algorithm development [35].

To date, the process of introducing PMUs in power systems is costly and requires more time to see the full benefits of WAMS. In the meantime, the studies must concentrate on making the most of the information provided by the few installed PMUs until the gradual insertion of PMUs will make the system fully observable.

The methodologies proposed in this thesis to prevent blackouts through ICI strategies and to accelerate PPSR through system sectionalising strategies can be supported in practical implementations by WAMS. In practical and current applications, they would utilise actual information from hybrid state estimators [33]. However, as the number of PMUs is

expected to increase in the near future, these methodologies would then use information from the linear state estimators [28].

1.5. Research Background

The risk of cascading outages leading to large-area blackouts cannot be completely eliminated [3, 4, 7]. Nonetheless, their impact can be reduced through the effective and timely implementation of adaptive corrective control actions, such as ICI [3, 4, 7, 13]. Furthermore, the duration of the blackout can be minimised through the adequate planning of restorative control actions, such as system sectionalising strategies for PPSR [14-17]. Undertaking PPSR ensures faster restoration [17]; hence, PPSR is usually referred to as faster PPSR.

Associated with the blackout phases (Figure 1.3), the four steps depicted in Figure 1.4 are used in this thesis to study the implementation of ICI strategies for blackout prevention and the adequate planning of sectionalising strategies for PPSR following a complete blackout.

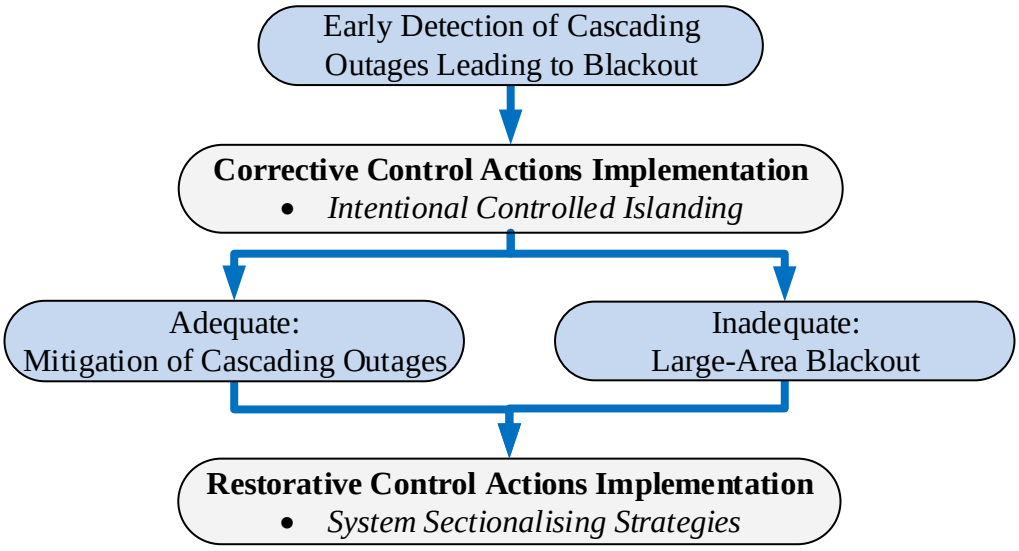

Figure 1.4: Introduced steps to study the blackout prevention and system restoration

The early detection of cascading outages leading to large-area blackouts – commonly defined in the literature as early warning of instability issues – is significantly important in the blackout prevention [8, 9, 36-40]. This step seeks to assist the operators on defining the

optimal timing of the implementation of ICI strategies. Although this stage is not covered in this thesis, as it is out of its scope and involves an immense research field that is associated with the early detection of instabilities, it is known that such detection should be rapidly performed during the steady-state progression of the cascade events (Figure 1.3), and must be capable of predicting the future behaviour of the system [8, 9, 36, 38].

ICI, which is usually seen as a Remedial Action Scheme (RAS), Special Protection Scheme (SPS) or System Integrity Protection Scheme (SIPS) depending on the region [3, 4, 7], must be undertaken when the risk of cascading outages increases and the vulnerability analysis indicates that the system is approaching a potential catastrophic failure. The first part of this thesis focuses on the development of ICI methodologies that can be used as the very last resort to mitigate the cascading outages that may lead to catastrophic blackouts followed with massive consequences to the society and the system. The methodologies that are developed within this thesis for the controlled separation of the power system are motivated by the initial work that had been carried at The University of Manchester by Dr Lei Ding, Dr Francisco Gonzalez-Longatt, Peter Wall and Prof Vladimir Terzija, which produced [49]. Indeed, the initial findings from [49] are used as a basis to further improve the accuracy and computational complexity of the spectral clustering-based methodologies, as it is explained in the following chapters.

As shown in Figure 1.4, the controlled separation of the system is defined as adequate if its timely implementation mitigates, or significantly reduces, the impact and consequences of a large-area blackout. However, its implementation will otherwise be inadequate, and it is highly likely that multiple areas, or even the entire power system, will be in blackout [3, 4].

In spite of adequate or inadequate controlled separation, restorative control actions must always be undertaken to restore the blackout area(s) of the power system to a normal and secure state of operation. In this context, the second part of this thesis considers the scenario of complete blackout – the most severe disturbance in the power system – and focuses on the development of basic guidelines that can assist system operators in determining system sectionalising strategies for PPSR. By restoring the system in parallel,

the restoration process is considerably accelerated [4, 14-17], and therefore, the duration of the blackout is significantly reduced [2].

1.5.1. Intentional Controlled Islanding (ICI)

Interconnected power systems are prone to cascading outages leading to large-area blackouts, and ICI is an effective corrective and adaptive approach to avoid these cascading outages [11, 12]. ICI – also referred to in the literature as controlled separation, system islanding or system splitting – aims to avoid the uncontrolled splitting of the power system that is commonly caused by the loss of synchronism between groups of machines [41-43].

A major concern related to any ICI scheme is the computational efficiency and accuracy of the method, as this control strategy must be undertaken in a very limited timeframe (of just a few seconds) and must ensure the creation of electrically separated and stable islands [44-49]. The simplicity of the ICI scheme and its scalability to large-scale networks will also factor when determining if an ICI method is appropriate for practical installations.

The ICI problem can be modelled as a constrained combinatorial optimization problem, and its complexity increases exponentially with the size of the power system [44-49]. Therefore, determining an islanding solution in real-time – quickly enough to ensure effective islanding within a limited timeframe – is an extremely complex analytical, computational and practical problem [44, 45].

There are two primary aspects related to ICI [41-43]: 1) when to island and 2) where to island. While the former is associated with the early detection of cascading outages leading to blackouts and refers to the optimal timing for system splitting (first block in Figure 1.4), the latter is associated with the actual implementation of this, and aims to determine the optimal set of transmission lines that must be disconnected across the power system to create electrically isolated and stable islands. This thesis focuses on answering the question of *"where to split"*.

When answering the question "*where to split*", multiple constraints such as generator coherency, load-generation balance, thermal limits, voltage and transient stability should be

taken into account. However, including all of these in the ICI problem may result in a very complex problem that could not be solvable in a limited timeframe; thus, only a subset of constraints can be considered [44-49]. The exclusion of some constraints and the inherent characteristics of the electrical network mean that additional (post-islanding) corrective measures, e.g., load shedding and generation rescheduling [11, 12] are necessary to ensure that each island retains its stability and security margins in the post-islanding stage.

Among the conditions mentioned above, the generator coherency constraint which is used as a practical substitution of the true transient stability constraint, is crucial for the success of the controlled separation [11, 12]. A group of generators is referred to as coherent if their rotor angle oscillates coherently following a major disturbance [1, 5, 6]. This critical constraint refers to the creation of electrically isolated islands such that only coherent generators are included in each island [41-49]. As a result, current approaches for ICI aim to split the transmission system such that each island contains only coherent generators. The creation of electrical islands for a given operating point with only coherent generators considerably helps the transient stability of the future islands, as all the machines within the same island possess a relatively constant angular deviation [5].

Extensive research into the development of ICI schemes has been carried out in the past, as it has been concluded that the effective and timely implementation of these schemes could have avoided numerous large-area blackouts in the past [50-52]. Furthermore, the existing methods are based on the rule that the controlled separation of the transmission system has to be undertaken before the triggering events stage in Figure 1.3 occurs [8, 9, 40-52].

The existing ICI methods seek to partition the power system in a controlled manner such that the islands created by the ICI method are optimal for a given objective function with a predefined set of physical and operational constraints. In this context, they can be classified according to the objective function used, of which there are three major classes: minimal dynamic coupling [53-56], minimal power imbalance [44-47, 50-52, 57-61], and minimal power flow disruption [48, 49, 62, 63].

Each approach has different advantages and disadvantages and they produce different islanding solution, as detailed below. However, they all are special cases of searching

problems on *graphs*, which are generally *NP-hard*. A problem is *NP-hard* if it cannot be optimally solved in polynomial time [64]. Thus, to rapidly determine an islanding solution, computationally more efficient algorithms that approximate the optimal solution must be used instead. The utilisation of scaled and representative systems, as well as the reduction of the search space to determine a suboptimal solution could also benefit the determination of islanding solutions [50-52].

1.5.1.1. Minimal Dynamic Coupling

Methods for minimal dynamic coupling seek to minimise the dynamic interaction between generators and, more specifically, between dynamically coherent areas [53-56]. An area in the power system is defined to be coherent if all the system buses included in the coherent area have a similar dynamic response [56]. Approaches for minimal dynamic coupling are based on the slow coherency theory [53] – introduced to develop dynamic equivalents for transient stability studies [65-67] – and they study the coherency of the electrical machines using the system state matrix, as well as the dynamic interaction between the load buses using the *Jacobian* matrices associated with the dynamic system [56].

More specifically, these methods employ information associated with the rotor angle of the generators and the voltage phase angle of the load buses to identify islanding solutions across the weak connections between strong dynamically connected buses. This approach creates coherent areas, in the sense that the angular deviations of the electrical buses within each island are closely related to the rotor angle variations of the generators within the same coherent area. In other words, the oscillations in the voltage phase angle of all the system buses within each coherent area have similar dynamic response after a disturbance [56].

The minimisation of the dynamic interaction between coherent areas also produces an islanding solution with only coherent generators, as the generator coherency occurs between machines that are strong dynamically coupled [54].

Research considering only the dynamic coupling between buses is very limited. Initial investigations were mainly focused on identifying coherent groups of generators [53, 54]. The singular perturbation technique is used in [55] to determine the slow coherent areas of

a power system. The aggregation performed in [55] forms slow coherent subsystems that model the dynamics of the interchange between the coherent areas.

The concept of slow coherency has been recently extended in [56] using the *Jacobian* matrices of the dynamic power system to group both generators and load buses within the same island. The existing method, which initially determines a reference generator for each island using a computationally demanding Gaussian elimination with complete pivoting technique, can determine the weak connections between coherent areas. However, it only considers the dynamic coupling between the load buses in the system and the reference generators previously identified for each island. Failure to consider the dynamic coupling between load buses and the non-reference generators in the same island may lead to inaccurate islanding solutions for minimal dynamic coupling. Therefore, the islanding solution produced by the ICI method introduced in [56] may not be determined across the absolute weakest connections in the power system, i.e., the islands created by the existing method may not be as strong dynamically coupled as they could be.

Methods that consider only the dynamic coupling between electrical buses cannot ensure adequate load-generation balance and the implementation of such solutions may produce overloads in the transmission lines that remain connected in the islands. These problems are caused because the ICI methods for minimal dynamic coupling cannot include in the ICI problem the actual power flow in the branches [49, 50]. Nevertheless, the concept of minimal dynamic coupling considers the dynamic properties of the electrical power system. Thus, it presents very interesting physical meanings which can be further explored to improve the dynamic performance of the islands [53, 54].

1.5.1.2. Minimal Power Imbalance

Methods for minimal power imbalance seek to create islands with load-generation balance [44-47, 50-52, 57-61]. This approach produces a solution that requires the least amount of load to be shed, and the least amount of generation to be rescheduled following splitting.

The transient stability of the future islands can be enhanced in these methods by including the generator coherency constraint in the ICI problem [44-46, 50-52]. Therefore, the

existing ICI methods for minimal power imbalance seek to create islands with reduced load-generation imbalance containing only coherent generators.

Research into the development of ICI schemes for minimal power imbalance is extensive. Several methods have been proposed, and various optimization techniques have been used. The existing methods use: Ordered Binary Decision Diagrams (OBDDs) [44-46], tracing power flows [47], slow coherency-based cutset determination algorithms [50-52], mixed integer linear programming [57], metaheuristic optimization [58, 59], and simulated annealing algorithms [61].

The existing ICI methods for minimal power imbalance can effectively find an islanding solution. However, due to the complexity of the ICI problem, the determination of an islanding solution for minimal power imbalance using various existing methods [44-46] may not satisfy the vital real-time requirement [49]. In fact, many of these methods [44-46, 57-59, 61] require extensive off-line simulations to reduce the searching space, and thus, to make them applicable in large-scale power systems Another proposed solution to improve the computational efficiency of these methods is by using network reduction approaches to limit the number of nodes to be included in the combinatorial optimization [44-46]. For example, in order to utilise the OBDD-based methods in real-time applications (less than two seconds), the size of the power system must be reduced to contain no more than 40 nodes [44-49]. Reducing the size of the network reduces the solution space. However, the solutions that are lost during the network reduction may be better than the final solution found by the algorithm using the simplified network. Additionally, these approaches may not be capable of coping with complex future systems with high spatial variety in generation locations due to the proliferation of renewable energy resources installations.

Effective and computationally efficient algorithms that combine the concept of slow coherency with reduced load-generation imbalance to help the transient stability of the islands and to minimise the amount of load to be shed are presented in [50-52]. The method in [50] initially uses the concept of slow coherency to identify the coherent groups of generators, and then applies brute force to find an islanding solution between the coherent groups for minimal power imbalance. The study in [50] demonstrates through time-domain

simulations that small variations in the islanding solution are achieved when the location, the size of the disturbance and the loading conditions change.

These empirical results suggest the existence of an area between the slowly coherent generators where islanding solutions are more likely to occur based on the dynamic performance of the power system, i.e., they suggest the existence of a weak area. The determination of this area, using mathematical and physical means, is a motivation of this research as such area can be used to limit the buses to be included in the combinatorial optimization, reducing thus the searching space and improving the efficiency of the ICI scheme. Moreover, these areas could be potentially used for multiple applications such as the optimal PMU placement to support operators on the determination of islanding solutions, as well as the monitoring during the resynchronisation of the islands.

The concept of slow coherency is also utilised in [52] to identify the slowly coherent generators in large-interconnected power systems. The method utilises an offline stage that reduces the size of the original power system by a factor of approximately twenty percent. When a scaled system is obtained, a real-time stage determines the islanding solution between the previously identified coherent groups of generators. In order to determine the islanding solution, the method in [52] uses *multi-way graph* partitioning libraries [68], and aims to minimise the load-generation imbalance while keeping the coherent groups of generators in separated islands. This method is effective and efficient but requires the reduction of the original system [49], and as previously commented, the use of simplified networks may not produce the best islanding solution.

1.5.1.3. Minimal Power Flow Disruption

Methods for minimal power flow disruption seek to minimise the change of the power flow pattern within the network following system islanding [48, 49, 62, 63]. This approach reduces the possibility of overloading the branches in the created islands [48, 49]. Similar to the previous approach, the transient stability of the future islands can be enhanced by including the generator coherency constraint in the ICI problem [49].

The concept of system islanding for minimal power flow disruption has been recently introduced in [48]. Thus, limited research is available in the literature. In order to determine an islanding solution for minimal power flow disruption, initial investigations presented in [48] and [62] use graph theory based techniques such as *spectral clustering* and *multi-level kernel k-means* algorithms, respectively. Even though these methods are computationally efficient and can determine an islanding solution for minimal power flow disruption in a considerable short period of time (few seconds in practice), they do not include the generator coherency constraint in the ICI problem. Failure to consider this crucial constraint restricts the use of these approaches [49]; nevertheless, the ICI problem introduced in [48, 62] can be improved by considering the transient stability of the machines.

A Spectral Clustering Controlled Islanding (SCCI) algorithm has been recently proposed in [49] to determine an islanding solution for minimal power flow disruption, while ensuring that each island contains only coherent generators. However, the SCCI algorithm cannot determine in one single calculation an islanding solution when the number of islands is larger than two, i.e., it can only find an islanding solution for the *bisection case* (two islands). When the transmission system has to be split into more than two islands, the SCCI algorithm requires applying *recursive bisection* [49]. However, the iterative bipartition of the interconnected power system is computationally demanding as it involves the repeated *eigendecomposition* of a matrix associated with the graph, and this approach can also affect the quality of the islanding solution [69-74].

1.5.2. Power System Restoration (PSR)

PSR is the task of re-energising a system after a blackout by progressively restoring each of its individual elements. The restoration process seeks to restore power systems affected by partial or complete blackouts as rapidly and safely as possible [75-81]. PSR is divided into several consecutive stages. Its general objective, namely the minimization of the time required for the restoration of all customer services, is divided for each stage into multiobjective functions that include the minimization of restoration time of key network components or plants and the maximization of customer load restoration at each stage [82].

The difficulties during restoration are mainly due to the need of a large amount of data from various origins and of different type, and the variety of the several criteria to be satisfied.

The availability and deployment of system blackstart units – generators capable of starting without external network support such as hydro units – are key elements of PSR as they provide the cranking power that allows the system non-blackstart units such as steam turbine units to be brought online [76]. The cranking power – also referred to in the literature as the starting power – is the amount of active power that is required to restart the non-blackstart unit after the blackout (approximately 10% of the rated power) [83]. A non-blackstart unit is a generator that needs external network support to start operation [76].

It should be mentioned that the blackstart units will commonly send cranking power to only the non-blackstart units included in the same cranking group [81]. A cranking group is defined as the set of blackstart units and those non-blackstart units that will receive starting power from the blackstart units in the same group [83]. Defining suitable cranking groups that accelerate the cranking task, and thus the restoration process, requires a large number of studies [78, 79, 81, 83] that are out of the scope of this thesis.

A review of numerous restoration plans in multiple power systems demonstrates that every restoration process is different. However, it shows that the restoration process can be divided into three generic stages as shown in Figure 1.5 [76].

The **restart and preparation** phase takes place first, and a large number of tasks are performed during this stage [75-81]. Initially, the status of the blackout area is assessed. This assessment is crucial as the evaluation of the network in blackout may eventually lead to changes in the restoration plan. In practice, restoration guidelines are defined even before the blackout occurs [76]. Nevertheless, multiple adjustments are commonly made to the restoration plan after the disturbance occurs [84]. These modifications seek to consider the true topology and availability of elements in the post-blackout system [75-81]. Information such as the available blackstart capability, the availability of interconnection assistance, the status of non-blackstart units, the status of lines and circuit breakers and the predicted load levels are extremely important for system operators for updating the restoration plan [81, 85]. When the assessment is completed, the availability of elements (lines, transformers,

generators, etc.) determined and adjustments on the restoration plan made, one of the restoration strategies explained in Section 1.5.2.1 – the "*build-down*" or the "*build-up*" – must be selected [76]. In spite of the selected restoration strategy, system blackstart units are restarted, as they will send cranking power to non-blackstart units in the same cranking group. Power system operators are allowed at this stage to restore load only for the purpose of stabilising frequency and voltage [81].

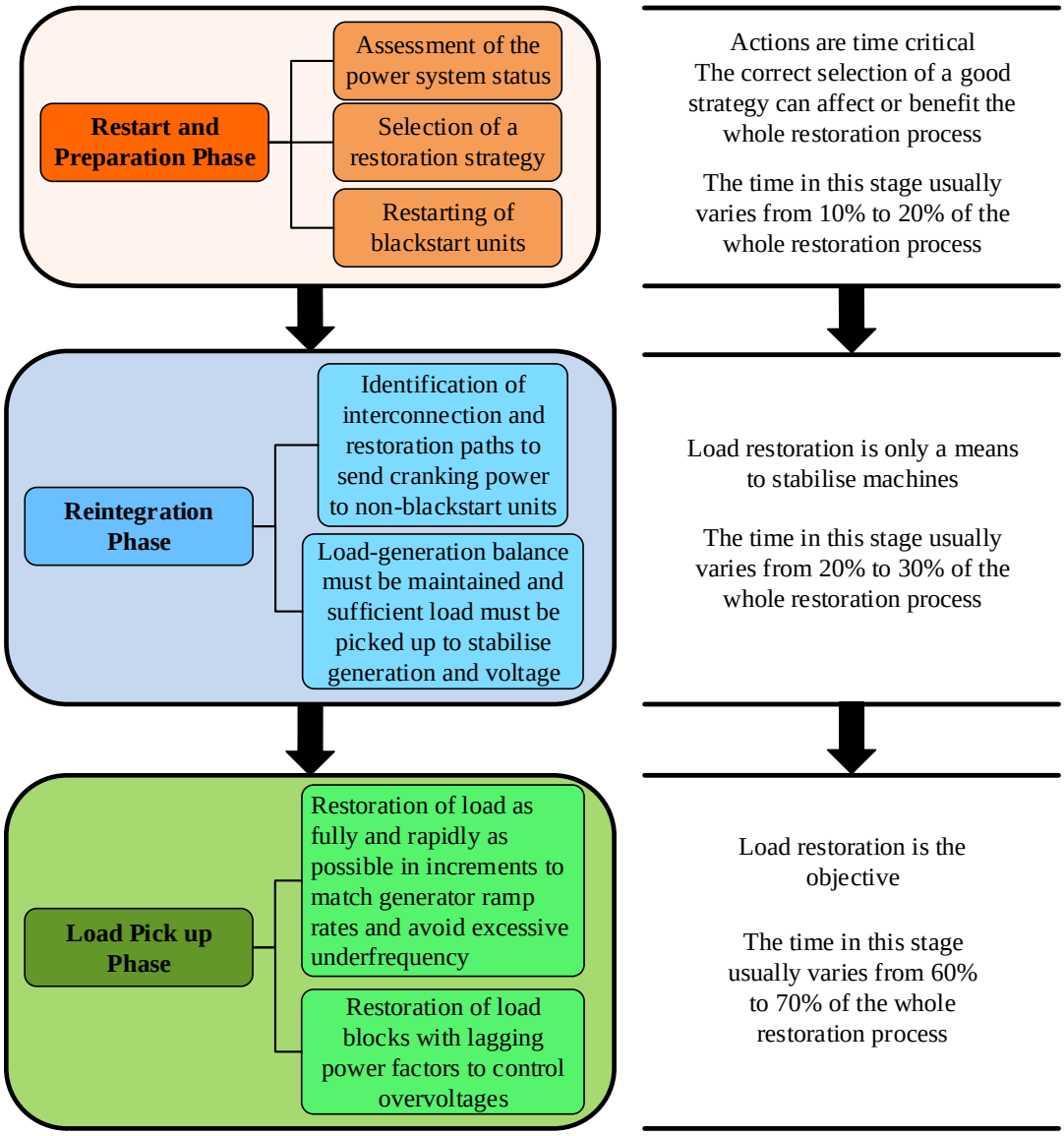

Figure 1.5: Power system restoration overview

The **reintegration** phase seeks to restore the skeleton of the blackout area – or correspondingly the skeleton of each island [76]. During this phase, restoration paths must

be adequately selected to send cranking power from the system blackstart units to the system non-blackstart units. The correct selection of the transmission loops to be energised is vital during the reintegration stage as high charging currents produced by the reconnection of long and unloaded lines may cause the sudden disconnection of the line [76]. Hence, system operators must avoid their reconnection, when possible, or connect shunt reactors at the remote end of the line to adsorb the reactive power produced by the re-establishment of the long line [86-89]. When the non-blackstart units are stable, they are resynchronised with the other machines to improve the stability margins, and to increase the probability of a successful restoration. Similar to the first stage, only sufficient load is restored during the reintegration phase to stabilise frequency and voltage.

The **load pick up** stage is the last phase of the restoration process, and aims to restore the remaining system load as fully and rapidly as possible. The size of the load block to be picked up depends on the generators response to frequency deviations [76, 78, 81, 90]. During the early stages of the load pick up phase, it is recommended to restore radial circuits with lagging power factor to control overvoltages [80].

1.5.2.1. Power System Restoration Strategies

The restoration process of a particular system requires several studies [76, 81]. Each restoration plan is different. Nonetheless, there are two general restoration strategies – the "*build-down*" and the "*build-up*" – that are commonly used by system operators as basis to develop the restoration plan of their power system [76, 79, 81]. The determination of the restoration strategy to be used depends on the relative size of the blackout area, and the amount and location of blackstart capacity and emergency backup power supplies [76, 79].

1.5.2.1.1. The Build-Down Strategy

The "*build-down*" strategy – also called centralised or sequential strategy – aims to energise the main part of the entire blackout area – also called the skeleton or backbone of the system. Loads and power stations are energised in parallel [76]. To perform a centralised restoration, the main blackstart unit must be capable of generating sufficient power to maintain system voltages within acceptable limits and to deliver sufficient power until the

other units are connected to the grid. This strategy is typical in power systems with large hydro stations, as they satisfy the requirements to perform centralised restoration [76].

In order to restore the blackout area, sequential restoration follows the three generic stages shown in Figure 1.5. The main advantage of this strategy is that the stability margins are high. Therefore, the reliability and probability of a successful restoration increase. However, the time needed for restoring the entire blackout area using the centralised strategy may be considerably long, and this commonly restricts its use [17]. Moreover, extremely high charging currents may be obtained after reconnecting long and unloaded high-voltage transmission lines. Finally, in case of a large electrical disturbance during the centralised restoration process, the entire blackout area may again be affected, leading in many cases to a recurrent large-area blackout [79, 86].

1.5.2.1.2. The Build-Up Strategy

The "*build-up*" strategy – typically referred to as PPSR – sectionalises in advance the entire blackout area into multiple islands by implementing a suitable sectionalising strategy, restores each island in parallel using their own cranking sources, and then resynchronises the restored islands to bring the entire power system back to normal operation [81].

PPSR allows more elements of the network in blackout to be restored simultaneously, as the restoration of each island is performed independently. Furthermore, it significantly accelerates restoration [76-81, 85, 91, 92]. Hence, it is usually adopted by utilities in system restoration plans. This approach has the additional advantage that in case of a disturbance in any of the islands, a recurrent blackout would happen only in the affected area [81]. However, different blackstart units are required to be available across the power system.

This strategy also follows the generic stages shown in Figure 1.5. Hence, the system status following the blackout is firstly assessed. Then, a sectionalising strategy that considers this new system status and satisfies multiple PPSR constraints is defined, and the blackstart units are restarted in each island. During the reintegration stage, the skeleton of each island is energised to allow the blackstart units to send cranking power to the non-blackstart units in each island, and load is restored for the purpose of stabilising frequency and voltage. The

load restoration stage finally involves the load in each island being restored as fully and as quickly as is reasonable [81]. When most of the load is restored and the islands are stable, the islands that have been restored independently are reconnected. Even though the resynchronisation of the islands is time consuming [85], monitoring equipment in the tie-lines between adjacent islands can extensively support system operator when resynchronising the islands [76, 79].

The definition of a suitable sectionalising strategy is a critical task performed by system operators in the control centre during the preparation stage of PPSR [81]. This strategy defines the set of transmission lines that optimally sectionalises the entire blackout area into multiple islands while considering various PPSR constraints [76, 78, 79, 81, 85]. It is important that the sectionalising strategy is defined using updated system information that is received after the blackout has occurred, which represents the actual topology of the system and the availability of its elements [76, 81, 85].

A suitable sectionalising strategy will help system operators restore the critical load – load that must be rapidly restored, e.g., hospitals and traffic lights – in a timely fashion [81, 85]. Furthermore, it will aid in restoring significant load – i.e., the non-critical load, e.g., households – as quickly as possible, when capacity becomes available. This will also facilitate the resynchronisation of the islands, as islands with more load restored are more likely to endure any unexpected voltage related issues during the resynchronization of the islands [81, 85]. In order to ensure a reliable PPSR, it is important that system security is considered during the design of the sectionalising strategy. Therefore, the following criteria should be considered when determining a sectionalising strategy [76, 81, 85].

1. Each island must have at least one blackstart unit and the cranking groups must be preserved;

2. Each island should have sufficient capacity to maintain a satisfactory frequency by matching generation and load;

3. Each island should have sufficient voltage control resources to maintain a suitable voltage profile;

4. Each island should be monitored at the system control center to ensure correct operation; and,

5. The tie-lines between the islands should all have monitoring equipment that allows the synchronization of the adjacent islands that they separate to be measured.

Numerous transmission system operators have designed sectionalising strategies for the PPSR of their systems, e.g., the Mexican system [75], the PJM interconnection [93] and the British network [94], based upon factors like historical asset ownership and operator experience, rather than on the study of the physical and inherent properties of the electrical network. This simplifies the determination of the solution but raises questions regarding the quality of the restoration planning, the proper consideration and exploitation of the physical properties of the system, and the delays that have been experienced in the past [85, 91, 92].

Furthermore, the existing methods [85, 91, 92] available in the literature to solve a sectionalising problem are focused on finding a solution with reasonable load-generation balance while considering only the blackstart availability within each island, i.e., they aim to find a sectionalising strategy that satisfies only Constraints 1 and 2 above. In order to solve the problem formulated in the existing methods, OBDDs implemented in simplified network models of the actual system [85] and heuristic search algorithms [91, 92] have been used in the past. However, it is known that the use of simplified network models may cause the loss of a better solution than that found by the algorithm using the simplified network. In addition, the use of heuristic search algorithms may produce a local minimal, instead of the global minimal.

One of the major issues identified in the current body of research is associated with the assumption of predefined active power schedules. The existing methods have assumed predefined power generation, and this assumption is certainly not suitable as the power output of the machines depends on how the restoration process progresses (cranking sequence) and the true topology of the system during restoration [76]. Furthermore, the existing methods lack of constraints to exclude critical lines that maintain system stability (Constraint 3) and those that cannot monitor resynchronisation with the adjacent islands (Constraint 5). These two constraints are vital to ensure that the lines that maintain voltage

stability within the islands and those that cannot measure synchronisation during the reconnection of the islands are not included in the sectionalising strategy.

As noticed, systematic methodologies to determine system sectionalising strategies for PPSR are required. Thus, the second part of this thesis considers the scenario of complete blackout and focuses on the determination of sectionalising strategies for PPSR. Although a suitable sectionalising strategy increases the likelihood of a successful restoration and reduces the restoration time, it cannot guarantee success due the inherent complexity and risk of restoration [85, 91, 92]. Hence, when proposing sectionalising strategies, the adequate use of the provided resources and the correct actions taken during the actual restoration of the islands must be assumed.

1.5.3. Current Practices of Transmission System Operators (TSOs)

This section details current practices of TSOs regarding defence plans, system islanding and restoration processes.

1.5.3.1. Defence Plans and Controlled Islanding Strategies

The operation of power system close to the stability limits has caused TSOs to recently update their defence plans [3]. In most of the cases, the defence plans to avoid wide-area blackouts are divided into control levels. When the risk of blackout increases, TSOs implement control actions such as automatic load shedding and ICI to limit the impact of the blackout. The purpose of this section is to give general ideas of defence plans, and not to describe all the possible plans because each TSO has its own methods. TSOs typically operate the system to ensure the continuity of load supplying, while guarantying a certain level of voltage quality, i.e., the criteria are respect the operation constraints, safe-keeping of equipment's, safe-keeping of the network, and system restoration [95].

The defence plan includes preventive and corrective actions that are carried out in control centres by operators before and during an incident. The corrective actions can be divided into actions taken by operators and automatic actions, and examples are shown below [95].

- Operators control actions

  - fast redispatching of active/reactive productions;
  - modifications of the topology of the network;
  - starting of production units;
  - actions on under load tap changers (decrease of voltage reference or manual locking, if needed);
  - manual load shedding.
- Automatic actions
  - tripping of production units (to solve line overloads);
  - actions on under load tap changers (decrease of voltage reference or locking, if needed);
  - frequency or voltage load shedding;
  - intentional controlled islanding of the bulk power system;
  - islanding of nuclear and thermal units.

1.5.3.2. Restoration Practices

As previously mentioned, every restoration process is different, and it depends mainly on the topology of the system, the availability of the elements after the blackout, and the cause of the blackout. The restoration tasks can be classified in the following areas [82].

- load balancing and frequency regulation (e.g., [90]), based on the amount of rapidly active reserve available to preserve the system frequency;
- transmission line energisation and voltage regulation (e.g., [86, 88, 96], based on the reactive reserve mainly provided by underexcitation capability limits of generators, shunt compensation, and early energisation of selected loads (preloading);
- switching strategies (e.g., [97]), which take into account the occurrence of severe transient overvoltages particularly in the case of harmonic resonance due to the nonlinear magnetizing characteristic of the energized transformers;
- protective system issues and reclosing maneuvers between restored islands by means of synchroscope and check synchronizing relays (e.g., [98]).

Typical restoration problems can be classified into the following areas [75-81, 88, 99-103].

- Reactive power unbalance and voltage control
- Active power unbalance
- Inadequate load and generation coordination
- Inadequate monitoring and control strategies
- Failure in the protective systems
- Depletion of energy storage (batteries)
- Restoration plans inadequacies
- Inadequate switching strategies
- Unavailability of sufficient remote cranking power
- Creation of inadequate subsystems to be restored in parallel
- Lack of interconnection assistance
- Pickup of large blocks of loads
- Excessive standing phase angle differences

1.5.4. Introduction of Graph Theory

This section introduces the mathematical tool used in this thesis to determine ICI strategies for blackout prevention and system sectionalising strategies for PPSR. Appendix A significantly extends the graph theory concepts and provides a much broader review of the graph theoretic techniques used in this thesis.

Graph theory is a powerful tool for mathematically representing complex systems through a graph that allows a number of well-established and powerful techniques to be used [104-106]. The first paper in the field of graph theory is commonly attributed to Euler, and it dates to 1736, when the paper on the *Seven Bridges of Königsberg* problem was published [104]. The problem is to find a walk through the city of Königsberg (see Figure 1.6) that would cross each bridge exactly once. Euler showed that the problem has no solution, as he noted that if every bridge is traversed exactly once then the number of bridges touching each land mass must be even (except possibly for the land masses chosen for the start and finish). By noting that all four land masses in Figure 1.6 are touched by an odd number of bridges and since at most two land masses can serve as the endpoints of a walk, the existence of a walk traversing each bridge exactly once leads to a contradiction. Euler's

solution of the *Seven Bridges of Königsberg* problem laid the foundations of graph theory and led to the concept of Eulerian graphs [106].

Graph theory can be used to study and solve many mathematical problems in major fields such as computer programming and networking, economics, communications and electrical engineering [105]. Graphs have become a convenient, practical and efficient tool to model power system problems [107], particularly when analysing large amount of data.

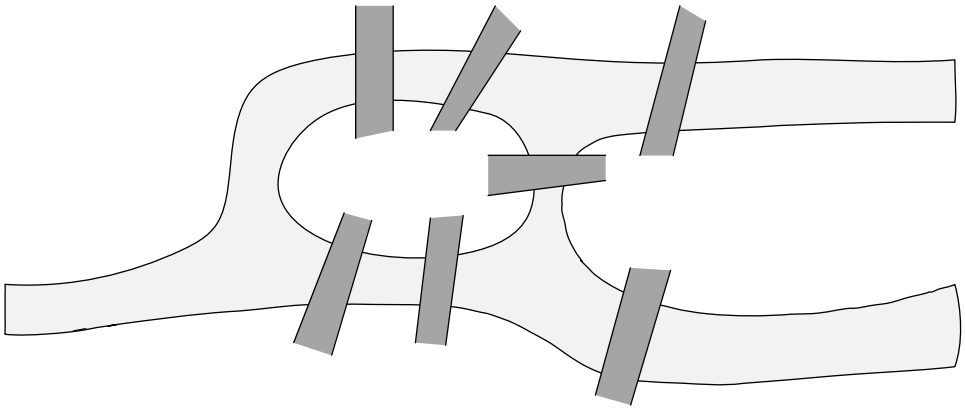

Figure 1.6: Layout of the seven bridges, highlighting the river Pregel and the bridges

In the graph representation of a power system, only connections, certain levels of strength (power flows, dynamic coupling or electrical distance) through those connections, and information of the system buses (power injection, inertia constant of the generator at the bus) are required [107]. No other information, such as type of generators, type of loads, transformer connections, presence of FACTS devices or the voltage level of a bus, is necessary. Therefore, it is more convenient and less complex to analyse the highly simplified graph representation of a power system than it is to directly analyse a complete power system [52, 107]. The opportunity to omit non-relevant information from the graph representation is one of the attractive characteristics of employing graph theory.

Graph theoretic techniques are used in this thesis to determine ICI strategies for blackout prevention and sectionalising strategies for faster PPSR. Algorithms based on graph theory are also used to optimally place monitoring equipment that can be used to gather real-time information during cascading outages and during the resynchronisation of the islands. In particular, *normalised spectral graph clustering*, which uses the eigenvalues and

eigenvectors of a matrix associated with the graph and improves the quality of the results compared to the classical *spectral graph clustering*, is used in this thesis to find islanding solutions and system sectionalising strategies due to its computational efficiency and efficacy to partition graphs [71]. Furthermore, the concept of *cutset matrix* [106], which represents multiple cutsets to partition graphs, is also used in this thesis to find islanding solutions and system sectionalising strategies due to its possibility to explore the vast combinatorial space to always find the optimal partition. Finally, this thesis uses the concept of a *dominating set* and *tree search* algorithms to optimally place PMUs due to their efficacy on searching solutions in graphs.

1.6. Research Aims and Objectives

The main aims of this thesis are to develop graph theory based methodologies that minimise the impact of large-area power system blackouts through adaptive corrective Intentional Controlled Islanding (ICI) schemes and to reduce the duration of these catastrophic events through system sectionalising strategies for Parallel Power System Restoration (PPSR).

Therefore, the research objectives of this thesis are as follows:

- To summarise and thoroughly examine existing ICI and system sectionalising methods for blackout prevention and PPSR, respectively.
- To develop methodologies to improve existing ICI approaches for minimal dynamic coupling and minimal power flow disruption.
- To develop a new ICI methodology for minimal power imbalance.
- To develop systematic methodologies for determining system sectionalising strategies for PPSR.
- To test and validate the proposed methodologies according to their computational efficiency and accuracy.

1.7.Main Contributions of the Thesis

The work within this thesis contributes to a number of technical areas of power systems research, particularly those linked to the question of how to create power system islands for blackout prevention and how to sectionalise a network affected by a complete blackout to support parallel restoration.

The contributions achieved and presented in this thesis are listed below.

- **A new methodology for determining islanding solutions for minimal dynamic coupling.**

  A new methodology based on normalised spectral clustering is developed to determine the absolute weakest connections between dynamically coherent groups of generators, i.e., islanding solutions for minimal dynamic coupling. In contrast to the previous approach [56], the new methodology proposed in this thesis uses normalised spectral clustering, considers the dynamic coupling between all the generators and all the load buses within each coherent group, and avoids implementation of computationally demanding algorithms, such as Gaussian elimination with complete pivoting. These characteristics significantly improve the computational efficiency and the accuracy of the proposed methodology compared to the existing islanding approach [56].

- **Determination of the areas in the network where islanding solutions are more likely to occur based on the assessment of the dynamic coupling between the system buses.**

  A new methodology that extends the concept of weak connections to determine the areas in the power system (the so-called *weak areas*) that contain multiple weak connections between strong dynamically connected areas is introduced. The weak areas comprise several weak connections between the dynamically coherent groups of generators, and represent the areas where islanding is more likely to occur based on the dynamic coupling between the system buses. The determination of the weak areas can benefit the controlled islanding, as these areas can be used to reduce the search space for ICI methodologies while preserving the expected level of accuracy.

- **A new methodology for optimal placement of PMUs across the weak areas to monitor the electrical variables during the determination of islanding solutions and during the resynchronisation of the islands.**

  Two graph theory based algorithms – the concept of a dominating set and a tree search algorithm – are implemented in this thesis to optimally place PMUs across the weak areas. This analysis allows ensuring that the electrical variables (voltage magnitudes, voltage phase angles and power flows) across the weak areas (the areas where islanding is more likely to occur) are monitored for the purpose of ICI for blackout prevention and the resynchronisation of the islands during PPSR.

- **A new methodology for determining islanding solutions for minimal power imbalance.**

  A methodology based on constrained cutset matrix is developed to determine islanding solutions for minimal power imbalance, while ensuring that each island contains only coherent generators. In contrast to the existing OBDD-based methods [44-46], the methodology proposed in this thesis can also constrain branches to be excluded from the solution space. This is important to exclude branches that are deemed to be unsuitable for islanding, e.g., transformer. Furthermore, it uses the constrained cutset matrix and the previously identified weak areas, avoiding thus the search for islanding solutions in the vast search space. This feature significantly improves the computational efficiency of the new methodology while maintaining the accuracy of the results compared to the existing OBDD-based methods [44-46].

- **A new methodology for determining islanding solutions for minimal power flow disruption.**

  A methodology based on normalised and constrained spectral clustering is developed to determine islanding solutions for minimal power flow disruption, while ensuring that each island contains only coherent generators. In contrast to the existing islanding approach [49], the methodology proposed in this thesis can also constrain branches to be excluded from the solution space. Furthermore, it uses normalised spectral clustering, and this approach improves the quality of the islanding solutions compared to the existing ICI approach [49]. The new

methodology solves the associated eigenproblem only once, even if multiple islands are required, avoiding thus recursive bisection. This feature significantly accelerates the determination of an islanding solution and simultaneously improves its quality. It also reduces the order of a similarity matrix and avoids the use of iterative approaches, which help accelerate the determination of an islanding solution.

- **New systematic methodologies for determining sectionalising strategies for parallel power system restoration following a complete system blackout.**

  Two systematic methodologies are developed to determine system sectionalising strategies for PPSR. These methodologies could benefit PPSR as they provide guidance to operators during the preparation stage of PPSR on how the blackout area can be sectionalised into multiple islands that satisfy PPSR constraints. The first methodology uses the concept of a constrained cutset matrix, and provides a list of feasible sectionalising strategies that can ultimately be used by system operators to define, based upon their knowledge and experience, the islands that will be restored in parallel. This approach could benefit the PPSR as system operators have multiple options to sectionalise the blackout area and independently restore the islands in parallel. Likewise, the second methodology uses the concept of electrical cohesiveness, as expressed by the electrical distances between buses, and formulates the sectionalising strategy problem to create islands that, in addition to satisfying multiple PPSR constraints, have strong internal connections, taking the electrical distance into account, and weak external connections. This second approach could benefit PPSR as the number of tie-lines between islands is reduced, whilst simultaneously increasing the number of internal connections. It also sectionalises the system across electrically long and weak transmission lines, helping to reduce the effects of high charging currents, high overvoltages, and other voltage related issues that may arise when reconnecting these long and unloaded lines.

A full list of international journal and conference publications is included in Appendix E at the end of the thesis.

1.8. Thesis Overview

This thesis consists of eight chapters in total. The seven chapters which follow this introduction are outlined below:

Chapter 2 – Intentional Controlled Islanding for Minimal Dynamic Coupling: A Spectral Clustering-Based Methodology

Chapter 2 presents an improved methodology that can determine islanding solutions for minimal dynamic coupling. The chapter initially reviews the dynamic modelling of the power system and the classical slow coherency theory. It then introduces a normalised spectral clustering-based methodology to identify coherent groups of generators. When the coherent groups of generators are identified, the improved methodology to determine the absolute weakest connections between strong dynamically connected buses is presented.

Chapter 3 – Weak Areas Determination and Optimal PMU Placement

Chapter 3 extends the concept of weak connections, and introduces the notion of weak areas. The weak areas are defined as the zones across the power system, and between the coherent groups of generators, where, based on the dynamic coupling between the system buses, islanding solutions are more likely to be found. The identified weak areas are used to optimally place PMUs based on two different graph theoretic techniques. The proposed PMU placement could potentially be used to monitor bus voltages, power flows and frequency for the purpose of ICI and resynchronisation of the systems after the controlled separation or after parallel restoration.

Chapter 4 – Intentional Controlled Islanding for Minimal Power Imbalance: A Constrained Cutset Matrix-Based Methodology

Chapter 4 presents a very efficient methodology that can determine islanding solutions for minimal power imbalance, while ensuring that each island contains only coherent generators. The proposed methodology is based on the concept of cutset matrix, and it explores the vast combinatorial space to find the optimal solution. In order to reduce this search space, and improve thus the efficiency of the new methodology, the previously determined weak areas are used. Hence, strong dynamically connected islands with reduced power imbalance are ultimately created.

Chapter 5 – Intentional Controlled Islanding for Minimal Power Flow Disruption in Large-Scale Power System: A Constrained Spectral Clustering-Based Methodology

Chapter 5 introduces a novel constrained spectral clustering-based methodology that is computationally more efficient than previous approaches, and can directly determine an islanding solution for minimal power flow disruption for any given number of islands while ensuring that each island contains only coherent generators. The proposed methodology also enables operators to constrain any branch to be excluded from the solution.

Chapter 6 – Sectionalising Strategies for Parallel Power System Restoration: A Constrained Cutset Matrix-Based Methodology

Chapter 6 introduces a methodology that can determine system sectionalising strategies for PPSR. The proposed methodology uses the concept of constrained cutset matrix, and creates islands that satisfy multiple PPSR constraints, enabling system operators to restore the created islands in parallel, and accelerate the overall restoration process.

Chapter 7 – Sectionalising Strategies for Parallel Power System Restoration: A Constrained Spectral Clustering-Based Methodology

Chapter 7 presents a novel methodology based on spectral clustering that can determine sectionalising strategies for PPSR, taking into account the physical and inherent properties of the power system. The methodology uses the concept of electrical cohesiveness, as expressed by electrical distance between buses, to create islands that, in addition to satisfy multiple PPSR, are highly connected among themselves – taking the electrical distance into account – but weakly connected to buses in other islands. The methodology also seeks to create suitable islands that would facilitate the parallel restoration.

Chapter 8 – Conclusions and Future Work

Chapter 8 summarises the conclusions drawn from this research project, discusses the applicability of the proposed methodologies, and suggests areas of further research.

Chapter 2. Intentional Controlled Islanding for Minimal Dynamic Coupling: A Spectral Clustering-Based Methodology

Chapter 2 initially describes the dynamic model of the system that is used for the study of islanding and reviews the classical slow coherency theory that has been used in the past to study generator coherency. It then proposes a methodology for identifying dynamically coherent groups of generators in interconnected power systems that is based on normalised spectral clustering and is computationally more efficient than conventional methods. Finally, this chapter introduces a new effective methodology that also uses normalised spectral clustering and can determine islanding solutions for minimal dynamic coupling.

The determination of islanding solutions for minimal dynamic coupling considerably enhances the transient stability of the future islands. Thus, the probability that the generators in each island will remain in synchronism after a disturbance is significantly increased. The advantage of the proposed methodology is that it requires less computational time than the conventional islanding methods and improves the level of accuracy.

2.1. Dynamic Modelling of a Power System

The dynamic time constants of power systems range from microseconds – electromagnetic phenomena – to hours – thermal phenomena [5]. The time constants of interest in Intentional Controlled Islanding (ICI) correspond to a small window, usually on the order of few seconds [41, 49, 50]. This enables the synchronous generators of a system to be modelled using the classical model of the generators, where only the motion of the rotor is considered [5]. This motion can be described using the swing equation as follows [5]:

$$\frac{2H}{\omega_0}\frac{d^2\delta_m}{dt^2} = P_m - P_e \tag{2.1}$$

where H is the inertia constant of the generator, ω_0 is the nominal system frequency, δ is the rotor angle of the machine, P_m is the mechanical power and P_e is the electrical power.

Then, the dynamic behaviour – the dynamic coupling between buses – of the entire power system during the time period considered in ICI can be described by a system of nonlinear differential and algebraic equations as follows [5]:

$$\mathbf{M_I}\ddot{\boldsymbol{\delta}} = \mathbf{f}\left(\boldsymbol{\delta}, \mathbf{V}\right) \tag{2.2}$$

$$0 = \mathbf{g}\left(\boldsymbol{\delta}, \mathbf{V}\right) \tag{2.3}$$

where $\mathbf{M_I}$ is an $m \times m$ diagonal matrix involving the machine inertia constants, $\boldsymbol{\delta}$ is an m-state vector of machine angles and $\mathbf{V} = \begin{bmatrix}\boldsymbol{\theta} & \mathbf{v}\end{bmatrix}^T$ is a $2n$-vector of bus voltage angles and magnitudes. Furthermore, the m-vector $\mathbf{f}$ is a vector of acceleration torques and $\mathbf{g}$ is the load flow function of the power network [5].

The nonlinear system (2.2)-(2.3) can be linearised about a given operating point $\boldsymbol{\delta_0}$, $\mathbf{V_0} = \begin{bmatrix}\boldsymbol{\theta_0}, \mathbf{v_0}\end{bmatrix}$ to obtain the following augmented system state equation,

$$\Delta\ddot{\boldsymbol{\delta}} = \left.\frac{\partial \mathbf{f}\left(\boldsymbol{\delta}, \mathbf{V}\right)}{\partial \boldsymbol{\delta}}\right|_{\boldsymbol{\delta}_0, \mathbf{V}_0} \Delta\boldsymbol{\delta} + \left.\frac{\partial \mathbf{f}\left(\boldsymbol{\delta}, \mathbf{V}\right)}{\partial \mathbf{V}}\right|_{\boldsymbol{\delta}_0, \mathbf{V}_0} \Delta\mathbf{V} = \mathbf{J_A}\Delta\boldsymbol{\delta} + \mathbf{J_B}\Delta\mathbf{V} \tag{2.4}$$

$$0 = \left.\frac{\partial \mathbf{g}\left(\boldsymbol{\delta}, \mathbf{V}\right)}{\partial \boldsymbol{\delta}}\right|_{\boldsymbol{\delta}_0, \mathbf{V}_0} \Delta\boldsymbol{\delta} + \left.\frac{\partial g\left(\boldsymbol{\delta}, \mathbf{V}\right)}{\partial \mathbf{V}}\right|_{\boldsymbol{\delta}_0, \mathbf{V}_0} \Delta\mathbf{V} = \mathbf{J_C}\Delta\boldsymbol{\delta} + \mathbf{J_D}\Delta\mathbf{V} \tag{2.5}$$

where, $\boldsymbol{\Delta\delta}$ is an m-vector of machine angle deviations from $\boldsymbol{\delta_0}$, and $\Delta\mathbf{V} = \begin{bmatrix}\Delta\boldsymbol{\theta} & \Delta\mathbf{v}\end{bmatrix}^T$ is a $2n$-vector of the bus voltage angle and magnitude deviations from $\mathbf{V_0}$. Moreover, the matrices $\mathbf{J_A}$, $\mathbf{J_B}$, $\mathbf{J_C}$ and $\mathbf{J_D}$ are *Jacobian* matrices comprised of the partial derivatives of the terms in equations (2.2)-(2.3). The linearised system (2.4)-(2.5) can also be expressed in the matrix form as follows:

$$\begin{bmatrix} \Delta\ddot{\boldsymbol{\delta}} \\ 0 \end{bmatrix} = \begin{bmatrix} \mathbf{J_A} & \mathbf{J_B} \\ \mathbf{J_C} & \mathbf{J_D} \end{bmatrix} \begin{bmatrix} \Delta\boldsymbol{\delta} \\ \Delta\mathbf{V} \end{bmatrix}. \tag{2.6}$$

This system can be reduced to derive the system state matrix $\bar{\mathbf{A}}$ as follows:

$$\bar{\mathbf{A}} = \mathbf{J_A} - \mathbf{J_B}\mathbf{J_D}^{-1}\mathbf{J_C} \tag{2.7}$$

where it is considered that the matrix $\mathbf{J_D}$ is invertible. The matrix $\mathbf{J_B}\mathbf{J_D}^{-1}\mathbf{J_C}$ is commonly referred to as a *degradation matrix*, as it degrades the stability of the matrix $\mathbf{J_A}$ [5]. The system state matrix $\bar{\mathbf{A}}$ can be used to define the linearised second-order dynamic model of an *m*-generator power system as follows.

$$\Delta\ddot{\boldsymbol{\delta}} = \bar{\mathbf{A}}\Delta\boldsymbol{\delta} \tag{2.8}$$

The dynamic modelling presented above is used in this chapter to identify dynamically coherent groups of generators and to create dynamically coherent areas. This model describes the inter-area modes in the power system [53]. Hence, it can effectively be used to identify the slowly coherent groups of generators in the network [5]. Additionally, it does not require analysing the dynamic behaviour of the power system following severe disturbances, which can serve to accelerate the determination of islanding solutions [50, 52]. Nevertheless, the system operating conditions and network configuration are constantly changing. Additionally, the accuracy of the system parameters (inertia constants, impedances and load levels) influences the efficacy of model-based techniques [27, 32]. Therefore, the linearised model described by (2.8) may result in slightly different groups of generators in complex future systems with high spatial variety in generation locations due to the proliferation of renewable energy resources installations.

2.1.1. Underlying Assumptions of the Dynamic Modelling

The following assumptions are made during the dynamic modelling presented above:

- Generators are represented by the classical 2nd order model given by (2.1), i.e., a constant internal voltage behind a constant transient reactance and the inertia constant.

- The losses in transmission lines are neglected.

- Loads are modelled as constant impedance loads.

While the first two assumptions would not affect the coherency results presented in this thesis, as the level of modelling given to the generators would not change the coherent groups [5], and the consideration of the resistance would not change the dynamic coupling between system buses, the modelling of the loads may cause weak machines between strong connected generators to switch from one group to another [50, 53, 60].

2.2. Coherent Generators and Slow Coherency Theory

A group of generators is referred to as coherent if their rotor angles oscillate coherently following a disturbance [1, 5, 6]. Slow coherency theory – originally used to develop dynamic equivalents for transient stability studies [65-67] and previously used to identify coherent groups of generators for ICI [50-52, 60] – is an effective way of identifying dynamically coherent groups of generators in large-interconnected power systems [50, 52].

In order to determine coherent groups, slow coherency theory assumes that [50, 53, 60]:

i. the coherent groups of generators are almost independent of the size of the disturbance; and

ii. the coherent groups are independent of the level of detail used when modelling the generators.

Assumption (i) is based on the observation that the coherency behaviour of the generators is not significantly affected by the clearing time of a specific disturbance [53, 60]. Moreover, assumption (ii) is based on the consideration that the inter-area modes do not radically change when the level of detail is increased [53]. Therefore, the linearised model (2.8) of

the dynamic power system is commonly employed when using slow coherency theory to identify the coherent groups of generators in large-interconnected power systems.

Slow coherency theory shows that partitioning a dynamic power system according to the *r* slowest modes of the system state matrix $\bar{\mathbf{A}}$ (2.7) will produce *r* groups of slowly coherent generators [60]. Furthermore, it details how generators in large-interconnected power systems with strong dynamic coupling will swing together after a disturbance, whereas generators with weak dynamic coupling will swing against one another. These two features are key factors that are used to identify dynamically coherent groups of generators.

In addition, the inherent exposure of the power system to electromechanical oscillations following a major disturbance causes different dynamic speeds (the frequency of the generators are different) in interconnected power systems. These different speeds can be interpreted as the separation in time between dynamically slow generators. A similar conclusion can be drawn from observing the motion of the centre of angle associated with each area, which is much slower than the "synchronizing" oscillations between any two machines in the same area [53].

The oscillations between generators and the frequency differences between these can be physically interpreted as strong connections between machines in the same area, and weak connections between machines in different areas [60]. Thus, machines within the same coherent group will commonly only interact in the short-term (few seconds) and when these fast dynamics have decayed it is expected that the they will move coherently; in other words, the rotor angle difference between any two machines in the same group decreases in the long-term (several seconds or even minutes) [5]. These physical properties are used to determine islanding solutions with minimal dynamic coupling.

2.3. Coherency Identification: A Normalised Spectral Clustering-Based Methodology

The dynamic behaviour of the interconnected power system described by the augmented system state matrix given by (2.6) is studied in this section from a graph theoretic point of

view, i.e., using graphs. This section proposes a methodology based on normalised spectral clustering that can identify dynamically coherent groups of generators. In this thesis, the coherency identification is focused solely upon the scenario of unstable electromechanical oscillations that are not accompanied by voltage instability.

2.3.1. Dynamic Graph Representation of the Dynamic Power System

The dynamic behaviour of a power system with *n* buses and *m* generators is initially represented in this chapter as an undirected graph. This graph will be called the *dynamic graph*, as it seeks to represent the dynamic interaction between electrical buses and the inertia constants of the generators modelled by the augmented system state equation (2.6).

The proposed dynamic graph is defined as follows:

$$G_D = \left(V_D, E_D\right) \tag{2.9}$$

where,

- the elements $v_i \in V_D$, $i = 1,\ldots,n+m$, denote the nodes of the dynamic graph, and they represent the buses of the extended power system. In the following discussion, the load buses and the terminal generator buses of the extended power system are all referred to as load buses. These load buses are distinguished from the internal generator buses by separating the node set V_D into two node subsets $V_{DGN} \subset V_D$, which represents the *m* internal generator buses, and $V_{DLD} = V_D \setminus V_{DGN}$, which represents the *n* load buses. In this chapter, the elements $v_{Gi} \in V_{DGN}$ and $v_{Li} \in V_{DLD}$ are referred to as internal- and load-nodes, respectively.

- the elements $e_{ij} \in E_D$, $i, j = 1,\ldots,n+m$, denote the edges of the dynamic graph, and they represent the connections between the internal generator buses and the load buses, and the connections between the load buses.

In order to illustrate the graph defined by (2.9), Figure 2.1 shows the dynamic graph of the IEEE 9-bus test system. In this chapter, the black dots represent the *m* internal generator buses modelled by the elements $v_{Gi} \in V_{DGN}$ and the grey dots represent the *n* load buses modelled by the elements $v_{Li} \in V_{DLD}$. The lines shown in Figure 2.1 represent the edges.

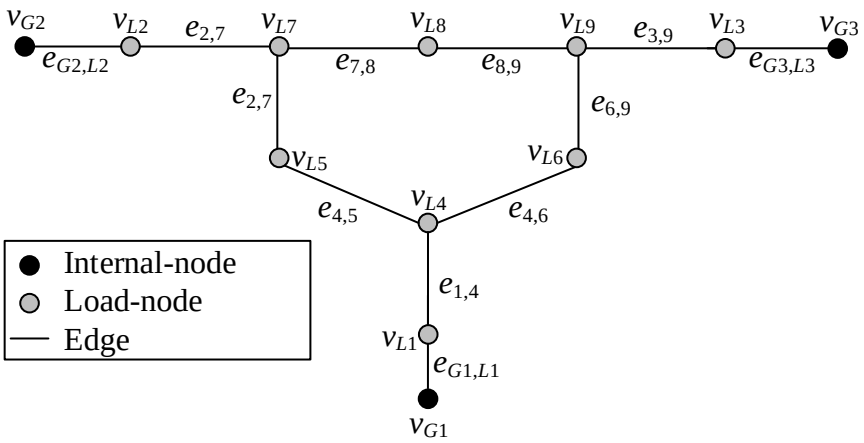

Figure 2.1: Dynamic graph of the IEEE 9-bus test system for coherency identification and islanding for minimal dynamic coupling

2.3.1.1. Kron Reduction of the Dynamic Graph G_D

Kron reduction is a well-known technique used in power systems to eliminate a bus from the network representation when the voltage or the current injection at that bus is zero [108]. *Kron* reduction, in the context of power systems, has been recently studied using graphs in [109]. Given the graph G_D, an associated Laplacian matrix **L**, the set of internal-nodes and the set of load-nodes, the *Kron* reduction of the dynamic graph G_D, with respect to the internal-nodes, is a graph whose Laplacian matrix $\mathbf{L_{RED}}$ is by the *Schur complement* [108] of the original Laplacian matrix **L**, with respect to the set of internal-nodes [109]. The *Kron* reduction of graphs is further explained in Appendix C.

Performing the *Kron* reduction of the dynamic graph reduces the graph G_D, which represents the extended power system, to a smaller graph that represents only the set of internal-nodes [109]. The new graph will then model the dynamic behaviour of the extended power system reduced to only the internal generator buses [109]. Henceforth, the new graph with Laplacian matrix $\mathbf{L_{RED}}$ that is obtained after the *Kron* reduction is referred

to as the reduced dynamic graph. In transient stability studies, this technique is the well-known reduction of the extended power system to the internal generator buses [108].

In principle, the full dynamic graph can be used to represent the augmented admittance matrix $\mathbf{Y_{FULL}}$ of the extended power system [109]. As detailed in Appendix A.6.3.1, the augmented admittance matrix $\mathbf{Y_{FULL}}$ is equal to the unnormalised Laplacian matrix **L** (A.27) of the dynamic graph, when the weight factors associated with the edges $e_{ij} \in E_D$ represent the line admittance (including the effect of the generators' transient reactance $x_d^{'}$) between the applicable buses [108].

After performing the *Kron* reduction of the dynamic graph G_D, with respect to the internal-nodes, the *reduced dynamic graph* given by (2.10) is obtained.

$$G_{DGN} = \left(V_{DGN}, E_{DGN}\right) \tag{2.10}$$

In (2.10):

- the elements $v_{Gi} \in V_{DGN}$, $i = 1,\ldots,m$, denote the nodes of the reduced dynamic graph and they represent the power system when it is reduced to only the internal generator buses; and
- the elements $e_{ij} \in E_{DGN}$, $i, j = 1,\ldots,m$, denote the edges of the reduced dynamic graph and they represent the connections between the internal generator buses.

As mentioned above, the reduced dynamic graph G_{DGN} can be seen as a reduction of the power system to the internal generator buses. The reduced dynamic graph given by (2.10) is by definition a simple and complete graph with m nodes and $m\left(m+1\right)/2$ edges [108, 109]. Hence, each internal-node $v_{Gi} \in V_{DGN}$ in the graph G_{DGN} is connected to each of the other internal-nodes $v_{Gj} \in V_{DGN}$, with $i \neq j$, by only one edge $e_{ij} \in E_{DGN}$.

When performing the *Kron* reduction of the dynamic graph G_D, whose Laplacian matrix **L** is equal to the full admittance matrix $\mathbf{Y_{FULL}}$ with respect to the internal-nodes, the new edge

weights would correspond to the admittances between the machines [108]. In other words, the *ij*-th entry of the reduced Laplacian matrix $\mathbf{L_{RED}}$ that is associated with the reduced dynamic graph will be the admittance Y_{ij} between the internal generators buses *i* and *j*.

In order to illustrate the previous concepts, Figure 2.2 shows the reduced dynamic graph of the IEEE 9-bus test system. It can be seen that the reduced dynamic graph is simple and complete. Furthermore, since this network has three generators [110], the reduced dynamic graph consists of three nodes and, in this case, three edges. Figure 2.2 also presents the susceptance b_{ij} between the internal generator buses *i* and *j*. Remark that only the susceptance matrix **B** is used in this chapter. As previously mentioned, these values can be obtained by computing the *Schur complement* [108] of the matrix $\mathbf{L} = \mathbf{B_{FULL}} = \text{Im}(\mathbf{Y_{FULL}})$.

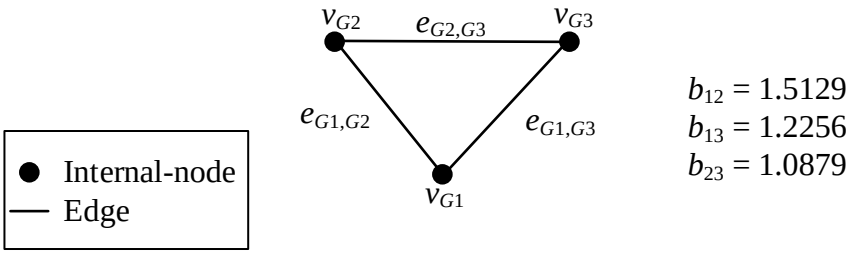

Figure 2.2: Reduced dynamic graph of the IEEE 9-bus test system for coherency identification

In order to represent the inertia constant of the generators and the dynamic coupling between them, node weights and edge weights are now defined for the reduced dynamic graph G_{DGN}. These node and edge weights seek to represent the functional information of the extended power system reduced to only the internal generation buses. Therefore, the reduced dynamic graph (2.10) can be augmented with node and edge weights to form the reduced dynamic graph described as follows:

$$G_{DGN} = \left(V_{DGN}, E_{DGN}, \sigma_{DGN}, \rho_{DGN}\right) \tag{2.11}$$

where,

- the values $u_i = \sigma_{DGN}(v_{Gi})$, $i = 1,\ldots,m$, are the weight factors associated with the nodes of G_{DGN}. Each value u_i is given by (2.12) and involves the inertia constant of the generator connected at bus *i* (H_i) and the nominal system frequency (ω_0).

$$u_i = \begin{cases} 2H_i/\omega_0 & \text{if } v_i \in V_{DGN}; \\ 0 & \text{otherwise.} \end{cases} \tag{2.12}$$

- the values $w_{ij} = \rho_{DGN}(e_{ij})$, $i, j = 1,\ldots,m$, are the weight factors associated with the edges of G_{DGN}. Each value w_{ij} is given by (2.13) and represents the synchronising coefficient $\partial P_{ij}/\partial \delta_{ij}$ between the internal generator buses *i* and *j*.

$$w_{ij} = w_{ji} = \begin{cases} \partial P_{ij}/\partial \delta_{ij} = \left|\tilde{V}_i\right|\left|\tilde{V}_j\right| b_{ij} \cos\left(\delta_i - \delta_j\right) & \text{if } e_{ij} \in E_{DGN}; \\ 0 & \text{otherwise.} \end{cases} \tag{2.13}$$

In (2.13), $\left|\tilde{V}_i\right|$ and $\left|\tilde{V}_j\right|$ are the bus voltage magnitudes at the internal generator buses *i* and *j*, respectively; b_{ij} is the imaginary component of the *ij*-th entry of the reduced admittance matrix $\mathbf{Y_{RED}} = \mathbf{L_{RED}}$; and δ_i and δ_j are the rotor angle at the internal generator buses *i* and *j*, respectively. The resistance is neglected in (2.13) as the resistance R_{ij} is generally much smaller than the reactance X_{ij} [5]. It should be noted that the edge weights defined in (2.13) take into account the admittances b_{ij} included in $\mathbf{L_{RED}}$.

As noticed, the weight factors associated with G_{DGN} seek to represent the dynamic properties – the inertia constant of the generators and the synchronising coefficients between machines – of the power system reduced to only the internal generator buses. Figure 2.3 presents the node weights and the edge weights of the reduced dynamic graph G_{DGN} of the IEEE 9-bus test system. This graph representation is equivalent to the graph shown in Figure A.3(c). These node weights and edge weights are used in Section 2.3.5.1 to identify the coherent groups of generators in this test network.

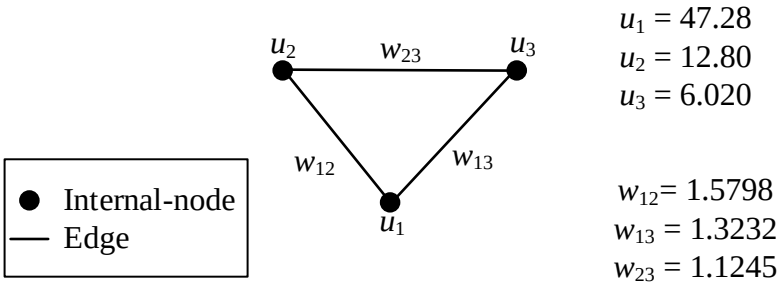

Figure 2.3: Reduced dynamic graph of the IEEE 9-bus test system and weight factors associated with the nodes and edges for coherency identification

The use of the reduced dynamic graph G_{DGN} with these node and edge weights enables the defition of the *graph theoretic system state matrix*. The graph theoretic system state matrix seeks to represent the classical power system state matrix $\bar{\mathbf{A}}$. Hence, it aims to model the dynamic behaviour of the power system when it is reduced to only the internal generator buses and each generator is modelled using a classical 2nd order generator model.

In this thesis, the graph theoretic system state matrix of the reduced dynamic graph G_{DGN} is denoted as $\mathbf{L_N}$ and is computed as follows:

$$\mathbf{L_N} = \left[\mathbf{M_G}\right]^{-1}\mathbf{L_{DGN}} \tag{2.14}$$

where,

$$\left[\mathbf{M_G}\right]_{ii} = diag\left(u_1, u_2, ..., u_m\right) \tag{2.15}$$

and

$$\left[\mathbf{L_{DGN}}\right]_{ij} = \begin{cases} 1 & \text{if } i = j; \\ -w_{ij}\Big/\sqrt{d_i d_j} & \text{if } i \neq j \text{ and } e_{ij} \in E_{DGN}; \\ 0 & \text{otherwise.} \end{cases} \tag{2.16}$$

In (2.16), d_i is the weighted degree of the node $v_{Gi} \in V_{DGN}$ and its value is calculated using (A.4) with respect to the edge weights given by (2.13). Since the reduced dynamic graph

G_{DGN} is by definition a complete graph, the *ij*-th entry of $\mathbf{L_{DGN}}$ is non-zero. Moreover, it should be noted that $\mathbf{L_{DGN}}$ is the normalised Laplacian matrix associated with the reduced dynamic graph (2.11). Hence, it is symmetrical and its first eigenvalue is by definition zero [71]. Additionally, the diagonal matrix $\mathbf{M_G}$ in (2.14) normalises the *ij*-th entry of $\mathbf{L_{DGN}}$ with respect to the term $\mathbf{M_G}$ (*i*, *i*) that involves the inertia constants of the generators and serves as a balancing matrix. Since $\mathbf{L_{DGN}}$ is a normalised Laplacian matrix, the matrix $\mathbf{L_N}$ (2.14) satisfies the properties of the normalised Laplacian matrices described in Appendix A.7.2.4. Thus, the first eigenvalue of $\mathbf{L_N}$ is zero, and the associated eigenvector is equal to $\boldsymbol{\psi}_1 = \left[\sqrt{d_1},\ldots,\sqrt{d_m}\right]$. The matrix $\mathbf{L_N}$ is used as part of the proposed methodology to identify the dynamically coherent groups of generators.

The proposed approach uses the dynamic graph G_D (2.9) of the extended power system to determine the reduced dynamic graph G_{DGN} (2.11) by performing the *Kron* reduction of G_D with respect to the internal-nodes [109]. Using the dynamic graph of the power system extended to the internal generator buses enables a more realistic modelling of the dynamic network to be achieved. It also allows the study of the dynamic properties of the system, and the determination of islanding solutions for minimal dynamic coupling, as explained in Section 2.4. Finally, this section has shown the mathematical justification (*Kron* reduction) of why the reduced dynamic graph can be used to find the coherent groups of generators.

2.3.2. Definition of Graph Theoretic Concepts

The normalised spectral clustering-based methodology uses the following graph theoretic concepts to identify the dynamically coherent groups of generators.

2.3.2.1. Cutset and Cut

The cutset $E_S \subset E_{DGN}$ is the set of edges that must be removed to split the reduced dynamic graph into *r* disjoint dynamic subgraphs $G_{DGN1},\ldots,G_{DGNr}$, with node sets $V_{DGN1},\ldots,V_{DGNr}$. The value of *r* is the number of coherent groups of generators to be identified, and each node set V_{DGNk}, $k = 1,\ldots,r$, represents a coherent group. The cut associated with the cutset E_S is the sum of the weight factors associated with the edges in E_S and can be calculated

using (A.8) with respect to the edge weights given by (2.13). The cut physically represents the total dynamic coupling between each of the coherent groups of generators.

2.3.2.2. Weight of the Dynamic Subgraph

The weight of the subgraph G_{DGNk} with node set V_{DGNk}, denoted by $wei\,(V_{DGNk})$, is the sum of the node weights included in the subset V_{DGNk} and can be calculated using (A.7) with respect to the node weights given by (2.12). The weight of a dynamic subgraph physically represents the total inertia constant within each of the coherent groups of generators.

2.3.2.3. Quality of a Cutset

The quality of the coherency identification can be measured using the ratios between the boundary (cut) (A.5) and the weight (A.7) of each of the clusters. In this application, the boundary of the cluster V_{DGNk}, denoted by $cut\left(V_{DGNk}, \bar{V}_{DGNk}\right)$, physically corresponds to the dynamic coupling between the machines that are represented by the nodes $v_{Gi} \in V_{DGNk}$ and the other machines. Furthermore, the weight of a node set, denoted by $wei\,(V_{DGNk})$, physically represents the total inertia constant within the corresponding island.

The quality of the node set V_{DGNk}, $k = 1,\ldots,r$, is measured as follows.

$$\eta\left(V_{DGNk}\right) = 1 - \frac{cut\left(V_{DGNk}, \bar{V}_{DGNk}\right)}{wei\left(V_{DGNk}\right)} \tag{2.17}$$

In (2.17), the expansion of the node set V_{DGNk} is $\phi\left(V_{DGNk}\right) = cut\left(V_{DGNk}, \bar{V}_{DGNk}\right) \big/ wei\left(V_{DGNk}\right)$ and measures the size of the cut relative to the weight of the coherent group. The quality index given by (2.17) can be physically interpreted as a quantity that compares the dynamic coupling between machines – expressed by the synchronising coefficients – and the total inertia constant within the islands. Indeed, the greater the value of $\eta\left(V_{DGNk}\right)$ – the lower the dynamic coupling will be between the machines in the separated groups and the larger the total inertia of each group will be – the better the coherent groups of generators are considered to be in terms of clustering.

The methodology will then evaluate the quality of the coherency solution using the quality index $\eta(V_{DGNk})$ of the cluster with lowest quality, i.e., the quality of the coherency solution is defined as the minimum value of $\eta(V_{DGNk})$ for all k: $\min_{k=1,...,r}\left(\eta(V_{DGNk})\right)$.

As described in Section 2.3.3, finding the maximum of the worst quality – solving (2.18) – will be the objective function of the coherency identification problem.

$$\max_{V_{DGN1},...,V_{DGNr}} \min_{k=1,...,r}\left(\eta(V_{DGNk})\right) \tag{2.18}$$

2.3.3. Formulation of the Coherency Identification Problem

The problem of identifying coherent groups of generators in power systems can be studied by analysing the dynamic coupling between the electrical machines [54]. Given the r partitions $V_{DGN1},\ldots,V_{DGNr}$ of the reduced dynamic graph G_{DGN}, which are defined by the cutset E_S, the dynamic coupling between the r groups of generators is calculated as follows.

$$cut(V_{DGN1},...,V_{DGNr}) = \sum_{e_{ij}\in E_S} w_{ij} \tag{2.19}$$

Then, the problem of identifying the dynamically coherent groups of generators in the system is equivalent to determining the weakest dynamic coupling over the r partitions of the reduced dynamic graph G_{DGN} [54], which is mathematically defined as follows:

$$\min_{V_{DGN1},...,V_{DGNr}} cut(V_{DGN1},\ldots,V_{DGNr}) \tag{2.20}$$

However, the solution to (2.20) may be trivial, as the node with the smallest node degree will likely be partitioned from the main graph [71], as detailed in Appendix A.3.8. For example, the weakest dynamic coupling between the internal-nodes shown in Figure 2.3 is achieved by separating the node v_{G3} from the rest of the graph. Nevertheless, this solution is

not dynamically suitable as the generator represented by the internal-node v_{G1} has a much higher inertia constant than the other generators (Table B.3). Thus, it is expected that generator G1 will be separated from the other generators [110].

In order to reduce the likelihood of obtaining the undesirable solutions that may be produced using the objective function (2.20), this thesis reformulates the objective function and introduces the new objective function defined as follows.

$$\min_{V_{DGN1},\ldots,V_{DGNr}} \max_{k=1,\ldots,r} \left(\frac{cut\left(V_{DGNk}, \bar{V}_{DGNk}\right)}{wei\left(V_{DGNk}\right)} \right) \tag{2.21}$$

This new objective function seeks to minimise the worst (maximum) expansion $\phi\left(V_{DGNk}\right)$ of the subsets. As the expansion and the quality index given by (2.17) of each node set is related $\left(\eta\left(V_{DGNk}\right)=1-\phi\left(V_{DGNk}\right)\right)$, the new objective function given by (2.21) is equivalent to maximising the worst (minimum) quality over the *r* partitions, which is given by (2.18).

Physically, the objective function given by (2.21) seeks to minimise the dynamic coupling between the groups, whilst balancing the total inertia constant within each coherent group of generators. Performing this type of min-max optimization problem for graphs is related to the eigenvalues of the graph Laplacian (see *Normalised Cut* in Appendix A.7.4), and this is the key connection between coherency identification and spectral clustering [71]. The solution to (2.21) returns the *r* coherent groups of generators, which is an essential step for the success of the ICI scheme [42, 47, 49].

2.3.4. Methodology for Solving the Coherency Identification Problem

The coherency identification problem defined by the new objective function (2.21) is solved in this chapter using a normalised spectral clustering algorithm. The proposed methodology initially builds the dynamic graph G_D (2.9). It then performs the *Kron* reduction of the dynamic graph with respect to the internal-nodes to obtain the reduced dynamic graph G_{DGN} (2.11). The node weights (2.12) and the edge weights (2.13) are used

to compute the matrices $\mathbf{M_G}$ (2.15) and $\mathbf{L_{DGN}}$ (2.16), respectively, and the eigenproblem $\mathbf{L_N}\boldsymbol{\psi} = \nu\boldsymbol{\psi}$ is solved to compute the eigenvalues and eigenvectors.

The value of r is then defined. In order to do so, the methodology uses the relative eigengaps of the spectrum (eigenvalues) of the reduced dynamic graph. As explained in Appendix A.7.8, spectral clustering provides a theoretical formulation that suggests, based on the spectrum of the graph, the most suitable number of clusters to be created. In practice, the number of coherent groups of generators to be identified could also be defined using different criteria such as those described in [27], e.g., number of transmission operators. When the value of r is defined, the eigenvectors $\boldsymbol{\psi}_1,\ldots,\boldsymbol{\psi}_r$ associated with the r smallest eigenvalues of $\mathbf{L_N}$ (2.14) are placed as columns to create the matrix $\mathbf{X} \in \mathbb{R}^{m\times r}$ with rows $\mathbf{x}_i$, $i = 1,\ldots,m$. As explained earlier, the vector $\mathbf{x}_i$ represents the coordinates of the internal-node $v_{Gi} \in V_{DGN}$ in an r-dimensional Euclidean space $\mathbb{R}^r$. Thus, they are denoted in $\mathbb{R}^r$ by the data-points $\mathbf{x}_i^{GND}$ (see Figure 2.4 for an example).

The methodology then normalises the vectors $\mathbf{x}_i \in \mathbf{X}$ to compute the normalised vectors $\mathbf{y}_i$, $i = 1,\ldots,m$, that form the rows of the matrix $\mathbf{Y} \in \mathbb{R}^{m\times r}$. The vector $\mathbf{y}_i$ represents the coordinates of the internal-node $v_{Gi} \in V_{DGN}$ on the unit (r–1)-dimensional sphere $\mathbb{S}^{r-1} = \left\{\mathbf{y}_i \in \mathbb{R}^r \text{ such that } \|\mathbf{y}_i\| = 1\right\}$. For consistency, the vector $\mathbf{y}_i$ will be denoted on $\mathbb{S}^{r-1}$ by $\mathbf{y}_i^{GND}$ (see Figure 2.5 for an example). The projection of the vector $\mathbf{x}_i$ on the unit sphere $\mathbb{S}^{r-1}$ improves the quality of the clustering, as detailed in Appendix A.7.9. Furthermore, it enables a visualisation of the clusters to be created (see Figure 2.5 for an example). This could potentially serve to accelerate the identification of coherent groups of generators.

In the coherency results presented in this chapter, the *k-means* algorithm described in Appendix A.7.11 is not required, as the clusters could always be visualised on $\mathbb{S}^{r-1}$. In practical implementations, this iterative algorithm may be needed when the clusters cannot be observed, e.g., when the dimension is higher than three. This algorithm would not significantly affect the computational efficiency of the proposed methodology, as the normalisation of the vectors $\mathbf{x}_i$ naturally tends to create clusters [70, 73], thus reducing the

number of iterations performed by the *k-means* algorithm. It is important to mention that the complexity of the *k-means* algorithm is proportional to the number of iterations [71]. It is important to remember that, in the eventual use of the *k-means* algorithm, the separation between the points in the spectral embedding should be described using the well-known spherical distance, explained in Appendix A.7.10.3, as the points are clustered on $\mathbb{S}^{r-1}$.

The partition of the data-points $\mathbf{y}_i^{GND}$ embedded on the unit sphere $\mathbb{S}^{r-1}$ produces the r sets $V_{DGN1},\ldots,V_{DGNr}$, and each set then represents a dynamically coherent group of generators, as previously mentioned. For example, the sets $V_{DGN1} = \{v_{G1}\}1$ and $V_{DGN2} = \{v_{G2}, v_{G3}\}$ that are visualised in Figure 2.5 indicate that the coherent groups of generators in the case of two islands for the IEEE 9-bus system are {G1} in one island and {G2, G3} in the other island.

2.3.5. Simulation Examples

This section illustrates the proposed methodology for coherency identification using three test networks. The simulation results obtained using the new methodology are compared with those of an implementation of the slow coherency algorithm, which is explained in the Appendix D.1. [53, 56].

2.3.5.1. IEEE 9-Bus Test System

The IEEE 9-bus test system is initially used to illustrate the new methodology. First, the dynamic graph G_D shown in Figure 2.1 is built. Then, the *Kron* reduction of the dynamic graph G_D with respect to the internal-nodes is performed, and the reduced dynamic graph G_{DGN} shown in Figure 2.2 is obtained. The weight factors shown in Figure 2.3 are then used to create the matrices $\mathbf{M_G}$ given by (2.22) and $\mathbf{L_{DGN}}$ given by (2.23). Finally, the matrix $\mathbf{L_N}$ is constructed using (2.14).

$$\mathbf{M_G} = \begin{bmatrix} 47.28 & 0 & 0 \\ 0 & 12.80 & 0 \\ 0 & 0 & 6.02 \end{bmatrix} \tag{2.22}$$

$$\mathbf{L}_{\mathbf{DGN}} = \begin{bmatrix} 1.0000 & -0.5638 & -0.4964 \\ -0.5638 & 1.0000 & -0.4371 \\ -0.4964 & -0.4371 & 1.0000 \end{bmatrix} \tag{2.23}$$

The eigenproblem $\mathbf{L_N}\boldsymbol{\psi} = \nu\boldsymbol{\psi}$ is then solved, and the eigenvalues and eigenvectors are determined. The methodology then determines the suitable number of coherent groups of generators to be created. In the case of the IEEE 9-bus test system, the relative eigengaps between consecutive eigenvalues suggest partitioning the graph G_{DGN} into two groups ($r = 2$). Thus, the matrix $\mathbf{X} = [\boldsymbol{\psi}_1 \quad \boldsymbol{\psi}_2]$ is used to create the spectral embedding of the reduced dynamic graph G_{DGN} in the Euclidean space $\mathbb{R}^2$ that is shown in Figure 2.4.

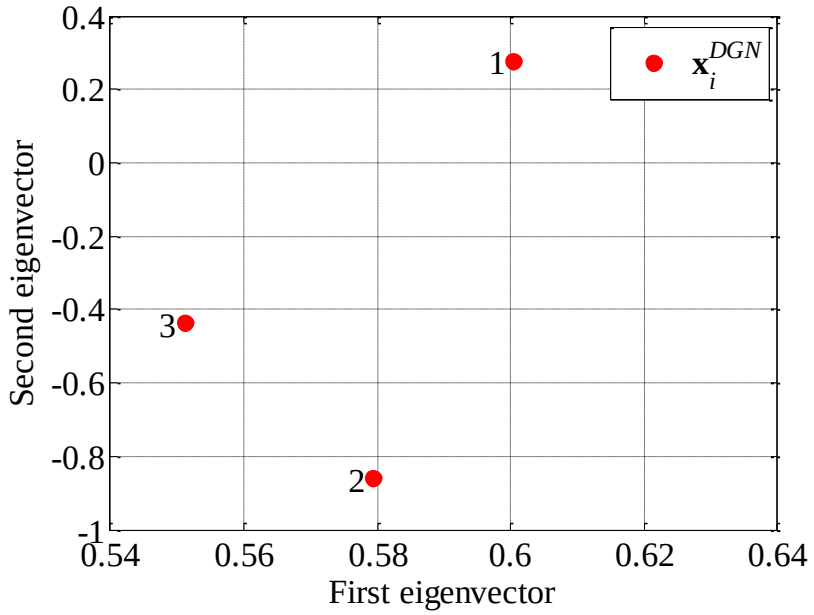

Figure 2.4: Spectral Embedding into $\mathbb{R}^2$ of the reduced dynamic graph of the IEEE 9-bus test system for coherency identification

The vectors $\mathbf{x}_i \in \mathbf{X}$ in $\mathbb{R}^2$, $i = 1,2,3$, are then projected on to the unit circle $\mathbb{S}^1$, and the normalised vectors $\mathbf{y}_i \in \mathbf{Y}$, $i = 1,2,3$, are obtained. Figure 2.5 shows the data-points $\mathbf{y}_i^{DGN}$ and two clusters, identified using any clustering algorithm (e.g., *k-means*), can be seen. The coherent generators groups are represented by the node subsets $V_{DGN1} = \{v_{G1}\}$ and

$V_{DGN2} = \{v_{G2}, v_{G3}\}$. The results obtained were actually expected as the inertia constant of generator G1 is much higher than the inertia constant of the other generators (G2 and G3).

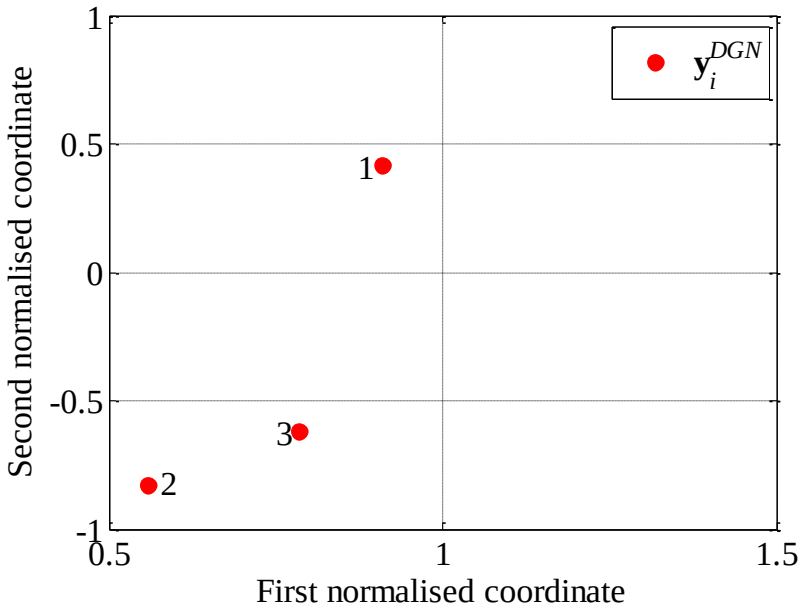

Figure 2.5: Spectral embedding onto the unit circle $\mathbb{S}^1$ of the reduced dynamic graph of the IEEE 9-bus test system for coherency identification

The accuracy of the coherent groups of generators obtained using the proposed methodology is compared with the results obtained using the classical slow coherency algorithm [53, 54, 56]. The steps used in this technique are explained in Appendix D.1. The result of the classical slow coherency theory defines G1 and G2 as the references (step 3). The matrix **T** that contains the cosine similarities between the generation buses and the buses that represent a reference generator (G1 and G2) is shown in Table 2.1.

Table 2.1: Results of the slow coherency algorithm for the IEEE 9-bus test system

Generator	Cosine similarity to G1	Cosine similarity to G2
G1	1.0000	0.0615
G2	0.0615	1.0000
G3	0.2027	0.9649

Then, by identifying the largest entry in each row, the coherent groups of generators can be defined. As noticed, the same two coherent groups of generators are identified using the

classical slow coherency algorithm. In this case, the proposed methodology was found to be as accurate as the existing slow coherency algorithm.

2.3.5.2. New England 39-Bus Test System

The New England 39-bus test system is now used to illustrate the methodology in a larger system. The single line diagram of the network is shown in Figure A.15. First, the dynamic graph G_D is built. Then, the *Kron* reduction of G_D with respect to the internal-nodes is performed to produce the reduced dynamic graph G_{DGN} (not shown in this thesis).

The weight factors associated with the nodes and edges of the reduced dynamic graph are then computed to build the matrices $\mathbf{M_G}$ and $\mathbf{L_{DGN}}$ using (2.15) and (2.16), respectively. These matrices are then used to create the graph theoretic system state matrix $\mathbf{L_N}$ that is defined in (2.14). The eigenproblem $\mathbf{L_N}\boldsymbol{\psi} = \nu\boldsymbol{\psi}$ is then solved to compute the eigenvalues and eigenvectors of $\mathbf{L_N}$. The eigenvalues are then used to define the number of coherent groups of generators. In this case, the relative eigengaps between consecutive eigenvalues suggest that the system has two coherent groups ($r = 2$). It must be mentioned that the generator at bus 39 (G10) represents a dynamic equivalent of the New York system [111] and its inertia constant is much higher than the inertia constant of the other generators (see Table B.6). Hence, the separation of this system into two coherent groups of generators was indeed expected. Moreover, the high inertia constant of generator G10 means that it can be anticipated that this machine will be separated from the other nine generators.

Since two coherent groups of generators have to be identified, the matrix $\mathbf{X} = \begin{bmatrix} \boldsymbol{\psi}_1 & \boldsymbol{\psi}_2 \end{bmatrix}$ is created. Then, the spectral embedding of the reduced dynamic graph is computed and the results of this embedding are illustrated in Figure 2.6. The vectors $\mathbf{x}_i$, $i = 1,\ldots,10$, are then normalised to compute the vectors $\mathbf{y}_i$. Then, the normalised vectors are represented as the data-points $\mathbf{y}_i^{DGN}$ on the unit circle $\mathbb{S}^1$ shown in Figure 2.7. As noticed, a clustering structure clearly emerges and the visualised clusters are $V_{DGN1} = \{v_{G10}\}$ and $V_{DGN2} = \{v_{G1}, v_{G2}, v_{G3}, v_{G4}, v_{G5}, v_{G6}, v_{G7}, v_{G8}, v_{G9}\}$.

The classical slow coherency algorithm explained in Appendix D.1 is now used to compare the accuracy of the new methodology. Table 2.2 shows the matrix **T** that contains the

cosine similarities between each generator and the reference generators (G5 and G10), and highlights the two coherent groups of generator. Table 2.2 indicates that the new approach is as accurate as the classical slow coherency theory.

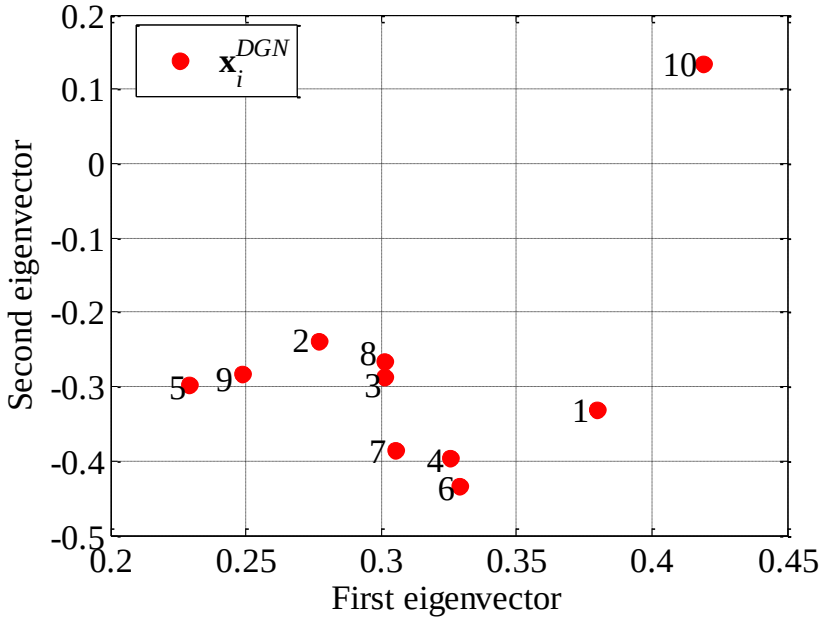

Figure 2.6: Spectral Embedding into $\mathbb{R}^2$ of the reduced dynamic graph of the New England 39-bus test system for coherency identification

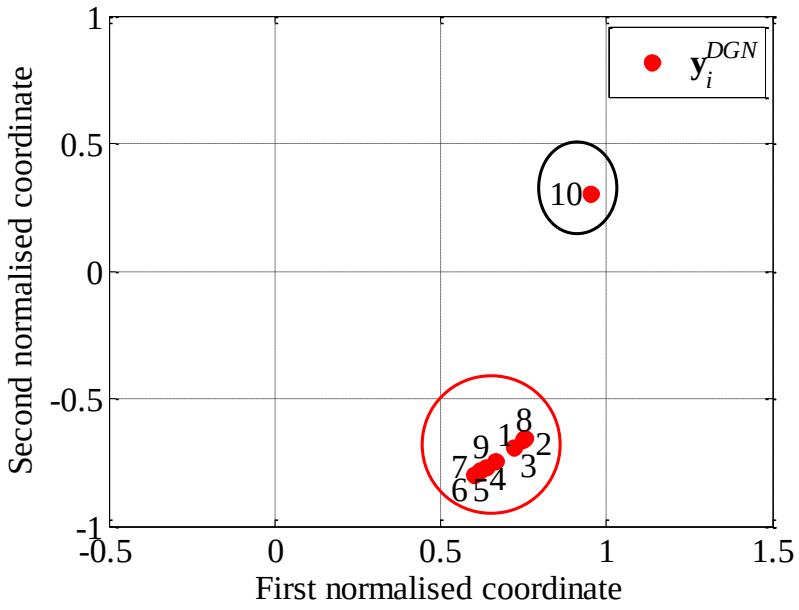

Figure 2.7: Spectral embedding onto the unit circle $\mathbb{S}^1$ of the reduced dynamic graph of the New England 39-bus test system for coherency identification

Table 2.2: Results of the slow coherency algorithm for the New England 39-bus test system

Element in the electrical system	Cosine similarity to G5	Cosine similarity to G10
G1	0.8916	0.2597
G2	0.9169	0.3167
G3	0.9520	0.4091
G4	0.9953	0.5940
G5	1.0000	0.6689
G6	0.9949	0.5903
G7	0.9940	0.5870
G8	0.9332	0.3571
G9	0.9951	0.5922
G10	0.6689	1.0000

Impact of the loading condition in the generator coherency

The simulation results presented here aim to demonstrate the effect of different loading conditions (changes in the level of load) in the coherent groups of generators. Two different loading conditions are considered: 50% and 130%.

For the first case, the base load level is reduced by 50%, while maintaining the same power factor. This change has been equally distributed among all of the generators. The implementation of the methodology then determines two coherent groups of generators. Figure 2.8 shows the spectral embedding onto the unit sphere of the reduced dynamic graph. As noticed, since the load level was distributed equally among the generators, the same coherent groups are obtained. This is because the ratio between synchronising coefficient is maintained, and thus, the coherent groups are the same.

In another set of simulations, it is now considered that the base load level is increased by 30%, while maintaining the same power factor. This increment has been equally distributed among the generators G2–G7. The output power of the other generators remains the same. This is done to highlight the effects of different generator rescheduling in the generator coherency. The implementation of the methodology then determines two coherent groups of generators. Figure 2.9 shows the spectral embedding onto the unit sphere of the reduced dynamic graph for this new scenario. As noticed, the loading level along with generation

rescheduling affects the generator coherency results. This is because the ratio between synchronising coefficient is different, and thus, the coherent groups are the different.

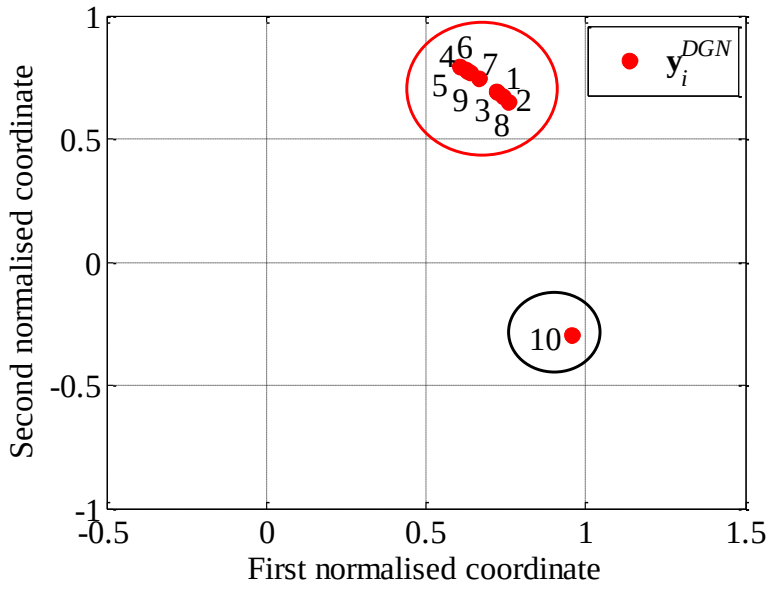

Figure 2.8: Spectral embedding onto the unit circle $\mathbb{S}^1$ of the reduced dynamic graph of the New England 39-bus test system for coherency identification considering 50% of load level

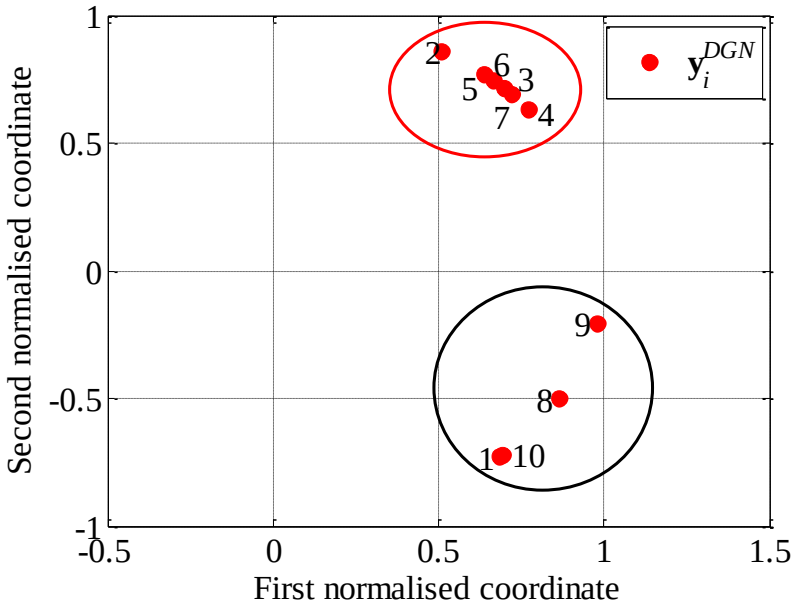

Figure 2.9: Spectral embedding onto the unit circle $\mathbb{S}^1$ of the reduced dynamic graph of the New England 39-bus test system for coherency identification considering 130% of load level

2.3.5.3. IEEE 118-Bus Test System

The IEEE 118-bus test system that is shown in Figure A.17 is finally used to illustrate the proposed methodology in a much larger system. The implementation of the novel methodology for this test case suggests the creation of three coherent groups of generators, which can be observed in Figure 2.10, and they are $V_{DGN1}=\{v_{G1},v_{G2},v_{G3},v_{G4},v_{G5}\}$, $V_{DGN2}=\{v_{G6},v_{G7},v_{G8},v_{G9},v_{G10},v_{G11},v_{G12},v_{G13},v_{G14}\}$ and $V_{DGN3}=\{v_{G15},v_{G16},v_{G17},v_{G18},v_{G19}\}$.

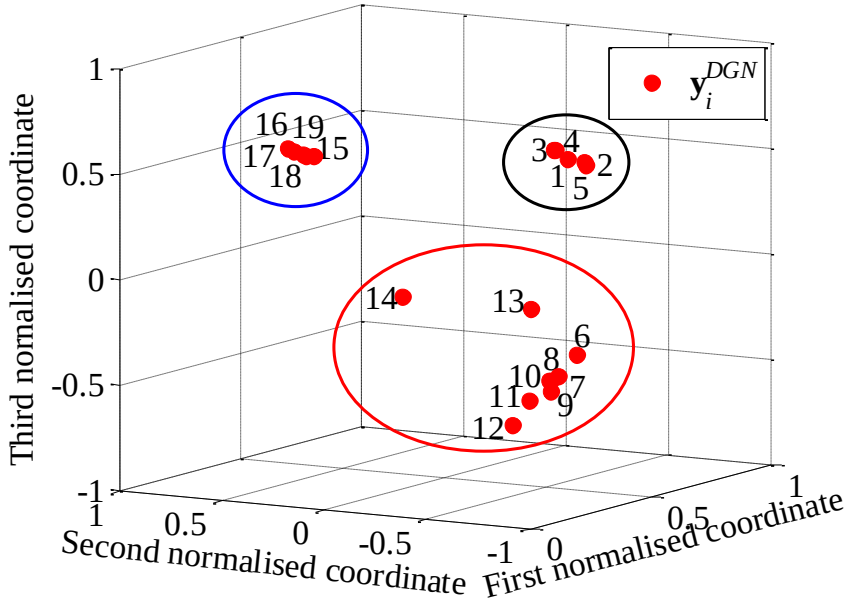

Figure 2.10: Spectral embedding onto the unit sphere $\mathbb{S}^2$ of the reduced dynamic graph of the IEEE 118-bus test system for coherency identification

The accuracy of the new methodology is now compared with the results of the slow coherency algorithm explained in Appendix D.1. Table 2.3 contains the cosine similarities between the machines and the reference generators and highlights the three coherent groups of generators identified by the classical technique. As noticed, the slow coherency algorithm produces similar coherent groups of generators. However, the cosine similarity between generator G14 and reference generator G8 is very close to the cosine similarity between generator G14 and reference generator G15. This kind of similarity may cause some generators to move from one group to another. In contrast, the proposed methodology projects the data-points on to the unit sphere and clusters are naturally created [70, 73].

Table 2.3: Results of the slow coherency algorithm for the IEEE 118-bus test system

Generator	Cosine similarity to G1	Cosine similarity to G8	Cosine similarity to G15
G1	1.0000	0.2490	0.2891
G2	0.9983	0.1928	0.3249
G3	0.9998	0.2494	0.2775
G4	0.9995	0.2230	0.2961
G5	0.9981	0.1910	0.3200
G6	0.1751	0.9971	0.6512
G7	0.2197	0.9994	0.6242
G8	0.2490	1.0000	0.6229
G9	0.2550	0.9986	0.5857
G10	0.2533	0.9966	0.5665
G11	0.2251	0.9792	0.4910
G12	0.2333	0.9952	0.5657
G13	0.3391	0.8634	0.1698
G14	0.3604	0.5875	0.5545
G15	0.2891	0.6229	1.0000
G16	0.5131	0.3224	0.9391
G17	0.5554	0.2429	0.9072
G18	0.5370	0.3054	0.9314
G19	0.4900	0.4095	0.9647

This test system is now used to analyse the results. To do so, the quality index (2.17) introduced in Section 2.3.2.3 is used. This quality index $\eta(V_{DGN})$ compares the dynamic coupling between machines – expressed by the synchronising coefficients – and the total inertia constant within the islands. Table 2.4 shows the dynamic coupling between the coherent groups $\left(cut\left(V_{DGNk},\bar{V}_{DGNk}\right)\right)$ (A.5), the total inertia within the group $\left(wei\left(V_{DGNk}\right)\right)$ (A.6) and the quality of each coherent group (2.17) for the results of the methodology, which are the same as those of the implementation of the slow coherency algorithm.

Table 2.4: Coherency identification results of the IEEE 118-bus test system for *r* = 3

	Group No.	Cut	Weight	$\eta(V_k)$
Results using the proposed methodology	1	7.23	82.10	91.19
	2	15.40	178.45	91.37
	3	9.19	78.88	88.35

2.3.5.4. Evaluating the Computational Efficiency of the Proposed Methodology

The runtime of the methodology is dominated by that of the eigendecomposition. Hence, the computational complexity of the new approach is approximately $O\left(m^3\right)$ [74]. The mean runtime of the methodology for 100 trials of each test system is shown in Table 2.5.

Table 2.5: Computational time for the coherency identification using the proposed methodology and the classical slow coherency algorithm

Test System	Runtime using the Proposed Methodology (ms)	Runtime using the Slow Coherency Algorithm (ms)
IEEE 9-bus	3.98	8.72
New England 39-bus	6.33	15.85
IEEE 118-bus	12.92	35.80

In order to compare the efficiency of the new methodology, similar studies were carried out using the classical slow coherency theory, and the results are also shown in Table 2.5. It is important to mention that the slow coherency algorithm applies Gaussian elimination with complete pivoting to determine the reference generators of each coherent group, and the computational complexity of this technique is approximately $O\left(m^3\right)$ [112]. Hence, the aggregated complexity of the slow coherency algorithm is determined by the eigendecomposition of the matrix $\bar{\mathbf{A}}$ plus the Gaussian elimination. In other words, its complexity is approximately double the complexity of the proposed methodology.

Table 2.5 shows that the proposed methodology is computationally more efficient than the slow coherency algorithm. Indeed, it can be observed that the average runtime of the methodology introduced in this section is approximately 60% faster than the existing approach. Furthermore, it can be noted that the larger the network, the faster the proposed methodology. The results presented using the proposed methodology avoids the use of recursive algorithms such as the *k-means* to cluster the data, as the groups could be visualised on the unit sphere. In practical implementations in power system with thousands of buses and hundreds of generators, it is expected that the reduction in the average time would be even higher, and this would represent a significant benefit of the methodology when compared to previous approaches [53, 56].

2.4. Determination of Islanding Solutions for Minimal Dynamic Coupling: A Normalised Spectral Clustering Approach

It has been observed in large-interconnected power systems that following a severe disturbance some generators will tend to swing together. The electromechanical oscillations between groups of machines – interpreted as the separation in time between dynamically slow generators [56] – are the result of the inherent weak connections between groups of generators with strong dynamic coupling. Hence, the identification of these weak connections plays an important role in the design of islanding solutions [50, 52, 56], as the transient stability of the future islands can be significantly enhanced by separating the transmission system across these weak connections [5, 53].

Therefore, this section presents a new ICI methodology based on normalised spectral clustering that can identify the weakest connections between strongly connected machines. The determination of weak connections is a natural extension of the slow coherency theory and is associated with the determination of islanding solutions for minimal dynamic coupling [56]. This can be physically interpreted as the identification of the dynamically coherent buses in the entire power system and the creation of dynamically coherent areas, i.e., areas that will have similar dynamic behaviour, where this dynamic behaviour is measured in terms of the dynamic coupling between buses.

In this thesis, the weak connections in the power system are determined by studying the *Jacobian* matrices $\mathbf{J_C}$ and $\mathbf{J_D}$ that are shown in the augmented system state matrix given by (2.6). These matrices contain information regarding the dynamic coupling between the internal generator buses and the load buses of the extended power system [1, 5, 56]. The determination of the coherent buses within each area is studied in the sense that the angular deviations between buses within the same coherent area are small. The voltage magnitude deviations are not included in this thesis as the coherency identification considers only the rotor angle of the machines. Hence, the determination of the coherent areas by taking into account deviations in the voltage phase and voltage magnitude remains an open question and represents a future area of research.

As further detailed in Section 2.4.4, the methodology introduced here aims to include the load-nodes of the full dynamic graph G_D, which represent the load and generator terminal buses of the system, in the spectral embedding. The new approach will then determine the weak connections between the previously identified coherent groups of generators. In other words, this technique seeks to determine the actual lines that are weak connections between the groups of buses that have strong internal connections. The new approach uses sensitivity factors associated with the changes in the voltage phase angles of the load buses with respect to the changes in the rotor angle of the generators, and these sensitivity factors are computed from the Jacobian matrices $\mathbf{J_C}$ and $\mathbf{J_D}$, as further detailed below.

2.4.1. Using Voltage Phase Angle Sensitivity Factors to Define New Dynamic Graph Weight Factors

The *Jacobian* matrices $\mathbf{J_C}$ and $\mathbf{J_D}$ given in (2.6) are utilised in this section to determine sensitivity factors between the phase angles at the load buses, including the generator terminal buses, and changes in the rotor angles of the generators. The sensitivity matrix, denoted by $\mathbf{S_L}$, is computed as follows.

$$\mathbf{S_L} = -\mathbf{J_D^{-1}}\mathbf{J_C} \tag{2.24}$$

The *ij*-th entry of the first *n* row vectors of the matrix $\mathbf{S_L}$ represents the sensitivity of the voltage phase angle at the load bus *i* to a change in the rotor angle at the internal bus of generator *j*. Since the spectral embedding of the *m* internal generator buses for the coherency identification performed in the previous section considered only the rotor angle of the generators (the angle of the voltage behind the transient reactance), only the first *n* row vectors of the matrix $\mathbf{S_L}$ are taken into account in this section to study the dynamic coupling (angular deviation) between the load bus *i* and the internal generator bus *j*.

It is important to mention that the sum of each row vector of the matrix $\mathbf{S_L}$ (2.24) is equal to one (see (2.33) for an example). Furthermore, the higher the *ij*-th entry of the row vector is,

the more sensitive the voltage phase angle at the load bus *i* is to variations in the rotor angle at the internal generator bus *j*.

The sensitivity factors in (2.24) are used as edge weights between the load-nodes and the internal-nodes. The higher the *ij*-th entry of $\mathbf{S_L}$, the stronger the connection between the load-node v_{Li} and the internal-node v_{Gj}. Hence, the load-node v_{Li} will be grouped with to an internal-node v_{Gj} based on the highest value in the *ij*-th entry of $\mathbf{S_L}$.

2.4.2. Definition of Graph Theoretic Concepts

The normalised spectral clustering-based methodology uses the following graph theoretic concepts to determine the weak connections between coherent zones. It should be noted that the weak connections will represent the islanding solution for minimal dynamic coupling.

2.4.2.1. Cutset and Cut

In order to determine islanding solutions for minimal dynamic coupling, the extended system that is represented by the dynamic graph G_D is partitioned into *r* electrical islands, where *r* represents the number of coherent groups of generators, as current practices suggest that the number of islands should be equal to the number of coherent groups [13, 44-50, 52]. To split the dynamic graph G_D, a cutset $E_S \subset E_D$ must be determined. In the application introduced here, a cutset $E_S \subset E_D$ is the set of edges that must be removed to cluster the graph G_D into *r* disjoint subgraphs $G_{D1},\ldots,G_{Dr}$, with node sets $V_{D1},\ldots,V_{Dr}$.

The cut associated with the cutset E_S is the sum of the weight factors associated with the edges included in E_S and is given by (A.8). In the ICI problem for minimal dynamic coupling, a cutset E_S consists of the edges that represent the branches in the extended power system that must be disconnected to create the islands. When defined in this way, the cut of the cutset E_S corresponds to the total dynamic coupling between the islands. Furthermore, the node set V_{Dk}, $k = 1,\ldots,r$, would contain the nodes that represent the buses of the extended power system that are included in the k^{th} dynamically coherent area.

2.4.2.2. Quality of a Cutset

The quality of an islanding solution for minimal dynamic coupling can be measured using the ratio between the boundary (cut) (A.5) and the volume (A.6) of the clusters. In this application, the cut of the node set V_{Dk}, denoted by $cut\left(V_{Dk},\bar{V}_{Dk}\right)$, physically corresponds to the dynamic coupling between the buses that are represented by the nodes $v_i \in V_{Dk}$ and the other buses, i.e., the dynamic coupling between the buses in the island represented by V_{Dk} and the rest of the system. Furthermore, the volume of that node set, denoted by $vol\left(V_{Dk}\right)$, represents the total dynamic coupling between the buses within the dynamically coherent island that is represented by the node set V_{Dk}.

The quality of the node set V_{Dk}, $k = 1,\ldots,r$, is measured as follows.

$$\eta\left(V_{Dk}\right) = 1 - \frac{cut\left(V_{Dk},\bar{V}_{Dk}\right)}{vol\left(V_{Dk}\right)} \tag{2.25}$$

In this application, the expansion $\phi\left(V_{Dk}\right) = cut\left(V_{Dk},\bar{V}_{Dk}\right)\Big/vol\left(V_{Dk}\right)$ of the node set V_{Dk} measures the size of the cut relative to the volume of the dynamically coherent islands. The quality index (2.25) of an island can be physically interpreted as a measure of the dynamic interaction between the buses in that island and the rest of the system with respect to the dynamic interaction between the buses in that island, where the dynamic interaction is measured using the sensitivity factors in $\mathbf{S_L}$ (2.24). Indeed, the greater the value of $\eta\left(V_{Dk}\right)$ – the smaller the dynamic interaction between islands and the more dynamic interaction between buses in the island – the better the island is considered to be in terms of clustering.

The methodology will then evaluate the quality of the islanding solution for minimal dynamic coupling using the worst quality index $\eta\left(V_{Dk}\right)$ from the k islands, i.e., the overall quality of a solution is the minimum value of $\eta\left(V_{Dk}\right)$ for all of the islands: $\min_{k=1,2,\ldots,r}\left(\eta\left(V_{Dk}\right)\right)$.

As detailed in Section 2.4.3, finding the maximum of the worst quality – solving (2.26) – will be the objective function in the islanding problem for minimal dynamic coupling.

$$\max_{V_{D1},\ldots V_{Dr}} \min_{k=1,2,\ldots,r} \left(\eta\left(V_{Dk}\right)\right) \tag{2.26}$$

2.4.3. Formulation of the ICI Problem for Minimal Dynamic Coupling

The determination of the weak connections in a power system is an inherent extension of the identification of the coherent groups of generators, and seeks to determine the dynamically coherent areas, i.e., the areas that contain buses with similar angular behaviour [56]. In order to determine the weakest connections – and the solution for minimal dynamic coupling – the load-nodes of G_D must be included in the spectral clustering, as previously mentioned. The similarities between the ICI problem for minimal dynamic coupling and the coherency identification problem mean that it lends itself to being formulated in a similar way as in the previous section. Since the aim is to partition the dynamic power system, the dynamic graph representation G_D (2.9) of the extended electrical network is considered. In other words, the internal-nodes and the load-nodes are taken into account.

Given the r partitions $V_{D1},\ldots,V_{Dr}$, the value of the cut – the dynamic coupling – between the clusters can be computed as follows.

$$cut\left(V_{D1},\ldots,V_{Dr}\right) = \sum_{e_{ij}\in E_S} w_{ij} \tag{2.27}$$

In (2.27), w_{ij} is the edge weight between the load-node v_{Li} and the internal-node v_{Gj}, and as previously mentioned, these values are calculated using the sensitivity matrix $\mathbf{S_L}$. It is important to remember that ij-th entry of the matrix $\mathbf{S_L}$ represent the sensitivity of the voltage phase angle at the load bus i to a change in the rotor angle at the internal bus of generator j, and this is the reason for defining the edge weights w_{ij} in this way.

Thus, the problem of identifying weak connections between coherent groups of generators is equivalent to determining the minimal dynamic coupling over the *r* partitions while including in each partition only coherent generators. This is equivalent to solving (2.28),

$$\min_{V_{D1},\ldots,V_{Dr}} cut\left(V_{D1},\ldots,V_{Dr}\right) \tag{2.28}$$

subject to each island containing only coherent generators (2.29):

$$V_{DGNk} \subset V_{Dk}\,. \tag{2.29}$$

As noticed in (2.28)-(2.29), the weak connections problem aims to partition the dynamic system into *r* islands, such that the k^{th} island contains the k^{th} group of coherent generators. The value of *r* is the number of islands to be created.

However, the solution to (2.28) may be trivial, as the node with smallest node degree could be partitioned from the graph [71], which is similar to the case of the coherency identification problem. To avoid the spurious solutions that may be obtained when solving (2.28)-(2.29), the problem of identifying weak connections is modified as follows.

$$\min_{V_{D1},\ldots,V_{Dr}} \max_{k=1,\ldots,r}\left(\frac{cut\left(V_{Dk},\bar{V}_{Dk}\right)}{vol\left(V_{Dk}\right)}\right) \tag{2.30}$$

subject to

$$V_{DGNk} \subset V_{Dk}$$

The objective function given by (2.30) seeks to minimise the worst (maximum) relative cut of each island with respect to its volume, while ensuring that each island contains only coherent generators. Since $\eta\left(V_{Dk}\right)=1-cut\left(V_{Dk},\bar{V}_{Dk}\right)\big/vol\left(V_{Dk}\right)$, this new objective function is equivalent to maximising the worst (minimum) quality over the *r* partitions (2.26).

The new objective function given by (2.30) creates balanced partitions, in the sense that the voltage phase angles of the load buses within each cluster are more sensitive to the rotor angle deviations of the generators in the same island than they are to the rotor angle deviations of the generators in the other islands. Solving (2.30) enhances the transient stability of the islands, as the electrical buses within the islands possess similar voltage phase angles, i.e., they have similar dynamic behaviour [5].

2.4.4. Methodology for Solving the ICI Problem for Minimal Dynamic Coupling

The methodology proposed in this section is a natural extension of the methodology presented in the previous one. Hence, it aims to embed the load-nodes of the dynamic graph G_D (2.9) in an r-dimensional Euclidean space $\mathbb{R}^r$ and then project the corresponding vectors on to the unit (r–1)-dimensional sphere $\mathbb{S}^{r-1}$. These projected vectors are then clustered to the nearest coherent group of generators, as explained below.

To embed the load-nodes v_{Li}, $i = 1,\ldots,n$, in $\mathbb{R}^r$ the geometric coordinates of the points that represent these nodes in $\mathbb{R}^r$ must be computed. These coordinates are calculated as follows.

$$\mathbf{X_L} = \mathbf{S_L}\mathbf{X} \tag{2.31}$$

In (2.31), the matrix $\mathbf{X}$ – calculated in the previous section using the eigenvectors $\boldsymbol{\psi}_1,\ldots,\boldsymbol{\psi}_r$ associated with the r smallest eigenvalues of the matrix $\mathbf{L_N}$ (2.14) – serves as a projection matrix. The matrix $\mathbf{X}$ embeds the load-nodes v_{Li}, $i = 1,\ldots,n$, close to the internal-nodes v_{Gj}, $j = 1,\ldots,m$, based on the sensitivity factors contained in the matrix $\mathbf{S_L}$ (2.24) (see Figure 2.11 for an example). The row vectors $\mathbf{x}_i^L \in \mathbf{X_L}$, $i = 1,\ldots,n$, represent the geometric coordinates of the node $v_{Li} \in V_{DLD}$ in $\mathbb{R}^r$. For consistency, the vector $\mathbf{x}_i^L$ are denoted by $\mathbf{x}_i^{DLD}$ in $\mathbb{R}^r$ (see Figure 2.11 for an example). The proposed methodology then normalises the vectors $\mathbf{x}_i^L$ to have length one. This normalisation projects the data-points $\mathbf{x}_i^{DLD}$, $i = 1,\ldots,n$, on to the unit sphere $\mathbb{S}^{r-1}$ and creates the new data-points $\mathbf{y}_i^{DLD}$ (see Figure 2.12

for an example). The creation of the data-points $\mathbf{y}_i^{DLD}$ not only improves the quality of the solution, as previous discussed, but also enables certain nodes to be defined as belonging to the "core" of the island and other nodes as belonging to the "periphery" of the islands. For example, it can be observed in Figure 2.12 that the load-node v_{L4} (represented by the asterisk 4) belongs to the core of the island created by generator 1 (G1), and that the nodes v_{L5} and v_{L6} (asterisks 5 and 6) are in the "periphery" of the islands. The nodes in the periphery will be called peripheral-nodes.

When the load-nodes v_{Li} and the internal-nodes v_{Gj} are embedded on the unit sphere $\mathbb{S}^{r-1}$, the dynamic centroids, denoted by $\boldsymbol{\mu}_k$, $k = 1,\ldots,r$, are calculated as follows.

$$\boldsymbol{\mu}_k = \frac{1}{\left|V_{DGNk}\right|} \sum_{v_{Gj} \in V_{DGNk}} \mathbf{y}_j^{DGN}\ ,\ k = 1,\ldots,r \tag{2.32}$$

A dynamic centroid is the mean point of the data-points representing the internal-nodes v_{Gi} that were used in Section 2.3 to create the set V_{DGNk}. For example, the centroid $\boldsymbol{\mu}_2$, marked in Figure 2.12, is the mean point of the data-points $\mathbf{y}_2^{DGN}$ and $\mathbf{y}_3^{DGN}$. Remark that each dynamic centroid must also be normalised to project it on to the unit sphere $\mathbb{S}^{r-1}$.

In contrast to the previous approach [56], which uses Gaussian elimination with complete pivoting to define a reference generator in each cluster, the new approach defines a dynamic centroid for each group considering the mean point of the generators included in each area. This improves the quality of the islanding solution as the dynamic centroid contains information for all of the generators in each coherent group. That is, the clusters created will contain buses with stronger dynamic coupling, as demonstrated below. Furthermore, the proposed approach partitions the data-points projected on to the unit sphere, which, as highlighted throughout this thesis, improves the quality of the clustering.

When the data-points $\mathbf{y}_i^{DLD}$, $i = 1,\ldots,n$, and the dynamic centroids $\boldsymbol{\mu}_k$, $k = 1,\ldots,r$, are embedded on to the unit sphere $\mathbb{S}^{r-1}$, the spherical distance between each data-point $\mathbf{y}_i^{DLD}$ and each dynamic centroid $\boldsymbol{\mu}_k$ is calculated. The results of this calculation are represented in

the similarity matrix $\mathbf{S} := \left(\mathbf{y}_i^{DLD}, \boldsymbol{\mu}_k \right)$. The similarity matrix **S** is used to determine the proximity between the load-nodes and the coherent groups of generators that are represented by the dynamic centroid. The smaller the spherical distance between the data-point $\mathbf{y}_i^{DLD}$ and the dynamic centroid $\boldsymbol{\mu}_k$, the stronger the connection between the load bus *i* and the k^{th} coherent group of generators.

Therefore, the load-node v_{Li} is grouped with the cluster V_{DGNk} based on the minimum entry of the *ij*-th entry of the matrix **S**. This clustering produces the sets (clusters) $V_{D1},\ldots,V_{Dr}$, in which the cluster V_{Dk}, $k = 1,\ldots,r$, contains the load-nodes V_{DLDk} that are closer to the cluster V_{DGNk}. Moreover, these clusters V_{Dk} represent the electrical islands that have minimal dynamic coupling. For example, the weak connections in the IEEE 9-bus test system for the case of two islands are found across the cutset $E_S = \left\{ e_{4,5}, e_{6,9} \right\}$, and the clusters are $V_{D1} = \left\{ v_{G1}, v_{L1}, v_{L4}, v_{L6} \right\}$, and $V_{D2} = \left\{ v_{G2}, v_{G3}, v_{L2}, v_{L3}, v_{L5}, v_{L7}, v_{L8}, v_{L9} \right\}$.

Lemma 2.4.1. Let a power system be represented by the full dynamic graph $G_D = (V_D, E_D)$. In addition, let the subset $V_{DGNk} \subset V_{Dk}$, $k = 1,\ldots,r$, contain only the internal-nodes v_{Gj} that represent coherent generators. If the graph is split into the subgraphs V_{Dk} such that the ratio $cut\left(V_{Dk}, \bar{V}_{Dk}\right) / vol\left(V_{Dk}\right)$ is minimum for all of the subgraphs, the obtained subsystems will exhibit an increased angular stability criterion.

2.4.5. Simulation Examples

This section illustrates the proposed methodology that determines islanding solutions for minimal dynamic coupling using the same three test systems. The simulation results obtained using the methodology are compared to those obtained using an implementation of the approach presented in [56], which is describe in Appendix D.1.

2.4.5.1. IEEE 9-Bus Test System

The IEEE 9-bus test system is initially used to illustrate the methodology. The dynamic graph shown in Figure 2.1 is used to partition this system. It must be noted from Section 2.3

that there are two coherent groups of generators: $V_{DGN1} = \{v_{G1}\}$ and $V_{DGN2} = \{v_{G2}, v_{G3}\}$. The methodology computes the sensitivity matrix $\mathbf{S_L}$, using (2.24) and the *Jacobian* matrices $\mathbf{J_C}$ and $\mathbf{J_D}$ given by (2.6). The matrix $\mathbf{S_L}$ for this test system is shown in (2.33).

$$\mathbf{S_L} = \begin{bmatrix} 0.8389 & 0.0874 & 0.0737 \\ 0.1931 & 0.6778 & 0.1291 \\ 0.2435 & 0.1931 & 0.5634 \\ 0.6851 & 0.1704 & 0.1445 \\ 0.5665 & 0.2710 & 0.1625 \\ 0.3060 & 0.4956 & 0.1984 \\ 0.3219 & 0.3867 & 0.2914 \\ 0.3250 & 0.2523 & 0.4227 \end{bmatrix} \tag{2.33}$$

The embedding of the load-nodes v_{Li}, $i = 1,\ldots,9$, into $\mathbb{R}^2$ is then performed, the results of which are shown in Figure 2.11. The methodology then projects the data-points $\mathbf{x}_i^{DLD}$ on to the unit circle $\mathbb{S}^1$ to create the normalised vectors shown in Figure 2.12. It should be noted that the peripheral-nodes identified in Figure 2.12 are v_5 and v_6.

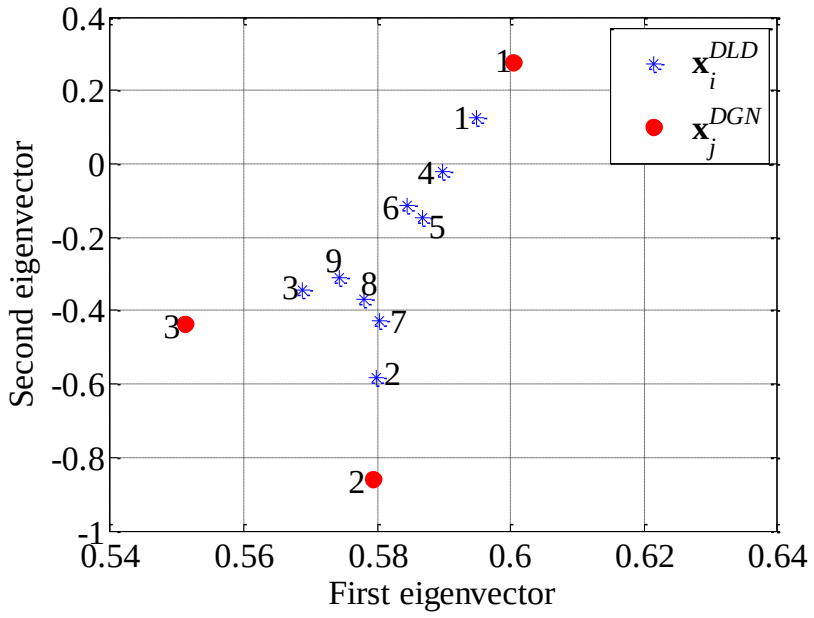

Figure 2.11: Spectral Embedding into $\mathbb{R}^2$ of the load-nodes of the dynamic graph of the IEEE 9-bus test system for minimal dynamic coupling

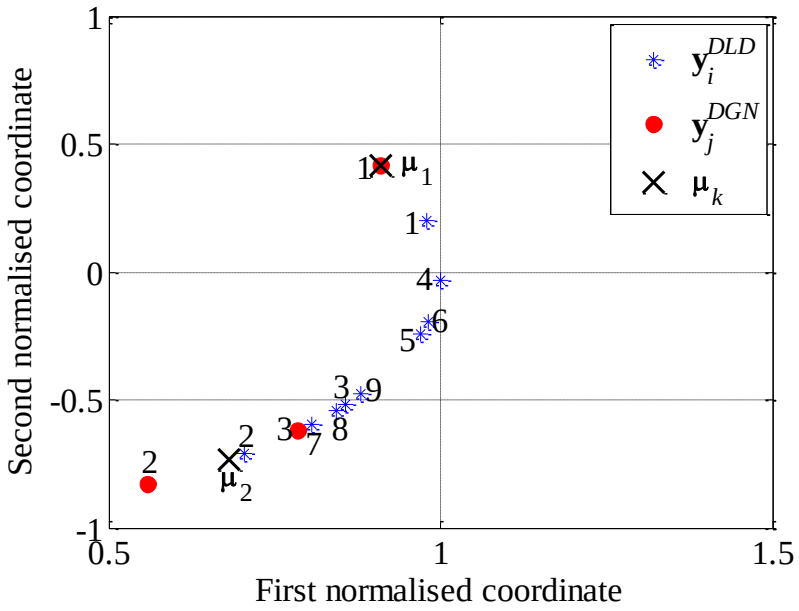

Figure 2.12: Spectral embedding onto the unit circle $\mathbb{S}^1$ of the load-nodes of the dynamic graph of the IEEE 9-bus test system for minimal dynamic coupling

The methodology then computes the dynamic centroids $\boldsymbol{\mu}_1$ and $\boldsymbol{\mu}_2$ using (2.32), which are shown in Figure 2.12, and calculates the spherical distance (A.64) between each point $\mathbf{y}_i^{DLD}$ and each dynamic centroid $\boldsymbol{\mu}_k$. This creates the similarity matrix **S** shown in Table 2.6.

Table 2.6: Spherical distance between load-nodes and dynamic centroids of the dynamic graph of the IEEE 9-bus test system for minimal dynamic coupling

Node	Spherical distance to Centroid $\boldsymbol{\mu}_1$	Spherical distance to Centroid $\boldsymbol{\mu}_2$
v_{L1}	**0.225**	1.027
v_{L2}	1.219	**0.033**
v_{L3}	0.973	**0.279**
v_{L4}	**0.464**	0.787
v_{L5}	0.675	**0.576**
v_{L6}	**0.624**	0.628
v_{L7}	1.064	**0.187**
v_{L8}	0.999	**0.253**
v_{L9}	0.925	**0.326**

The methodology then groups each data-point $\mathbf{y}_i^{DLD}$ with the nearest dynamic centroid $\boldsymbol{\mu}_k$ based on the minimum spherical distance. This grouping is highlighted in Table 2.6 and it

defines the islands that have the minimal dynamic coupling as they are separated by the weakest connections between the coherent areas. In this case, the methodology returns the cutset $E_S = \{e_{4,5}, e_{6,9}\}$ and creates the two islands shown in Figure 2.13.

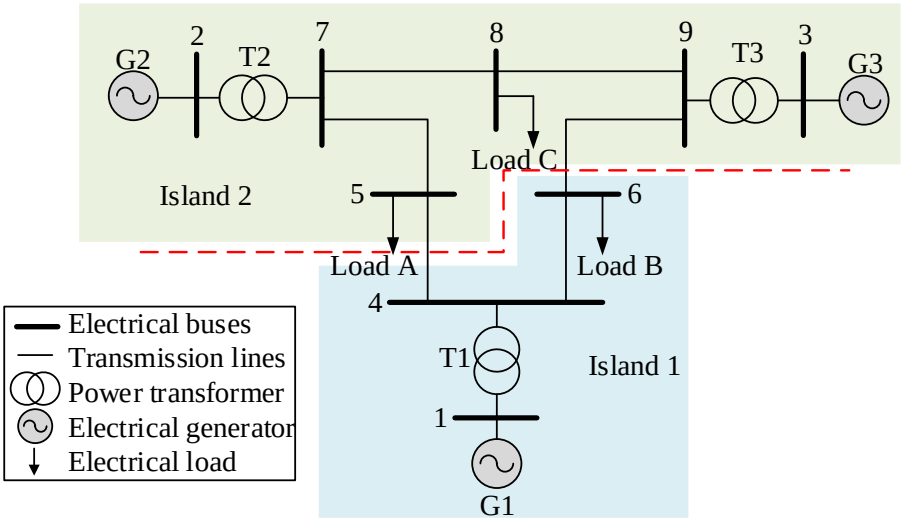

Figure 2.13: Islanding solution for minimal dynamic coupling of the IEEE 9-bus test system split into two islands

In order to evaluate the quality of the solution obtained, the quality index (2.25) for each island is then calculated. Using the edge weights given by the sensitivity matrix $\mathbf{S_L}$, it can be determined that the quality of islands 1 and 2 are 67.2% and 83.5%, respectively. Therefore, the quality of the islanding solution $\left(\min_{k=1,2,\ldots,r}\left(\eta\left(V_{Dk}\right)\right)\right)$ is 67.2%.

The efficiency of the ICI methodology is also compared with the existing approach [56]. Both methods tend to find the solution in a very short period of time (average time of 17.60 ms in all of the simulations). This excludes the eigendecomposition used to identify the coherent groups of generators. In Section 2.4.5.4, the overall computational efficiency (coherency identification plus determination of the islanding solution) is evaluated.

2.4.5.2. New England 39-Bus Test System

The New England 39-bus test system is now used to illustrate the proposed methodology. The methodology considers the two coherent groups of generator that were previously identified when computing the sensitivity matrix $\mathbf{S_L}$ and embedding the load-nodes in $\mathbb{R}^2$.

Figure 2.14 shows this embedding in $\mathbb{R}^2$, and Figure 2.15 the projection on to the unit circle $\mathbb{S}^1$. It can be noted that the normalisation improves the visualisation of the data, and that this key feature helps to cluster the data-points into well-defined groups.

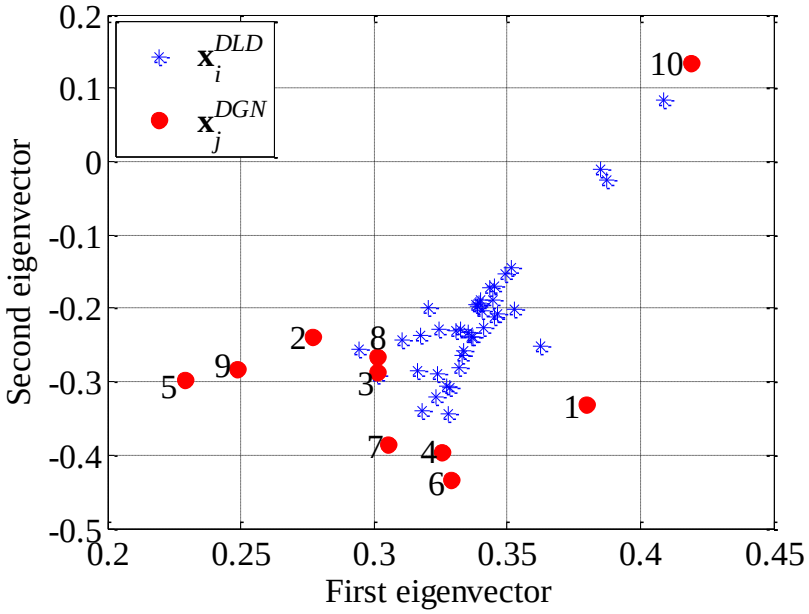

Figure 2.14: Spectral Embedding into $\mathbb{R}^2$ of the load-nodes of the dynamic graph of the New England 39-bus test system for minimal dynamic coupling

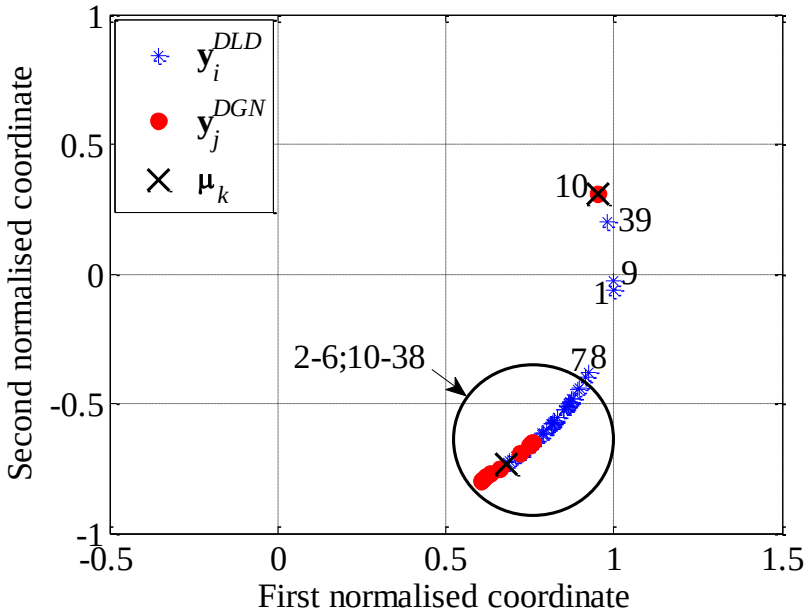

Figure 2.15: Spectral embedding on to the unit circle $\mathbb{S}^1$ of the load-nodes of the dynamic graph of the New England 39-bus test system for minimal dynamic coupling

It should also be noted that the peripheral nodes identified in Figure 2.15 are $\{v_1. v_9\}$. The methodology then calculates the spherical distance between the data-points that represent the load-nodes and the dynamic centroids to create the similarity matrix **S**. The matrix **S** is then used to determine the weak connections shown in Figure 2.16.

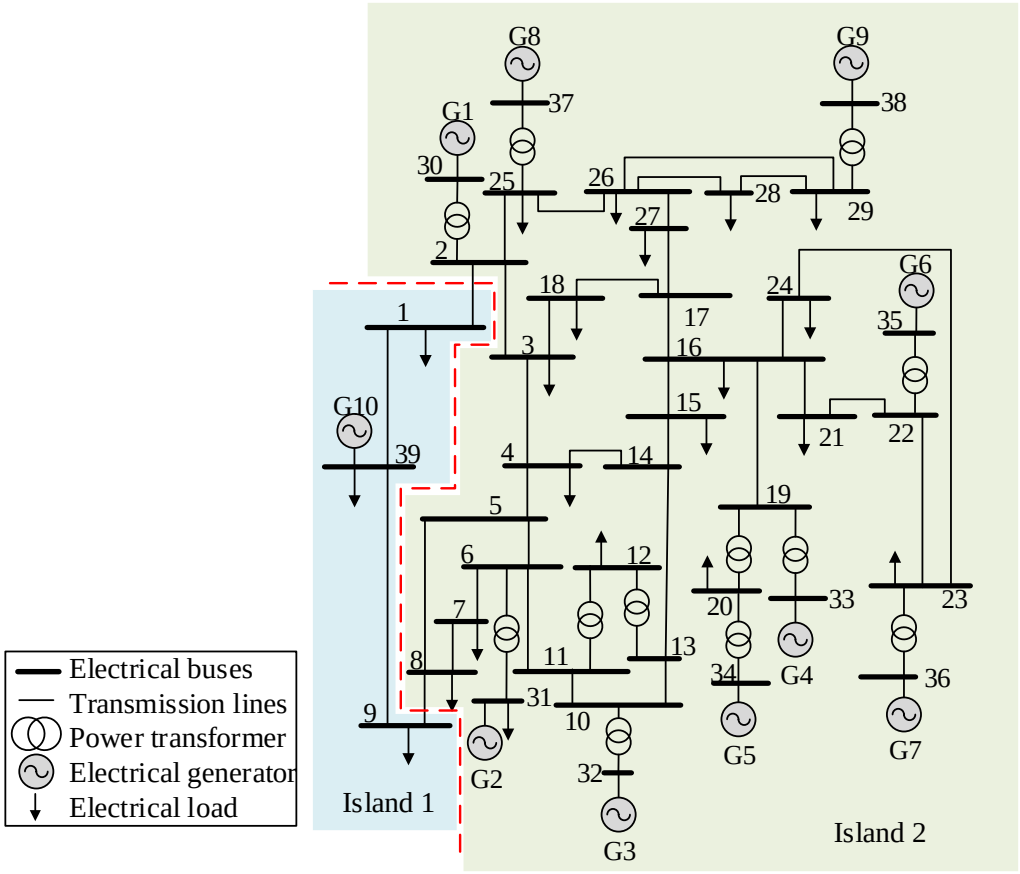

Figure 2.16: Islanding solution for minimal dynamic coupling of the New England 39-bus test system split into two islands

In this particular test system, and due to the dynamic properties (high inertia constant) of generator G10 that represents the dynamic equivalent of the New York system [111], the same weak connections were found using the existing approach [56]. In this case, the quality of islands 1 and 2 using both approaches are 68.3% and 97.9%, respectively. Thus, the quality of the islanding solution for minimal dynamic coupling is 68.3%. In terms of the efficiency of each approach, similar computational times were also obtained, and in both cases the average runtime was found to be approximately 39.40 ms.

2.4.5.3. IEEE 118-Bus Test System

The IEEE 118-bus test system is now used to illustrate the proposed ICI methodology for minimal dynamic coupling. This system is to be split into three islands, as three coherent groups of generators were previously identified. After implementing the methodology, the islanding solution for minimal dynamic coupling shown in Figure 2.17 can be determined. Then, by computing the dynamic coupling between the coherent areas $\left(cut\left(V_{Dk},\bar{V}_{Dk}\right)\right)$ and the total dynamic coupling between the buses in the same coherent area $\left(vol\left(V_{Dk}\right)\right)$, the quality index (2.25) of the islands can be calculated. In this case, the quality of islands 1, 2 and 3 is 95.7%, 93.6% and 96.5%, respectively. Thus, the overall quality of the islanding solution for minimal dynamic coupling determined by the methodology is 93.6%.

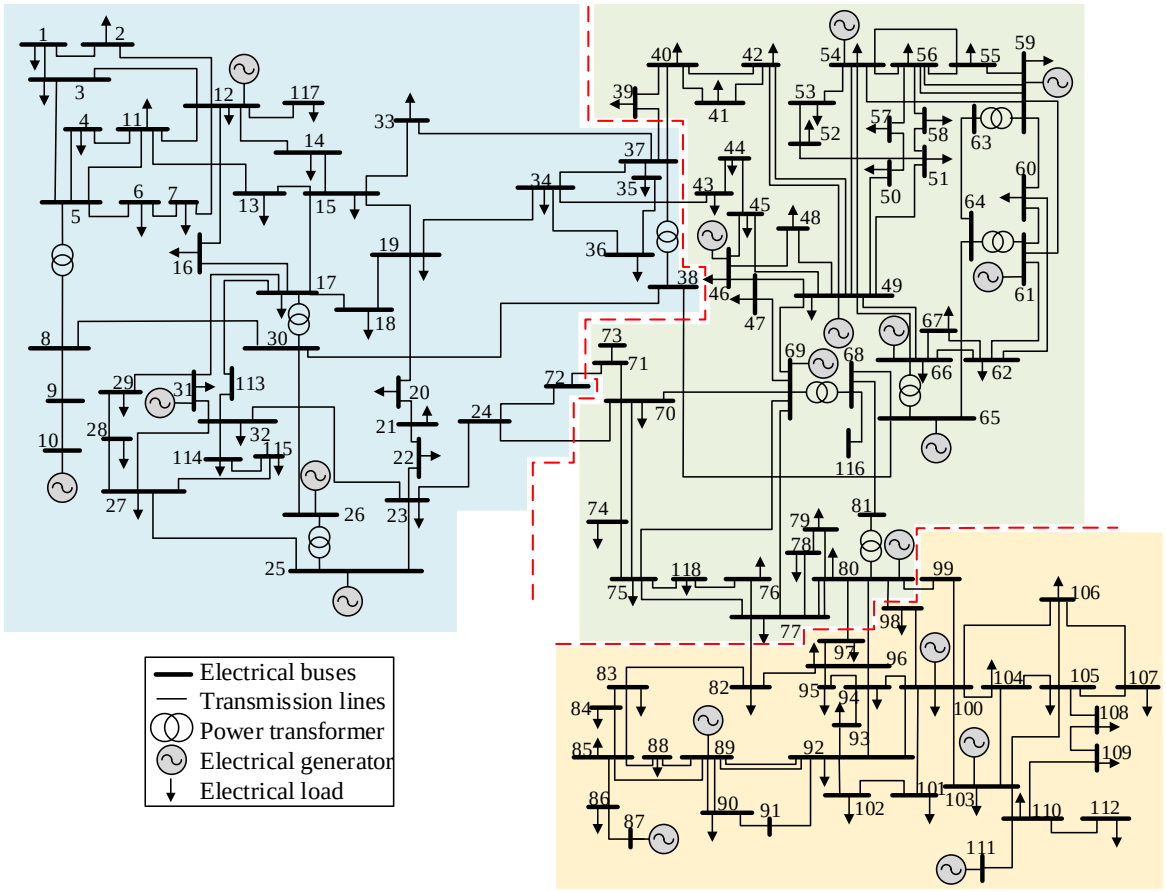

Figure 2.17: Islanding solution for minimal dynamic coupling of the IEEE 118-bus test system split into three islands

The solution found using the existing approach [56] is compared to this solution to verify the accuracy of the proposed methodology. When considering the same coherent groups of generators, the existing approach identifies the following weak connections 24-70; 71-72; 38-65; 43-44; 40-41; 40-42; 75-77; 76-77; 69-77; 77-78; 77-80; 80-97; 80-98; 80-99. The quality of islands 1, 2 and 3 (measured in terms of the quality index (2.25)) are 95.9%, 89.7% and 93.2%, respectively. Thus, the quality of the islanding solution for minimal dynamic coupling identified using the existing approach is 89.7%.

As it can be noticed, the proposed methodology improves the quality of the clustering over the existing approach [56]. In terms of the computational efficiency of the proposed methodology, it was found in the simulations that no significant improvement was achieved and both techniques determined the solution in approximately 163.20 ms.

2.4.5.4. Evaluating the Computational Efficiency of the Proposed Methodology

The runtime of the proposed methodology is equal to the runtime of the coherency identification plus the runtime of the determination of the weak connections. Table 2.7 shows the average runtime (over 100 trials) of the proposed methodology. In order to compare the computational efficiency of the new methodology, a similar study was carried out using the existing approach [56], and the results are also shown in Table 2.7.

As it can be noticed, the proposed methodology for determining islanding solutions with minimal dynamic coupling is computationally more efficient than the existing approach. The computational times shown in Table 2.7 highlight the benefits of the new methodology. It is important to mention that the improvement in computational efficiency offer by the methodology is due to the improvement achieved in the coherency identification.

Table 2.7: Computational time for determining islanding solutions for minimal dynamic coupling using the proposed methodology and the existing approach

Test System	Runtime using the proposed methodology (ms)	Runtime using the existing approach (ms)
IEEE 9-bus	21.58	26.32
New England 39-bus	45.73	55.25
IEEE 118-bus	176.12	199.00

2.5. Summary

This chapter has presented a methodology that can rapidly identify coherent groups of generators in large-interconnected power systems. The normalised spectral clustering-based methodology uses the eigenvectors associated with the normalised Laplacian matrix of a reduced dynamic graph (the graph that represents the extended power system reduced to only the internal generator buses) to embed this graph in a Euclidean space, and then projects the data-points on to a unit sphere. The projection of the data-points on to a unit sphere enables the visualisation of the coherent groups of generators to be created. Overall, the methodology avoids the use of recursive algorithms (*k-means*) and, more importantly, it does not require Gaussian elimination with complete pivoting to determine the reference generators of each coherent group, representing an important improvement in the computational efficiency of the approach compared to the classical slow coherency theory.

This chapter has also proposed a methodology that can determine islanding solutions for minimal dynamic coupling, i.e., a technique that can determine the weak connections between buses with strong dynamic coupling. The weak connections are determined using sensitivity factors between the voltage phase angles of the load buses and the variations in the rotor angles of the generators. The new methodology clusters the points on the unit sphere and takes into account the overall dynamic coupling between buses. These factors have considerably improved the computational efficiency and the accuracy of the proposed methodology compared to the existing approach.

The methodologies proposed in this chapter have been illustrated using the IEEE 9-bus, New England 39-bus and IEEE 118-bus test systems. Simulation results have demonstrated that the proposed methodology for identifying coherent groups of generators offers the same level of accuracy as the slow coherency algorithm but is computationally more efficient. Furthermore, these results also have also shown that the proposed methodology for determining an islanding solution with minimal dynamic coupling improves the accuracy of the results whilst maintaining the same efficiency as the existing approach for determining weak connections.

Chapter 3. Weak Areas Determination and Optimal PMU Placement

Chapter 3 introduces a methodology that is used to determine the weak areas across a power system. These weak areas are physically interpreted as the areas in the electrical network where, based on the dynamic coupling between the system buses, multiple weak connections between the coherent groups of generators can be found. This chapter also implements two graph theory based techniques – the concept of a dominating set and a tree search algorithm – that can be used to optimally place PMUs to monitor these weak areas.

The weak areas consist of the load buses that are on the periphery of the islands. Hence, the electrical buses contained in the weak areas are as strongly connected to buses in one island as they are to buses in another island. These areas can be used to determine islanding solutions using a second objective function; for example, minimal power imbalance. Furthermore, the optimal placement of PMUs to monitor the weak areas can support Intentional Controlled Islanding (ICI) schemes, as real-time information will be available to compute the power flow in the lines and thus the power balance in the islands. Additionally, this optimal placement can assist operators during Parallel Power System Restoration (PPSR) as the electrical variables – voltage magnitudes and phase angles – at the boundary buses can be constantly monitored.

3.1. Determination of the Weak Areas

The islanding of the power system across the absolute weakest connections determined in the previous chapter enhances the transient stability of the islands [5, 56]. However, the load generation balance within the future islands is not taken into account, and this may unnecessarily increase the amount of load to be shed and generation to be rescheduled after the controlled separation [54]. Moreover, splitting the power system across the weakest connections may cause excessive power flow disruption. This may cause the lines that

remain connected in the islands to become overloaded, and lead to the deterioration of the integrity of the islands and increase the risk of cascading outages [4].

Therefore, this chapter presents a methodology that is used to determine the weak areas across the power system. These weak areas are physically interpreted as the areas (zones) in the network where, based on the dynamic coupling between the system buses, multiple weak connections between the coherent groups of generators can be found. Hence, the load buses included in the weak areas are as strongly connected to one adjacent island as they are to another adjacent island, where the strength of connection is measured in terms of the dynamic coupling between the system buses. Therefore, it is more likely that islanding solutions will separate the system within these areas. The set of electrical buses included in the weak areas can potentially be used to determine islanding solutions that take into consideration a second objective function, such as minimal power imbalance.

In this chapter, the weak areas consist of the peripheral nodes that can be visualised on the unit sphere created in the previous chapter. Since these nodes are on the periphery of the islands, they can be moved from one island to another in order improve the load generation balance within the islands, without affecting the transient stability of the future islands.

This chapter only aims to identify these weak areas only, which will be used in the next chapter to determine islanding solutions that will create electrical islands with reduced load generation imbalance, while taking into account the transient stability of the future islands.

3.1.1. Graph Representation of the Electrical Power System

This chapter utilises the dynamic graph G_D given by (2.9) to determine the weak areas. The weak areas are defined as an extension of the weak connections. Determining the weak areas in the power system is equal to determining the load-nodes in the dynamic graph G_D that have similar strength of connection to both subgraphs. The load buses of the system that are more likely to be included in the weak areas are represented by those load-nodes of the dynamic graph that are on the periphery of the clusters, i.e., the load-nodes that are represented by the data-points between the clusters visualised on the unit sphere created in the previous chapter.

3.1.2. Definition of Graph Theoretic Concepts

The methodology uses the same graph theoretic concepts as those presented in Section 2.4.2 to determine the weak areas between coherent groups of generators. It is important to note that there are (r–1) weak areas for the r electrical islands to be created.

3.1.3. Formulation and Methodology for Determining Weak Areas in the Power System

The problem of determining weak areas can be seen as the problem of determining a set of cutsets for reduced dynamic coupling. Hence, the problem of determining the weak areas is a natural extension of the problem of determining the weak connections. Indeed, the weak areas are the areas across the power system where multiple weak connections can be found.

The concept of weak areas emerges from observing during the determination of the weak connections that certain load-nodes can be defined as belonging to the "core" of the island and other nodes as belonging to the "periphery" of the islands. For example, the spectral embedding on the unit circle $\mathbb{S}^1$ shown in Figure 2.12 for the dynamic graph of the IEEE 9-bus test system indicates that the load-nodes v_{L5} and v_{L6} are as close to the dynamic centroid $\boldsymbol{\mu_1}$ as they are to the dynamic centroid $\boldsymbol{\mu_2}$, i.e., these nodes are on the periphery of both groups. Indeed, it can be observed in Table 2.6 that the spherical distance between the data-points that represent these load-nodes and the dynamic centroids $\boldsymbol{\mu_1}$ and $\boldsymbol{\mu_2}$ is similar.

The concept of weak areas defines areas between the buses with strong dynamic coupling, which can be used to implement a second objective function for ICI. This would allow a final islanding solution to be created that offers reduced dynamic coupling between the islands and either reduced load generation imbalance or reduced power flow disruption. This is explained in the next chapter.

In order to determine the weak areas in the power system, the similarity matrix **S**, previously used to create the sets $V_{D1},\ldots,V_{Dr}$, is used. The weak areas are identified by extending the weak connections based on the strength of the connectivity of each load-node

with the rest of their set. In order to extend the weak connections, a threshold ε is defined. Section 3.1.3.1 introduces a heuristic way used in this thesis to compute value of ε.

A load-node will be assigned to the weak area between its set and another set if the relevant entries in **S** are sufficiently similar, where similarity is determined by a predefined threshold ε. For example, let the load-node $v_{Li} \in V_{DLD}$ be a member of the set V_{Dk}. This load-node is then assigned to the weak area between the set V_{Dk} and the set V_{Dl} if the inequality (3.1) is satisfied.

$$\mathbf{S}(i,l) \le (1+\varepsilon)\mathbf{S}(i,k)^{\min} \tag{3.1}$$

In (3.1), $\mathbf{S}(i,k)^{\min}$ is the smallest element in the i^{th} row of **S**, and $\mathbf{S}(i,l)$ corresponds to the entry for the l^{th} dynamic centroid. This inequality (3.1) defines the membership of the load-node v_{Li}.

3.1.3.1. Determination of the Value of ε in the Weak Area

The methodology explained above requires the definition of the threshold ε to determine the weak areas. This section introduces a heuristic approach for defining the value of ε. In the simulations, this approach was found to provide suitable results, i.e.,, only electrical buses that are between strongly-connected areas are included in the weak areas. The heuristic approach considers the results of the weak connection solution, and studies the spherical distances between the data-points that represent the load-nodes in the defined set and the dynamic centroid of that cluster. The approach is explained below.

Let $V_{DLDk} \subset V_D$, $k = 1,\ldots,r$, be the subsets of load-nodes created by the weak connection solution. The load-node v_{Li}, $i = 1,\ldots,n$, belongs to the cluster V_{DLDk} if, and only if, the spherical distance on the unit sphere $\mathbb{S}^{r-1}$ between the data-point $\mathbf{y}_i^{DLD}$ and the dynamic centroid $\boldsymbol{\mu}_k$ is the minimum value in the i^{th} row of the similarity matrix **S**.

For example, consider Table 2.6 in the case of the IEEE 9-bus system, and note that the spherical distance between the load-node v_{L1} and the dynamic centroid $\boldsymbol{\mu_1}$ is the minimum entry of that row. Hence, the load-node v_{L1} belongs to Island 1. Similar analysis can be performed for the remaining nodes, and the weak connections shown in Figure 2.13 can be obtained. When the subsets $V_{DLD1},\ldots,V_{DLDr}$ are all determined, the mean spherical distance between the data-points included in the set V_{DLDk}, $k=1,\ldots,r$, and the dynamic centroid $\boldsymbol{\mu}_k$, denoted by $aveg(\mathbf{S}_k)$, is computed for each cluster as follows:

$$aveg(\mathbf{S}_k)=\frac{1}{|V_{DLDk}|}\sum_{v_{Li}\in V_{DLDk}}\mathbf{S}(i,k) \tag{3.2}$$

where $\mathbf{S}(i,k)$ is the spherical distance between the data-points $\mathbf{y}_i^{DLD}$ that represent the load-nodes v_{Li} and the centroids $\boldsymbol{\mu}_k$. When (3.2) is computed for each cluster, the minimum mean $\min_{k=1,2,\ldots r}\left(aveg(\mathbf{S}_k)\right)$ and maximum mean $\max_{k=1,2,\ldots r}\left(aveg(\mathbf{S}_k)\right)$ are used to calculate the value of ε as follows.

$$\varepsilon=\frac{\min_{k=1,2,\ldots r}\left(aveg(\mathbf{S}_k)\right)}{\max_{k=1,2,\ldots r}\left(aveg(\mathbf{S}_k)\right)}*100 \tag{3.3}$$

The following example is used to illustrate the empirical approach. Consider Table 2.6 in the case of the IEEE 9-bus test system. The average spherical distance for Island 1 and Island 2 are $aveg(\mathbf{S}_1)=0.4376$ and $aveg(\mathbf{S}_2)=0.2576$, respectively. Using (3.3), the value of ε is then found to be 63%. This corresponds to the value of ε used in the example of the weak areas in the IEEE 9-bus test system shown in Section 3.1.4.

3.1.4. Simulation Examples

The weak areas in the three test networks previously used are determined in this section. These weak areas are used in the next sections for potential applications.

3.1.4.1. IEEE 9-Bus Test System

The weak areas are initially determined for the IEEE 9-bus system. Thus, Table 2.6 is used. In order to determine the weak areas in this test system, the threshold beyond the weak connections must be defined. Using the empirical approach explained in Section 3.1.3.1, the threshold ε is found to be 63%. As noticed in Table 2.6, the spherical distances between the load-nodes v_{L5} and v_{L6} and the dynamic centroids $\boldsymbol{\mu_1}$ and $\boldsymbol{\mu_2}$ are relatively similar. Thus, these nodes were previously defined to be in the "periphery" of the clusters. In the case of the load-node v_{L5}, the smallest spherical distance is to the centroid $\boldsymbol{\mu_2}$ (0.5760). Hence, this load-node was included in Island 2 in the previous section (see Figure 2.13).

The threshold ε is then used in the inequality (3.1) and the range $[0.2016\text{-}0.9504]$ is defined. Since the spherical distance between the data-point representing the load-node v_{L5} and the centroid $\boldsymbol{\mu_1}$ (0.6754) is within that range, the load-node v_{L5} is included in the weak area. Physically, this means that the connection between bus 5 and Island 2 is approximately as strong as the connection between bus 5 and Island 1. A similar conclusion is drawn for the load-node v_{L6}. Therefore, the weak area is as shown in Figure 3.1.

3.1.4.2. New England 39-Bus Test System

The weak areas are also determined for the New England 39-bus test system. Since two islands were created in the previous section, there is only one weak area. The implementation of the heuristic approach for determining a value of ε defines a threshold ε = 75%. Then, by using the similarity matrix **S** created in Section 2.4.5.2 and associated with the spectral embedding of the network on the unit circle (Figure 2.15), the weak area shown in Figure 3.2 can be found. As noticed, only the load-node v_{L8} is included in the weak area. This means that the buses 1 and 9 are strongly connected to the generator G10.

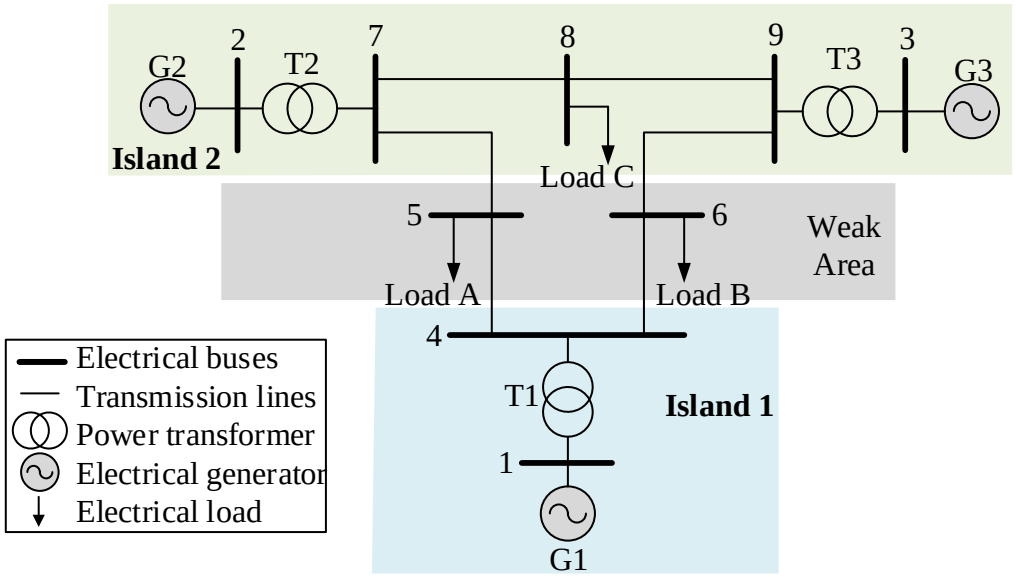

Figure 3.1: Weak area in the IEEE 9-bus test system for two islands

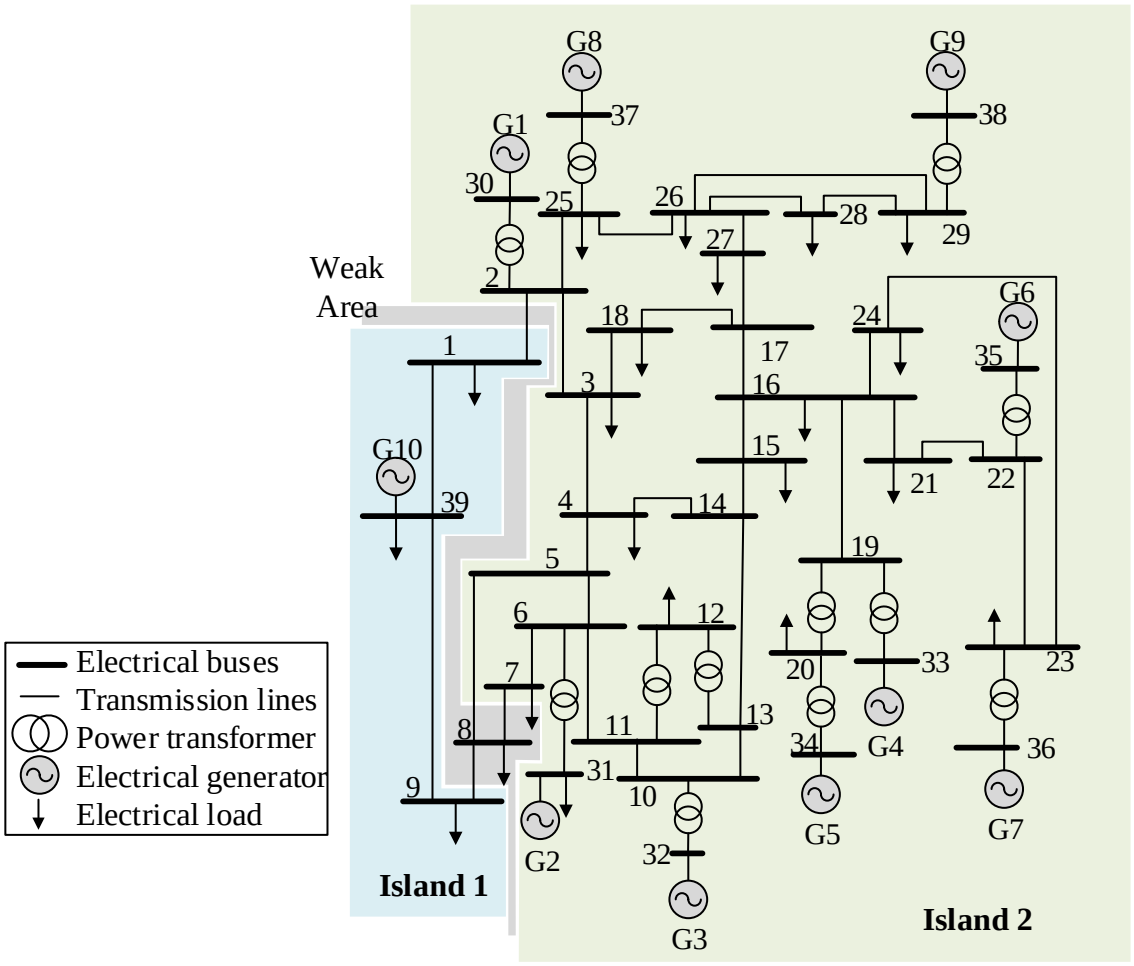

Figure 3.2: Weak area in the New England 39-bus test system for two islands

3.1.4.3. IEEE 118-Bus Test System

The weak areas in the IEEE 118-bus test system can also be found. In this test case, the scenario of three islands is considered, thus, two weak areas are identified. A threshold $\varepsilon = 75\%$ is defined using the heuristic approach explained in Section 3.1.3.1. It is important to note that the threshold ε varies for every system. In practical implementations, this value depends on the dynamic properties of the system (inertia constant of the machines and dynamic coupling between generators). Figure 3.3 shows the weak areas. It must be noted that the weak area between Island 1 and Island 2 is different to the weak area between Island 2 and Island 3.

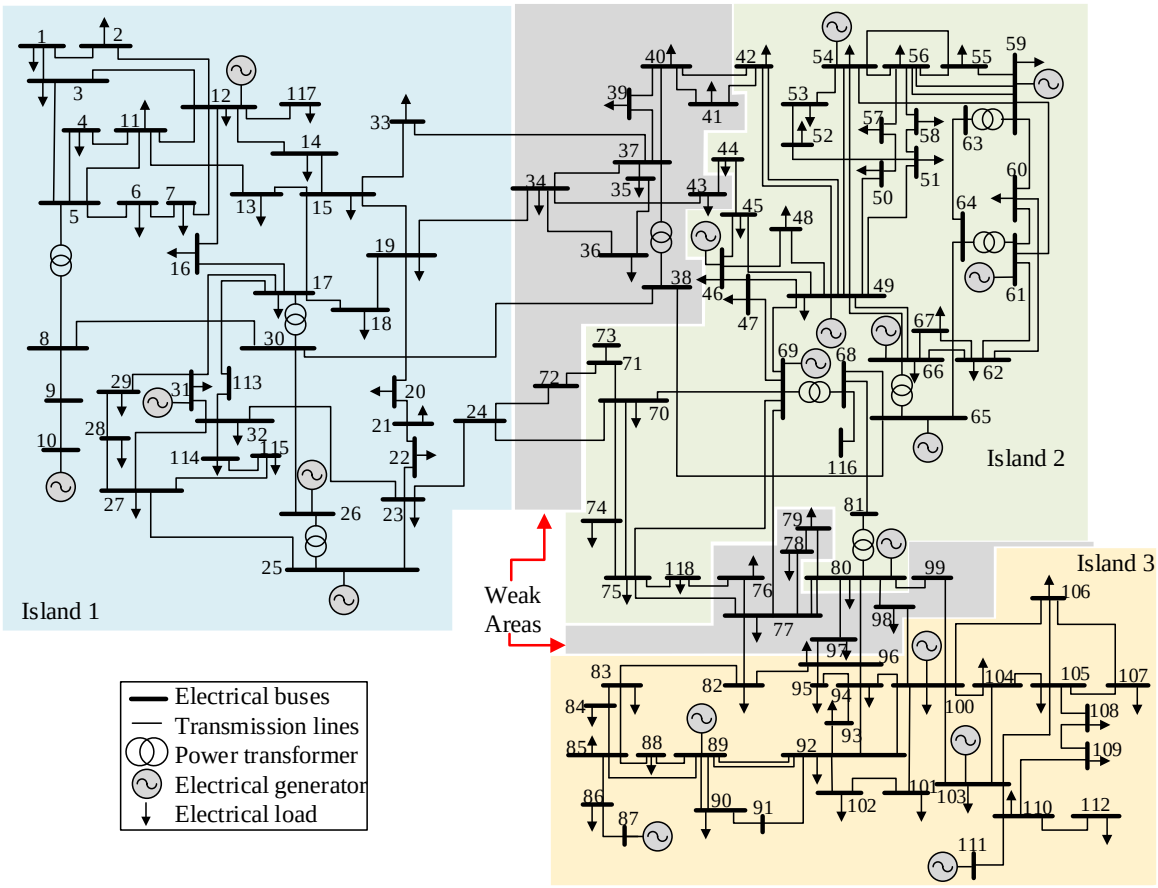

Figure 3.3: Weak areas in the IEEE 118-bus test system for three islands

3.2. Optimal PMU Placement across the Weak Areas

The optimal placement of PMUs refers to the determination of the minimum number of these devices that need to be placed across the network to monitor the power system [113]. This is important to ensure observability of the system, whilst reducing the number of these devices, as they are costly and cannot be allocated, at the moment, at every system bus.

In this chapter the optimal placement of PMU is constrained to the optimal allocation of these devices across the weak areas and the boundary buses only. The boundary buses are represented by the nodes that belong to an island but are connected to a node in a weak area. For example, buses 19 and 33 in Figure 3.3 are boundary buses as they are connected to bus 34 and 37, respectively, which are in the weak areas of the IEEE 118-bus test system. The criterion that is used in this thesis is full observability of the buses in the weak areas. In practice, this may not be very accurate due to the multi-objective nature of the PMU placement problem. Two different graph theory based techniques are implemented for the optimal placement of PMUs across the weak areas. The first approach is based on the concept of a dominating set and the second approach is based on a tree search algorithm.

The optimal placement of PMUs presented in this chapter is important to monitor the weak areas. This can benefit ICI schemes, as real-time information will be available to compute the power flow in the lines and thus the power balance in the islands or power flow disruption between islands. This can also assist operators during PPSR as the electrical variables – voltage magnitudes and phase angles – at the boundary buses can be constantly monitored and such information can be used during the resynchronisation of the islands.

When the (r–1) weak areas are determined, r – 1 new undirected graphs that describe these weak areas are defined. Each of these graphs is defined as follows:

$$G_S = (V_S, E_S) \tag{3.4}$$

where,

- the elements $v_i \in V_S$, $i = 1,\ldots,|V_S|$, denote the nodes of the new graph, and they represent the buses within the weak areas and the boundary buses. The set V_S is divided into two node subsets: the weak area-node subset representing the buses defined as being in the weak area, and the boundary-node subset that represent the boundary buses; and
- the elements $e_{ij} \in E_S$, $i, j = 1,\ldots,|V_S|$, denote the edges of the new graph, and they represent the branches connecting the buses within the weak area with one another, and the boundary buses.

Figure 3.4 shows the graph G_S produced by the weak area of the IEEE 9-bus test system. As noticed, the nodes are relabelled, and the boundary nodes represent the load-nodes v_{L4}, v_{L7} and v_{L9} of the dynamic graph G_D given by (2.9). It should be mentioned that the graph maintains the existing load-node v_{L8} as this connects two different boundary-nodes with weak area-nodes, i.e., it is another boundary-node.

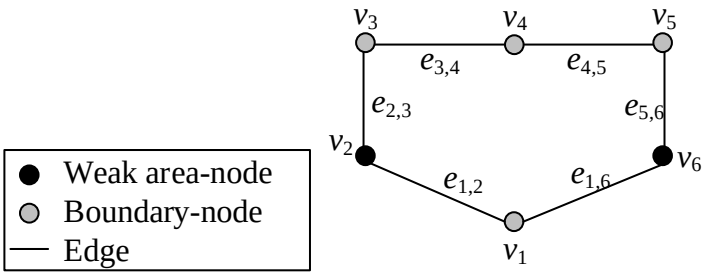

Figure 3.4: IEEE 9-bus test system reduced to represent the weak area and its boundary

3.2.1. Optimal PMU Placement

The undirected graph G_S can be used to place PMUs. However, this solution will be equivalent to the case when zero injection buses are not taking into account in the PMU placement problem. Considering zero injection buses increases the number of PMUs to be allocated, and this is neither optimal nor economical [113]. Thus, graph reductions are introduced to take advantage of zero injection buses, and thus reduce the number of PMUs.

Without loss of generality, it is assumed in this thesis that every PMU has a sufficient number of channels to measure the current phasors through all of the branches incident to the corresponding PMU buses (i.e., the buses in which PMUs are installed). This thesis does not consider conventional measurements; rather, it is a pure PMU solution, taking advantage of the uniquely high reporting rates possessed by the PMUs.

3.2.2.1. Graph Reductions Rules for PMU Placement

The main graph reduction used to take advantage of zero injection buses is achieved by arbitrarily merging each node of the graph G_S that represents a zero injection bus with a neighbour node that represents a non-zero injection bus. For example, the nodes v_3 and v_5 in Figure 3.4 represent the buses 7 and 9 in the IEEE 9-bus test system and these buses are zero injection buses. Therefore, these nodes are merged with the node v_4 to produce the new graph shown in Figure 3.5. The resulting graph, denoted by G_{SN}, is then used to optimally place PMUs using the two techniques described below.

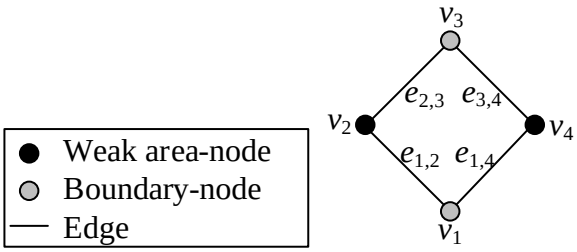

Figure 3.5: IEEE 9-bus test system reduced to optimally place PMUs

3.2.2.2. Optimal PMU Placement based on the Concept of Dominating Set

The concept of using a dominating set to place PMUs in power systems was initially implemented in [114]. However, the effect of zero injection buses was not taken into account. In this thesis, the concept of a dominating set is implemented to optimally place PMUs across only the weak areas, while taking into consideration the zero injection buses.

As detailed in Appendix A.8, the concept of a dominating set aims to find the set $S \subset V_{SN}$ such that every node $v_i \in V_{SN}$ is a neighbour of at least one node $v_j \in S$. Solving the

minimal dominating set problem for the graph G_{SN} will define the location of the minimal number of PMUs to be placed across the weak areas.

For example, the solution to the minimal dominating set problem in the graph shown in Figure 3.5 is $S = \{v_1, v_3\}$. This means that the optimal PMU placement in the IEEE 9-bus test system is at buses 4 and 8 as shown in Figure 3.6.

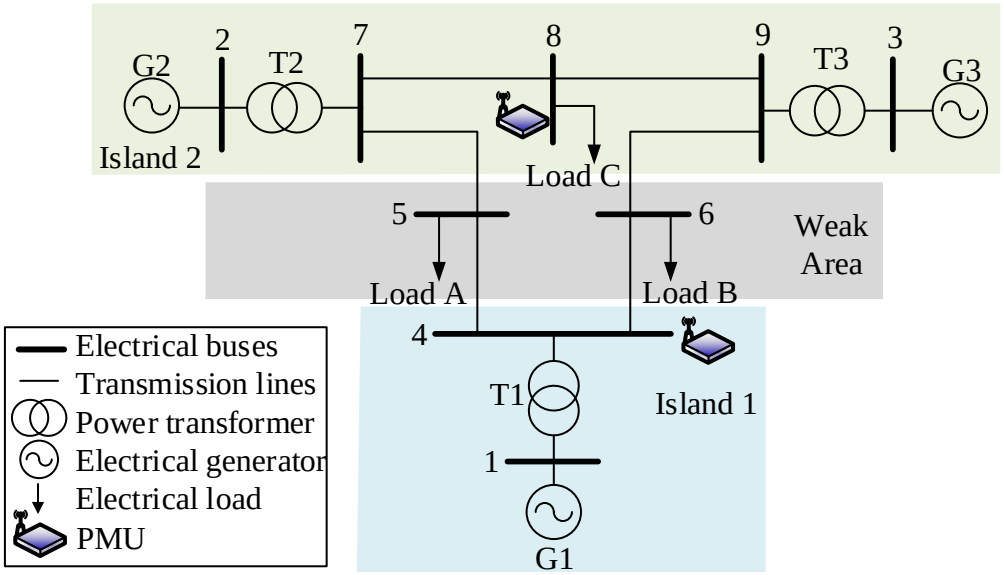

Figure 3.6: Optimal PMU placement to monitor the weak area of the IEEE 9-bus test system

3.2.2.3. Optimal PMU Placement based on a Tree Search Algorithm

A tree search algorithm can also be used to optimally place PMUs across the weak areas. Tree search algorithms were initially used to place PMUs across the entire power system in [113]. While the existing approach [113] aims to place PMUs across the entire power system for incomplete observability, the approach proposed in this thesis aims to place PMUs across only the weak areas for complete observability of these weak areas, which would serve to monitor these areas for the purpose of ICI for blackout prevention and resynchronisation of the islands during PPSR.

The technique uses the reduced graphs G_{SN} (Figure 3.5). When the reduced graphs of the weak areas are obtained, the Depth First Search (DFS) algorithm, described in Appendix

A.9.1, is used to determine a DFS-tree of each graph, and a PMU is placed every two nodes in the tree, i.e., at alternate nodes in the tree. The root node of each DFS-tree is selected as the node with the greatest degree in the graph G_{SN}, i.e., the node with the largest number of edges connected to it. When all of the nodes have the same degree, the root node is selected as the node with the lowest number as its label.

For example, the DFS-tree of the graph G_{SN} shown in Figure 3.5 takes the node v_1 as the root node, as presented in Figure 3.7. If a PMU is allocated at node v_1, the next PMU is then placed at node v_3. In the actual power system, this means that PMUs are placed at buses 4 and 8, as shown in Figure 3.6. As noticed, in this particular case, the solutions given by both techniques (the concept of a dominating set and a tree search algorithm) are the same. Although these techniques may produce different PMU placements, as shown in Table 3.1, they will both result in the same number of PMUs to be allocated across the weak areas.

Figure 3.7: DFS-tree of the reduced IEEE 9-bus test system to optimally place PMUs

3.2.2.4. Optimal PMU Placement: Examples

The two approaches presented above are used to optimally place PMUs across the weak areas of the other two test networks that have previously been used. The optimal PMU placement for these two test networks is shown in Table 3.1. As noticed, the number of PMUs required in the case of the New England 39- and IEEE 118-bus test systems are four and ten, respectively.

Table 3.1: Optimal PMU placement to monitor the weak areas of the New England 39- and IEEE 118-bus test systems

Test System	Method	Location
New England 39-bus	Dominating set	3; 4; 8; 39
	Tree Search (root node at bus 39)	3; 7; 9; 39
IEEE 118-bus	Dominating set	24; 34; 40; 42; 44; 65; 75; 77; 80; 96
	Tree Search (root nodes at bus 34 and 80)	24; 34; 38; 40; 42; 44; 75; 77; 80; 96

3.3. Summary

This chapter has presented a methodology that extends the concept of weak connections to define weak areas. The weak areas are the zones across the power system where, based on the dynamic coupling between the system buses, multiple weak connections between the coherent groups of generators can be found. The weak areas contain the buses that are as strongly connected to buses in one island as they are to buses in another island; hence, they could be used to determine islanding solutions using a second objective function. These weak areas are used in the next chapter to determine islanding solutions that will ultimately contain reduced power imbalance while taking into account the transient stability of the islands.

This chapter has also presented two graph theory based techniques that can be used to optimally place PMUs across the weak areas and the boundary buses. The criterion that is used in this thesis is full observability of the buses in the weak areas. In practice, this may not be very accurate due to the multi-objective nature of the PMU placement problem. Hence, further research is required to adequately allocate PMUs across the entire power system. The optimal PMU placement that is suggested in this thesis aims to support ICI schemes, as real-time information will be available to compute the power flow in the lines and the power balance in the islands. Additionally, the optimal PMU placement can assist system operators during PPSR as the electrical variables – voltage magnitudes and phase angles – at the boundary buses can be constantly monitored.

Chapter 4. Intentional Controlled Islanding for Minimal Power Imbalance: A Constrained Cutset Matrix-Based Methodology

Chapter 4 introduces a constrained cutset matrix-based methodology to determine islanding solutions for minimal power imbalance, while ensuring that each island contains only coherent generators. The new Intentional Controlled Islanding (ICI) methodology can also constrain any branch to be excluded from the solution, and can explore the vast combinatorial space to always find the islanding solution that produces the minimal power imbalance within the islands. The previously determined weak areas are utilised to consider the transient stability of the interconnected power system. This also reduces the search space and improves the efficiency of the proposed islanding methodology.

The introduced ICI methodology benefits the controlled islanding of power systems as strong-dynamically connected islands with reduced power imbalance are ultimately created. Hence, the transient stability of the islands is expected to be enhanced, and the amount of load to be shed and generation to be rescheduled following system splitting is significantly reduced. Furthermore, the methodology requires much less computation compared to the conventional islanding methods while maintaining the accuracy of the islanding solution.

ICI methods for minimal power imbalance minimise the amount of load to be shed and the amount of generation to be rescheduled following splitting, and they enhance the transient stability of the islands by creating subsystems with only coherent generators. As discussed in Section 1.5.1.2, there are numerous ICI methods for minimal power imbalance [44-47, 50-52, 57-61]. However, most of these ICI techniques do not satisfy the vital real-time requirement that is required during the practical implementation of ICI schemes.

Therefore, this chapter introduces a novel ICI methodology that uses the concept of a constrained cutset matrix to create electrical islands with reduced power imbalance, while ensuring that each subsystem contains only coherent generators. The concept of constrained

cutset matrix is an inherent extension of the cutset matrix – the matrix that contains multiple cutsets to partition a graph, as presented in Appendix A.6.4 – and aims to improve the efficiency of the new methodology, by reducing the complexity of the combinatorial problem. The general idea of the new approach is to constrain certain buses to be in a specific island and to allow other buses – referred to as the "*free nodes*" – to be included in any of the possible islands. This defines a set of suitable cutsets – islanding solutions – that is then used to determine the solution that produces the minimal imbalance within the islands, as further detailed in Section 4.4.

By constraining certain buses to be in a given island, several branches are excluded from the solution space. This is important to exclude branches that are deemed to be unsuitable for islanding, e.g., transformer. Moreover, by considering only a suitable and small subset of buses that can be included in any of the future islands – the subset of "*free nodes*" – the computational efficiency of the new methodology is significantly improved, while the accuracy of the results is maintained. It is important to mention that the subset of "*free nodes*" must be adequately selected. Therefore, the constrained cutset matrix-based methodology uses the results of Chapter 3, and defines the nodes within the determined weak areas as the "*free nodes*". As discussed earlier, the nodes in the weak areas represent the buses in the system that can be clustered in any island based on a second criterion, for example, minimal power imbalance. Indeed, this can be seen as another application of the previously defined weak areas.

By defining the "*free nodes*" as those buses within the weak areas only, the proposed methodology not only accelerates the determination of an islanding solution for minimal power imbalance, but also creates islands that are strong-dynamically connected. The latter is achieved as the weak areas were determined between coherent groups of generators and they consist of load buses only (Section 3.1). Therefore, the islands created by the proposed methodology for minimal power imbalance contain only coherent generators, and this enhances the transient stability of the future islands, as previously discussed.

In the following sections of this chapter, the proposed methodology is presented and steady-state studies are performed to demonstrate its effectiveness – computational

efficiency and accuracy. It is assumed that the weak areas have been firstly determined. Thus, the "*free nodes*" are known prior to the implementation of the approach.

4.1. Graph Representation of the Electrical Power System

The behaviour of a power system with *n* buses, *m* generators and *l* branches following a disturbance is represented in this chapter as an edge weighted and directed graph. This digraph represents the active power flow in the branches, considering the associated direction, and is defined as follows:

$$H = \left(V, \bar{E}, \rho\right) \tag{4.1}$$

where,

- the elements $v_i \in V$, $i = 1, \ldots, n$, denote the nodes of the digraph, and they represent the buses of the power system. To distinguish the generation buses from the load buses, the node set *V* is divided into two node subsets $V_{GN} \subset V$ representing the *m* generation buses, and $V_{LD} = V \setminus V_{GN}$ representing the $n - m$ load buses. The elements $v_i^{GN} \in V_{GN}$ and $v_i^{LD} \in V_{LD}$ are called generation- and load-nodes, respectively.

- the elements $e_{ij} \in \bar{E}$, $i, j = 1, \ldots, n$, denote the arcs of the directed graph, and they represent the branches of the actual power system. The direction of these arcs is given by the direction of the power flow in the branches. In this chapter, the notation $e_k = \left(v_i, v_j\right)$ is conveniently used.

- the number $w_{ij} = \rho\left(e_{ij}\right)$, $i, j = 1, 2, \ldots, n$, $\left(w_k = \rho\left(e_k\right), k = 1, 2, \ldots, \left|\bar{E}\right| = l\right)$, represents the weight factor associated with each arc $e_{ij} \in \bar{E}$ (active power flow). To accommodate network losses, the value of w_{ij} is calculated as follows.

$$w_{ij} = w_k = \begin{cases} \dfrac{|P_{ij}| + |P_{ji}|}{2} & \text{if } e_{ij} \in \bar{E}; \\ 0 & \text{otherwise.} \end{cases} \tag{4.2}$$

In (4.2), P_{ij} and P_{ji} represent the active power flow in the branch from bus *i* to bus *j*, and from bus *j* to bus *i*, respectively. It should be noted that the arc weights are all positive. As explained later, the direction of these weight factors is represented by the oriented incidence matrix $\mathbf{M_H}$ (A.25) associated with the digraph *H*.

Figure 4.1 shows the digraph representation of the IEEE 9-bus test system. The black dots – defined by the elements in the subset V_{GN} – represent the *m* generator buses. Furthermore, the grey dots – defined by the elements in the subset V_{LD} – represent the *n* – *m* load buses. The arrows illustrated in Figure 4.1 represent the arcs.

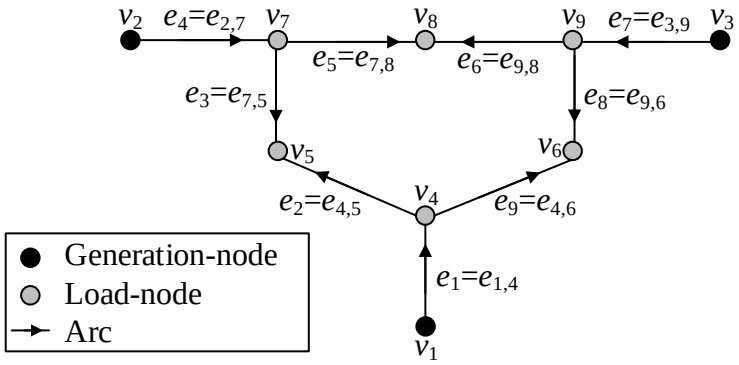

Figure 4.1: Digraph representation of the IEEE 9-bus test system for minimal power imbalance

4.2. Definition of Graph Theoretic Concepts

The constrained cutset matrix-based methodology presented in this chapter uses the following graph theoretic concepts to determine islanding solutions for minimal power imbalance, while ensuring that each island contains only coherent generators.

4.2.1. Oriented Incidence Matrix

The oriented incidence matrix $\mathbf{M_H}$ of the digraph *H* is given by (A.25). As detailed in Appendix A.6.2.2, this matrix represents the directed incidence between the nodes of the digraph and its arcs. In this application, the matrix $\mathbf{M_H}$ represents the direction of the power flow. The matrix $\mathbf{M_H}$ of the digraph shown in Figure 4.1 is presented in (A.26).

4.2.2. Oriented Cutset and Oriented Cut

As discussed in Appendix A.4.1.2, the oriented cutset $\bar{E}_S \subset \bar{E}$ is the set of arcs that must be removed to split the digraph *H* into *r* directed subgraphs $H_1,\ldots,H_r$, with node sets $V_1,\ldots,V_r$. Without loss of generality and due to the complexity of the islanding problem for minimal power imbalance, only the case of splitting the digraph into two disjoint digraphs is considered in this chapter. By applying parallel analysis, the case of splitting the network into more than two islands can be obtained, as explained in Section 4.5.3.

The oriented cut from V_1 to V_2, denoted by $cut(V_1,V_2)$, associated with the cutset $\bar{E}_S$ is the absolute value of the sum of the weight factors associated with the arcs from V_1 to V_2 minus the weight factors associated with the arcs from V_2 to V_1, and is given by (4.3).

$$cut(V_1,V_2) = \left| \sum_{\substack{v_i \in V_1 \\ v_j \in V_2}} w_{ij} - \sum_{\substack{v_i \in V_2 \\ v_j \in V_1}} w_{ij} \right| \tag{4.3}$$

For example, if the digraph shown in Figure 4.1 is partition across the oriented cutset $\bar{E}_S = \{e_2, e_8\}$, the cut associated with this oriented cutset will be equal to $|w_2 - w_8| = 19.88$ MW, where the arc weights can be obtained from Table A.2. In the islanding problem for minimal power imbalance an oriented cutset $\bar{E}_S$ consists of the arcs that represent the branches in the system that must be disconnected to create the islands, and the value of the cut corresponds to the power imbalance.

4.2.3. Label of the Node

The label of the node refers to the number of the island that the node belongs to. For example, the partition of the digraph shown in Figure 4.1 across the cutset $\bar{E}_S = \{e_2, e_8\}$ creates the node subsets $V_1 = \{v_1, v_4, v_6\}$ and $V_2 = \{v_2, v_3, v_5, v_7, v_8, v_9\}$. Then, the label of the nodes $\{v_1, v_4, v_6\}$ is "1" and the label of the nodes $\{v_2, v_3, v_5, v_7, v_8, v_9\}$ is "2", as they belong to Island 1 and 2, respectively.

In power system applications, certain nodes must have a specific label, i.e., they must be in a given island. For example, the generation-nodes that represent generators in a coherent group should have the same label, as the coherent generators must be grouped together and separated from the others. On the other hand, some nodes (mainly load-nodes) can be defined as "*free nodes*", as they can be included in any of the possible islands according to the results of a combinatorial optimization. The degree of freedom given to certain nodes creates multiple combinations. For example, consider that only the node v_5 in Figure 4.1 could be clustered in any of the two islands, and that all the other nodes must be in a specific island as shown in (4.4). Consequently, there are two possible combinations to label the nodes, and thus, to split *H* into two subgraphs (see (4.4)).

	v_1	v_2	v_3	v_4	v_5	v_6	v_7	v_8	v_9
$comb_1$	1	2	2	1	1	1	2	2	2
$comb_2$	1	2	2	1	2	1	2	2	2

(4.4)

4.2.4. Indicator Matrix

The indicator matrix, denoted by **C**, is the matrix that contains multiple combinations of node labels that would partition the digraph *H* into multiple digraphs. Each combination in **C** labels some nodes to be in a given island and combines the free-node labels. This is a combinatorial problem that can be effectively solved computing the permutations with repetitions [115] of the free-node labels. Each combination in **C** also includes the labels for the generation-nodes and any other constrained nodes so that each combination supplies a full set of labels that defines which island each node will be clustered into. Therefore, the *ij*-entry of the matrix **C** is equal to the label – the number $k = 1, 2$ – assigned to the node

$v_i \in V$ for the j^{th} combination. If there are χ "free nodes", then there will be $\zeta = 2^{\chi}$ possible combinations, i.e., the size of **C** is $n \times \zeta$.

For example, consider that the digraph shown in Figure 4.2 will be partitioned into two digraphs H_1 and H_2. Additionally, all the nodes are assumed to be "free nodes". Mathematically, there are 16 possible combinations (permutations with repetitions) to split H into two digraphs (see (4.5)); hence, the size of the matrix **C** in this case is 4×16. Nevertheless, this mathematical solution possesses some combinations that are not suitable in power systems. That is, they do not actually split the digraph, or the number of directed subgraphs induced by the corresponding cutset is larger than two. Furthermore, it should be noted that some combinations, e.g., $comb_2$ and $comb_{15}$ will produce the same cutset.

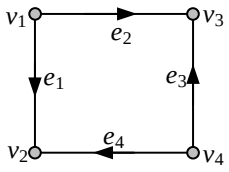

Figure 4.2: Example of a digraph with four nodes and four edges

$$\mathbf{C}^T = \begin{array}{|c|cccc|}\hline & v_1 & v_2 & v_3 & v_4 \\ \hline comb_1 & 1 & 1 & 1 & 1 \\ comb_2 & 1 & 1 & 1 & 2 \\ comb_3 & 1 & 1 & 2 & 1 \\ comb_4 & 1 & 1 & 2 & 2 \\ comb_5 & 1 & 2 & 1 & 1 \\ comb_6 & 1 & 2 & 1 & 2 \\ comb_7 & 1 & 2 & 2 & 1 \\ comb_8 & 1 & 2 & 2 & 2 \\ comb_9 & 2 & 1 & 1 & 1 \\ comb_{10} & 2 & 1 & 1 & 2 \\ comb_{11} & 2 & 1 & 2 & 1 \\ comb_{12} & 2 & 1 & 2 & 2 \\ comb_{13} & 2 & 2 & 1 & 1 \\ comb_{14} & 2 & 2 & 1 & 2 \\ comb_{15} & 2 & 2 & 2 & 1 \\ comb_{16} & 2 & 2 & 2 & 2 \\ \hline \end{array} \quad (4.5)$$

In order to determine whether a cutset is suitable or not, the rank of the digraph induced by the corresponding cutset can be utilised. As explained in Appendix A.3.9, the rank of the

digraph equals the number of nodes minus the number of connected components. Hence, if two islands will be created, the rank of the induced digraph must be equal to $n - 2$. For example, the implementation of the cutset induced by the $comb_2$ produces two digraphs. Thus, the rank of the resulting digraph is equal to 2 (4 – 2). Hence, it is concluded that the cutset induced by the $comb_2$ is feasible. Following this analogy, it can be concluded that the cutset induced by the $comb_7$ is not feasible as the rank of the resulting digraph is equal to $0 \neq 2$. Finally, it is concluded that the digraph shown in Figure 4.2 has six feasible cutsets, named $comb_2$, $comb_3$, $comb_4$, $comb_5$, $comb_6$ and $comb_8$ in (4.5).

The indicator matrix **C** can also be used to constrain certain nodes to belong to a given island. For example, assume that the nodes v_1 and v_4 must be in Island 1 and in Island 2, respectively. Furthermore, consider that the nodes v_2 and v_3 are "free nodes". Hence, they can be clustered in any of the two islands. Since two islands will be created and there are two "free nodes", four combinations $\left(\zeta = r^{\chi} = 2^2\right)$ will be obtained (see (4.6)). Again, to determine whether an induced cutset is feasible or not, the rank of the digraph produced by the removal of the induced cutset can be calculated. For this particular case, the four combinations presented in (4.6) are suitable in the sense that they certainly split the digraph into two disjoint digraphs.

$$\mathbf{C}^T = \begin{array}{|c|c|c|c|c|} \hline & v_1 & v_2 & v_3 & v_4 \\ \hline comb_1 & 1 & 1 & 1 & 2 \\ \hline comb_2 & 1 & 1 & 2 & 2 \\ \hline comb_3 & 1 & 2 & 1 & 2 \\ \hline comb_4 & 1 & 2 & 2 & 2 \\ \hline \end{array} \tag{4.6}$$

4.2.5. Oriented Constrained Cutset Matrix

A cutset matrix, also known as a *cut-edge* incidence matrix, is a well-known matrix used in graph theory to represent all the possible cutsets of a digraph [105]. The constrained cutset matrix $\mathbf{Q_H}$ is an extension of the cutset matrix that enables to constrain certain nodes to be clustered into a specific group. The constrained cutset matrix $\mathbf{Q_H}$ of the digraph H is the $\zeta \times l$ matrix computed in this thesis as follows.

$$\mathbf{Q_H} = -\mathbf{C}^T\mathbf{M_H} \tag{4.7}$$

The sign included in (4.7) aims to always define the orientation of the cutsets from V_1 to V_2. The non-zero entries in the i^{th} row of the constrained cutset matrix $\mathbf{Q_H}$ represent the arcs that must be disconnected to create the islands defined in the i^{th} column of the indicator matrix **C**. The *ij*-entry of $\mathbf{Q_H}$ is different from zero if the implementation of the i^{th} cutset requires the j^{th} arc to be removed to partition the digraph. For example, the constraint cutset matrix $\mathbf{Q_H}$ of the digraph shown in Figure 3.2 considering the indicator matrix **C** shown in (4.6) is presented in (4.8). The $cutset_1$, which produces the node subsets $V_1 = \{v_1, v_2, v_3\}$ and $V_2 = \{v_4\}$, requires the removal of the arcs e_3 and e_4. This solution can be confirmed observing Figure 3.2. It must be noted that the *ij*-entry of $\mathbf{Q_H}$ is equal to -1, 0 or 1, and the sign depends on the orientation of the arc, respect to the cutset orientation, see Appendix A.6.4 for details. It is positive when the arc goes from V_1 to V_2, and negative otherwise.

$\mathbf{Q_H}$ =

	e_1	e_2	e_3	e_4
$cutset_1$	0	0	-1	-1
$cutset_2$	0	1	0	-1
$cutset_3$	1	0	-1	0
$cutset_4$	1	1	0	0

(4.8)

4.3. Formulation of the ICI Problem for Minimal Power Imbalance

The proposed ICI methodology seeks to minimise the power imbalance – generation minus load – within each island, while ensuring that each island contains only coherent generators and that the islanding solution excludes certain branches. In this chapter, the coherent groups of generators are denoted by the node subsets V_{GN1} and V_{GN2}. Each of these dynamically coherent groups of generators must be separated into different islands to help the transient stability of the system when determining an islanding solution [44, 45, 47-49]. For example, the solution shown in Figure 4.3 assumes that the two coherent groups of generators are $V_{GN1} = \{v_1\}$ and $V_{GN2} = \{v_2, v_3\}$, and the islanding solution determined by the methodology clusters these coherent groups of generators in different islands.

The problem of minimising the power imbalance within each island can be formulated considering the power generation and consumption at the buses [44-46]. This active power balance within the islands is associated with the power transfer between them [58]. Hence, the ICI problem for minimal power imbalance can be reformulated to as minimising the power transfer between the partitions V_1, V_2 defined as follows:

$$\min_{V_1,V_2}\left(\left|\sum_{\substack{v_i\in V_1\\ v_j\in V_2}} w_{ij}-\sum_{\substack{v_i\in V_2\\ v_j\in V_1}} w_{ij}\right|\right) \tag{4.9}$$

subject to each island containing only coherent generators (4.10).

$$V_{GNk}\subset V_k \tag{4.10}$$

As noticed in (4.9)-(4.10), the ICI problem for minimal power imbalance aims to partition the power system into two islands, such that the k^{th} island contains the k^{th} group of coherent generators. The new methodology will also aim to constrain any branch to be excluded from islanding solutions. This is important to exclude branches that are deemed to be unfeasible for islanding, e.g., transformers, lines with unavailable circuit breakers or critical lines that based on stability studies are defined as lines that maintain the stability of the islands. To exclude the branches, a new arc subset $\bar{E}_C\subset\bar{E}$ that represents branches that must not be disconnected is defined. Given this new set of constraints, the new ICI problem that the methodology attempts to solve is finally reformulated as follows.

$$\min_{V_1,V_2} cut\left(V_1,V_2\right) \tag{4.11}$$

subject to

$$V_{GNk}\subset V_k,\ \text{and}\ \bar{E}_C\cap\bar{E}_S=\varnothing.$$

The condition $\bar{E}_C\cap\bar{E}_S=\varnothing$ means that the proposed ICI methodology only considers partitions with cutsets $\bar{E}_S$ not containing any excluded-arcs from $\bar{E}_C$.

4.4. Methodology for Solving the ICI Problem for Minimal Power Imbalance

The proposed methodology to solve the ICI problem for minimal power imbalance (4.11) initially uses (A.25) to create the oriented incidence matrix $\mathbf{M_H}$ associated with the digraph *H*. It then builds the indicator matrix **C**, providing thus the label $k = 1, 2$ to the nodes. As previously explained, all the nodes could mathematically be assigned to any island. Nevertheless, in power system application some nodes are constrained to be in a specific island. Therefore, the nodes within the previously determined weak areas are used with the objective to reduce the size of the combinatorial optimization, create islands that are strong-dynamically connected and group together the coherent groups of generators. Hence, only the nodes that belong to the weak areas are defined as "free nodes". For example, in the case of the IEEE 9-bus test system, only the nodes v_5 and v_6 are "free nodes". Hence, the indicator matrix **C** shown in (4.13) is obtained. It should be noted that only nodes included in the subset of load-nodes $\left(v_i^{LD} \in V_{LD}\right)$ are considered as "free nodes", as the nodes included in the subset of generation-nodes $\left(v_i^{GN} \in V_{GN}\right)$ are assigned to a specific island based on the coherency results.

To constrain any branch to be excluded from islanding solutions, the ICI methodology provides the same label to the nodes incident to the corresponding arc. For example, if the arc e_3 in Figure 4.1 must be excluded from the islanding solution, the label associated with the nodes v_5 and v_7 will be equal to "2", as node v_7 already belongs to Island 2. The branches that should not be included in islanding solutions are detailed in [44-46]. For example, transformer should not be included in the islanding solution as sudden disconnections of these elements can deteriorate them and cause aging problems [44].

The proposed methodology then computes the oriented constrained cutset matrix $\mathbf{Q_H}$ using (4.7). For example, the constrained cutset matrix of the digraph shown in Figure 4.1 is illustrated in (4.14). The matrix $\mathbf{Q_H}$ then contains multiple cutsets, and some of these cutset may not be feasible, as previously explained. Therefore, the methodology computes the rank of the digraph (A.12) induced by the removal of the corresponding arcs for each

combination. For example, consider Figure 3.1 and its matrix $\mathbf{Q_H}$ shown in (4.14). Furthermore, remove from Figure 3.1 the arcs e_3 and e_8 and note that the resulting digraph is indeed split into two disjoint digraphs. Hence, the cutset $\bar{E}_S = \{e_3, e_8\}$ is feasible. This procedure is repeated for all the cutsets shown in $\mathbf{Q_H}$, removing the unfeasible cutsets and maintaining only those solutions than could actually be implemented in power systems.

The methodology then computes the *l*-vector **w**, which is a column vector with the j^{th} row equal to the edge weight (4.2). For example, in the case of the IEEE 9-bus test system, the vector **w** is shown in (4.15). Then, by calculating the absolute value of the product between the matrix $\mathbf{Q_H}$ and the vector **w**, the power imbalance induced by each cutset can be determined. The islanding solution that produces the minimal power imbalance is then determined by minimising the value of the cut, i.e., $\min\left(cut\left(V_1, V_2\right)\right)$, where the cut $cut\left(V_1, V_2\right)$ can be computed as in (4.12).

$$cut\left(V_1, V_2\right) = \left|\mathbf{Q_H}\mathbf{w}\right| \tag{4.12}$$

For example, the islanding solution producing the minimal power imbalance in the case of the IEEE 9-bus test system is obtained across the cutset $\bar{E}_S = \{e_2, e_8\}$, and the cut associated with this cutset is equal to 19.88 MW.

4.5. Simulations Examples

This section presents three simulation examples of islanding solutions for minimal power imbalance. The results of the new methodology are compared with those obtained using an implementation of the OBDD-based method [44-46]. As detailed in [44-46], the OBDD-based method uses Boolean theory, and requires the definition of a threshold β to indicate the power imbalance allowed with each island, usually very small. The definition of this threshold represents a major disadvantage of the existing approach [49]. Moreover, OBDD-based methods can only be implemented in scaled systems containing no more than 40

nodes (Section 1.5.1.2) [49]. The solution to the problem formulated in [44-46] is resolved using an OBDD software package, for example Buddy [116].

4.5.1. IEEE 9-Bus Test System

The proposed methodology is initially tested using the IEEE 9-bus test system. Figure 4.1 shows the digraph representation of this test system, and such digraph was used to create the oriented incidence matrix $\mathbf{M_H}$ shown in (A.26). As previously discussed, there are two coherent groups of generators: $V_{GN1} = \{v_1\}$ and $V_{GN2} = \{v_2, v_3\}$. Moreover, the weak area determined in Chapter 3 and shown in Figure 3.1 should be utilised. Hence, this test system is split into two islands, and the "free nodes" are v_5 and v_6. Finally, it is assumed that any branch can be included in the islanding solution represented by the cutset $\bar{E}_S$, i.e., $E_C = \varnothing$.

Using the information above, the methodology computes the matrix **C** as follows.

$\mathbf{C}^T =$

	v_1	v_2	v_3	v_4	v_5	v_6	v_7	v_8	v_9
$comb_1$	1	2	2	1	1	1	2	2	2
$comb_2$	1	2	2	1	1	2	2	2	2
$comb_3$	1	2	2	1	2	1	2	2	2
$comb_4$	1	2	2	1	2	2	2	2	2

(4.13)

The matrices **C** and $\mathbf{M_H}$ are then used by the new ICI methodology to compute the constrained cutset matrix $\mathbf{Q_H}$ (4.7), which is shown in (4.14).

$\mathbf{Q_H} =$

	e_1	e_2	e_3	e_4	e_5	e_6	e_7	e_8	e_9
$cutset_1$	0	0	-1	0	0	0	0	-1	0
$cutset_2$	0	0	-1	0	0	0	0	0	1
$cutset_3$	0	1	0	0	0	0	0	-1	0
$cutset_4$	0	1	0	0	0	0	0	0	1

(4.14)

The methodology then evaluates whether the cutsets included in $\mathbf{Q_H}$ are feasible or not. Hence, the rank of the digraph induced by each cutset is computed. In this case, the four cutset shown in (4.14) are feasible. The methodology then computes the vector **w** using the weight factors associated with the arcs (4.2), and this vector is shown in (4.15).

$$\mathbf{w} = \begin{bmatrix} 71.64 & 40.95 & 86.61 & 163.00 & 76.39 & 24.17 & 85.00 & 60.83 & 30.69 \end{bmatrix}^T \quad (4.15)$$

Then, the value of the cut produced by each cutset is determined using (4.12), and these are presented in (4.16). The final islanding solution with the minimal power imbalance is then identified by searching for the minimum entry in (4.16). As noticed, the optimal islanding solution for minimal power imbalance is represented by the $\bar{E}_S = \{e_2, e_8\}$. This cutset creates the two islands shown in Figure 4.3, and each island has a power imbalance of 19.88 MW. Island 1 has an excess of load, and that Island 2 has an excess of generation.

$$cut(V_1, V_2) = \begin{bmatrix} 147.44 \\ 55.92 \\ 19.88 \\ 71.64 \end{bmatrix} \quad (4.16)$$

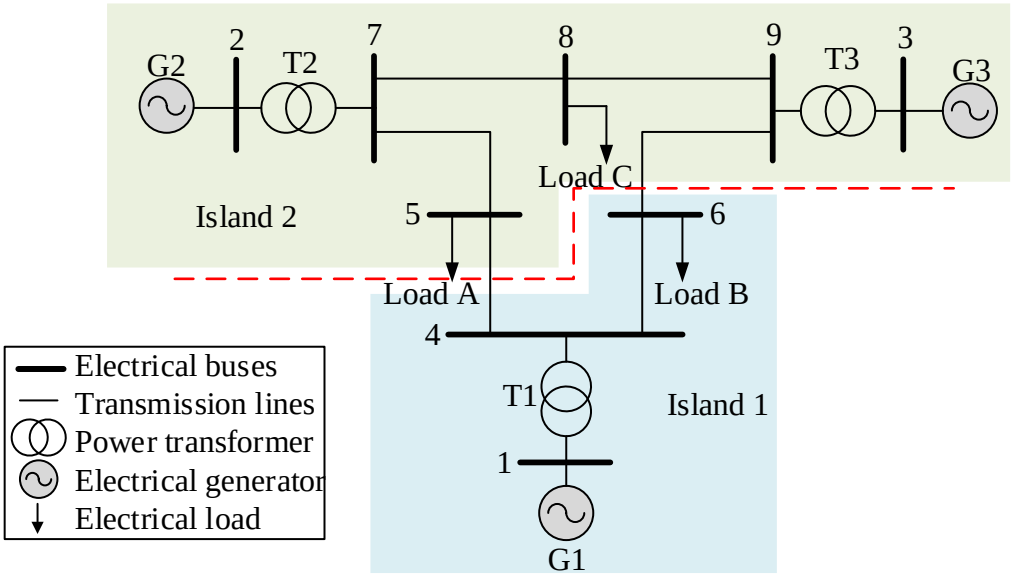

Figure 4.3: Islanding solution for minimal power imbalance of the IEEE 9-bus test system split into two islands

In order to compare the quality of the islanding solution determined by the proposed methodology, the existing OBDD-based method [44-46] is implemented. In this test

system, the same coherent groups of generators are considered, and a threshold of $\beta = 100$ is defined. The OBDD-based method found the four cutsets shown in Table 4.1. As noticed, the proposed methodology can determine the same islanding solution as the OBDD-based method. Hence, it is demonstrated that the new approach is as accurate as the existing methods. Furthermore, an important advantage of the new method is that no threshold is required to be defined. Furthermore, and as detailed in Section 4.5.4, the proposed methodology is computationally more efficient than the OBDD-based method.

Table 4.1: Results of the OBDD-based method for the IEEE 9-bus test system

Cutset	Power Imbalance (MW)
4-5; 6-9	19.88
5-7; 4-6	55.92
4-5; 4-6	71.64

4.5.2. New England 39-Bus Test System

The proposed methodology is also tested using the New England 39-bus test system. Initially, it is considered that any branch can be included in the cutset $\bar{E}_S$, i.e., $\bar{E}_C = \varnothing$. Furthermore, the coherent groups of generators previously determined are $V_{GN1} = \{v_{G10}\}$ and $V_{GN2} = \{v_{G1}, v_{G2}, v_{G3}, v_{G4}, v_{G5}, v_{G6}, v_{G7}, v_{G8}, v_{G9}\}$, and the weak area shown in Figure 3.2 should be used. Nevertheless, and since the weak area in this network is significantly small due to the dynamic properties of the test system (the inertia constant of G10), the subset of "free nodes" is extended for simulation purposes, and the nodes v_1, v_5, v_7, v_8 and v_9 are arbitrarily defined as the "free nodes".

The implementation of the methodology then determines that the islanding solution with minimal power imbalance considering the given coherent groups of generators is across the cutset $\bar{E}_S = \{e_{1,39}, e_{9,39}\}$. Figure 4.4 shows this islanding solution, which produces an imbalance of 104.04 MW – excess of load in Island 1 and excess of generation in Island 2.

The quality of the islanding solution obtained using the proposed methodology is also compared with the solution of the implementation of the existing OBDD-based method [44-46]. Assuming the same coherent groups of generators and a threshold of $\beta = 250$, the OBDD-based method found the four cutsets shown in Table 4.2. As noticed, the proposed methodology is at least as accurate as the existing OBDD-based methodx. However, the new methodology is significantly faster than existing islanding methods for minimal power imbalance, as further detailed in Section 4.5.4.

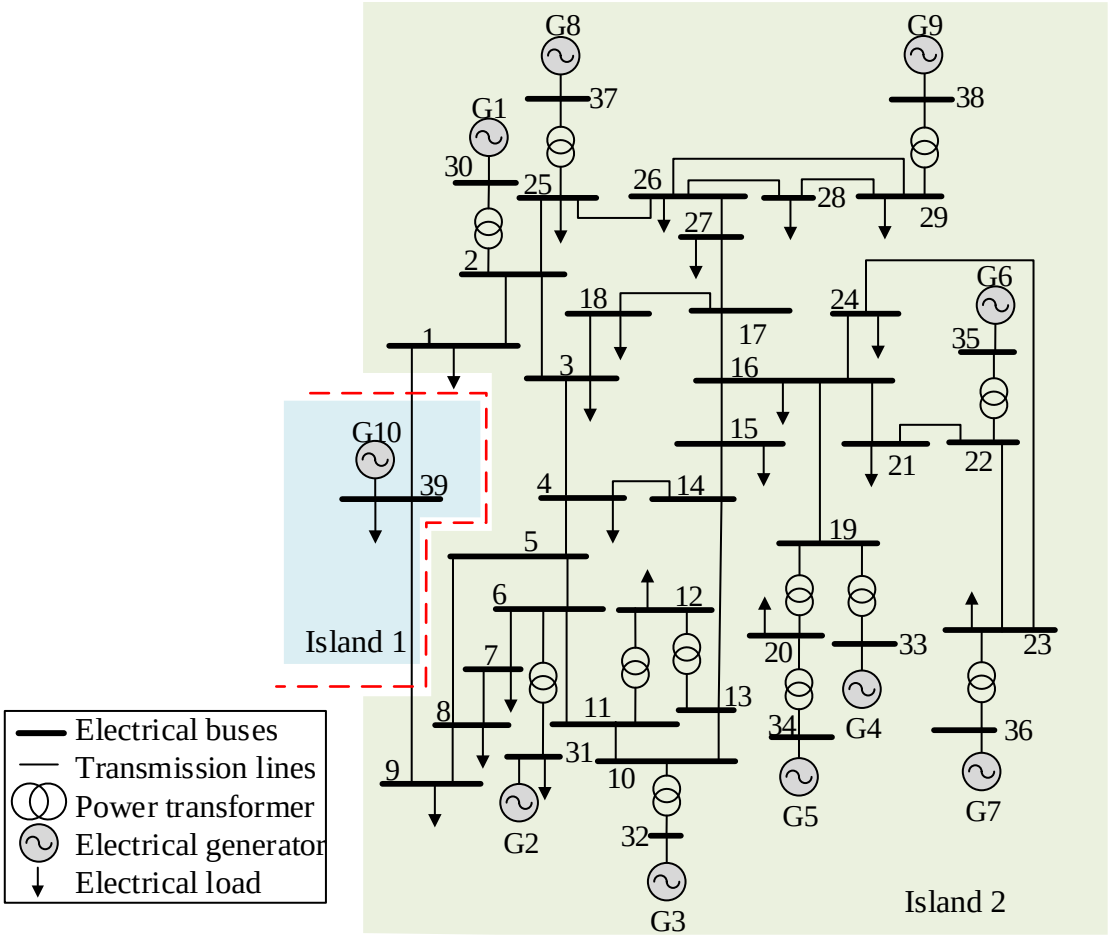

Figure 4.4: Islanding solution for minimal power imbalance of the New England 39-bus test system split into two islands

The methodology can constrained any branch to be excluded from islanding solutions. To demonstrate this feature, it is assumed that the line 9-39 cannot be disconnected. Thus, the set $\bar{E}_C = \{e_{9,39}\}$ is defined. The same coherent groups of generators are assumed. The

proposed methodology then excludes the node v_9 from the subset of "free nodes", and defines the label of the node v_9 to be "1", including thus the node v_9 in the same island as the node v_{39} (G10). In this case, the methodology found ten feasible cutsets, and the optimal solution for minimal power imbalance was found across the cutset $\bar{E}_S = \{e_{1,39}, e_{8,9}\}$. This new solution produces a power imbalance of 110.71 MW within each island.

Table 4.2: Results of the OBDD-based method for the New England 39-bus test system

Cutset	Power Imbalance (MW)
1-39; 9-39	104.04
1-39; 8-9	110.71
1-2; 9-39	202.16
1-2; 8-9	208.83

4.5.3. IEEE 118-Bus Test System

The proposed methodology is finally illustrated using the IEEE 118-bus test system. The coherent groups of generators previously determined are $V_{GN1} = \{v_{G1}, v_{G2}, v_{G3}, v_{G4}, v_{G5}\}$, $V_{GN2} = \{v_{G6}, v_{G7}, v_{G8}, v_{G9}, v_{G10}, v_{G11}, v_{G12}, v_{G13}\}$ and $V_{GN3} = \{v_{G14}, v_{G15}, v_{G16}, v_{G17}, v_{G18}, v_{G19}\}$, and the two weak areas shown in Figure 3.3 should be used. Finally, as the transformer 37-38 should not be included in the islanding solution, the set $\bar{E}_C = \{e_{37,38}\}$ is defined. Since there are three coherent groups of generators and two weak areas, this test system is used in this section to demonstrate the splitting of the power system into three islands for minimal power imbalance. As previously discussed, this is achieved by computing in parallel the cutset between each island. In this case a matrix $\mathbf{C_{12}}$ is created between Island 1 and Island 2 and a matrix $\mathbf{C_{23}}$ is created between Island 2 and Island 3.

Two constrained cutset matrices, $\mathbf{Q_{H12}}$ and $\mathbf{Q_{H23}}$, are then computed in parallel and the feasible cutsets for each matrix are determined. In this case, 54 and 10 feasible cutsets between Island 1 and Island 2 and between Island 2 and Island 3 were identified, respectively. Then, the combination of cutsets, one from each constrained cutset matrix,

that produces the minimum cut (4.3) between the applicable islands, is defined as the optimal islanding solution for minimal power imbalance. This optimal solution is presented in Figure 4.5. In this case, Island 1 was found to have an excess of generation equal to 1.87 MW, Island 2 was found to have an excess of load 2.97 MW and Island 3 has an excess of generation equal to 1.10 MW.

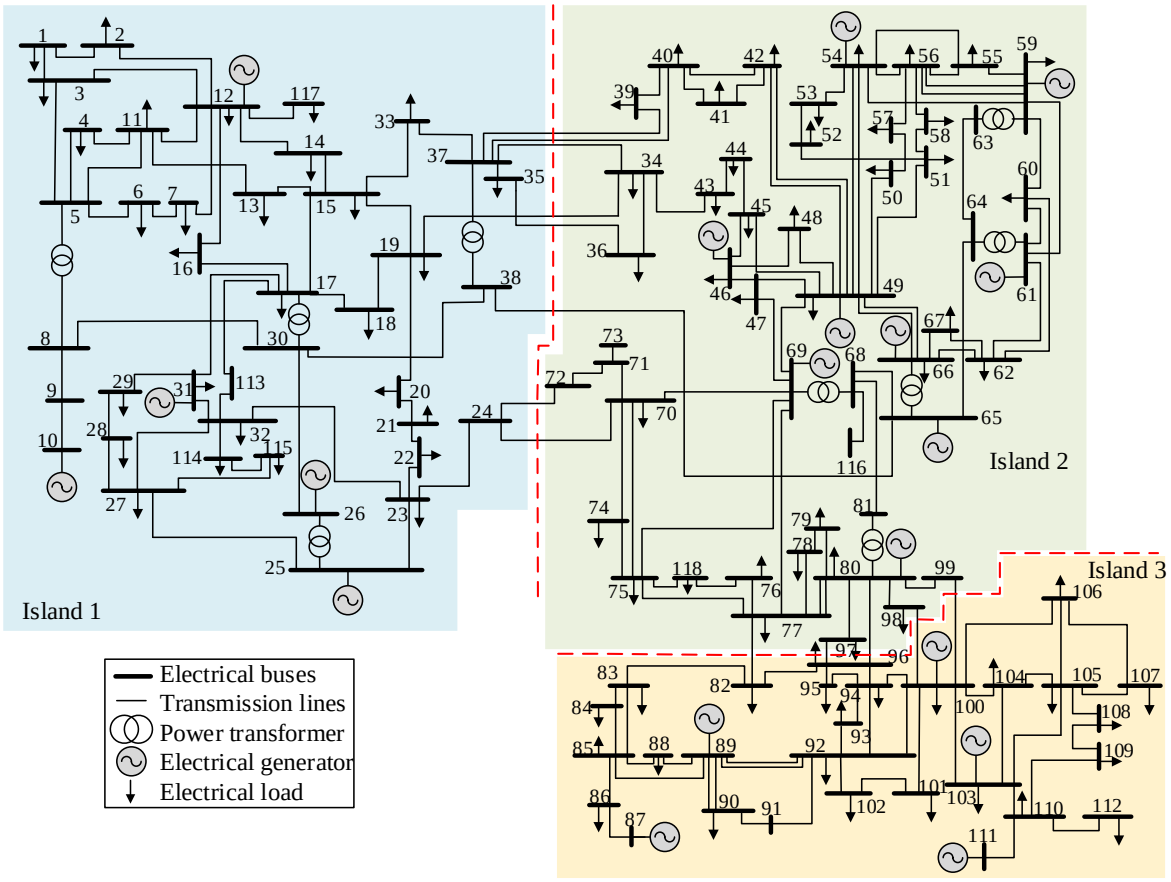

Figure 4.5: Islanding solution for minimal power imbalance of the IEEE 118-bus test system split into two islands

The OBDD-based method [44-46] is also implemented to compare the quality of the islanding solutions determined by the proposed methodology. In this test system, the same coherent groups of generators are considered, and a threshold $\beta = 25$ is defined. The OBDD-based method found 23 cutsets between Island 1 and Island 2, and 2 cutsets between Island 2 and Island 3. The first three combinations of cutsets that produce the minimal power imbalance within the islands are shown in Table 4.3.

In this particular case, and since the search space of the proposed methodology was limited to consider only the node within the weak areas, the first islanding solution determined by the OBDD-based method has a slightly lower power imbalance, i.e., a slightly better islanding solution. Nevertheless, the computational time required by the existing method was significantly slow, as shown in Section 4.5.4.

Table 4.3: Results of the OBDD-based method for the IEEE 118-bus test system

Cutset	Power Imbalance (MW)		
	Island 1	**Island 2**	**Island 3**
18-19;19-20;15-19;35-36;34-37;37-40;39-40; 38-65;24-70;70-71; 77-82;80-96;96-97;98-100;99-100	1.32	–2.42	1.10
19-34;35-36;34-37;37-39;37-40;38-65; 24-70;24-72;77-82;80-96;96-97;98-100;99-100	1.87	–2.97	1.10
18-19;19-20;15-19;34-36;34-37;37-39;37-40; 38-65;24-70;70-71;77-82;80-96;96-97;98-100;99-100	– 2.15	1.05	1.10

4.5.4. Computational Efficiency of the new Methodology

The proposed methodology has the key advantage that it uses the weak areas previously identified to limit the nodes to be included in the combinatorial optimization. This feature considerably accelerates the determination of an islanding solution, particularly when dealing with large-scale power systems. Indeed, the runtime of the proposed methodology is dominated by that of the computation of the rank of the induced graph. Since this computation is performed c times only, and the value of c depends on the number of "free nodes", the utilisation of the weak areas significantly improves the efficiency of the introduced methodology, and ultimately creates islands that are strong-dynamically connected with reduced power imbalance.

The methodology was run 1000 times for the same loading condition and the average runtime, on different systems and for different number of islands, was computed. To compare the efficiency of the proposed methodology with that of the existing OBDD-based method, similar study was performed using the existing approach. Table 4.4 shows the results of this comparison.

As noticed, the proposed methodology is significantly more efficient compared to the existing OBDD-based methodology. The improvement achieved by the methodology is significantly important when dealing with large-scale power systems.

Table 4.4: Computational time for determining islanding solutions for minimal power imbalance using the proposed methodology and the existing islanding method

Test System	Runtime using the proposed methodology (s)	Runtime using the OBDD-based method (s)
IEEE 9-bus	0.0002	0.0032
New England 39-bus	0.0045	9.01
IEEE 118-bus	1.96	280.39

4.6. Summary

This chapter has presented a novel constrained cutset matrix-based methodology that can determine islanding solutions for minimal power imbalance, while ensuring that each island contains only coherent generators. It can also constrain any branch to be excluded from the islanding solution, allowing thus the exclusion of transformers and unavailable lines. This is important to exclude branches that are deemed to be unsuitable for islanding. The new methodology has the possibility to explore the vast combinatorial space to always find the islanding solution with the minimum power imbalance. Nevertheless, the previously determined weak areas have been utilised to reduce the search space, and thus to considerably accelerate the determination of an islanding solution.

The proposed methodology creates electrical islands with reduced power imbalance, while ensuring that each island contains only coherent generators. Hence, the methodology enhances the transient stability of the islands and reduces the amount of load to be shed and generation to be rescheduled following system splitting.

The methodology has been illustrated using the IEEE 9-bus test system, New England 39- and IEEE 118-bus test systems. Simulation results demonstrate that the new methodology is significantly faster than the conventional ICI methods for minimal power imbalance, while maintaining the same level of accuracy of the solution.

Chapter 5. Intentional Controlled Islanding for Minimal Power Flow Disruption of Large-Scale Power Systems: A Constrained Spectral Clustering-Based Methodology

Chapter 5 introduces a novel constrained spectral clustering-based methodology to determine islanding solutions for minimal power flow disruption, while ensuring that each island contains only coherent generators. The proposed Intentional Controlled Islanding (ICI) methodology is computationally very efficient, it can directly determine an islanding solution for any given number of islands, and it can constrain any branch to be excluded from the islanding solution.

The proposed ICI methodology benefits the controlled separation of large-scale power systems as the possibility of overloading the branches in the islands is reduced, and the probability that the generators in each island will remain in synchronism is increased. Furthermore, it has the advantage that it requires much less computation compared to the conventional islanding methods while improving the accuracy of the islanding solution.

ICI methods for minimal power flow disruption seek to minimise the change of the power flow pattern within the network following system islanding, and they enhance the transient stability of the islands by creating these with only coherent generators [48, 49]. As discussed in Section 1.5.1.3, solutions for this ICI approach can be obtained using graph theory based techniques such as *spectral clustering*. This powerful technique – explained in Appendix A.7 – has been used in the past to determine islanding solutions with minimal power flow disruption [48, 49]. However, these existing ICI methods do not consider the generator coherency constraint [48], or they require recursive bisection to determine an islanding solution for cases when more than two islands are required [49]. As explained earlier, failure to consider the coherency constraint may create unstable islands, from the transient stability point of view [5], and recursive bisection is computationally demanding and may affect the quality of the islanding solution [70-74].

Therefore, this chapter introduces a novel ICI methodology based on constrained spectral clustering to determine islanding solutions for minimal power flow disruption, while ensuring that each island contains only coherent generators. As an extra feature, the new technique can also constrain any branch to be excluded from the islanding solution, and this allows the exclusion of transformers and unavailable transmission lines from the islanding solution. The general idea of the constrained spectral clustering-based methodology proposed in this chapter is to embed the graph representing the active power flow of the system into the Euclidean space, manipulate this to create Voronoi diagrams as explained in Appendix A.7.12, and then group together the Voronoi diagrams based on the coherency constraint, as further explained in Section 5.4.

Compared to the ICI approach presented in [48], the proposed methodology enhances the transient stability of the islands by creating these with only coherent generators. Hence, comparing these two approaches will be irrelevant. In comparison to the Spectral Clustering Controlled Islanding (SCCI) algorithm introduced in [49], which also considers the transient stability of the future islands and creates islands with only coherent generators, the new methodology is computationally more efficient, as it has the key advantages of (i) solving the associated eigenproblem only once, even if numerous islands are required and (ii) avoiding application of iterative algorithms (e.g., *k-means*). Furthermore, it possesses the extra advantage over the existing SCCI algorithm that it can directly determine an islanding solution for minimal power flow disruption for any given number of islands. Hence, the proposed methodology not only accelerates the determination of the islanding solution by computing the corresponding eigenvectors only once, but also improves its quality, as recursive bisection is not required. Accelerating the determination of islanding solutions and their quality is important for real-time applications and from the speed of blackouts' mitigation perspective [41-43]. The proposed methodology is more efficient and at least as accurate as the existing SCCI algorithm [49] for cases of two islands, and significantly more efficient and more accurate for cases of more than two islands.

In the following sections of this chapter, the proposed methodology is presented and steady-state studies are performed to demonstrate its effectiveness – computational efficiency and accuracy. It is assumed in this chapter that the coherent groups of generators

have been previously identified. Indeed, the coherent groups of generators identified in Section 2.3 are used in this chapter.

5.1. Graph Representation of the Electrical Power System

The behaviour of a power system with *n* buses and *m* generators following a disturbance is represented in this chapter as an edge weighted and undirected graph. This graph represents the active power flow in the branches, without the directions, and is defined as follows:

$$G = (V, E, \rho) \tag{5.1}$$

where,

- the elements $v_i \in V$, $i = 1,\ldots,n$, denote the nodes of the graph, and they represent the buses of the actual power system. To distinguish the generation buses from the load buses, the node set V is divided into two node subsets $V_{GN} \subset V$ representing the m generation buses, and $V_{LD} = V \setminus V_{GN}$ representing the $n - m$ load buses. The elements $v_i^{GN} \in V_{GN}$ and $v_i^{LD} \in V_{LD}$ are called generation- and load-nodes, respectively.

- the elements $e_{ij} \in E$, $i, j = 1,\ldots,n$, denote the edges of the graph, and they represent the branches of the actual power system.

- the number $w_{ij} = \rho(e_{ij})$, $i, j = 1,\ldots,n$, represents the weight factor associated with each edge $e_{ij} \in E$, and it represents the average active power flow in the branch. To accommodate network losses, the value of w_{ij} is defined as follows.

$$w_{ij} = w_{ji} = \begin{cases} \dfrac{|P_{ij}| + |P_{ji}|}{2} & \text{if } e_{ij} \in E; \\ 0 & \text{otherwise.} \end{cases} \tag{5.2}$$

  In (5.2), P_{ij} and P_{ji} represent the active power flow in the branch from bus i to bus j, and from bus j to bus i, respectively.

Figure 5.1 shows the graph representation of the IEEE 9-bus test system. The black dots – defined by the elements $v_i^{GN} \in V_{GN}$ – represent the m generator buses, and the grey dots – defined by the elements $v_i^{LD} \in V_{LD}$ – represent the $n - m$ load buses. The lines illustrated in Figure 5.1 represent the edges.

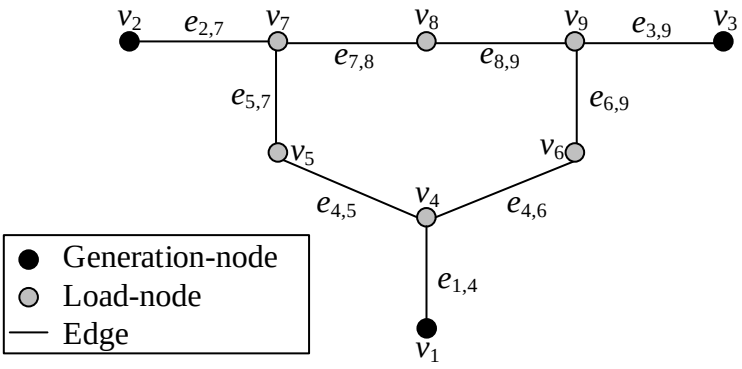

Figure 5.1: Graph representation of the IEEE 9-bus test system for minimal power flow disruption

5.2. Definition of Graph Theoretic Concepts

The methodology presented in this chapter is based on constrained spectral clustering. Hence, it uses the concepts introduced in Appendix A.7, which are summarised below.

5.2.1. Graph Laplacian Matrices

The methodology proposed here uses a Laplacian matrix associated with the graph G to represent the active power flow in the branches of the system. Using a normalised Laplacian matrix $\mathbf{L_N}$ given by (A.28) for clustering purposes is more advantageous (see Appendix A.7.5). Thus, the proposed methodology will use the matrix $\mathbf{L_N}$ considering the edge weights given by (5.2).

5.2.2. Spectral Embedding

When the normalised Laplacian matrix $\mathbf{L_N}$ is computed, the eigenproblem given by (A.33) can be solved. The eigenvectors $\boldsymbol{\psi}_1, \ldots, \boldsymbol{\psi}_r$ associated with the r smallest eigenvalues

$0 = \nu_1 \leq \ldots \leq \nu_r$ of $\mathbf{L_N}$ are then used to create the matrix $\mathbf{X} = \left[\boldsymbol{\psi}_1, \ldots, \boldsymbol{\psi}_r\right] \in \mathbb{R}^{n \times r}$ with rows $\mathbf{x}_i$, $i = 1, 2, \ldots, n$. The value of r is the number of islands to be created. This value corresponds to the number of identified coherent groups of generators.

The matrix $\mathbf{X}$ is then used to perform the spectral embedding of the graph G in r-dimensional Euclidean space $\mathbb{R}^r$. As detailed in Appendix A.7.9, the vector $\mathbf{x}_i$ then represents the coordinates of the node $v_i \in V$ in $\mathbb{R}^r$. The vectors $\mathbf{x}_i$ can be normalised using (A.61). This normalisation improves the quality of the solution, as explained in Appendix A.7.9, projects the vectors $\mathbf{x}_i$ to the unit (r–1)-dimensional sphere $\mathbb{S}^{r-1}$, and creates the matrix $\mathbf{Y} \in \mathbb{R}^{n \times r}$ with rows $\mathbf{y}_i$. After computing the spectral embedding, the nodes $v_i \in V$ can be seen as data-points $\mathbf{x}_i$ in $\mathbb{R}^r$, or $\mathbf{y}_i$ on $\mathbb{S}^{r-1}$. For example, Figure 5.2 and Figure 5.3 show the vectors $\mathbf{x}_i$ and $\mathbf{y}_i$ for the spectral embedding of the IEEE 9-bus test system for minimal power flow disruption when $r = 2$, respectively. The numbers on the diagrams correspond to node numbers.

5.2.3. Representative data-points

The subset $\mathbf{X_{GN}} \subset \mathbf{X}$, and equivalently $\mathbf{Y_{GN}} \subset \mathbf{Y}$, are defined as the subset of data-points representing the m generation-nodes $v_i^{GN} \in V_{GN}$. It should be noted that $\left|\mathbf{X_{GN}}\right| = \left|\mathbf{Y_{GN}}\right| = m$. These data-points are called centroids and denoted by $\mathbf{x}_i^{GN}$ and $\mathbf{y}_i^{GN}$ in $\mathbb{R}^r$ and on $\mathbb{S}^{r-1}$, respectively. The function of these centroids is further detailed in Section 5.4. The advantages of using centroids are to: (i) satisfy the generator coherency constraint, (ii) accelerate the identification of an islanding solution, and (iii) reduce the memory usage by reducing the order of the similarity matrix. Figure 5.2 and Figure 5.3 show the centroids as red-dots and the remaining data-points representing load-nodes as blue-asterisks.

5.2.4. Similarity Matrix

Since the data-points $\mathbf{x}_i$ are projected on the unit sphere $\mathbb{S}^{r-1}$ to create the new data-points $\mathbf{y}_i$, the spherical distance (Appendix A.7.10.3) between the applicable data-points should be

calculated [73, 117]. These results are used to build a similarity matrix $\mathbf{S} := s\left(\mathbf{y}_i, \mathbf{y}_j\right)$, as further explained in Section 5.4.

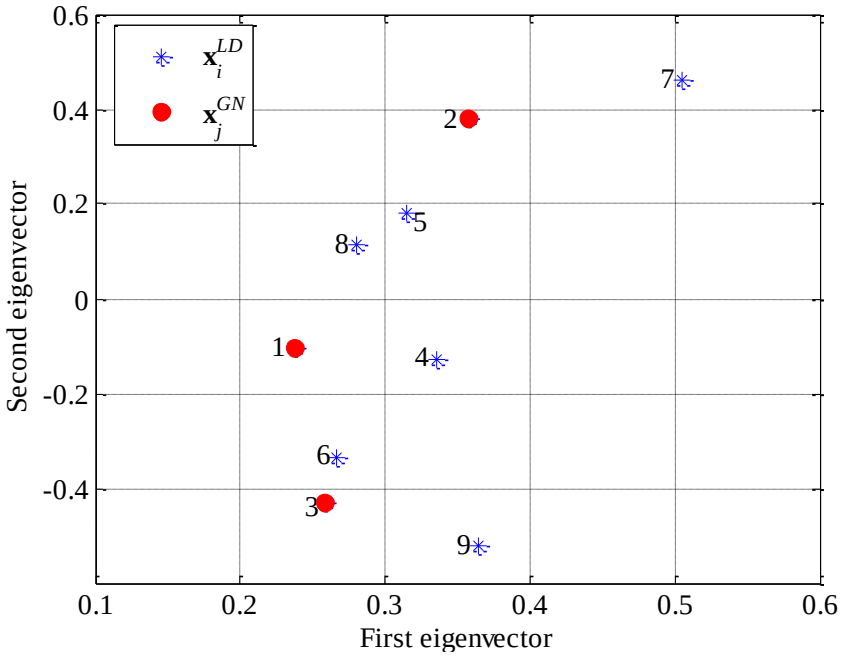

Figure 5.2: Spectral embedding into $\mathbb{R}^2$ of the IEEE 9-bus test system for minimal power flow disruption

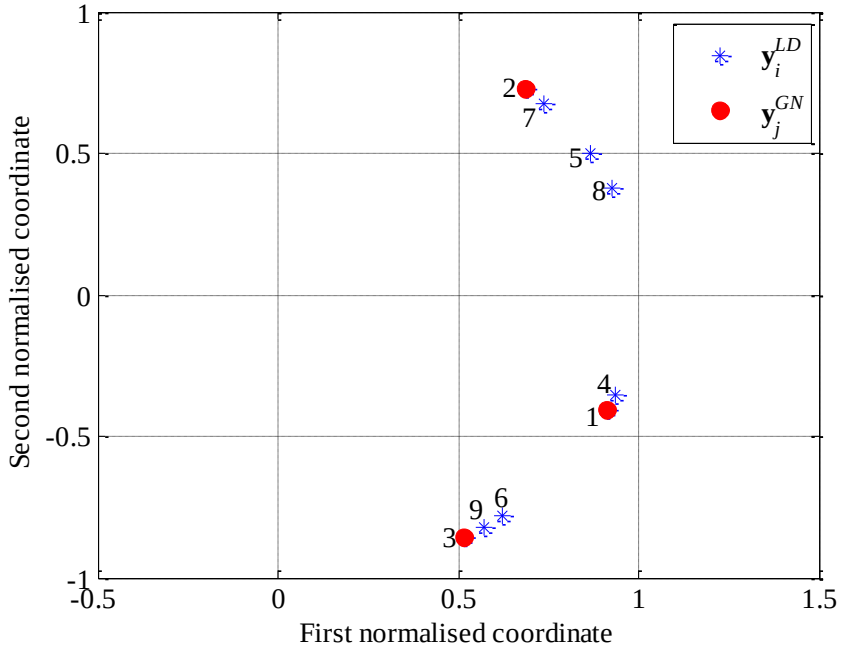

Figure 5.3: Spectral embedding onto the unit circle $\mathbb{S}^1$ of the IEEE 9-bus test system for minimal power flow disruption

5.2.5. Cutset and Cut

The cutset $E_S \subset E$ is the set of edges that must be removed to split the graph G into the r disjoint subgraphs $G_1,\ldots,G_r$, with node sets $V_1,\ldots,V_r$. Then, the cut associated with the cutset E_S is the sum of the weight factors associated with the edges in E_S, and is given by (A.8). In the ICI problem for minimal power flow disruption, a cutset E_S consists of the edges that represent the branches in the actual power system that must be disconnected to create the islands and the value of the cut corresponds to the total power flow disruption.

5.2.6. Quality of a Cutset

The quality of an islanding solution – represented by the cutset E_S – is measured using the ratios between the boundary (cut) (A.5) and the volume (A.6) of the islands. In this application, the cut of the node set V_k, denoted by $cut\left(V_k,\bar{V}_k\right)$, physically corresponds to the power flow disruption between the buses that are represented by the nodes $v_i \in V_k$ and the other buses, i.e., the power flow between the buses in the island represented by V_k and the rest of the system. Furthermore, the volume of the node set V_k, denoted by $vol\,(V_k)$, represents the total power flow within the corresponding island that is represented by the node set V_k.

Then, the quality of the subset V_k, $k=1,\ldots,r$, is measured as follows.

$$\eta\left(V_k\right)=1-\frac{cut\left(V_k,\bar{V}_k\right)}{vol\left(V_k\right)} \tag{5.3}$$

In this application, the expansion $\phi\left(V_k\right)=cut\left(V_k,\bar{V}_k\right)\big/vol\left(V_k\right)$ of the node subset V_k measures the size of the cut relative to the volume of the island. The quality index (5.3) can be physically interpreted as a measure of the energy exchange between the islands – expressed by the power flow in the lines – with respect to the energy flow within the islands. Hence, the greater the value of $\eta\left(V_k\right)$ – the less energy exchange and the more energy within the island – the better the island is considered to be in terms of clustering.

Note that the value of $\eta(V_k)$ varies from zero to one, and a partition with quality equal to zero means that the subset contains only one node, and that such node was indeed separated from the rest of the graph [71]. As further explained in Section 5.5.2, this type of solution may be found when the loss of synchronism occurs between one generator and the others.

The methodology will then evaluate the quality of the islanding solution using the worst quality index $\eta(V_k)$ among the clusters, i.e., the quality of the best cutset is the minimum value of $\eta(V_k)$ from all of the islands: $\min_{k=1,2,\ldots r}\left(\eta(V_k)\right)$.

As detailed in Section 5.3, finding the maximum of the worst quality – solving (5.4) – will be the objective function in the islanding problem for minimal power flow disruption.

$$\max_{V_1,\ldots V_r}\ \min_{k=1,2,\ldots r}\left(\eta(V_k)\right) \tag{5.4}$$

5.3. Formulation of the ICI Problem for Minimal Power Flow Disruption

The methodology proposed in this chapter seeks to minimise the power flow disruption between islands, while ensuring that each island contains only coherent generators. These coherent groups of generators are denoted by the node subsets $V_{GN1},\ldots,V_{GNr}$, and it is assumed that they are separately identified. This chapter uses the previously identified coherent groups of generators (Section 2.3). Nevertheless, it should be noted that the methodology could also be deployed using coherency results from approaches such as those described in [27]. As explained throughout this thesis, the dynamically coherent groups of generators must be separated into different islands to help the transient stability of the system when determining an islanding solution [49]. For example, the islanding solution shown in Figure 5.6 considers the two coherent groups of generators $V_{GN1} = \{v_1\}$ and $V_{GN2} = \{v_2, v_3\}$, and the islanding solution determined by the proposed methodology will cluster these groups in different islands.

The problem of minimising the power flow disruption between islands can be formulated using the absolute value of power flow exchange between islands [48]. Mathematically, this means that the proposed methodology will minimise the power flow disruption over the *r*-partitions $V_1,\ldots,V_r$ as follows:

$$\min_{V_1,\ldots,V_r}\left(\sum_{e_{ij}\in E_S}\frac{\left|P_{ij}\right|+\left|P_{ji}\right|}{2}\right) \tag{5.5}$$

subject to each island containing only coherent generators.

$$V_{GNk}\subset V_k \tag{5.6}$$

As noticed, the islanding problem (5.5) subject to (5.6) aims to partition the power system into *r* islands, such that the k^{th} island contains the k^{th} group of coherent generators.

However, the optimisation problem (5.5) has a trivial solution, namely partition of the graph into the node with smallest node degree, and the rest [71]. In order to minimise the probability of obtaining these spurious solutions, the objective function is modified to (5.7).

$$\min_{V_1,\ldots,V_r}\max_{k=1,2,\ldots,r}\left(\frac{cut\left(V_k,\bar{V}_k\right)}{vol\left(V_k\right)}\right) \tag{5.7}$$

The new objective function (5.7) indeed aims to minimise the worst (maximum) expansion (A.52) of each island. As the expansion $\phi\left(V_k\right)$ and the quality $\eta\left(V_k\right)$ of the subsets are related $\left(\eta\left(V_k\right)=1-\phi\left(V_k\right)\right)$, the new objective function (5.7) is certainly equivalent to maximise the worst (minimum) quality over the *r* partitions (5.4). Indeed, this type of min-max optimization problems on graphs are related to Laplacian eigenvalues (see Normalised Cut in Appendix A.7.4), and this is the key connection between islanding for minimal power flow disruption and spectral clustering [71].

The methodology can also constrain any branch to be excluded from the islanding solution. Thus, branches that must not be disconnected, e.g., unavailable lines, transformer and lines that are important for the stability of the islands, can be excluded from the solution space. In order to do so, a new subset $E_C \subset E$, with elements $e_{ij} \in E_C$, is defined to represent the branches in the power system that cannot be disconnected, e.g., transformers.

Having defined the set of coherent groups of generators (5.6), the set of excluded edges E_C and the new objective function (5.7), the ICI problem that the methodology attempts to solve is finally reformulated as follows.

$$\min_{V_1,\ldots,V_r} \max_{k=1,2,\ldots,r} \left(\frac{cut\left(V_k, \bar{V}_k\right)}{vol\left(V_k\right)} \right) \tag{5.8}$$

subject to

$$V_{GNi} \subset V_i \text{ and } E_C \cap E_S = \varnothing.$$

The condition $E_C \cap E_S = \varnothing$ in (5.8) means that the methodology only considers partitions with cutsets E_S not containing any excluded edge $e_{ij} \in E_C$. As previously explained, solving (5.8) reduces the possibility of overloading the branches in the created islands, and increases the probability that the generators in each island will remain in synchronism. Furthermore, it creates balanced partitions, in the sense that the power flow within each island is higher than the power flow exchange between the islands.

5.4. Methodology for Solving the ICI Problem for Minimal Power Flow Disruption

The proposed methodology seeks to minimise the power flow disruption while satisfying the generator coherency constraint and excluding the constrained branches from the islanding solution, i.e., the objective function is given by (5.8). It must be noted that while the problem of determining an optimal solution of (5.8) is in general *NP-hard*, the methodology produces an approximate solution in polynomial time (a few seconds in

practice). The approximate and the optimal solution can be related via the Cheeger inequality (Appendix A.7.6), and this is one of the main theoretical justifications of the spectral clustering methodology [71].

Figure 5.4 shows the flowchart of the proposed methodology. Each step is identified by an *S* (step) followed by a number. In practical implementations, the input information required by the new technique, in real-time and at the moment of islanding the power system, is: the actual power flow in the branches – the value of w_{ij} for all $e_{ij} \in E$ – the set of branches that must not be disconnected – $E_C \subset E$ – and the separately identified coherent groups of generators – the subsets $V_{GN1},\ldots,V_{GNr}$.

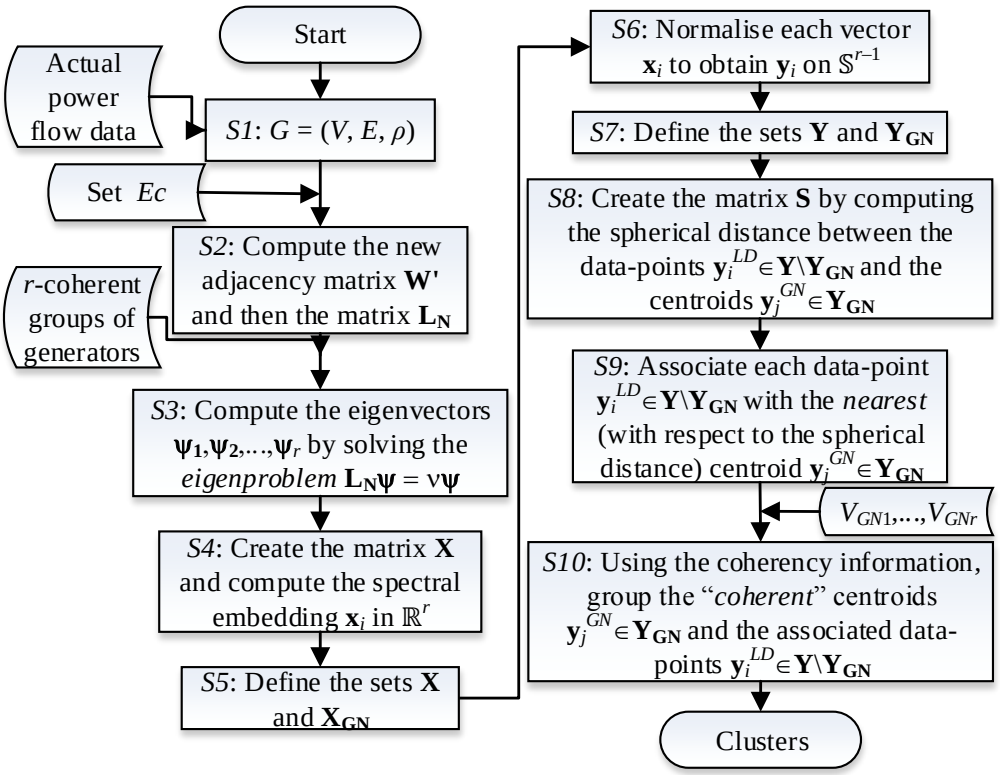

Figure 5.4: Flowchart of the proposed ICI methodology for minimal power flow disruption

In **Step 1**, the methodology uses the power flow data to build the graph *G*. Then, in the **Step 2**, it constrains the edges $e_{ij} \in E_C$ to be excluded from cutsets, by changing their associated weight factor to the largest value in **W**, i.e., $\max(\mathbf{W})$, as follows.

$$\text{for all } e_{ij} \in E_C, \text{let } w'_{ij} = w'_{ji} = \max(\mathbf{W}) \tag{5.9}$$

Changing the edge weight of the constrained edge to the highest value significantly increases the possibility that the edge will be excluded from the cutset [72, 74]. The weight factor of the excluded edge is modified to the largest value in **W**, as it has been found that defining infinity can considerably affected the *commute distance* between nodes [74]. The changes in (5.9) induce a new weighted adjacency matrix **W'**, which is then used to compute the corresponding normalised Laplacian matrix $\mathbf{L_N}$ using (A.28) or (A.29).

The eigenproblem $\mathbf{L_N}\boldsymbol{\psi} = \nu\boldsymbol{\psi}$ is then solved to compute the eigenvectors $\boldsymbol{\psi}_1, \ldots, \boldsymbol{\psi}_r$ associated with the r smallest eigenvalues of the new matrix $\mathbf{L_N}$ in **Step 3**. These eigenvectors are placed as columns to create the matrix $\mathbf{X} \in \mathbb{R}^{n \times r}$, which is finally used to perform the spectral embedding in **Step 4** (see Figure 5.2 for an example).

In **Step 5**, the methodology then defines the centroids $\mathbf{x}_i^{GN} \in \mathbf{X_{GN}}$ in r-dimensional Euclidean space $\mathbb{R}^r$ (e.g., the red-dots in Figure 5.2) as the data-points that represent the generation-nodes. The remaining data-points $\mathbf{x}_i \in \mathbf{X} \setminus \mathbf{X_{GN}}$ in $\mathbb{R}^r$ (e.g., the blue-asterisks in Figure 5.2) then represent the load-nodes in the graph. Thus, and for consistency, these data-points are denoted by $\mathbf{x}_i^{LD} \in \mathbf{X} \setminus \mathbf{X_{GN}}$.

In **Step 6**, the vectors $\mathbf{x}_i$ are then normalised to compute the vectors $\mathbf{y}_i$ which form the rows of the matrix $\mathbf{Y} \in \mathbb{R}^{n \times r}$. The normalised vectors $\mathbf{y}_i$ represent the nodes $v_i \in V$ as data-points on the unit (r–1)-dimensional sphere $\mathbb{S}^{r-1}$ (see Figure 5.3 for an example). In **Step 7**, the data-points $\mathbf{y}_i^{GN} \in \mathbf{Y_{GN}}$ (the red-dots in Figure 5.3) are defined as the centroids on $\mathbb{S}^{r-1}$.

In **Step 8**, the methodology then computes the spherical distance *only* between the data-points $\mathbf{y}_i^{LD} \in \mathbf{Y} \setminus \mathbf{Y_{GN}}$ and the centroids $\mathbf{y}_i^{GN} \in \mathbf{Y_{GN}}$. These distances are used to create the similarity matrix $\mathbf{S} := (s_{ij})$, where $s_{ij} = s(\mathbf{y}_i^{LD}, \mathbf{y}_j^{GN})$ is the spherical distance between these data-points (between the blue-asterisks and the red-dots in Figure 5.3). As it can be noted,

the order of the matrix **S** is reduced to $(n-m)\times m$ (see Table 5.1 for an example). The advantages of this reduction are discussed in Section 5.5.5.

In **Step 9**, each data-point $\mathbf{y}_i^{LD} \in \mathbf{Y} \setminus \mathbf{Y_{GN}}$ is associated with the nearest centroid $\mathbf{y}_i^{GN} \in \mathbf{Y_{GN}}$ (with respect to the spherical distance). Mathematically, this means that the minimum value in the i^{th} row of **S** is identified. All in all, each load-node $v_i^{LD} \in V_{LD}$ is grouped with one and only one generation-node $v_j^{GN} \in V_{GN}$. For example, Figure 5.3 (and equivalently Table 5.1) shows that the blue-asterisks (data-points $\mathbf{y}_i^{LD}$) marked as 6, and 9 are closer to the red-dot marked as 3 (generation-node or centroid $\mathbf{y}_j^{GN}$) than to any other centroid. Thus, the nodes v_6 and v_9 are grouped with v_3. When each load-node is associated with the closest generation-node, *m* disjoint subgraphs are obtained (see Figure 5.5). Each of these subgraphs is defined as the "domain of the generator for minimal power flow disruption". This is a special case of Voronoi diagrams [118]. In the proposed methodology, each generator has a different domain, and examples of generator domains are illustrated in Figure 5.5 and explained in detail in Section 5.5.

In **Step 10**, the methodology creates the final islands by grouping the domains of the coherent generation-nodes to satisfy the generator coherency constraint. For example, it is assumed in Figure 5.5 that the coherent groups of generators are $V_{GN1} = \{v_1\}$ and $V_{GN2} = \{v_2, v_3\}$, thus, the islands shown in Figure 5.6 are obtained by grouping the domains of v_2 and v_3. The final clusters $V_1,\ldots,V_r$ then represent the *r* islands to be created, and the islanding solution consists of the set of edges $e_{ij} \in E$, for which $v_i \in V_i$, $v_j \in V_j$ and $i \neq j$. For example, the islanding solution in Figure 5.6 is across lines 4-5 and 4-6.

5.5. Simulation Examples

This section presents the simulation examples of islanding solutions for minimal power flow disruption, while ensuring that each island contains only coherent generator and that the islanding solution excludes branches that cannot be used for islanding. In this chapter, the previously identified coherent groups of generators will be utilised. The methodology

will also be illustrated on the New England 39-bus test system using different coherent groups of generators, as further explained in Section 5.5.2. The results of the new methodology are compared, in all the cases, with those obtained using an implementation of the existing SCCI algorithm detailed in [49].

5.5.1. IEEE 9-Bus Test System

The proposed methodology is initially tested using the IEEE 9-bus test system. The graph G shown in Figure 5.1 is created using the power flow solution. It is assumed that any line can be included in the cutset E_S, i.e., $E_C = \varnothing$. Moreover, the two previously identified coherent groups of generators $V_{GN1} = \{v_1\}$ and $V_{GN2} = \{v_2, v_3\}$ are used. Hence, the methodology defines $r = 2$, solves the corresponding eigenproblem and considers the spectral embedding in $\mathbb{R}^2$ shown in Figure 5.2. It then defines the centroids as the data-points representing the generation-nodes (the red-dots in Figure 5.2).

The vectors $\mathbf{x}_i$ in $\mathbb{R}^2$, $i = 1,2,\ldots,9$, are then normalised to project these on the unit circle $\mathbb{S}^1$ (Figure 5.3). Observe in Figure 5.3 that a clustering structure starts to emerge. The methodology then computes the arc across the circumference only between the normalised vectors $\mathbf{y}_i^{LD} \in \mathbf{Y} \setminus \mathbf{Y}_{\mathbf{GN}}$ (blue-asterisks) and the normalised centroid $\mathbf{y}_j^{GN} \in \mathbf{Y}_{\mathbf{GN}}$ (red-dots). These spherical distances are used to build the similarity matrix **S** shown in Table 5.1.

Table 5.1: Similarity matrix S between points on the circumference created by the spectral embedding of the IEEE 9-bus test system for minimal power flow disruption

Node	Spherical distance to Centroid v_1^{GN}	Spherical distance to Centroid v_2^{GN}	Spherical distance to Centroid v_3^{GN}
v_4	**0.054**	1.113	0.655
v_5	0.906	**0.292**	1.402
v_6	0.476	1.512	**0.133**
v_7	1.094	**0.077**	1.548
v_8	0.783	**0.427**	1.302
v_9	0.537	1.552	**0.070**

Each load-node $v_i^{LD} \in V_{LD}$ is then grouped with the nearest generation-node $v_j^{GN} \in V_{GN}$ (with respect to the arc along the circumference). This preliminary grouping creates the "domain of each generator for minimal power flow disruption", or Voronoi diagrams. Figure 5.5 illustrates in different background colours the representation of the three Voronoi diagrams in the graph of the IEEE 9-bus test system when r = 2.

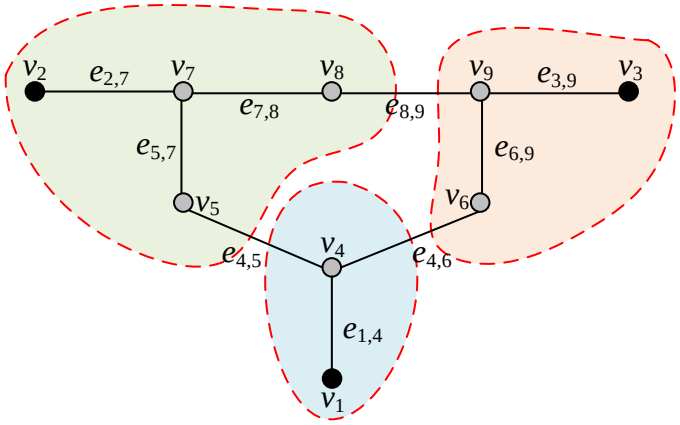

Figure 5.5: Representation of the Voronoi diagrams on the graph of the IEEE 9-bus test system for minimal power flow disruption

The methodology then groups the subgraphs that contain the centroids representing the coherent groups of generators. Hence, the subgraphs in Figure 5.5 that contain the generation-nodes v_2 and v_3 are grouped together to determine the islanding solution shown in Figure 5.6. Table 5.2 shows the power flow disruption of each island (cut) given by (A.5), the total power flow within each island (volume) given by (A.6) and the quality of each island $\eta(V_k)$ given by (5.3). Based on these results, the quality of the islanding solution (the minimum quality $\eta(V_k)$ among the created islands) is defined to be 66.67%.

The quality of the solution obtained with the new methodology is compared with that of the SCCI algorithm [49] using the same coherent groups of generators. Table 5.2 also shows the results obtained using the implementation of the existing ICI technique. As noticed, the islanding solution determined using the SCCI algorithm is the same; hence, the quality of the islanding solution – measured in terms of the qualities $\eta(V_k)$ (5.3) – is also 66.67%. In this particular scenario, the islanding solutions identified using both approaches are equally

accurate. Hence, the proposed methodology demonstrates in this case to be as accurate as the existing approach.

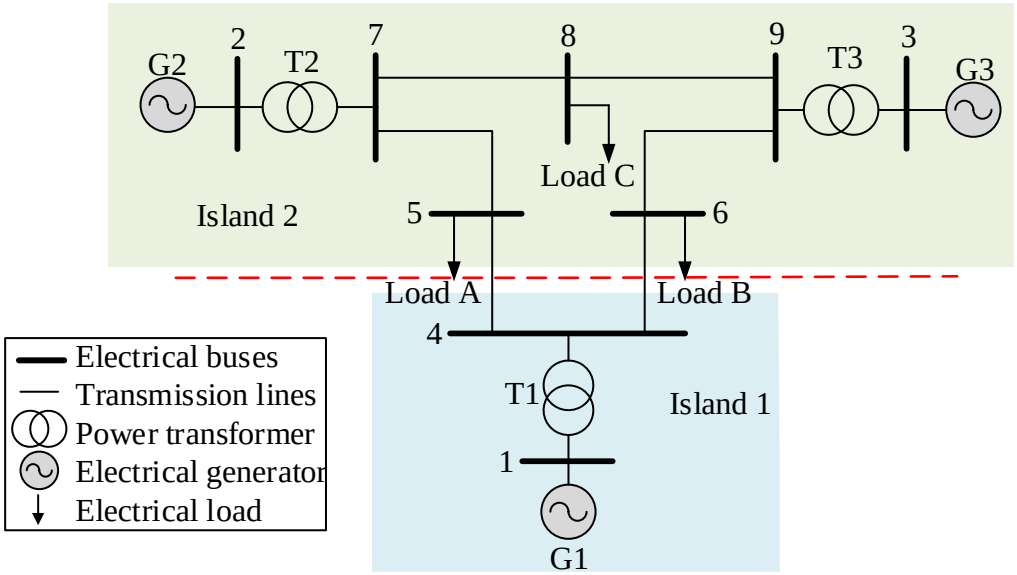

Figure 5.6: Islanding solution for minimal power flow disruption of the IEEE 9-bus test system split into two islands

Table 5.2: Results and comparison of the quality of the proposed methodology and the existing SCCI algorithm in the IEEE 9-bus test system split into two islands

	Cutset	Island No.	Cut (MW)	Volume (MW)	$\eta(V_k)$ (%)
Results using the proposed methodology	$e_{4,5}, e_{4,6}$	1	71.64	214.92	66.67
		2	71.64	1063.64	93.26
Results using the SCCI algorithm	$e_{4,5}, e_{4,6}$	1	71.64	214.92	66.67
		2	71.64	1063.64	93.26

5.5.2. New England 39-Bus Test System

The methodology is now tested using the New England 39-bus test system. It is considered that any branch can be included in the cutset E_S, i.e., $E_C = \varnothing$. The two previously identified coherent groups of generators $V_{GN1} = \{v_{G10}\}$ and $V_{GN2} = \{v_{G1}, v_{G2}, v_{G3}, v_{G4}, v_{G5}, v_{G6}, v_{G7}, v_{G8}, v_{G9}\}$ are used. Thus, the methodology defines $r = 2$, solves the corresponding eigenproblem and considers the spectral embedding in $\mathbb{R}^2$ shown in Figure 5.7. It also defines the centroids as representing the generation-nodes (see the red-dots in Figure 5.7). It

then normalises the vectors $\mathbf{x}_i$ in $\mathbb{R}^2$, $i = 1,\ldots,39$, to project these on the unit circle $\mathbb{S}^1$, and to create the vectors $\mathbf{y}_i$ (Figure 5.8).

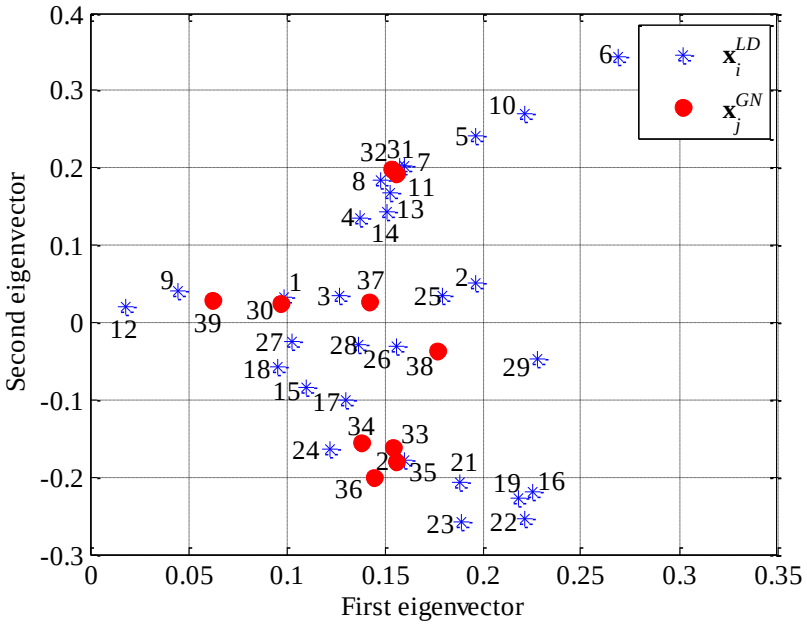

Figure 5.7: Spectral embedding into $\mathbb{R}^2$ of the New England 39-bus test system for minimal power flow disruption

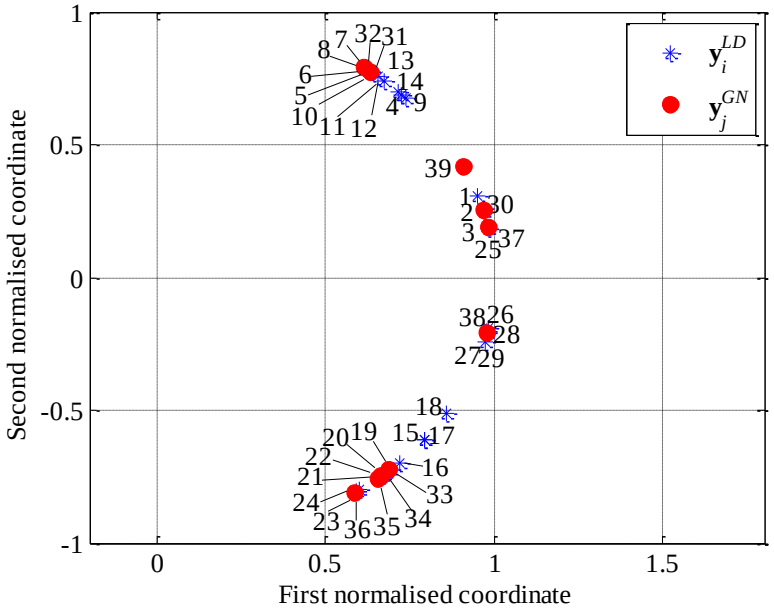

Figure 5.8: Spectral embedding onto the unit circle $\mathbb{S}^1$ of the New England 39-bus test system for minimal power flow disruption

The methodology then computes the arc across the circumference only between the normalised vectors $\mathbf{y}_i^{LD} \in \mathbf{Y} \setminus \mathbf{Y_{GN}}$ (blue-asterisks) and the normalised centroid $\mathbf{y}_j^{GN} \in \mathbf{Y_{GN}}$ (red-dots). These distances are then used to build the similarity matrix **S**. Each load-node $v_i^{LD} \in V_{LD}$ is then grouped with the nearest generation-node $v_j^{GN} \in V_{GN}$ (with respect to the arc along the circumference). This preliminary grouping creates the Voronoi diagrams illustrated in different background colours in Figure 5.9.

Then, the coherency groups are used, and the subgraphs in Figure 5.9 containing coherent generation-nodes are grouped together to determine the islanding solution across the cutset $E_S = \{e_{1,39}, e_{9,39}\}$. Table 5.3 shows the power flow disruption of each island (cut) given by (A.5), the total power flow within each island (volume) given by (A.6) and the quality of each island $\eta(V_k)$ given by (5.3).

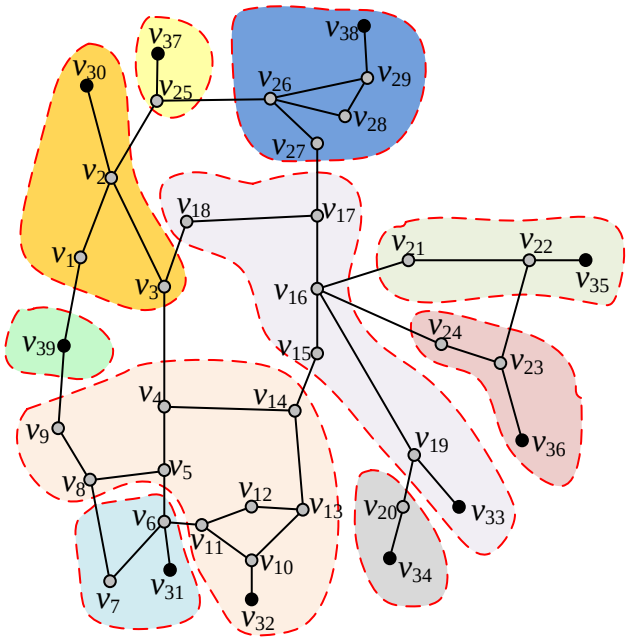

Figure 5.9: Representation of the Voronoi diagrams on the graph of the New England 39-bus test system for minimal power flow disruption

In this particular case, the quality of the islanding solution – the minimum quality $\eta(V_k)$ among the created islands – is 0%. Although this value may not provide a clear measure of optimality, it should be noted that this is indeed the best partition – smallest power flow

disruption – that can be obtained for the given coherent groups of generators. To support this outcome, the existing SCCI algorithm [49] is also implemented using the same coherent groups of generators, and the same islanding solution is found (see Table 5.3). Hence, the islanding solution determined by the proposed methodology is as accurate as the SCCI algorithm and both induce the same value of cut (104 MW).

Table 5.3: Results and comparison of the quality of the proposed methodology and the existing SCCI algorithm in the New England 39-bus test system for the case of two islands for the previously determined coherent groups of generators

	Cutset	**Island No.**	**Cut (MW)**	**Volume (MW)**	$\eta(V_k)$ **(%)**
Results using the proposed methodology	$e_{1,39}, e_{9,39}$	1	104	104	0.00
		2	104	26495	99.61
Results using the SCCI algorithm	$e_{1,39}, e_{9,39}$	1	104	104	0.00
		2	104	26495	99.61

It is important to note that the quality index $\eta(V_k)$ is zero only when the cut of a node set equals its volume (see (5.3)), and this solution occurs only when one node is separated from the main graph [71]. Spectral clustering tries to create balanced partitions [71]; nevertheless, constrained spectral clustering will create balanced partitions while satisfying the set of given constraints [74]. In the presented application of constrained spectral clustering, the graph *G* will be optimally split such that the generator coherency constraint is satisfied. Hence, the methodology will determine a cutset that induces the minimum ratio between the cut (A.5) and the volume (A.6), while ensuring that each cluster contains only coherent generators. Therefore, as the generator-node v_{39} should be separated from the other generation-nodes to satisfy the generator coherency constraint, the methodology will find the cutset that produces such separation at the optimal cost on the objective function (5.8), and in this particular case, the cost – the value of the objective function – of creating such clusters is equal to zero.

To illustrate the applicability of the proposed methodology with different coherent groups of generators, and to present a more illustrative example for the purpose of this thesis, the

methodology will now be implemented considering the following arbitrarily selected coherent groups of generators: $V_{GN1} = \{v_{30}, v_{31}, v_{32}, v_{37}, v_{38}, v_{39}\}$ and $V_{GN2} = \{v_{33}, v_{34}, v_{35}, v_{36}\}$.

Since the power flow in the branches remains the same, the spectral embedding of the corresponding graph is indeed the same as shown in Figure 5.7 and Figure 5.8. Thus, the Voronoi diagrams illustrated in different background colours in Figure 5.9 remain the same. Then, the coherency information abovementioned is used, and the clusters in Figure 5.9 containing coherent generation-nodes are grouped to determine the islanding solution presented in Figure 5.10. Table 5.4 shows the value of the power flow disruption of each island (cut) (A.5), the total power flow within each island (volume) (A.6) and the quality of each island $\eta(V_k)$ (5.3). As noted, the quality of the islanding solution is now 98.87%.

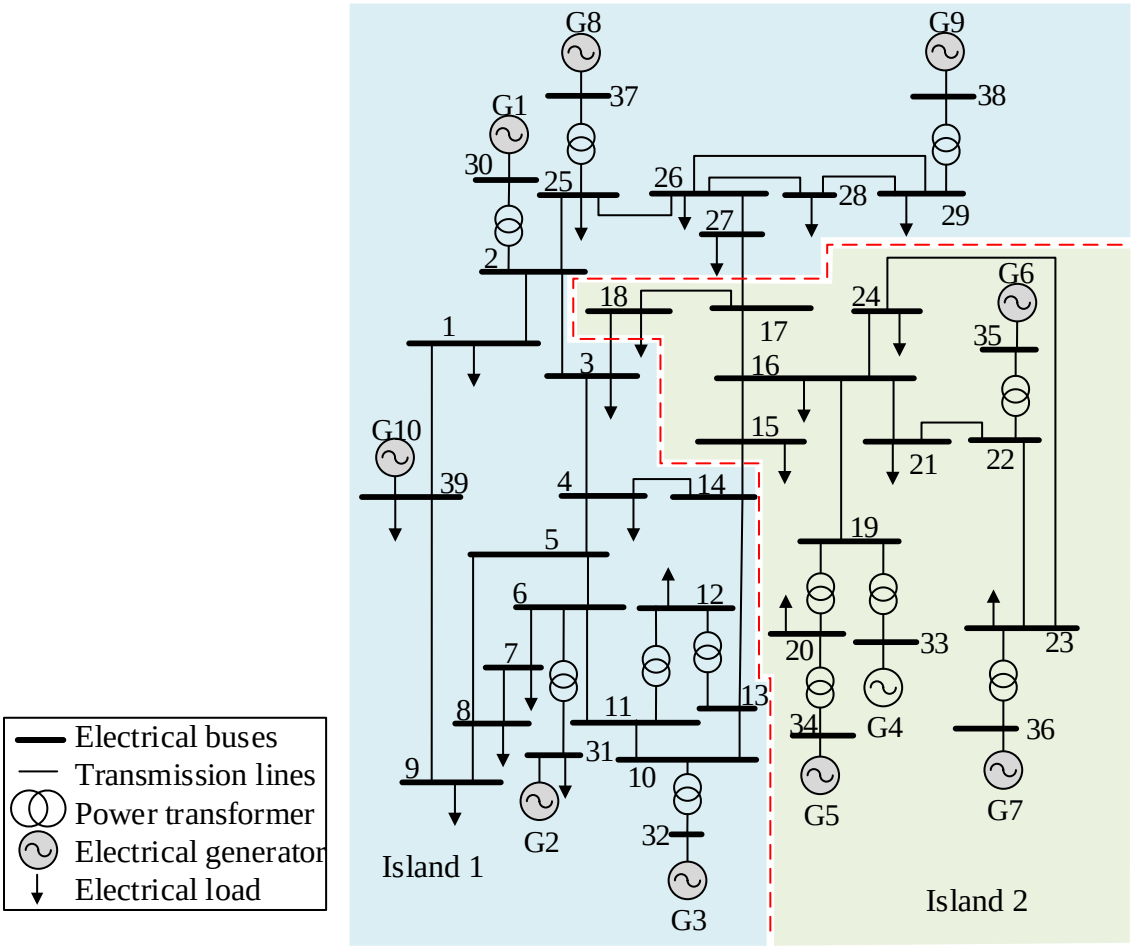

Figure 5.10: Islanding solution for minimal power flow disruption of the New England 39-bus test system split into two islands for the new coherent group of generators

Table 5.4: Results and comparison of the quality of the proposed methodology and the existing SCCI algorithm in the New England 39-bus test system split into two islands for the new coherent groups of generators

	Cutset	Island No.	Cut (MW)	Volume (MW)	$\eta(V_k)$ (%)
Results using the proposed methodology	$e_{3,18}, e_{17,27}, e_{14,15}$	1	115.69	16442	99.30
		2	115.69	10197	98.87
Results using the SCCI algorithm	$e_{3,18}, e_{17,27}, e_{15,16}$	1	335.55	16763	98.00
		2	335.55	9877	96.60

The quality of the solution determined by the proposed methodology is now compared with that of the existing SCCI algorithm [49] using the new coherent groups of generators. Table 5.4 also summarises the results of each island when using the SCCI algorithm. As noticed, the quality of the solution found by the SCCI algorithm is 96.60%. Hence, the quality of islanding solution determined by the new methodology is better (greater value of $\eta(V_k)$ and indeed smaller cut). One reason why the SCCI algorithm did not find a solution with less power flow disruption in this case is because it uses the unnormalised Laplacian matrix to partition *G* [49]. As explained in Appendix A.7.5, using the normalised Laplacian matrix instead in spectral clustering is more advantageous, particularly for weighted graphs [71].

The proposed methodology can also exclude any branch from the solution. This is important to exclude from the islanding solution any branch that operators deem to be unfeasible for islanding. To illustrate this, it is now assumed that the circuit breakers at the line 3-18 – previously included in the islanding solution – cannot be tripped. According to Figure 5.4, the methodology then defines the set $E_C = \{e_{3,18}\}$ and uses (5.9) to change the applicable edge weight. The implementation of the methodology considering $V_{GN1} = \{v_{30}, v_{31}, v_{32}, v_{37}, v_{38}, v_{39}\}$, $V_{GN2} = \{v_{33}, v_{34}, v_{35}, v_{36}\}$ and $E_C = \{e_{3,18}\}$ then reveals that the new islanding solution is as shown in Figure 5.11.

As noticed, the new islanding solution effectively excludes the line 3-18 (from Figure 5.10) and it now includes the line 17-18. Table 5.5 summarises the results of this new islanding solution. The inclusion of a constraint to the line 3-18 results in a reduction of the quality of the new islanding solution. Indeed, it can be noted in Table 5.5 that the quality $\eta(V_k)$ of

both islands is slightly reduced. Therefore, it is concluded that the quality of the new islanding solution is 97.39%. It must be mentioned that the existing SCCI algorithm does not offer the possibility to exclude branches from the islanding solutions.

Table 5.5: Results and comparison of the quality of the proposed methodology and the existing SCCI algorithm in the New England 39-bus test system split into two islands with constraint on the edge $e_{3,18}$

	Cutset	Island No.	Cut (MW)	Volume (MW)	$\eta(V_k)$ (%)
Results using the proposed methodology	$e_{17,18}, e_{17,27}, e_{14,15}$	1	261.04	16585	98.43
		2	261.04	10014	97.39

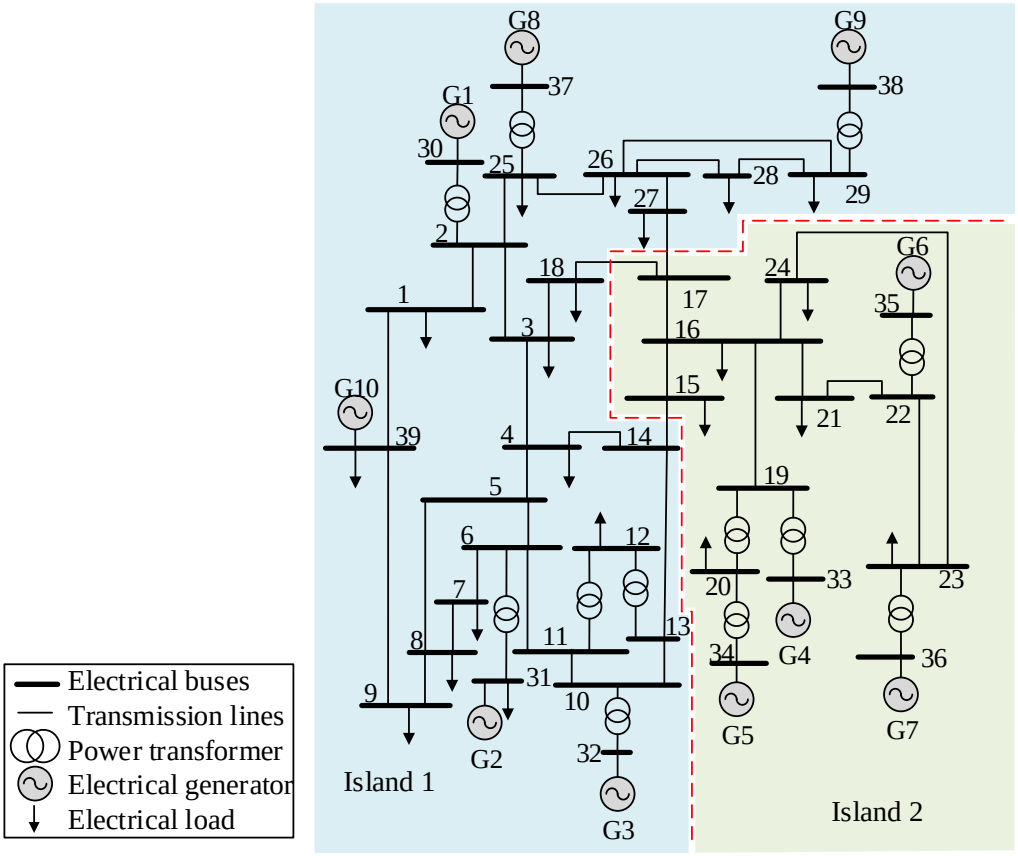

Figure 5.11: Islanding solution for minimal power flow disruption of the New England 39-bus test system split into two islands for the new coherent groups of generators with constraint on the edge $e_{3,18}$

5.5.2.1.Validation of the Hypothesis related to Dynamic Behaviour

This section attends to demonstrate that the dynamic behaviour of the system can be represented for islanding purposes using the model presented in Section 2.1. The New England 39-bus system is used. The data of this system and the controllers (Automatic Voltage Regulators and Power System Stabilisers only) can be found in [119]. All time-domain simulations are performed in DIgSILENT PowerFactory [120]. The times settings of the protective relays used in the simulations are carefully selected to show the desired oscillation mode, although, in practice, they may be shorter. Additionally, instantaneous power flows are used for disconnecting overloaded lines.

Testing case description: As in Section 2.3.5, the base load level has been increased by 30%, while maintaining the same power factor. This is done to stress the system and increase the likelihood of instability following a disturbance. This increment has been equally distributed among the generators G2–G7. The output power of the other generators remains the same. It is then considered that at time $t = 0$ s, a three phase to ground solid fault occurs near bus 16 at line 16-17, and is cleared after local relays open the faulty line at $t = 0.4$ s. If no control action is undertaken, it can be observed in Figure 5.12(a) that the system loses synchronism at about 2.8 s. Indeed, the software DIgSILENT PowerFactory [120] indicates out of step (pole slip) at $t = 2.85$ s.

Then, due to the power oscillations and the line overloads caused by the disconnection of line 16-17, multiple lines are disconnected in cascade. Line 13-14 is disconnected at time $t = 5.5$ s. This then triggers the uncontrolled cascading outages of lines 4-5, 3-4, 5-8 and 6-7 at the times 6.2 s, 6.7 s, 7.1 s and 7.3 s, respectively. These cascading outages lead to the uncontrolled separation of the system into three islands, which are eventually affected by blackouts. Figure 5.12(b) shows the frequency of the generators. As noticed, the system is partitioned into three groups, which are not balanced. Finally, Figure 5.12(c) illustrates that the voltage magnitudes at the system buses are considerably small, leading to a blackout of the system at about 7 s.

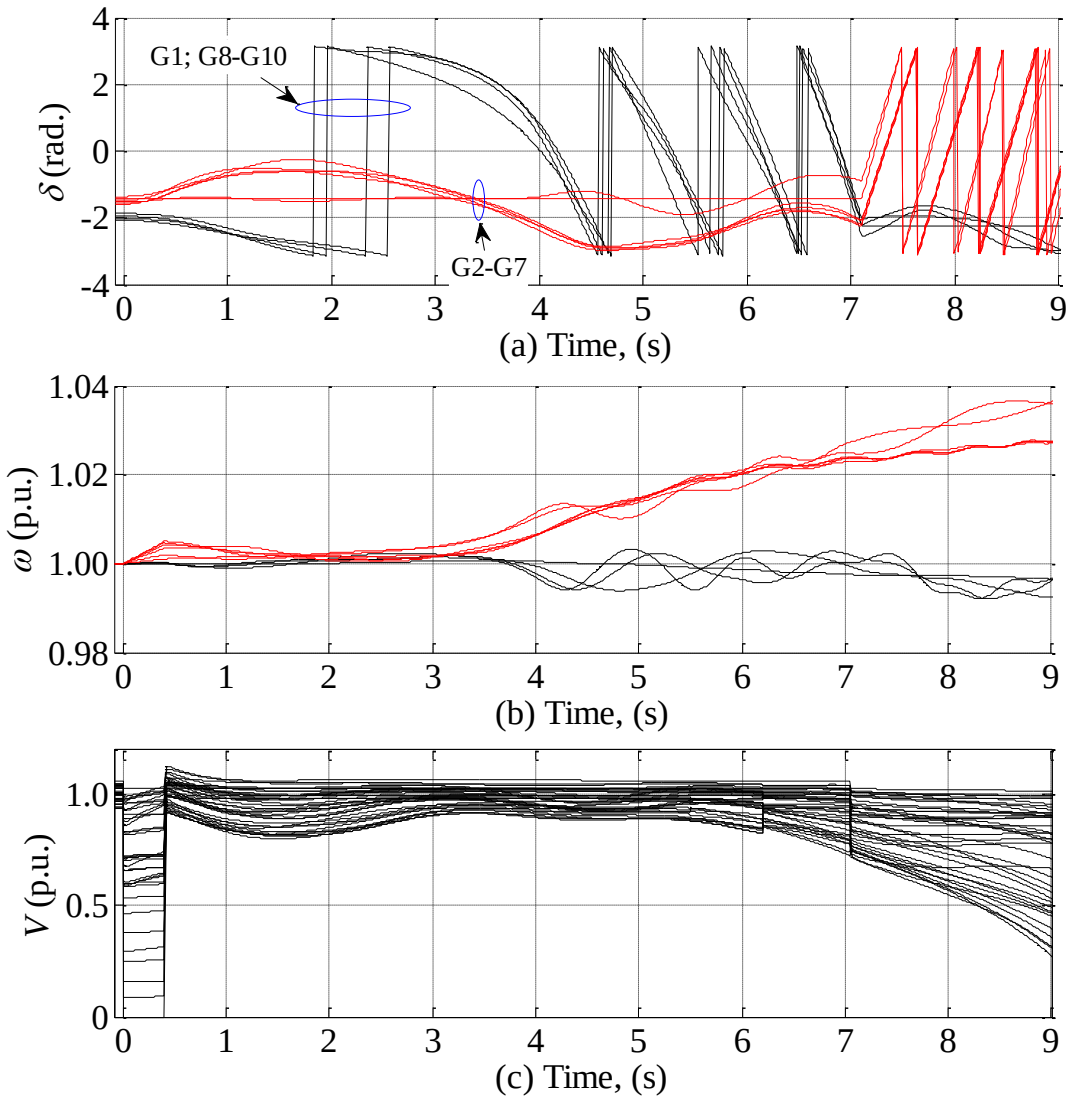

Figure 5.12: Results for the New England 39-bus system without islanding (a) Generator rotor angle (b) Generator speed (c) Voltage magnitudes.

The loss of synchronism and the frequency of the generators are clear indicators that the system should be split [46]. Here it is considered the necessity to partition the system at time $t = 3$ s. In practical implementations, this time depends on the vulnerability analysis performed following severe disturbances. The methodology is used to determine the most suitable islanding solution with respect to the actual power flow in the branches at $t = 3$ s. In the simulations presented here, it is assumed that any transmission line can be included in the cutset. The transformers are excluded from the solution. Since two coherent groups are identified at $t = 3$ s, $r = 2$ is defined. The implementation of the methodology determines that the islanding solution is across the lines 8-9, 3-4 and 16-17.

This solution was obtained in approximately 1.5 ms and thus the corresponding corrective controlled strategy was undertaken at $t = 3.0015$ s. Figure 5.13 presents the dynamic simulation results with islanding. It can be seen that the blackout has been successfully avoided, and two stable islands are created with frequency at $t = 15$ s between 0.989 pu and 1.035 pu, and voltages between 0.895 pu and 1.09 pu. Indeed, power flows computed in the post-islanding state demonstrate the feasibility of these results. Note that the machines are not equipped with governors.

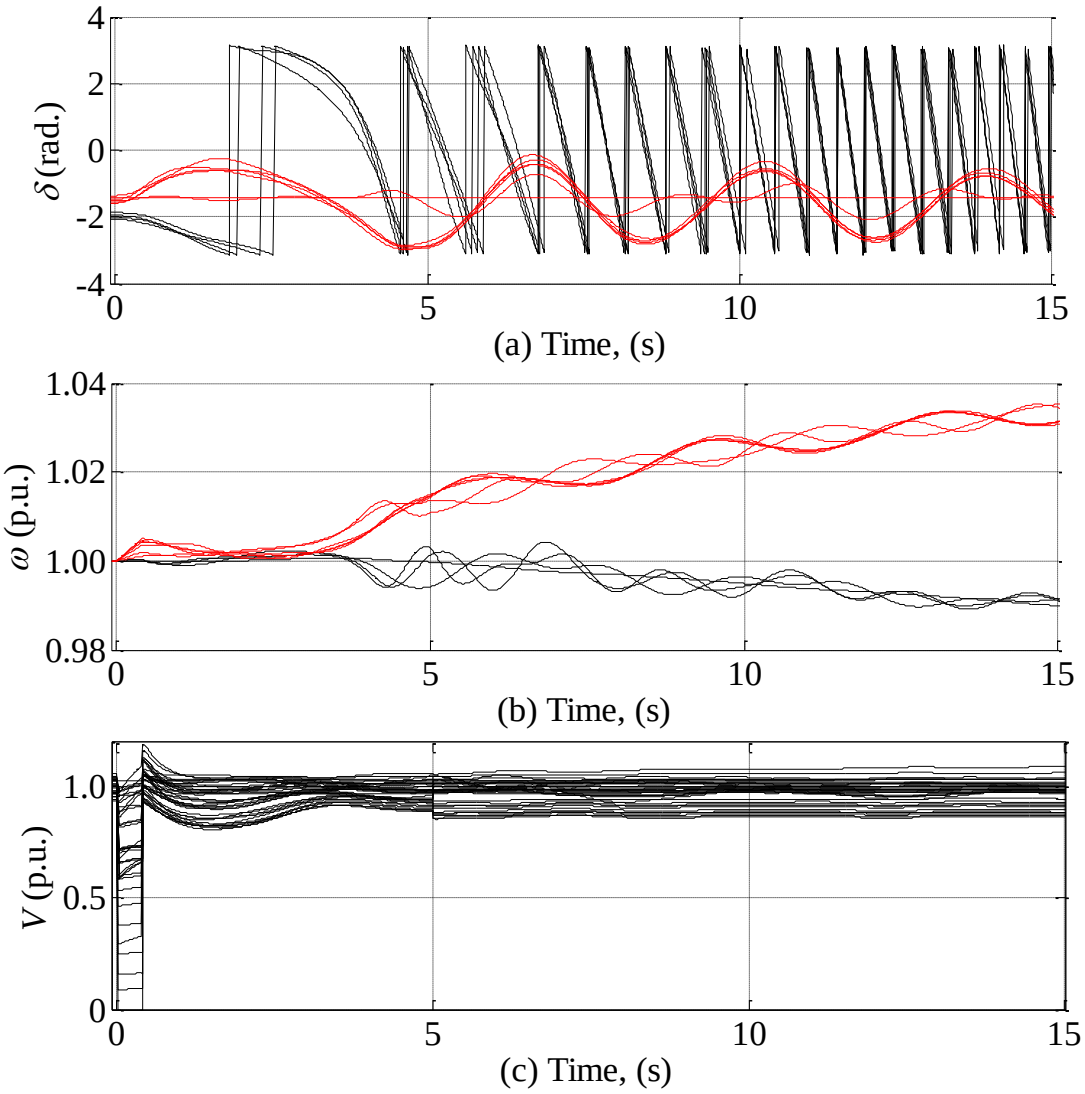

Figure 5.13: Results for the New England 39-bus system with islanding (a) Generator rotor angle (b) Generator speed (c) Voltage magnitudes.

5.5.3. IEEE 118-Bus Test System

The proposed methodology is now tested using the IEEE 118-bus test system. It is considered that transformers must be excluded from the islanding solution. Furthermore, the previously identified coherent groups of generators $V_{GN1}=\{v_{10},v_{12},v_{25},v_{26},v_{31}\}$, $V_{GN2}=\{v_{46},v_{49},v_{54},v_{59},v_{61},v_{65},v_{66},v_{69},v_{80}\}$ and $V_{GN3}=\{v_{87},v_{89},v_{100},v_{103},v_{111}\}$ are utilised. The methodology, previously explained in detail using smaller test networks, is then used in this network, and Figure 5.14 illustrates the islanding solution for this scenario. It is important to mention that the methodology does not require recursive bisection to identify such solution. Table 5.6 shows the value of the power flow disruption of each island (cut) (A.5), the total power flow within each island (volume) (A.6) and the quality of each island $\eta(V_k)$ (5.3). Based on these results, the quality of the islanding solution is 96.96%.

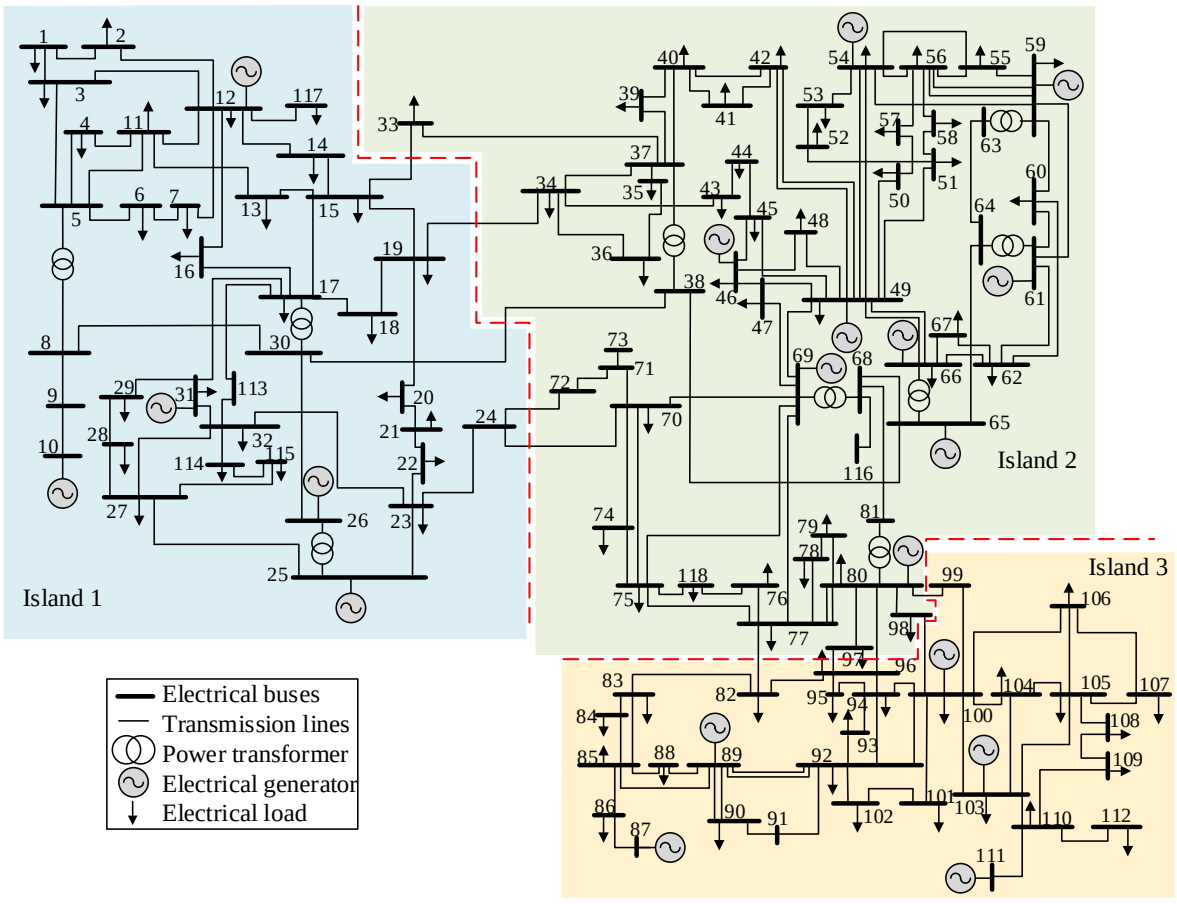

Figure 5.14: Islanding solution for minimal power flow disruption of the IEEE 118-bus test system split into three islands

Table 5.6: Results and comparison of the quality of the proposed methodology and the existing SCCI algorithm in the IEEE 118-bus test system split into three islands

	Island No.	**Cut (MW)**	**Volume (MW)**	$\eta(V_k)$ **(%)**
Results using the proposed methodology	1	81	6956	98.84
	2	139	8459	98.37
	3	58	3777	98.47
Results using the existing SCCI algorithm	1	81	6956	98.84
	2	166	8467	98.04
	3	85	3769	97.74

The quality of the obtained islanding solution is compared with the solution of the SCCI algorithm [49] using the same coherent groups of generators. It should be mentioned that as three islands will be created, recursive bisection will need to be applied using the existing SCCI algorithm, and this may affect the quality of the solution. The implementation of the SCCI algorithm found the islanding solution across the lines 15-33; 19-34; 30-38; 24-72; 24-70; 77-82; 96-97; 80-96; 80-98; 99-100, and the results of the islands are also shown in Table 5.6. In this case, it can be noticed that the quality of the islanding solution determined by the proposed methodology is, once again, better (98.37%) than the islanding solution obtained using the SCCI algorithm (97.74%).. Indeed, it can be observed in Table 5.6 that the cut of Island 2 is much smaller when using the proposed methodology than the case when using the existing SCCI algorithm. The improvements achieved by the proposed methodology are further explained in the next case (a realistically sized system), where considerable reductions in the power flow disruption are obtained.

5.5.4. Reduced Great Britain Network

A static model of a reduced Great Britain network with 815 buses is finally utilised to test the proposed methodology. This network does not contain dynamic data. Hence, the simulations presented in this section aim to demonstrate the improvements in both the accuracy and the computational efficiency achieved by the proposed methodology over the SCCI algorithm [49] when implementing both approaches on a realistically sized system.

This network has a total load consumption of approximately 60 GW, and is used to study the islanding of the network into multiple islands $(r = 2,3,4,5)$. The following simulations assume that any branch can be included in the islanding solution. Furthermore, the slowly coherent groups of generators are defined, for simulation purposes, based on the geographical areas of the Great Britain network. Table 5.7 shows the total power flow disruption and the quality of each islanding solution, i.e., $\min(\eta(V_k))$ among the islands, using both the proposed methodology and the existing SCCI algorithm.

As noticed, the results using the proposed methodology are as good (when $r = 2$) or significantly better (when $r = 3,4,5$) than those obtained using the SCCI algorithm. It is important to note that the proposed methodology improves the accuracy of the islanding results (measured as the ratio between the total power flow disruption difference and the power flow disruption using the existing technique) in 12.6%, 20.7% and 15.6% for the cases with r = 3, 4 and 5, respectively.

One reason why the SCCI algorithm did not find an islanding solution with less power flow disruption when $r > 2$ in these cases is because the existing SCCI algorithm uses recursive bisection [49], which affects, in many cases, the quality of the islanding solution [70, 71, 74]. These results reveal another important advantage – accuracy – of using the new methodology particularly in large-scale power systems. Finally, it will be shown in Section 5.5.5 that the introduced methodology is more efficient than the existing SCCI algorithm.

Table 5.7: Results and comparison of the quality of the proposed methodology and the existing SCCI algorithm in the reduced Great Britain network

No. of Islands	Proposed methodology		Existing algorithm	
	Total Cut (MW)	$\min(\eta(V_k))$ (%)	Total Cut (MW)	$\min(\eta(V_k))$ (%)
2	1869	98.79	1869	98.79
3	1895	98.72	2167	95.06
4	3332	94.73	4204	93.69
5	5333	96.95	6318	95.06

5.5.5. Computational Efficiency of the Proposed Methodology

The proposed methodology has the key advantage of solving the associated eigenproblem only once, even if multiple islands are required. This feature considerably accelerates the determination of an islanding solution, particularly when dealing with large-scale power systems that require the creation of multiple islands, i.e., when $r > 2$. The new methodology is capable of determining an islanding solution in real-time even for large-scale power systems (Table 5.8), and its runtime is dominated by that of the eigendecomposition of the normalised Laplacian matrix. The computation of the eigenvectors $\boldsymbol{\psi}_1,\ldots,\boldsymbol{\psi}_r$ approximately represents 75% of the total runtime of the proposed methodology. Hence, the computational complexity of the new technique is approximately $O\left(n^3\right)$ [74], although it can be reduced to $O\left(n^{4/3}\right)$ when utilising a sparse form of the matrix $\mathbf{L_N}$ [63].

The proposed methodology computes the spherical distance only between the data-points representing load-nodes and the centroids that represent generation-nodes, reducing the order of the similarity matrix **S** to $(n-m)\times m$ (see Table 5.1 for an example). Moreover, it computes this similarity matrix only once. The existing methods based on spectral clustering [48, 49] use iterative algorithms (e.g., *k-means*) to cluster the data. These approaches create, in each iteration, a similarity matrix of order $n \times n$ [71]. The reduction in the order of **S** and the avoidance of iterative procedures achieved by the introduced methodology represents a diminution in the memory occupied by this, particularly when dealing with large-scale power systems, and an important improvement in the computational efficiency of the introduced approach.

The methodology was run 1000 times for the same loading condition and the average runtime, on different systems and for different number of islands, is computed. To compare the efficiency of the methodology with that of the existing algorithm [49], similar study is performed using the SCCI algorithm. Table 5.8 shows the results of this comparison.

As noticed, the proposed methodology is very efficient and rapidly determines an islanding solution for any given number of islands. The methodology reduces by approximately a

factor of ten the computational time with respect to the existing SCCI algorithm [49]. This improvement is significantly important when dealing with large-scale power systems that require the creation of numerous islands. The proposed methodology can meet the demand of real-time controlled islanding.

Table 5.8: Comparison of the computational time of the proposed methodology and the existing SCCI algorithm for minimal power flow disruption

Test System	Computational time using the proposed methodology (s)	Computational time using the SCCI algorithm (s)
IEEE 9^2	0.0008	0.0071
New England 39^2	0.0014	0.0141
IEEE 118^3	0.0090	0.0636
Great Britain-815^2	1.1478	7.3884
Great Britain-815^3	1.1638	9.7664
Great Britain-815^4	1.1653	9.9415
Great Britain-815^5	1.1753	9.9901

*The superscript indicates the number of created islands

5.6. Summary

This chapter has presented a novel constrained spectral clustering-based methodology to determine islanding solutions for minimal power flow disruption, while ensuring that each island contains only coherent generators. The methodology enables the exclusion of any branch from the islanding solution, improving its flexibility and practicality. This is important to exclude from the islanding solution any branch that operators deem to be unfeasible for islanding. The proposed methodology uses the normalised Laplacian matrix associated with the graph, and this approach improves the quality of the islanding solutions in comparison with existing islanding methods that use the unnormalised Laplacian matrix.

The methodology proposed in this chapter has the significant advantage that it solves the associated eigenproblem only once, even if multiple islands are required. Since it avoids recursive bisection, the new methodology is significantly faster than existing islanding methods for minimal power flow disruption. This also helps improve the quality of the solution. The methodology also reduces the order of a similarity matrix and avoids the use

of iterative approaches. This is done by defining the vectors that represent the generation-nodes as centroids and computing just once the spherical distance only between the vectors that represent load-nodes and the centroids. These two features also contribute accelerating the determination of an islanding solution for minimal power flow disruption.

The methodology has been tested and validated using the IEEE 9-bus test system, New England 39- and IEEE 118-bus test systems and a model of the British network with 815 buses. Simulation results have demonstrated that the new methodology determines better islanding solutions and is significantly faster (approximately ten times faster) than the existing methods for solving the ICI problem with the same objective function (minimal relative power flow disruption while ensuring coherency). Moreover, these reveal that the new methodology can be used with practical power systems to determine, in a few seconds, a good islanding solution, i.e., a solution with minimal power flow disruption relative to the power in each island, for any given number of islands.

Chapter 6. Sectionalising Strategies for Parallel Power System Restoration: A Constrained Cutset Matrix-Based Methodology

Chapter 6 presents a constrained cutset matrix-based methodology that can determine sectionalising strategies for Parallel Power System Restoration (PPSR). The methodology explores the vast combinatorial space to provide a list of suitable sectionalising strategies that satisfy the constraints of blackstart availability, load-generation balance, voltage stability and the ability to monitor synchronisation between adjacent islands.

The sectionalising strategies determined by the proposed methodology can ultimately be used by system operators to define the electrical islands that will be restored in parallel for the purpose of faster restoration. This would allow more system elements to be restored simultaneously and would considerably accelerate the restoration process of power systems in complete blackout, as the restoration of each island is performed independently.

PPSR, which sectionalises the entire blackout area into multiple islands that are then restored in parallel using their own cranking sources, is commonly adopted by utilities as it considerably accelerates the restoration process [76, 78, 79, 81, 85, 91, 92]. As detailed in Section 1.5.2, PPSR can be divided into three stages: preparation, reintegration – also known as system restoration – and load restoration.

The definition of a suitable sectionalising strategy is a critical task performed by system operators in the control centre during the preparation stage of PPSR [81, 85]. A suitable sectionalising strategy defines the set of lines that creates multiple islands for PPSR [76, 78, 79, 81, 85]. As discussed in Section 1.5.2.1.2, it is important that the sectionalising strategy is defined using updated system information that is received after the blackout has occurred, which represents the actual topology of the system and the availability of its elements [76, 81, 85]. The most important information for the design of a suitable sectionalising strategy includes [81, 85]: the available blackstart capability, the availability of interconnection

assistance, the status of non-blackstart units, the cranking groups, the status of lines and circuit breakers, and the predicted load levels.

A suitable sectionalising strategy can assist system operators during PPSR in bringing the entire critical load to service and restoring significant load as quickly as possible. The restoration of large amount of load prior to the resynchronisation of the islands is important as islands with more load restored are more likely to endure any unexpected voltage related issues during the resynchronization of the islands [75, 77, 86, 91-94, 121].

To ensure a reliable PPSR, it is important that system security is considered during the design of the sectionalising strategy. Therefore, the following criteria should be taken into account when determining a suitable sectionalising strategy [76, 81, 85].

1. Each island must have at least one blackstart unit and the cranking groups must be preserved;

2. Each island should have sufficient capacity to maintain a satisfactory frequency by matching generation and load;

3. Each island should have sufficient voltage control resources to maintain a suitable voltage profile;

4. Each island should be monitored at the system control center to ensure correct operation; and,

5. The tie-lines between the islands should all have monitoring equipment that allows the synchronization of the adjacent islands that they separate to be measured.

Numerous system operators have designed sectionalising strategies for the PPSR of their systems, e.g., the Mexican system [75], the PJM interconnection [93] and the British network [94], based on factors like historical asset ownership and operator experience, rather than the study of the physical and inherent properties of the electrical network. This simplifies the determination of the solution but raises questions regarding the quality of the restoration planning, the proper exploitation of the physical properties of the system, and the delays that have been experienced in the past [85, 91, 92].

Therefore, this chapter presents a new methodology that uses the concept of constrained cutset matrix, also known as the *cut-edge* incidence matrix [106], to determine sectionalising strategies that satisfy constraints 1, 2, 3 and 5 above, which are referred to as the critical constraints for PPSR. It is assumed in this thesis that each island can effectively be monitored by the control centre, which satisfies constraint 4. The methodology proposed in this chapter to determine sectionalising strategies is an adaptation of the technique presented in Chapter 4 to determine islanding solutions for minimal power imbalance. Hence, it aims to constrain certain buses, e.g., the generators that belong to the same cranking group, to be in a specific island, and to allow other buses – also referred in this chapter to as the "*free nodes*" – to be included in any of the possible islands. This creates a set of feasible cutsets – sectionalising strategies – that satisfy the critical PPSR constraints. This set of feasible strategies can ultimately be then used by operators to select, based upon their knowledge and experience, the most suitable solution for their system.

The proposed methodology is for use during the preparation stage of PPSR and can assist system operators by providing in a few minutes feasible sectionalising strategies that satisfy the critical PPSR constraints, which should serve to help ensure the steady-state stability of the future islands. Although a suitable sectionalising strategy increases the likelihood of a successful restoration and reduces the restoration time, it cannot guarantee success due the inherent complexity and risk of restoration [85, 91, 92]. Hence, the adequate use of the provided resources and the correct actions taken during the actual restoration of the islands will have to be assumed. Finally, it is important that operators only implement the methodology after they have received updated system information that represents the true topology and availability of elements in the post blackout system.

6.1. Graph Representation of the Electrical Power System

The power system in blackout with n buses, m generators, l branches and κ blackstart units is represented in this chapter as a node weighted and directed graph. This directed graph is used to represent the difference between the available generation and the load to be restored at each bus prior to the resynchronisation of the islands, and is defined as follows:

$$H = \left(V, \bar{E}, \sigma\right) \tag{6.1}$$

where,

- the elements $v_i \in V$, $i = 1, \ldots, n$, denote the nodes of the digraph *H*, and represent the buses of the power system in blackout. In order to distinguish the generation buses, the generation buses with blackstart capabilities and the load buses, the node set V is divided into various node subsets. Therefore, the node subsets $V_{GN} \subset V$ and $V_B \subset V_{GN}$ are defined to respectively represent the *m* generation buses (generation-nodes) and the κ available blackstart units of the system. Moreover, the node subsets $V_{LD} = V \setminus V_{GN}$ and $V_{CLD} \subset V_{LD}$ are defined to represent the $n - m$ load buses (load-nodes) and the load buses with critical loads, respectively.

- the elements $e_{ij} \in \bar{E}$, $i, j = 1, \ldots, n$, denote the arcs of the digraph, and they represent the branches of the system in complete blackout. In order to assign the direction of these arcs, the direction of the power flow in the branches in the base case is used for convenience. However, the methodology also accepts any other direction assigned to the arcs of *H*. In this chapter, the notation $e_k = \left(v_i, v_j\right)$ is also used.

- the number $u_i = \sigma\left(v_i\right)$, $i = 1, 2, \ldots, n$, represents the weight factor associated with each node $v_i \in V$, and is calculated as follows.

$$u_i = \begin{cases} P_{GN,i}^{\max} - \alpha_i P_{LD,i}^{\text{pre}} & \text{if } v_i \in V; \\ 0 & \text{otherwise.} \end{cases} \tag{6.2}$$

In (6.2), $P_{GN,i}^{\max}$ and $P_{LD,i}^{\text{pre}}$ are the maximum active power capability and predicted active power demand at bus *i*, respectively. The value u_i provides a measure of the balance at each bus between the available generation and the predicted load to be

restored prior to the resynchronization of the islands. $P_{LD,i}^{\text{pre}}$ is multiplied by the scalar α_i in (6.2) to represent the percentage of the load at bus *i* that will be restored before resynchronizing the islands. The value of α_i can be different for every bus. As the entire critical load must be restored as quickly as possible [76, 78, 79, 122], $\alpha_i = 100\%$ will be defined if $v_i \in V_{CLD}$. A load connected to a generation bus is considered to be a critical load, as this commonly represents local services that support the generator [75]. Moreover, as the amount of significant load to be restored before the resynchronisation of the islands usually varies from 40% to 75% of the total system load [30], $\alpha_i = 70\%$ is arbitrarily selected for all non-critical loads, $v_i \in V_{LD} \setminus V_{CLD}$, in the results presented in this chapter. In practical implementations of the proposed methodology, the definition of α_i for the nodes $v_i \in V_{LD} \setminus V_{CLD}$ would require a highly accurate estimation of the load levels. A higher value of α_i would result only in a small reduction in the number of feasible sectionalising strategies, as this value is used when selecting the strategies that satisfy the load-generation balance, as further detailed in Section 6.3.3.

In order to illustrate the graph representation introduced in (6.1), Figure 6.1 presents the digraph representation of the IEEE 9-bus test system and the corresponding node weights.

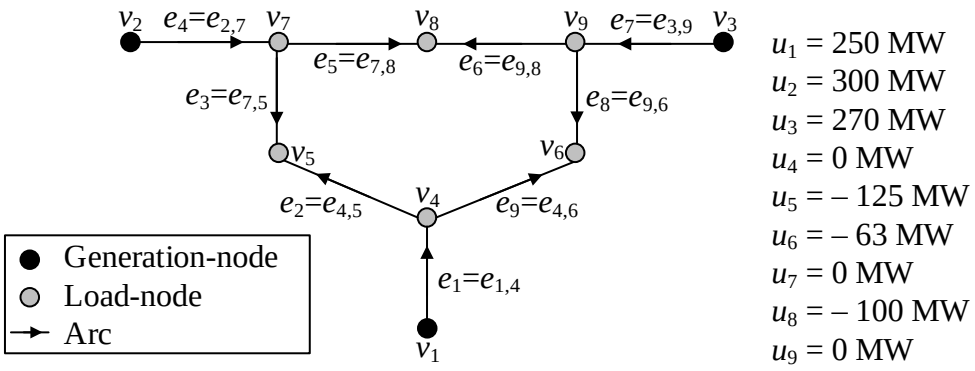

Figure 6.1: Digraph representation of the IEEE 9-bus test system with node weights for sectionalising strategies

As further detailed in Section 6.4.1, it is assumed in this chapter that the set of critical loads is $V_{CLD} = \{v_5, v_8\}$. As throughout this thesis, the black dots – defined by the elements in the

subset V_{GN} – represent the *m* generation buses. Furthermore, the grey dots – defined by the elements in the subset V_{LD} – represent the *n* – *m* load buses. The arrows presented in Figure 6.1 are defined by the arcs of the digraph, and they represent the branches of the system.

6.2. Definition of Graph Theoretic Concepts

The constrained cutset matrix-based methodology presented in this chapter to determine sectionalising strategies for parallel system restoration is an adaptation of the methodology presented in Chapter 4. Hence, it uses similar graph theoretic concepts as those described in Section 5.2. These graph theoretic concepts are summarised below.

6.2.1. Oriented Incidence Matrix

The oriented incidence matrix $\mathbf{M_H}$ of the digraph *H* is given by (A.25). As discussed earlier, the matrix $\mathbf{M_H}$ represents the directed incidence between the nodes $v_i, v_j \in V$ and the arcs $e_{ij} \in \bar{E}$. In order to maintain consistency with the concepts introduced in Chapter 4, the direction associated with the arcs $e_{ij} \in \bar{E}$ will be defined using the power flow in the branches in the base case. However, it is important to mention that the methodology also accepts any other direction associated with the arcs, and it will result in the same sectionalising strategies.

6.2.2. Oriented Cutset and Weight of the Subgraphs

As discussed in Section 4.2.2, the oriented cutset $\bar{E}_S \subset \bar{E}$ is the set of arcs that must be removed to split the digraph *H* into *r* directed subgraphs $H_1,\ldots,H_r$, with node sets $V_1,\ldots,V_r$. In the sectionalising problem presented in this chapter, an oriented cutset $\bar{E}_S$ consists of the arcs that represent the branches of the system to be included in the sectionalising strategy. Without loss of generality and due to the complexity of the sectionalising problem, only the case of partitioning the digraph into two disjoint digraphs is considered in this chapter. By applying recursive bisection, the methodology can determine sectionalising strategies for cases with more than two islands.

An oriented cutset $\overline{E}_S$ induces the creation of the node subsets V_1 and V_2. Then, the weight of the subgraph, denoted by $wei(V_k)$, $k = 1, 2$, can be calculated using (A.7) with respect to the node weights given by (6.2). The weight of the subgraph V_k represents the difference between the power generation capacity and the predicted load level within the island represented by the node subset V_k. Henceforth, it is called generation-load difference, and is used when ensuring that the islands satisfy the load-generation constraint, in other words, when ensuring that each island contains more generation than predicted load.

In order to illustrate the concept of weight of the subgraph in this application, consider that the digraph shown in Figure 6.1 is partitioned across the oriented cutset $\overline{E}_S = \{e_2, e_8\}$. Then the weight of the subgraphs H_1 and H_2 will be $wei(V_1) = \sum_{v_i \in V_1} u_i = u_1 + u_4 + u_6 = 187$ MW and $wei(V_2) = \sum_{v_i \in V_2} u_i = u_2 + u_3 + u_5 + u_7 + u_8 + u_9 = 345$ MW, respectively. This means that Island 1 and 2 respectively have an additional 187 MW and 345 MW generation capability available than predicted load level.

The weight of the subgraphs must be positive if a larger portion of the island will be restored to facilitate the synchronisation of islands, as the islands become more stable [85]. Hence, when an oriented cutset induces a negative subgraph weight, the methodology will exclude this from the set of feasible sectionalising strategies, as detailed in Section 6.3.

6.2.3. Label of the Node

As explained in Section 4.2.3, the label of the node refers to as the number of the island at which that node belongs to. For example, if the digraph shown in Figure 6.1 is split across the cutset $\overline{E}_S = \{e_2, e_8\}$, the node subsets $V_1 = \{v_1, v_4, v_6\}$ and $V_2 = \{v_2, v_3, v_5, v_7, v_8, v_9\}$ will be created, and this would mean that the label of the nodes $\{v_1, v_4, v_6\}$ is "1" and the label of the nodes $\{v_2, v_3, v_5, v_7, v_8, v_9\}$ is "2", as they belong to Island 1 and 2, respectively.

Certain nodes will have a specific label. For example, the generation-nodes that represent generators in a cranking group will have the same label, as they must be grouped in the

same island. It is important to remember that a cranking group consists of at least one blackstart unit and the non-blackstart units that will receive cranking power from the blackstart units in the same island. On the other hand, some load-nodes can be defined as "free nodes". Hence, they can be clustered in any of the possible islands. As in Section 4.2.3, the definition of certain "free nodes" creates multiple combinations that are used to build the indicator matrix described below.

6.2.4. Indicator Matrix

As extensively explained in Section 4.2.4, the indicator matrix **C** is the matrix that contains multiple combinations to cluster the nodes in different islands. Each combination in **C** labels certain nodes to be in a given island and combines the free-node labels. As explained earlier, this is a combinatorial problem that can be effectively solved computing the permutations with repetitions [115] of the free-node labels. Each combination in **C** defines the label of the node $v_i \in V$, and this causes the partition of the digraph H into disjoint digraphs. Each label indicates the number of the island at which that node should belong for that particular combination. Hence, the ij-entry of the matrix **C** is equal to the number $k = 1,2$ assigned to the node $v_i \in V$ for the j^{th} combination. If there are χ "free nodes", then there will be $\zeta = 2^{\chi}$ possible combinations, i.e., the size of **C** is $n \times \zeta$.

5.2.1. Oriented Constrained Cutset Matrix

As explained in Section 4.2.5, the oriented constrained cutset matrix $\mathbf{Q_H}$ is an extension of the oriented cutset matrix that enables to constrain certain nodes to be clustered into a specific group. The matrix $\mathbf{Q_H}$ of the digraph H is the $\zeta \times l$ matrix that represents the arcs that must be removed to cluster H for each given combination, and it can be computed using (4.7). As explained earlier, the ij-entry of $\mathbf{Q_H}$ is different from zero if the implementation of the i^{th} cutset requires the j^{th} arc to be removed to partition the digraph. Since the direction of the cutset is not of interest to determine sectionalising strategies, the sign obtained in the oriented cutset matrix $\mathbf{Q_H}$ will be ignored.

6.3. Proposed Sectionalising Methodology Based on a Constrained Cutset Matrix

The objective of PPSR is to accelerate the restoration process by restoring a number of separate and electrically isolated islands simultaneously. These islands are defined by a sectionalising strategy and the objective of this chapter is to propose a methodology based on the concept of a constrained cutset matrix that identifies a set of feasible sectionalising strategies which satisfy the critical constraints for PPSR. Presented in this section is the step-by-step execution of the proposed methodology.

6.3.1. Step 1: Blackstart Availability and Cranking Groups

Each island must contain at least one blackstart unit (Constraint 1) that can provide cranking power for the restoration of the island. The location and availability of the blackstart units are commonly known after the assessment of the system in blackout [76, 78, 79, 81], thus, this information is used in this chapter to define the subsets V_{B1} and V_{B2}. Then, two cranking groups, denoted by V_{GN1} and V_{GN2}, will be defined. Each group V_{GNk} consists of a subset V_{Bk} of blackstart units and another subset $V_{GNk} \setminus V_{Bk}$ representing the non-blackstart units. Defining suitable cranking groups requires a large number of studies [78, 79]. Hence, it is assumed in this thesis that they are separately defined, and as such the proper cranking groups for the systems considered in this chapter are assumed to be known.

In order to satisfy the availability of at least one blackstart unit within each island and to cluster together the cranking groups (Constraint 1), the methodology labels the generation-nodes – the nodes within the same cranking group – with the same label in all the possible combinations.

6.3.2. Step 2: Exclusion of Lines

In order to satisfy Constraints 3 and 5 of the system sectionalising problem, it is necessary to exclude certain branches from the solution space. A suitable sectionalising strategy cannot include lines that maintain the voltage stability within the islands (Constraints 3) or lines that lack the ability to monitor synchronization (Constraints 5).

In order to define critical lines that maintain system voltage stability, it is common practice to consider that the tie-lines between the islands are open during the restoration process [85]. Thus, to identify these critical lines, an $N-1$ voltage stability analysis is performed for every line in the network. The most severe outages are then selected using the contingency analysis method available in DIgSILENT Power Factory [120]. This tool computes the reactive power injection at that bus before the contingency, then disconnects the line in analysis, and computes the new reactive power injection after the contingency. A line is critical if its disconnection in the nominal case produces an excessive (i.e., considerably high compared to the other disconnections) reactive power difference between the pre-contingency and the post-contingency [85]. When the critical lines are identified, the subset $\bar{E}_{VS} \subset \bar{E}$ that consists solely of the arcs that represent these critical lines in the digraph of the power system is defined.

These critical lines are not the only type of branch that should be excluded from consideration when determining the cutset for the sectionalising strategy. As explained earlier, the tie-lines that separate the islands must be equipped with the ability to measure the synchronisation between the islands that they separate (Constraint 5). As with the lines critical to voltage stability, an arc subset $\bar{E}_C \subset \bar{E}$ that consists of the arcs that represent the branches that cannot measure resynchronisation is defined. This subset is commonly defined using information available following the blackout assessment [76, 81, 85].

Having defined the subsets of arcs to be excluded, the subset $\left(\bar{E}_{EX} = \bar{E}_{VS} \cup \bar{E}_C\right) \subset \bar{E}$ of excluded-arcs is defined. To exclude the arcs $e_{ij} \in \bar{E}_{EX}$ from the strategies, the methodology labels the nodes v_i and v_j incidence to the arc $e_{ij} \in \bar{E}_{EX}$ with the same number.

This mechanism for excluding arcs from sectionalising strategies is not limited to the branch types considered in this thesis. In practice, it could be extended to any branch, or branch type, that the operator deemed unsuitable for use as a tie-line between islands. For example, it is known that transformers should not be included in the sectionalising strategy, as they cannot be used during the resynchronisation of the islands [81]. Other branch types that should not be used as tie-lines between islands are provided in [78, 79, 81, 85, 91, 92].

6.3.3. Step 3: Sectionalising Strategies Determination

In step 3, the proposed methodology creates the oriented incidence matrix $\mathbf{M_H}$ (A.25) associated with the digraph *H*. It also builds the indicator matrix **C**, labelling thus the nodes with the number $k = 1,2$. The methodology utilises the set of "free nodes" and performs the combinatorial optimization with these nodes (permutations with repetitions [115]), to create several combinations of node labels.

It is important to remember that the labels of the generation-nodes are fixed based on the predefined cranking groups V_{GN1} and V_{GN2}, i.e., all generators in the same cranking group will have the same fixed label. Additionally, the nodes incident to the excluded-arcs had also been labelled with the same number. It should be noted that these labels can be different for different combinations but they would be changed together, which results in both nodes being always clustered in the same island. Labelling these nodes with the same number ensures that the branches that cannot be used as tie-lines are excluded from the sectionalising strategies. These steps limit the size of the indicator matrix **C** and consequently the number of sectionalising strategies that must be considered.

When the indicator matrix **C** is defined, the constrained cutset matrix $\mathbf{Q_H}$ is computed using (4.7). As previously discussed, the matrix $\mathbf{Q_H}$ contains multiple cutsets, and the non-zero entries in the i^{th} row of $\mathbf{Q_H}$ represent the arcs that must be removed to create the subgraphs defined in the i^{th} column of the indicator matrix **C**. The *ij*-entry of $\mathbf{Q_H}$ is different from zero if the implementation of the i^{th} cutset requires the j^{th} arc to be removed to split the digraph.

As explained in Section 4.4, the matrix $\mathbf{Q_H}$ may contain cutsets that are not feasible in the context of power systems, that is, they may sectionalise the system into more than two islands, and some of these islands will not have cranking sources. Therefore, the methodology computes the rank of the digraph (A.12) induced by the removal of the corresponding arcs for each combination. This procedure is repeated for all of the cutsets included in $\mathbf{Q_H}$, excluding the unfeasible cutsets and maintaining only those solutions than could actually be implemented in power systems. The resulting set of feasible cutsets would eventually define two islands, and they all will satisfy Constraint 1, 3 and 5.

The methodology then seeks to create islands with sufficient generation capacity (Constraint 2). In order to do so, it computes the *n*-vector **u**, which is a column vector with the j^{th} row equal to the node weight u_i given by (6.2). For example, in the case of the IEEE 9-bus test system, the vector **u** will be created using the information shown in Figure 6.1. Then, by calculating the weight of the subgraphs $wei(V_k)$ (A.7) with respect to the node weights given by (6.2), the power generation capacity minus the predicted load level within each island – the generation-load difference – induced by each cutset can be determined. The final set of feasible sectionalising strategies is defined as those cutsets that partition the power system into two islands and that produce positive subgraph weight in both islands.

It is important to note that the cutsets included in this final subset will all satisfy the four constraints, i.e., blackstart availability constraint (Constraint 1), load-generation balance represented by a positive generation-load difference (Constraint 2), exclusion of both critical lines from sectionalising strategies that maintain system voltage stability (Constraint 3) and those that cannot measure resynchronisation with adjacent islands (Constraint 5).

When more than two islands are required ($r > 2$), the set V_1 or V_2 that contains more than one blackstart unit should be selected as the node set of a new digraph, and the methodology should be implemented again. The process should be repeated until the required number of islands is achieved. When Step 3 is finished, the set of feasible sectionalising strategies will satisfy Constraints 1, 2, 3 and 5 for each island.

6.4. Simulations Examples

This section presents the simulation examples of sectionalising power systems in complete blackout considering the constraints of: blackstart availability, load-generation balance, voltage stability and the ability to monitor synchronisation between adjacent islands. The results of the methodology proposed in this chapter will be compared with those obtained using the methodology presented in Chapter 7 of this thesis.

6.4.1. IEEE 9-Bus Test System

The methodology is initially illustrated using the IEEE 9-bus test system. Figure 6.1 shows the digraph representation of this test system and the node weights. For simulation purposes, it is assumed that every blackstart unit, non-blackstart unit, line and breaker is available after the blackout. If any of these elements were to be unavailable, it would result in a reduction in the number of feasible cut-sets, as shown in the case studies developed in Section 6.4.2.2. The set of critical loads is defined as $V_{CLD} = \{v_5, v_8\}$.

In Step 1, the proposed methodology defines the cranking groups. For simulation purposes, it is assumed in this thesis that the subsets of blackstart units are $V_{B1} = \{v_1\}$ and $V_{B2} = \{v_2\}$. Then, the cranking groups separately defined are considered to be $V_{GN1} = \{v_1\}$ and $V_{GN2} = \{v_2, v_3\}$. These results are later used to build the indicator matrix **C** (see (6.3)).

In Step 2, the contingency screening method available in DIgSILENT Power Factory [120] is used to identify the critical lines that maintain system voltage stability. The results obtained from the contingency screening method are used to define the set $\bar{E}_{VS} = \{e_{1,4}, e_{2,7}, e_{3,9}\}$. Furthermore, it is assumed in this case that every line can measure synchronisation with adjacent islands. Therefore, the set $\bar{E}_C = \varnothing$ is defined. Then, the set of excluded-arcs is $\bar{E}_{EX} = \{e_{1,4}, e_{2,7}, e_{3,9}\}$. As explained earlier, these results are also used to build the indicator matrix **C**, as noticed in (6.3).

In Step 3, the methodology uses the digraph shown in Figure 6.1 to create the oriented incidence matrix $\mathbf{M_H}$. It then computes the indicator matrix **C** using the previous information. It should be noted that the label of the node v_1 must be "1", as the generator at bus 1 must be in one island (cranking group V_{GN1}), and the label of the nodes v_2 and v_3 must be "2", as the generators at buses 2 and 3 must be in another island (cranking group V_{GN2}). Furthermore, it should be noted that due to the set of excluded-arcs, the label of the node v_4 must be "1", and the label of the nodes v_7 and v_9 must be "2". Hence, the methodology determines that the "free nodes" are v_5, v_6 and v_8, and the indicator matrix **C** shown in (6.3) is obtained after the combinatorial optimization.

$\mathbf{C}^T =$

	v_1	v_2	v_3	v_4	v_5	v_6	v_7	v_8	v_9
$comb_1$	1	2	2	1	1	1	2	1	2
$comb_2$	1	2	2	1	1	1	2	2	2
$comb_3$	1	2	2	1	1	2	2	1	2
$comb_4$	1	2	2	1	1	2	2	2	2
$comb_5$	1	2	2	1	2	1	2	1	2
$comb_6$	1	2	2	1	2	1	2	2	2
$comb_7$	1	2	2	1	2	2	2	1	2
$comb_8$	1	2	2	1	2	2	2	2	2

(6.3)

It is important to remember that the labels given to the free nodes indicate that these nodes can be clustered in any island. The methodology then uses the matrices **C** and $\mathbf{M_H}$ to compute the constrained cutset matrix $\mathbf{Q_H}$ shown in (6.4). As explained earlier, the orientation of the cutsets is ignored in this chapter as such direction is not of interest to determine sectionalising strategies.

The methodology then evaluates whether the cutsets included in $\mathbf{Q_H}$ are feasible or not. Hence, the rank of the digraph induced by each cutset is computed. The rank of the induced digraph must be equal to $n - 2$. In this case, there are four feasible cutsets, and these are highlighted in (6.4). Note that although the node v_8 was defined as "free node", this cannot be grouped in Island 1 due to the inherent topology of the power system (see Figure 6.1).

$\mathbf{Q_H} =$

	e_1	e_2	e_3	e_4	e_5	e_6	e_7	e_8	e_9
$cutset_1$	0	0	1	0	1	1	0	1	0
$cutset_2$	0	0	1	0	0	0	0	1	0
$cutset_3$	0	0	1	0	1	1	0	0	1
$cutset_4$	0	0	1	0	0	0	0	0	1
$cutset_5$	0	1	0	0	1	1	0	1	0
$cutset_6$	0	1	0	0	0	0	0	1	0
$cutset_7$	0	1	0	0	1	1	0	0	1
$cutset_8$	0	1	0	0	0	0	0	0	1

(6.4)

The methodology then computes the different between the power generation capacity and the predicted system load within each possible island for the four feasible cutsets and the results are shown in Table 6.1. In this case, the four cutsets would results in islands with positive generation-load difference. When moving nodes between the islands, it should be noted that an action that causes an increase in the generation-load difference in Island 1 will cause a decrease in the generation-load difference in Island 2. It should be noted that the

four feasible sectionalising strategies satisfy the critical constraints for PPSR. The third sectionalising strategy is arbitrarily selected and shown in Figure 6.2. The generators highlighted in red represent the blackstart units.

Table 6.1: Sectionalising results of the constrained cutset matrix-based methodology for the IEEE 9-bus test system

Sectionalising Strategy	Generation-load difference (MW)	
	Island 1	Island 2
5-7; 6-9	62	470
5-7; 4-6	125	407
4-5; 6-9	187	345
4-5; 4-6	250	282

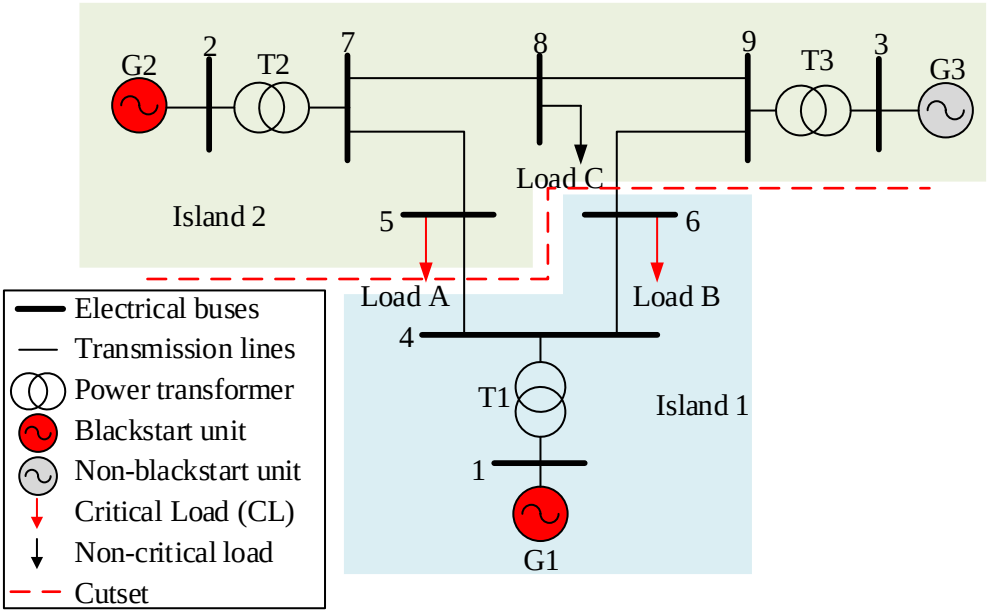

Figure 6.2: IEEE 9-bus test system sectionalised into two islands using the constrained cutset matrix-based methodology

6.4.2. New England 39-Bus Test System

The proposed methodology is now illustrated using the New England 39-bus test system. For simulation purposes, the set of critical loads is defined as $V_{CLD} = \{v_3, v_4, v_8, v_{16}, v_{20}\}$. It is assumed that the subsets of blackstart units are $V_{B1} = \{v_{37}\}$ and $V_{B2} = \{v_{33}\}$. Two cases are examined using this network to show the adaptability of the methodology to any system

condition, and to demonstrate that the unavailability of system assets would only result in a reduction in the number of feasible sectionalising strategies. In case study 1 it is assumed that all elements of the system are available after the blackout, and case study 2 examines the unavailability of system assets (a generator and a line) after the blackout.

6.4.2.1 Case Study 1: Availability of all System Assets

The first case study assumes that every blackstart unit, non-blackstart unit, line and breaker is available after the blackout. For the given blackstart units, the cranking groups are $V_{GN1} = \{v_{30}, v_{31}, v_{32}, v_{37}, v_{39}\}$ and $V_{GN2} = \{v_{33}, v_{34}, v_{35}, v_{36}, v_{38}\}$. These results are used to build the indicator matrix **C**. The critical lines that maintain system voltage stability are found to be represented by the arc subset $\bar{E}_{VS} = \{e_{5,6}, e_{6,7}, e_{6,11}, e_{10,11}, e_{13,14}, e_{21,22}, e_{23,24}, e_{28,29}, e_{26,29}\}$. It is initially assumed that every line can measure synchronisation with adjacent islands. Since the transformers should not be included in the sectionalising strategies [81], the edges that represent transformers are constrained to be excluded from the solution space by including the appropriate arcs in the subset $\bar{E}_C$. Then, the set of excluded-arcs is $\bar{E}_{EX} = \bar{E}_{VS} \cup \bar{E}_C$. These results will also be used to build the indicator matrix **C**.

The implementation of Step 3 then determines sixteen cutsets. These cutsets are then evaluated to exclude the unfeasible cutsets. In this case, there are only eight feasible cutsets, and they are shown in Table 6.2. The methodology then computes the weight of the subgraphs – generation-load difference – within each possible island for the eight feasible cutsets and the results are also shown in Table 6.2.

It can be noted that the strategy 2-3; 4-5; 4-14; 14-15; 25-26 defines Island 2 with more load level than power capability, i.e., negative subgraph weight (A.7). Thus, this strategy is defined as unfeasible and is excluded from the final list of feasible sectionalising strategies. Therefore, it is concluded that this system has seven feasible sectionalising strategies that can be used by system operators to define the islands that will be restored in parallel. Determining multiple feasible strategies enables operators to select, based upon their knowledge and experience, the most suitable for their system. Table 6.2 also shows that as the generation-load difference within Island 1 increases, it decreases within Island 2.

Table 6.2: Sectionalising results using the constrained cutset matrix-based methodology for the New England 39-bus test system in case study 1

Sectionalising Strategy	Generation-load difference (MW)	
	Island 1	Island 2
15-16; 17-18; 25-26	883.9	1065.3
3-18; 15-16; 25-26	994.5	954.7
14-15; 17-18; 25-26	1107.9	841.3
3-18; 14-15; 25-26	1218.5	730.7
2-3; 3-4; 15-16; 25-26	1316.5	632.7
2-3; 3-4; 14-15; 25-26	1540.5	408.7
2-3; 4-5; 4-14; 15-16; 25-26	1816.5	132.7
2-3; 4-5; 4-14; 14-15; 25-26	2040.5	-91.3

The final set of feasible sectionalising strategies satisfies the critical constraints. Figure 6.3 shows the sectionalising strategy that induces similar subgraph weights, i.e., the second in Table 6.2. As before, the generators highlighted in red represent the blackstart units.

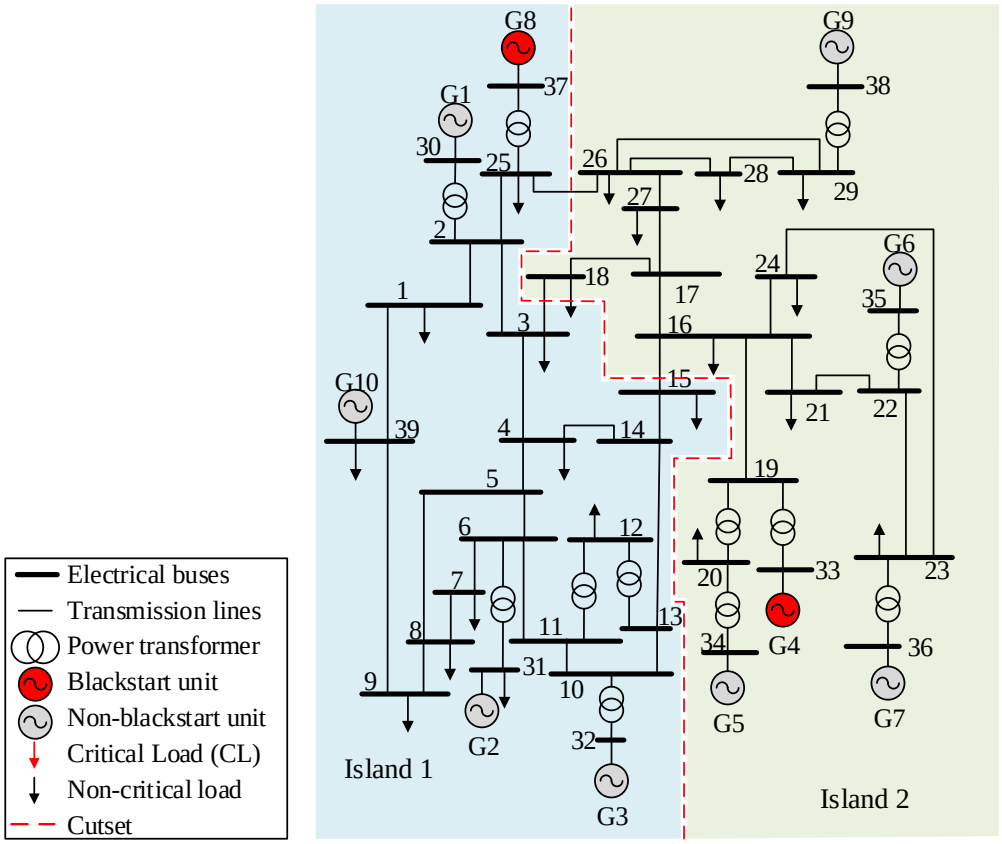

Figure 6.3: New England 39-bus test system sectionalised into two islands in case study 1 using the constrained cutset matrix-based methodology

6.4.2.2 Case Study 2: Unavailability of System Assets

The second case study aims to demonstrate the adaptability of the methodology to any system condition. It is assumed that the generator at bus 35 (G6) is not available after the blackout. Since this is the largest machine in the cranking group V_{GN2}, its unavailability would produce larger imbalances. In addition, it is considered that the line 3-18 (previously included in the set of feasible sectionalising strategies) has lost monitoring ability, thus it cannot measure resynchronisation. Losing a monitoring equipment on a line is equivalent to losing a line for sectionalising strategies due to Constraint 5. The cranking groups previously defined remain the same except the unavailability of the generator G6. Additionally, the new set of excluded-arcs must include the arc that represents the line 3-18.

The implementation of the methodology considering this new post-blackout state determines two feasible sectionalising strategies, which are shown in Table 6.3.

Table 6.3: Sectionalising results using the constrained cutset matrix-based methodology for the New England 39-bus test system in case study 2

Sectionalising Strategy	Generation-load difference (MW)	
	Island 1	Island 2
15-16; 17-18; 25-26	883.9	378.3
14-15; 17-18; 25-26	1107.9	154.3

It should be noted that the unavailability of G6results in the reduction of the generation-load difference within Island 2. In practical implementations, the unavailability of a non-blackstart unit may require updating the predicted load levels [79, 122]. Figure 6.4 shows the sectionalising strategy that induces the most similar subgraph weights.

6.4.3. IEEE 118-Bus Test System

The methodology proposed in this chapter is now illustrated using the IEEE 118-bus test system. For simulation purposes, it is assumed that every blackstart unit, non-blackstart unit, line and breaker is available after the blackout. The assumed critical loads are highlighted in Figure 6.5. It is considered that the blackstart units are located at buses 31

and 87. Thus, the cranking groups separately defined are $V_{GN1} = \{v_{10}, v_{12}, v_{25}, v_{26}, v_{31}\}$ and $V_{GN2} = \{v_{46}, v_{49}, v_{54}, v_{59}, v_{61}, v_{65}, v_{66}, v_{69}, v_{80}, v_{87}, v_{89}, v_{100}, v_{103}, v_{111}\}$. The critical lines that maintain system voltage stability are found to be {5-8, 8-9, 9-10, 37-38, 38-65}.

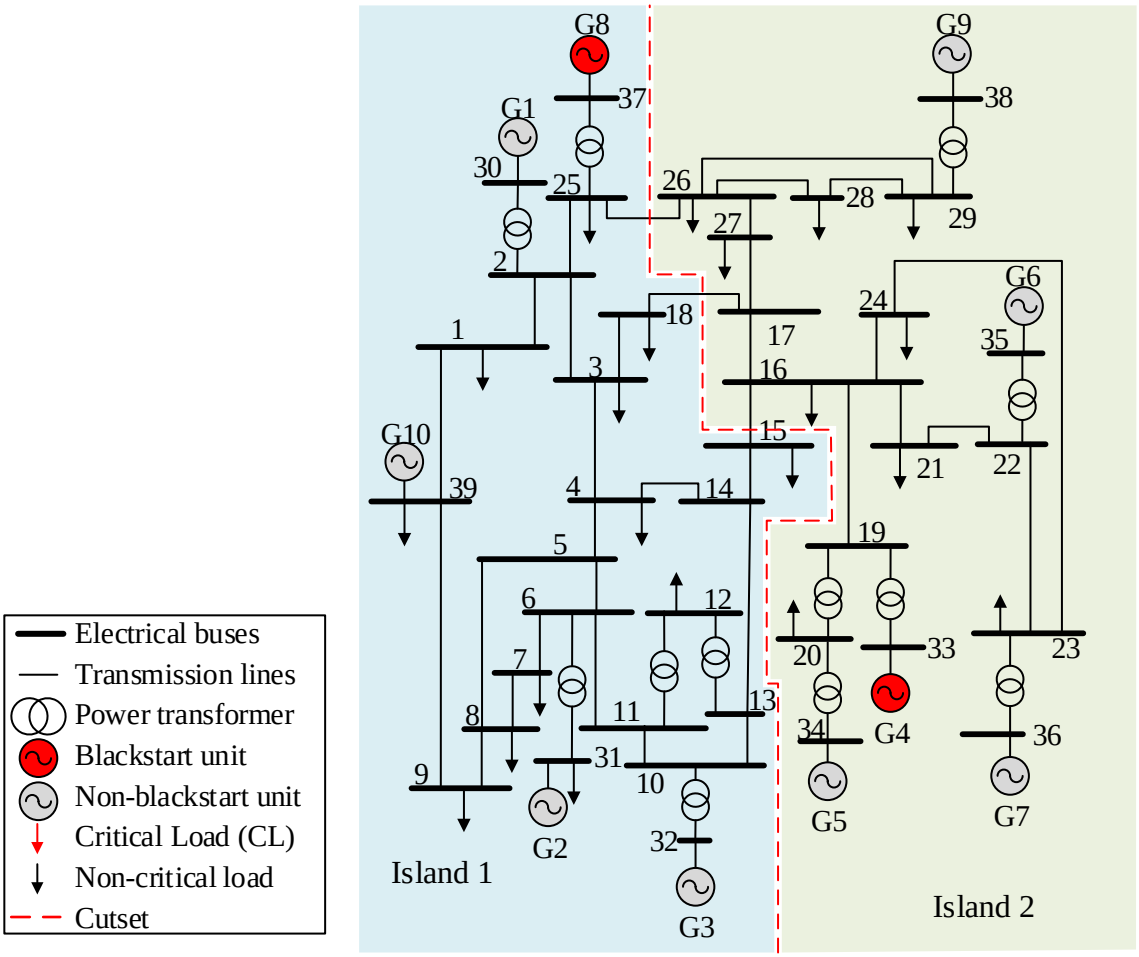

Figure 6.4: New England 39-bus test system sectionalised into two islands in case study 2 using the constrained cutset matrix-based methodology

Furthermore, it is considered, for simulation purposes, that every line can measure synchronisation with adjacent islands. Finally, it is known that in practical implementations transformers should not be included in the sectionalising strategies [81]; therefore, the arcs that represent transformers are also constrained to be excluded from the set of feasible sectionalising strategies by including the appropriate arcs in the subset $\bar{E}_C$. Thus, the subset of excluded-arcs $\bar{E}_{EX} = \bar{E}_{VS} \cup \bar{E}_C$ is defined, and these will be excluded from the sectionalising strategies by labelling the applicable nodes with the same island number.

The implementation of Step 3 then determines that there are 324 feasible sectionalising strategies. As previously mentioned, determining multiple feasible strategies enables operators to select, based upon their knowledge and experience, the most suitable for their system. The minimum and maximum generation-load difference within Island 1 (Island 2) are 433 MW (2023 MW) and 893 MW (2483 MW), respectively. Figure 6.6 shows the distribution of these 324 feasible cutsets into five groups of 92 MW ranges (i.e., maximum minus minimum generation-load difference over five).

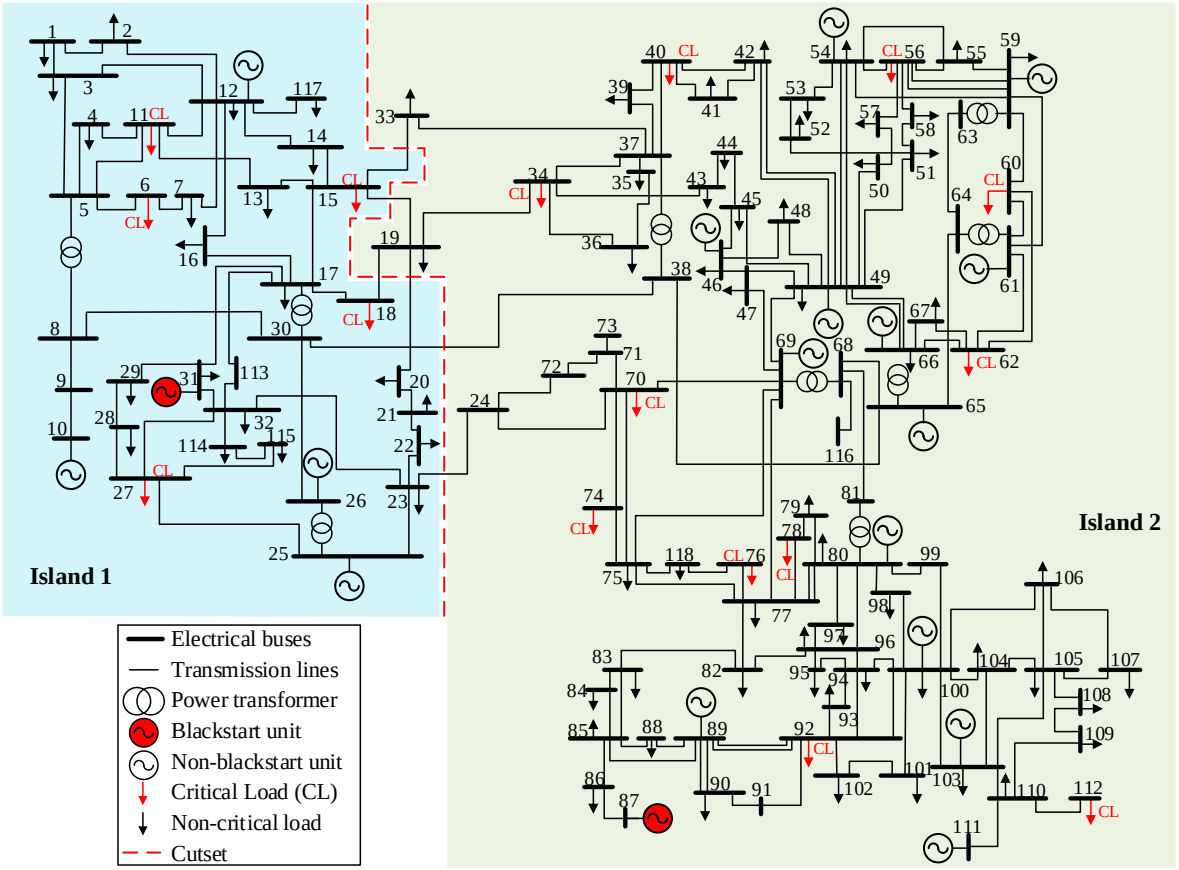

Figure 6.5: IEEE 118-bus test system sectionalised into two islands using the constrained cutset matrix-based methodology

As it can be noticed, the majority of feasible sectionalising strategies (219, approximately 68% of the total) has a generation-load difference in the range of 617-801 MW and 2115-2299 MW for Island 1 and 2, respectively. Figure 6.6 also shows that as the generation-load difference within Island 1 increases, it decreases within Island 2. Since the generation-load difference in Island 1 is higher in the range of 801-893 MW and this value remains high in

Island 2, it is considered that it is more suitable to select a sectionalising strategy that is within these 44 feasible cutsets, as this will create islands that will have a much larger generation capability than predicted load consumption. This potentially reduces the number of feasible cutsets to 44, facilitating thus operator's decision.

Figure 6.5 shows a sectionalising strategy that creates islands with generation-load difference equal to 804 MW in Island 1 and 2112 MW in Island 2. This SS is selected as it satisfies all the critical PPSR constraints, it is within the range of the 44 cut-sets that result in large generation capacity in Island 1, and it has a reduced number of tie-lines between the islands. Reducing the number of tie-lines potentially decreases the time required for the tie-line reconnections that must be performed during the resynchronisation of the islands.

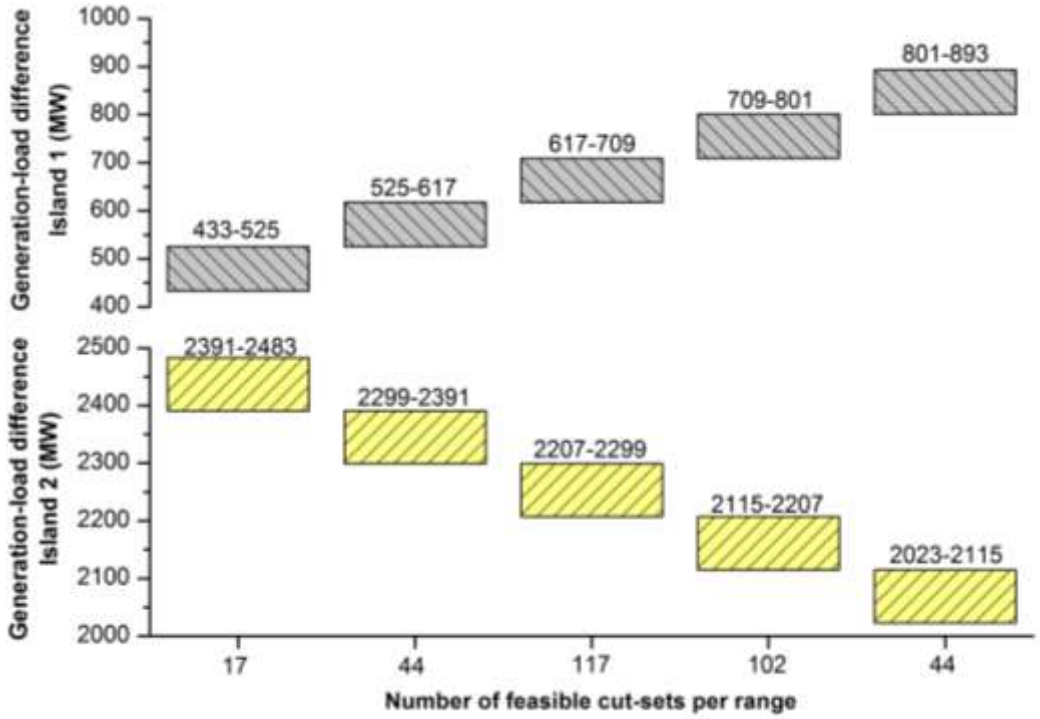

Figure 6.6: Distribution of the 324 feasible cutsets for the IEEE 118-bus test system

6.4.4. Computational Efficiency of the Proposed Methodology

It must be noted that sectionalising strategies are determined during the preparation stage of PPSR, and system operators commonly have several minutes during this stage to plan the most adequate sectionalising strategy. This section presents the runtime of the proposed

methodology in order to demonstrate that the methodology introduced in this chapter can find a suitable set of sectionalising strategies in only a few seconds or minutes. The methodology was run 100 times and the average runtime, on different systems, was computed. Table 6.4 shows the average runtime of the proposed methodology for the three test system considered in this thesis.

Table 6.4: Average runtime of the constrained cutset matrix-based methodology for sectionalising strategies

Test System	Runtime using the proposed methodology (s)
IEEE 9-bus	0.01
New England 39-bus	Scenario 1: 2.51 Scenario 2: 2.65
IEEE 118-bus	114.57

It can be observed in Table 6.4 that the methodology can determine the set of suitable sectionalising strategies in the case of the IEEE 118-bus test system in less than two minutes, which is considerably fast for the purposes of PPSR.

6.5. Summary

This chapter has presented a methodology that uses the concept of a constrained cutset matrix to determine system sectionalising strategies for the purpose of PPSR, which accelerates the restoration of a system in complete blackout. The methodology determines multiple feasible strategies to sectionalise the entire blackout area, whilst satisfying the constraint of blackstart availability within each island, preserving the integrity of the defined cranking groups, creating islands with more generation capacity than the predicted load level and excluding from the solution critical lines that maintain system voltage stability and those that cannot measure resynchronisation with adjacent islands.

Satisfying these constraints provides sufficient resources to maintain the steady-state stability of the islands within acceptable limits during the actual restoration. The proposed methodology is intended for use during the preparation stage of PPSR, after updated post-blackout system information is provided, and it aims to create islands that would facilitate

PPSR. The methodology proposed in this chapter is capable of exploring the vast combinatorial space to find sectionalising strategies that satisfy the given critical constraints. It can effectively determine a set of feasible sectionalising strategies that can ultimately be used by system operators to select, based upon their knowledge and experience, the most suitable sectionalising strategy. This will enable them to simultaneously restore more system components, as each island is restored independently.

The proposed methodology has been illustrated using the IEEE 9-bus test system, New England 39- and IEEE 118-bus test systems. Simulation results have indicated that the methodology is effective during the preparation stage of PPSR, as it quickly provides guidance to operator on how the blackout area can be sectionalised. Numerous cases have been examined to demonstrate the adaptability of the methodology to any system condition, e.g., assets unavailability. The solutions have been obtained in less than two minutes for the larger case with 118 buses, indicating that the methodology is computationally efficiency enough to be employed during the preparation stage of PPSR.

Chapter 7. Sectionalising Strategies for Parallel Power System Restoration: A Constrained Spectral Clustering-Based Methodology

Chapter 7 presents a constrained spectral clustering-based methodology that uses the physical and inherent properties of the system to quickly determine a suitable sectionalising strategy for Parallel Power System Restoration (PPSR). The methodology can find a strategy that satisfies the constraints of blackstart availability, load-generation balance, voltage stability and the ability to monitor synchronisation between adjacent islands.

The methodology uses the electrical distance between buses to define islands that have strong internal connections – in terms of the electrical distance – but weak external connections. This creates electrically cohesive islands, reduces the number of tie-lines that must be closed to reconnect the islands and increases the number of internal connections.

As previously detailed in Chapter 6, numerous system operators have designed sectionalising strategies for the PPSR of their systems based on factors like historical asset ownership and operator experience, rather than the study of the physical and inherent properties of the electrical network. This simplifies the determination of the solution but raises questions regarding the quality of the restoration planning and the proper consideration and exploitation of the physical properties of the system [85, 91, 92].

Therefore, this chapter proposes a methodology based on constraint spectral clustering that can determine a sectionalising strategy that satisfies the critical constraints 1, 2, 3 and 5 mentioned earlier. In addition to satisfy these critical constraints for PPSR, the methodology uses the physical and inherent properties of the network to create islands with the maximum electrical cohesiveness. The concept of electrical cohesiveness is expressed in terms of the electrical distance between buses and has previously been used to create electrical zones for system planning and control [123-126]. Introducing it as part of the formulation of the sectionalising strategy problem allows the creation of islands that not

only satisfy the critical PPSR constraints but also possess the quality of being strongly connected within themselves and weakly connected to other islands, where the strength of connectivity is assessed in terms of the electrical distance between buses.

Moreover, maximising the electrical cohesiveness of the islands allows reducing the number of tie-lines between the islands and consequently increases the number of internal connections. This reduces the number of potentially time-consuming tie-line reconnections needed during the resynchronisation of the islands, while increasing the number of paths available for the transmission of cranking power from the blackstart units to the non-blackstart units within each island. Furthermore, the emphasis on creating electrically cohesive islands means that the lines that separate these subsystems will tend to be the longest, electrically, and weakest transmission lines between the define cranking groups. Therefore, the effects of high charging currents and overvoltages that might arise when reconnecting these long and unloaded lines can be reduced, as these lines will be reconnected at the end of PPSR when the system is nearing full strength [76, 78, 79].

The nature of the sectionalising strategy problem presented in this chapter lends itself to being solved using spectral clustering. Thus, this chapter proposes the use of constrained spectral clustering to find a sectionalising strategy that satisfies the critical constraints with the maximum electrical cohesiveness within the islands [70-74]. This technique can directly determine an "initial sectionalising strategy", meaning a solution that ensures blackstart availability (Constraint 1), excludes critical lines that maintain system voltage stability within the islands (Constraint 3), and ensures that the tie-lines between islands can measure the synchronisation between adjacent islands (Constraint 5). A graph theory based refinement algorithm is then used to ensure that each island will possess sufficient power generation capacity to restore loads (Constraint 2).

The methodology proposed in this chapter is for use during the preparation stage of PPSR and can also assist operators by quickly providing a sectionalising strategy that satisfies constraints 1, 2, 3 and 5, which should serve to help ensure the steady-state stability of the future islands. As explained in Chapter 6, it is important that the methodology is implemented by operators in the control centre only after they have received updated

system information that represents the true topology and availability of elements in the post blackout system. In this chapter, simulation results for the same test systems are used to demonstrate the effectiveness of the methodology in determining the sectionalising strategy that maximises the internal electrical-cohesiveness of the islands whilst also satisfying the critical constraints for PPSR. A comparison between the methodology presented in the previous chapter and the new methodology introduced in this chapter is performed to highlight the benefits of both approaches and present certain limitations.

7.1. Graph Representation of the Electrical Power System

The power system in blackout with n buses, m generators and κ blackstart units is represented in this chapter as a node and edge weighted and undirected graph. This graph is used to represent the difference at each bus between the available generation and the load to be restored prior to the resynchronisation of the islands and the electrical distance between the buses, and is defined as follows:

$$G = (V, E, \rho, \omega) \tag{7.1}$$

where,

- the elements $v_i \in V$, $i = 1, \ldots, n$, denote the nodes of the graph, and represent the buses of the system in blackout. In order to distinguish the generation buses, the generation buses with blackstart capabilities and the load buses, the node set V is divided into various node subsets. Therefore, the node subsets $V_{GN} \subset V$ and $V_B \subset V_{GN}$ are defined to respectively represent the m generation buses (generation-nodes) and the κ blackstart units of the system. Moreover, the node subsets $V_{LD} = V \setminus V_{GN}$ and $V_{CLD} \subset V_{LD}$ are defined to represent the $n-m$ load buses (load-nodes) and the load buses with critical loads, respectively.

- the elements $e_{ij} \in E$, $i, j = 1, \ldots, n$, denote the edges of the graph, and they represent the branches of the system in blackout.

- the number $u_i = \sigma(v_i)$, $i = 1, 2, \ldots, n$, represents the weight factor associated with each node $v_i \in V$, and is calculated as follows.

$$u_i = \begin{cases} P_{GN,i}^{\max} - \alpha_i P_{LD,i}^{\text{pre}} & \text{if } v_i \in V; \\ 0 & \text{otherwise.} \end{cases} \tag{7.2}$$

  where, $P_{GN,i}^{\max}$ and $P_{LD,i}^{\text{pre}}$ are the maximum active power capability and predicted active power consumption at bus *i*, respectively. The value u_i also provides a measure of the balance at each bus between the available generation and the predicted load to be restored prior to the resynchronization of the islands. As in Chapter 6, $P_{LD,i}^{\text{pre}}$ is multiplied by the scalar α_i to represent the percentage of the load at bus *i* that will be restored before resynchronizing the islands. The value of α_i can be different for every bus. As before, $\alpha_i = 100\%$ is defined if $v_i \in V_{CLD}$, to ensure that the full critical load can be restored. As explained in the previous chapter, system loads connected to a generation bus are considered to be critical loads, as they usually represent local services that support the generator [75]. Moreover, $\alpha_i = 70\%$ is also defined in this chapter for all $v_i \in V_{LD} \setminus V_{CLD}$. It must be mentioned that changing the value of α_i for the application presented in this chapter would only result in a fewer number of feasible sectionalising strategies.

- the number $w_{ij} = \rho(e_{ij})$, $i, j = 1, 2, \ldots, n$, represents the weight factor associated with each edge $e_{ij} \in E$, and is calculated as follows.

$$w_{ij} = w_{ji} = \begin{cases} Y_{ij} = 1/X_{ij} & \text{if } e_{ij} \in E; \\ 0 & \text{otherwise.} \end{cases} \tag{7.3}$$

In (7.3), X_{ij} is the reactance in per unit of the branch between buses *i* and *j*. The resistance R_{ij} is ignored in (7.3) as, in general, $R_{ij} << X_{ij}$ [125]. The value w_{ij} can be interpreted as a measure of the strength of the connection between two nodes – the inverse of X_{ij} – as it is preferable to cluster together strongly connected nodes (nodes connected by large w_{ij}). This definition will become clearer in Section 7.2.5. The concept of strength is formalised using an electrical distance measure $1/X_{ij}$ because it associates the physical and inherent properties of the system with information found in the system susceptance matrix $\mathbf{B} = \mathrm{Im}(\mathbf{Y_{BUS}})$, which is available. The benefits of using the physical properties of the network, represented by the matrix **B**, for multiple power system partitioning problems have been discussed at length in the past [123-126]. Motivated by the successful creation of strongly connected – electrically cohesive – partitions that were reported in these works, this chapter proposes the use of **B** to determine sectionalising strategies for the purpose of PPSR, as further detailed below.

In order to illustrate the graph representation introduced in (7.1), Figure 7.1 shows the graph representation of the IEEE 9-bus test system and the corresponding node and edge weights. In this chapter, it is also assumed that the set of critical loads is $V_{CLD} = \{v_5, v_8\}$. The black dots represent the *m* generation buses, and the grey dots represent the $n-m$ load buses. The lines illustrated in Figure 7.1 represent the edges.

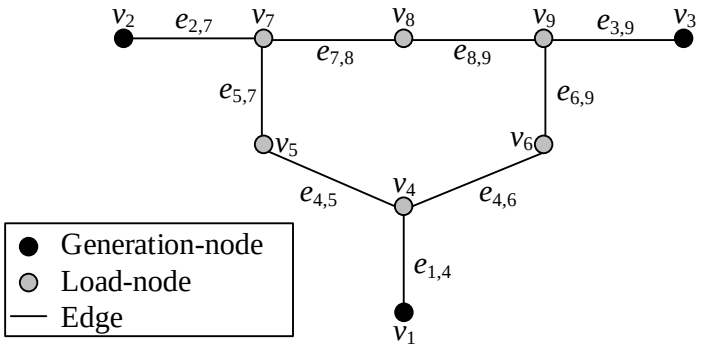

u_1 = 250 MW	$w_{1,4}$ = 17.36 S
u_2 = 300 MW	$w_{4,5}$ = 11.76 S
u_3 = 270 MW	$w_{5,7}$ = 6.21 S
u_4 = 0 MW	$w_{2,7}$ = 16.00 S
u_5 = – 125 MW	$w_{7,8}$ = 13.89 S
u_6 = – 63 MW	$w_{8,9}$ = 9.92 S
u_7 = 0 MW	$w_{3,9}$ = 17.06 S
u_8 = – 100 MW	$w_{6,9}$ = 5.88 S
u_9 = 0 MW	$w_{4,6}$ = 10.87 S

Figure 7.1: Graph representation of the IEEE 9-bus test system with node and edge weights for sectionalising strategies

7.2. Definition of Graph Theoretic Concepts

The methodology presented in this chapter is based on constrained spectral clustering. Hence, it uses most of the concepts introduced in Appendix A.7, which are summarised below.

7.2.1. Graph Laplacian Matrices

The proposed methodology uses a Laplacian matrix associated with the graph G to represent the electrical connectivity of the power system. By initially using the definition of the unnormalised Laplacian matrix **L** (A.27) considering the edge weights given by (7.3), this chapter directly associates the matrix **L** with the well-known susceptance matrix **B**. Indeed, it should be noted that **L** = **B** (neglecting shunt susceptances). The methodology then uses (A.28) to determine the normalised Laplacian matrix $\mathbf{L_N}$ of the graph G. The methodology uses the matrix $\mathbf{L_N}$, as it performs better for clustering purposes [70, 71, 73].

7.2.2. Constrained Spectral Clustering

As explained in Appendix A.7.13, constrained spectral clustering is an extension of spectral clustering that allows two types of constraints – Must-Link (ML-) and Cannot-Link (CL-) constraints – to be used [72, 74]. A ML-constraint between two nodes indicates that the pair of nodes must be clustered together and a CL-constraint specifies that the pair of nodes cannot be assigned to the same cluster.

7.2.3. Cutset and Cut

The cutset $E_S \subset E$ is the set of edges that must be removed to split the graph G into the r disjoint subgraphs $G_1,\ldots,G_r$, with node sets $V_1,\ldots,V_r$. In the sectionalising strategy problem presented in this chapter, a cutset E_S consists of the edges that represent the branches to be included in the sectionalising strategy. Then, the cut associated with the cutset E_S is the sum of the weight factors associated with the edges in E_S, and is given by (A.8). In the sectionalising problem of power systems in blackout, the value of the cut corresponds to the total electrical distance between the created islands.

7.2.4. Weight of the Subgraphs

As explained in Section 6.2.2, the weight of the subgraph V_k, denoted by $wei(V_k)$, that is induced by the cutset E_S can be calculated using (A.7) with respect to the node weights (7.2). The weight of the subgraph V_k represents the difference between the power generation capacity and the predicted load level within the island represented by the node subset V_k. Henceforth, it is also called in this chapter generation-load difference, and is also used when attempting to ensure the satisfaction of the load-generation constraint, that is, when ensuring that each island contains more generation than predicted load.

7.2.5. Quality of a Cutset

The quality of a sectionalising strategy – represented by the cutset E_S – is measured using the ratios between the boundary (cut) given by (A.5) and the volume given by (A.6) of the islands. In this application, the value of the boundary of the node set V_k, $k=1,\ldots,r$, denoted by $cut(V_k,\bar{V}_k)$, physically represents the total electrical distance between buses in the island represented by V_k and the rest of the system, i.e., the inter-cluster electrical distance. Furthermore, the volume of a subset V_k, denoted by $vol(V_k)$, represents the total electrical distance between nodes within V_k, i.e., the intra-cluster electrical distance.

Then, the quality of the subset V_k, $k=1,\ldots,r$, is measured as follows.

$$\eta(V_k) = 1 - \frac{cut(V_k,\bar{V}_k)}{vol(V_k)}. \tag{7.4}$$

In this application, the expansion $\phi(V_k) = cut(V_k,\bar{V}_k)/vol(V_k)$ of the node subset V_k measures the size of the cut relative to the volume of the island. The quality index (7.4) can be physically interpreted as a measure of the inter-cluster electrical distance with respect to the intra-cluster electrical distances. Indeed, the greater the value of $\eta(V_k)$ – the less electrical distance between that island and the others and the more electrical cohesiveness

within the island – the better the island is considered to be in terms of clustering. Furthermore, it should be noted that a suitable cutset would induce islands with nodes that are strongly interconnected between them (large $vol(V_k)$) and weakly connected with the rest of the network (small $cut(V_k, \bar{V}_k)$). This is physically interpreted as a small inter-cluster electrical distance and large intra-cluster electrical distances.

The methodology will evaluate the quality of the sectionalising strategy using the worst quality index $\eta(V_k)$ among the clusters, i.e., the quality of the best cutset is the minimum value of $\eta(V_k)$ from all of the islands: $\min_{k=1,2,...r}(\eta(V_k))$.

7.3. Proposed Sectionalising Methodology Based on Constrained Spectral Clustering

The objective of this chapter is to propose a methodology based on constrained spectral clustering that identifies a sectionalising strategy that satisfies the critical PPSR constraints. The proposed methodology seeks to create islands that will have the characteristic that the nodes in each island will be more highly connected to those nodes in the same island than they are to those nodes in a different island. Presented in this section is the step-by-step execution of the proposed methodology. Only the case of defining two islands ($r = 2$) is considered in the following sections. By applying recursive bisection [71], the proposed methodology can find a sectionalising strategy for values of $r > 2$.

7.3.1. Step 1: Blackstart Availability and Cranking Groups

As explained in Section 6.3.1, each island must contain at least one blackstart unit (Constraint 1) that can provide cranking power for the restoration of the island. It is assumed in this thesis that the cranking groups are separately defined, and as such, the proper cranking groups for the systems considered in this chapter are assumed to be known.

When the cranking groups are known the two node subsets V_{GN1} and V_{GN2} are defined. Each cranking group V_{GNk} consists of a subset V_{Bk} of blackstart units and another subset representing the non-blackstart units.

In order to satisfy the availability of at least one blackstart unit within each island (Constraint 1) and to cluster together the cranking groups, the methodology proposed in this chapter uses a subspace manipulation [127], which assigns a ML-constraint between generators in the same cranking group and a CL-constraint between machines in different groups. This space manipulation has been used to determine islanding solutions in [49]. Assuming that $|V_{GN1}| = m_1$ and $|V_{GN2}| = m_2$, where, $m = m_1 + m_2$, the subspace manipulation presented in [127] creates the projection matrix **P** as follows:

$$\mathbf{P} = \begin{pmatrix} \mathbf{1}_{m_1} & \mathbf{1}_{m_1} & \mathbf{0}_{m_1 \times (n-m)} \\ \mathbf{1}_{m_2} & -\mathbf{1}_{m_2} & \mathbf{0}_{m_2 \times (n-m)} \\ \mathbf{1}_{n-m} & \mathbf{0}_{n-m} & \mathbf{I}_{(n-m)\times(n-m)} \end{pmatrix}. \tag{7.5}$$

where **I** is the identity matrix, **1** is the all-ones column vector, and **0** is the zero matrix or zero column vector.

Mathematically, the matrix **P** gives the same geometric coordinates in $\mathbb{R}^r$ to the generation-nodes $v_i \in V_{GNk}$, $k = 1, 2$, i.e., to the nodes in each cranking group. The use of the matrix **P** ensures that nodes in the same cranking group (nodes with ML-constraint) will be clustered together and that nodes in different cranking groups (nodes with CL-constrain) will be separated, as it also projects the data-points into different hemispheres in $\mathbb{R}^2$. A mathematical explanation of the subspace manipulation can be found in [127]. The applicability of the projection matrix is illustrated using the graph of the IEEE 9-bus test system shown in Figure 7.1, which considers that the cranking groups are $V_{GN1} = \{v_1\}$ and $V_{GN2} = \{v_2, v_3\}$. In the spectral embedding shown in Figure 7.2 and Figure 7.3 the data-points that represent the generators within the cranking groups are marked with red dots. It can be seen that the coordinates of the data-points that represent the machines in the same cranking

group are the same, and that one group of data-points is in the positive y-axes and the other is in the negative y-axes (different hemispheres in $\mathbb{R}^2$). Hence, the sectionalising strategy will cluster the system in such a way that the cranking groups are clustered in different islands (see Figure 7.4).

7.3.2. Step 2: Exclusion of Lines

As previously explained, it is necessary to exclude certain lines from being considered as part of the cutset if the sectionalising strategy is to satisfy Constraints 3 and 5.

As described in Section 6.3.2, the set of critical lines can be defined using the contingency analysis method available in DIgSILENT Power Factory [120]. A line is critical if its disconnection in the nominal case produces an excessive reactive power difference between the pre-contingency and the post-contingency [85]. When the critical lines are identified, the subset $E_{VS} \subset E$ that consists solely of the edges that represent these critical lines in the graph of the power system is defined (Constraint 3).

Furthermore, the edge subset $E_C \subset E$ that consists of the edges that represent the branches that cannot measure resynchronisation is defined to ensure that all the tie-lines that separate the islands are equipped with the ability to measure the synchronisation between the islands that they separate (Constraint 5).

Having defined the lines to be excluded, the subset $\left(E_{EX} = E_{VS} \cup E_C\right) \subset E$ of excluded-edges can be defined. The edges $e_{ij} \in E_{EX}$ are constrained such that they are excluded from the cutset by changing the associated weight factors as follows:

$$\text{for all } e_{ij} \in E_{EX}, \text{let } w'_{ij} = w'_{ji} = max\left(\mathbf{W}\right) \tag{7.6}$$

where, *max* (**W**) represents the largest value in **W**. The changes in (7.6) create a new weighted adjacency matrix **W'**. This mechanism for excluding edges from the cut set is not limited to the branch types considered here. In practice, it could also be extended to any

branch, or branch type, that the operator deemed unsuitable for use in the cutset i.e., as a tie-line in the sectionalising strategy.

7.3.3. Step 3: Initial Sectionalising Strategy problem

Spectral clustering can find a sectionalising strategy that satisfies constraints 1, 3 and 5 only; henceforth, this section is referred to as the initial sectionalising strategy problem. The initial sectionalising strategy is refined in Section 7.3.4 to also ensure Constraint 2 and form the final sectionalising strategy. The initial sectionalising strategy problem consists of finding a strategy for PPSR that creates islands that have strong internal connections but weak external connections, i.e., the buses in the same island are electrically close to the other buses in that island and are electrically distant from the buses in other islands. The sectionalising strategy must also ensure that each island only contains generators that belong to the same cranking group and that the excluded lines are not included in the cutset.

In order to determine the initial sectionalising strategy, i.e., to solve the initial sectionalising strategy problem, the methodology proposed in this chapter uses a constrained spectral clustering algorithm that employs the projection matrix **P** given by (7.5) and the normalised Laplacian matrix $\mathbf{L_N}$ defined in (A.28) of the modified matrix of weights **W'** obtained after changing the edge weights of the excluded edges (7.6).

The methodology then solves the generalised eigenproblem $\mathbf{P^T L_N P \psi} = \nu \mathbf{P^T P \psi}$ to compute the two eigenvectors $\boldsymbol{\psi}_1$ and $\boldsymbol{\psi}_2$ associated with the two smallest eigenvalues. The matrix $\mathbf{X} \in \mathbb{R}^{n \times 2}$ is then created using the vectors $\mathbf{P}\boldsymbol{\psi}_1$ and $\mathbf{P}\boldsymbol{\psi}_2$ as columns. The vector $\mathbf{x}_i$, $i = 1, ..., n$, provides geometric coordinates for the nodes $v_i \in V$ in $\mathbb{R}^2$ (see Figure 7.2 for an example). It should be noted that the coordinates of the generation-nodes (red-dots) that represent the generators included in the same cranking group are the same. Moreover, the points that represent generators in different cranking groups are very different and in fact they are in different hemispheres in $\mathbb{R}^2$. The remaining data-points in $\mathbb{R}^2$ (e.g., the blue-asterisks in Figure 7.2) represent the load-nodes in the graph.

The vectors $\mathbf{x}_i$ are then normalised using (A.61) to compute the vectors $\mathbf{y}_i$, which form the rows of the matrix $\mathbf{Y} \in \mathbb{R}^{n\times 2}$. The normalised vectors $\mathbf{y}_i$ represent the nodes $v_i \in V$ as data-points on the unit circle $\mathbb{S}^1$ (see Figure 7.3 for an example). In particular, the data-points on $\mathbb{S}^1$ denoted by the red-dots represent the generation-nodes on the unit circle. Furthermore, this normalisation improves the quality of the solution [70, 73], and allows certain nodes to be defined as belonging to the core of the island and other nodes as belonging to the periphery of the islands. Nodes in the periphery will be used to determine the final sectionalising strategy, as further detailed in Section 7.3.4.

When the spectral embedding on the unit circle is performed, the nodes $\mathbf{y}_i$ are clustered into clusters V_1 and V_2 using a clustering algorithm, e.g., the *k-means* algorithm [71]. This clustering must consider the well-known length of the arc (Appendix A.7.10.3) between the points on the circumference [70] and not the Euclidean distance (Appendix A.7.10.1) [71] as the partitioning is being performed in a point cloud on $\mathbb{S}^1$.

When more than two islands are required (r > 2), the set V_1 or V_2 that contains more than one blackstart unit should be selected as the node set of a new graph and repeat the procedure starting from the generalised eigendecomposition. This recursive bisection [71] should be repeated until achieving r subgraphs. When Step 3 is finished, the initial sectionalising strategy will satisfy Constraints 1, 3 and 5 for each island. Nevertheless, to ensure Constraint 2, Step 4 must then be applied.

7.3.4. Step 4: Final Sectionalising Strategy

Step 4 seeks to create islands with sufficient generation capacity, i.e., it aims to ensure that the Constraint 2 is satisfied. In order to do so, Step 4 uses the results from Step 3. When the node sets V_1 and V_2 are known, the available capacity within each island is compared with the predicted load level within the same island. For this purpose, the total weight of the subgraphs is calculated using (A.7) with respect to the node weights given by (7.2).

By creating islands with sufficient active power generation capacity, the load-generation balance during PPSR can be ensured. If the available generation capacity is larger than the

predicted load level inside each island, a larger portion of the island can be restored to facilitate the synchronisation of islands, as the islands become more stable [85]. To ensure that the frequency of each island is maintained within prescribed limits during the restoration process, it is necessary to ensure that $wei(V_k) \geq 0$ for each island.

If $wei(V_k) < 0$ for any island, the refining algorithm detailed in [128] is used to reduce the load consumption within the island with $wei(V_k) < 0$ by moving the applicable nodes to the adjacent islands, as explained below.

In order to define the nodes that can be moved to the adjacent islands, the methodology defines the node set $N_L \subset V_{LD}$, which consists of the nodes that are in the periphery of the islands, in other words, the data-points between the clusters visualised on $\mathbb{S}^1$. The set N_L will not include generation-nodes, as these are in general within the core of the corresponding clusters (see Figure 7.3 for an example). When the set N_L is defined, the methodology exchanges one node $v_i \in N_L$ per iteration from one island to the adjacent island, and computes the corresponding quality index (7.4) and the total weight of the nodes $wei(V_k)$ within each island. The process is repeated for all $v_i \in N_L$, $i = 1, 2, \ldots, |N_L|$.

The process creates a list of candidate sectionalising strategies from which the final sectionalising strategy can be selected as the one with the highest quality. All candidate solutions will satisfy the four constraints, i.e., blackstart availability constraint (Constraint 1), load-generation balance (Constraint 2), exclusion of both critical lines from SSs that maintain system voltage stability (Constraint 3) and those that cannot measure resynchronisation with adjacent islands (Constraint 5).

7.4. Simulations Examples

This section presents the simulation examples of sectionalising systems considering the constraints of: blackstart availability, load-generation balance, voltage stability and the ability to monitor synchronisation between adjacent islands. The results of the methodology proposed in this chapter are compared in Section 7.4.5 with those obtained in Chapter 6.

7.4.1. IEEE 9-Bus Test System

The methodology is initially illustrated using the IEEE 9-bus test system. Figure 7.1 shows the graph representation of this test network and the node and edge weights. For consistency with the results presented in Chapter 6, it is also assumed that every blackstart unit, non-blackstart unit, line and breaker is available after the blackout. Moreover, the set of critical loads is defined as $V_{CLD} = \{v_5, v_8\}$.

In Step 1, the proposed methodology defines the cranking groups. As in the previous chapter, it is assumed that the subsets of blackstart units are $V_{B1} = \{v_1\}$ and $V_{B2} = \{v_2\}$. Then, the cranking groups are considered to be $V_{GN1} = \{v_1\}$ and $V_{GN2} = \{v_2, v_3\}$. These pre-defined cranking groups are used to create the projection matrix **P** according to (7.5).

In Step 2, the contingency screening method available in DIgSILENT Power Factory [120] is used to identify the critical lines that maintain system voltage stability. Hence, the set $E_{VS} = \{e_{1,4}, e_{2,7}, e_{3,9}\}$ is created as in the previous chapter. Furthermore, it is assumed that every line can measure synchronisation with adjacent islands. Therefore, the set $E_C = \varnothing$ is defined. Then, the set of excluded edges is $E_{EX} = \{e_{1,4}, e_{2,7}, e_{3,9}\}$. These excluded edges are used to change the applicable edge weights using (7.6).

In Step 3, the matrix $\mathbf{L_N}$ is created taking into consideration the modified weight matrix computed after changing the edge weights of the excluded edges. Then, the methodology solves the corresponding generalised eigenproblem, and performs the spectral embedding of the eigenvectors $\mathbf{P}\boldsymbol{\psi}_1$ and $\mathbf{P}\boldsymbol{\psi}_2$ in $\mathbb{R}^2$. The spectral embedding of this graph in $\mathbb{R}^2$ is shown in Figure 7.2. Then, the vectors $\mathbf{x}_i$ in $\mathbb{R}^2$, $i = 1, 2, \ldots, 9$ are normalised using (A.61). Hence, the points are projected to the unit circle $\mathbb{S}^1$ shown in Figure 7.3. It is clear that a clustering structure emerges. Indeed, the clusters found by the *k-means* algorithm are shown in Figure 7.4. The generators highlighted in red represent the blackstart units. This initial solution is known to satisfy Constraints 1, 3 and 5.

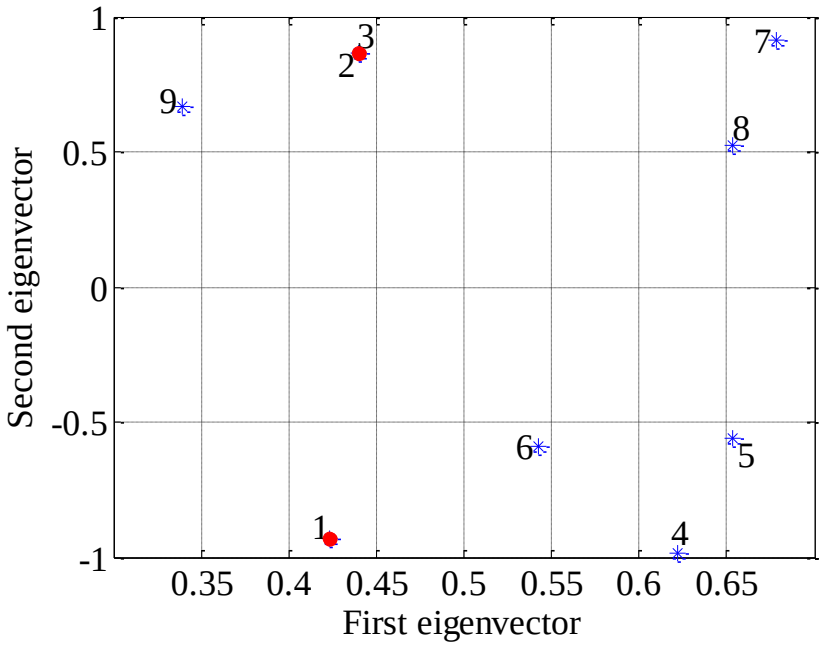

Figure 7.2: Spectral embedding into $\mathbb{R}^2$ of the IEEE 9-bus test system for sectionalising strategies

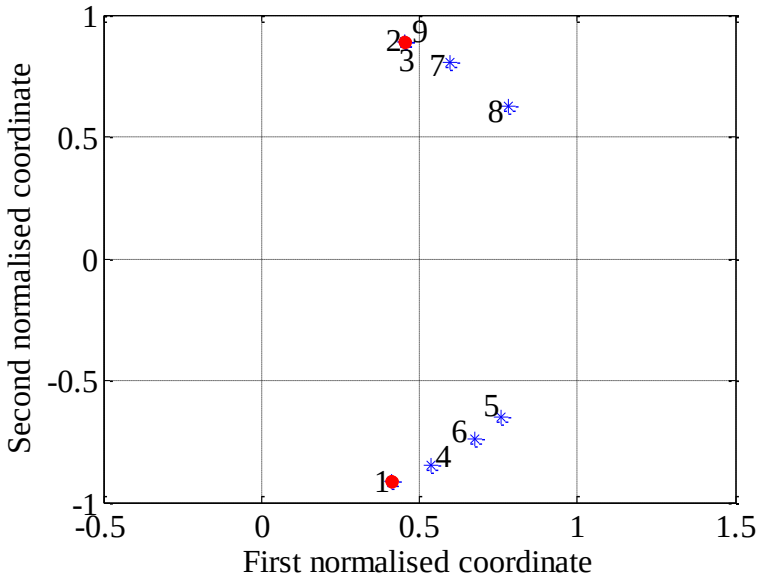

Figure 7.3: Spectral embedding onto the unit circle $\mathbb{S}^1$ of the IEEE 9-bus test system for sectionalising strategies

Then in Step 4, the difference between the available generation and predicted demand for each island is computed. The implementation of Step 4 reveals that the initial sectionalising strategy shown in Figure 7.4 also satisfies Constraint 2, i.e., $wei(V_k) \geq 0$ for both islands.

Table 7.1 shows the value of the total electrical distance between the islands (cut) given by (A.5), the total electrical distance within each island (volume) given by (A.6), the quality of each island given by (7.4) and the value of $wei(V_k)$ for each island given by (A.7). Then, the quality of this sectionalising strategy (the minimum value of $\eta(V_k)$ for the islands) is defined as 86.87%.

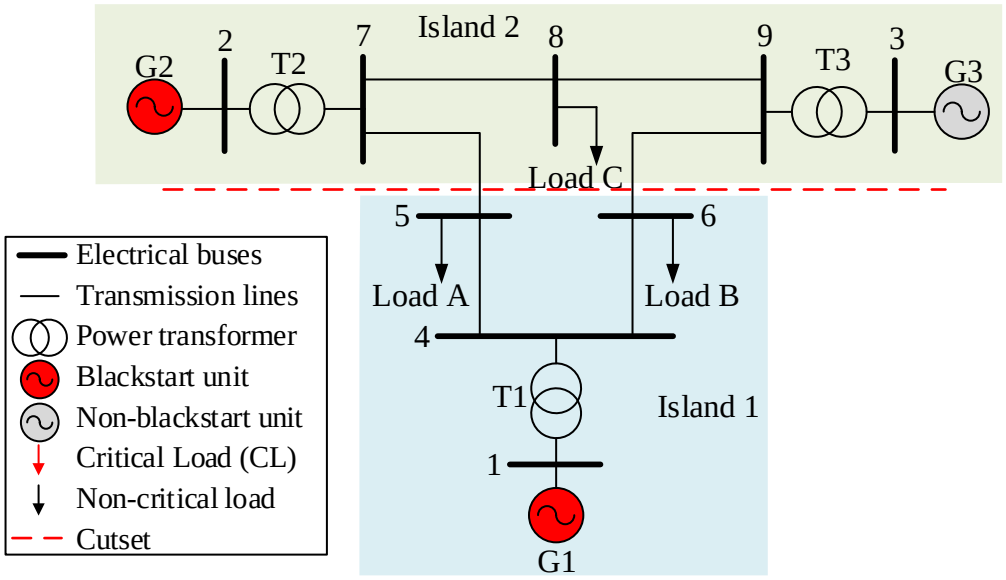

Figure 7.4: IEEE 9-bus test system sectionalised into two islands using the constrained spectral clustering-based methodology

Table 7.1: Sectionalising results using the constrained spectral clustering-based methodology for the IEEE 9-bus test system

	Cutset	**Island No.**	**Cut**	**Volume**	$\eta(V_k)$ **(%)**	$wei(V_k)$ **(MW)**
Results using the proposed methodology	$e_{5,7}, e_{6,9}$	1	12.09	92.08	86.87	62
		2	12.09	125.84	90.39	470

7.4.2. New England 39-Bus Test System

The proposed methodology is now illustrated using the New England 39-bus test system. For consistency with the examples presented in Section 6.4.2, the set of critical loads is defined as $V_{CLD} = \{v_3, v_4, v_8, v_{16}, v_{20}\}$. It is assumed that the subsets of blackstart units are $V_{B1} = \{v_{37}\}$ and $V_{B2} = \{v_{33}\}$. Two cases are also examined in this chapter using this network to

show the adaptability of the methodology to any system condition. As in the previous chapter, in case study 1 it is assumed that all elements of the system are available after the blackout, and case study 2 examines the unavailability of system assets after the blackout.

7.4.2.1 Case Study 1: Availability of all System Assets

The first case study assumes that every blackstart unit, non-blackstart unit, line and breaker is available after the blackout. For the given blackstart units, the cranking groups are $V_{GN1} = \{v_{30}, v_{31}, v_{32}, v_{37}, v_{39}\}$ and $V_{GN2} = \{v_{33}, v_{34}, v_{35}, v_{36}, v_{38}\}$. These cranking groups are used to create the projection matrix **P** defined by (7.5). The set of critical lines that maintain system voltage stability is found to be $E_{VS} = \{e_{5,6}, e_{6,7}, e_{6,11}, e_{10,11}, e_{13,14}, e_{21,22}, e_{23,24}, e_{28,29}, e_{26,29}\}$. It is initially assumed that every line can measure synchronisation with adjacent islands. Nevertheless, transformers will be excluded from the solution space. Thus, the set E_C consists of the edges that represent the transformers. The set of excluded edges is then defined as $E_{EX} = E_{VS} \cup E_C$, and the edges are excluded using (7.6).

The implementation of Step 3 creates the matrix $\mathbf{X} = [\mathbf{P}\boldsymbol{\psi}_1 \quad \mathbf{P}\boldsymbol{\psi}_2]$, which is then used to perform the spectral embedding of the nodes of the graph in $\mathbb{R}^2$ shown in Figure 7.5. The vectors $\mathbf{x}_i$, $i = 1, 2, \ldots, 39$ are then normalised using (A.61) to project the points to the unit circle $\mathbb{S}^1$, as shown in Figure 7.6. It should be noted that a clustering structure emerges again. The sectionalising strategy found by the *k-means* algorithm is shown in Figure 7.7. This initial solution satisfies Constraints 1, 3 and 5.

Step 4 is then used to compute the difference between the available generation and predicted demand for each island. The implementation of Step 4 reveals that the initial sectionalising strategy shown in Figure 7.7 also satisfies Constraint 2, i.e., $wei(V_k) \geq 0$ for both islands. It should be noted that if the generation-load difference in any island had been negative, the node subset *N* would have been defined as $N_L = \{v_2, v_3, v_{15}, v_{18}, v_{25}\}$, i.e., the nodes on the periphery of the islands (see Figure 7.6).

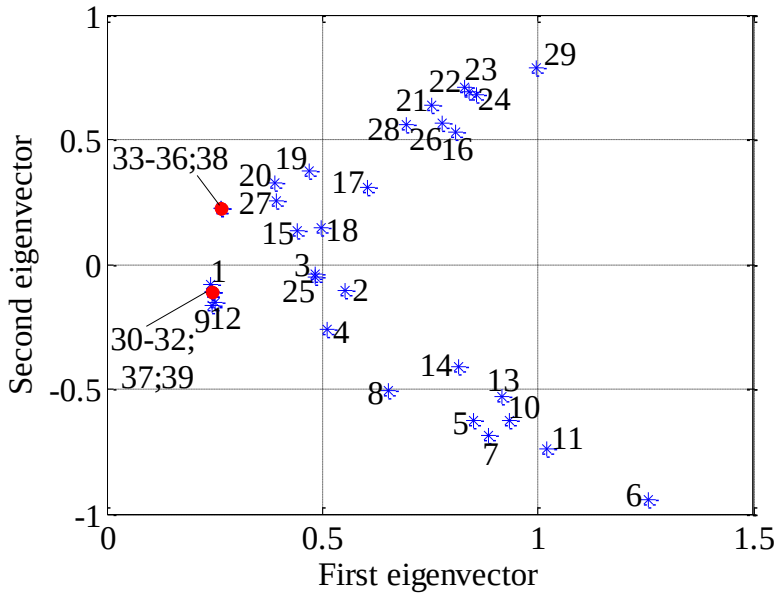

Figure 7.5: Spectral embedding into $\mathbb{R}^2$ of the New England 39-bus test system for sectionalising strategies in case study 1

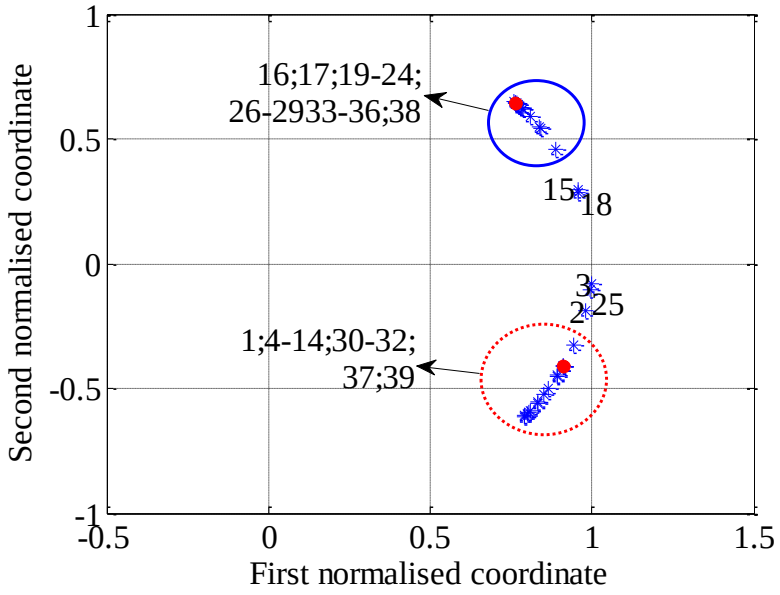

Figure 7.6: Spectral embedding onto the unit circle $\mathbb{S}^1$ of the New England 39-bus test system for sectionalising strategies in case study 1

Table 7.2 shows the value of the total electrical distance between the islands (cut) (A.5), the total electrical distance within each island (volume) (A.6), the quality of each island (7.4)

and the value of $wei(V_k)$ for each island (A.7). Then, the quality of this sectionalising strategy (the minimum value of $\eta(V_k)$ for the islands) is defined as 94.94%.

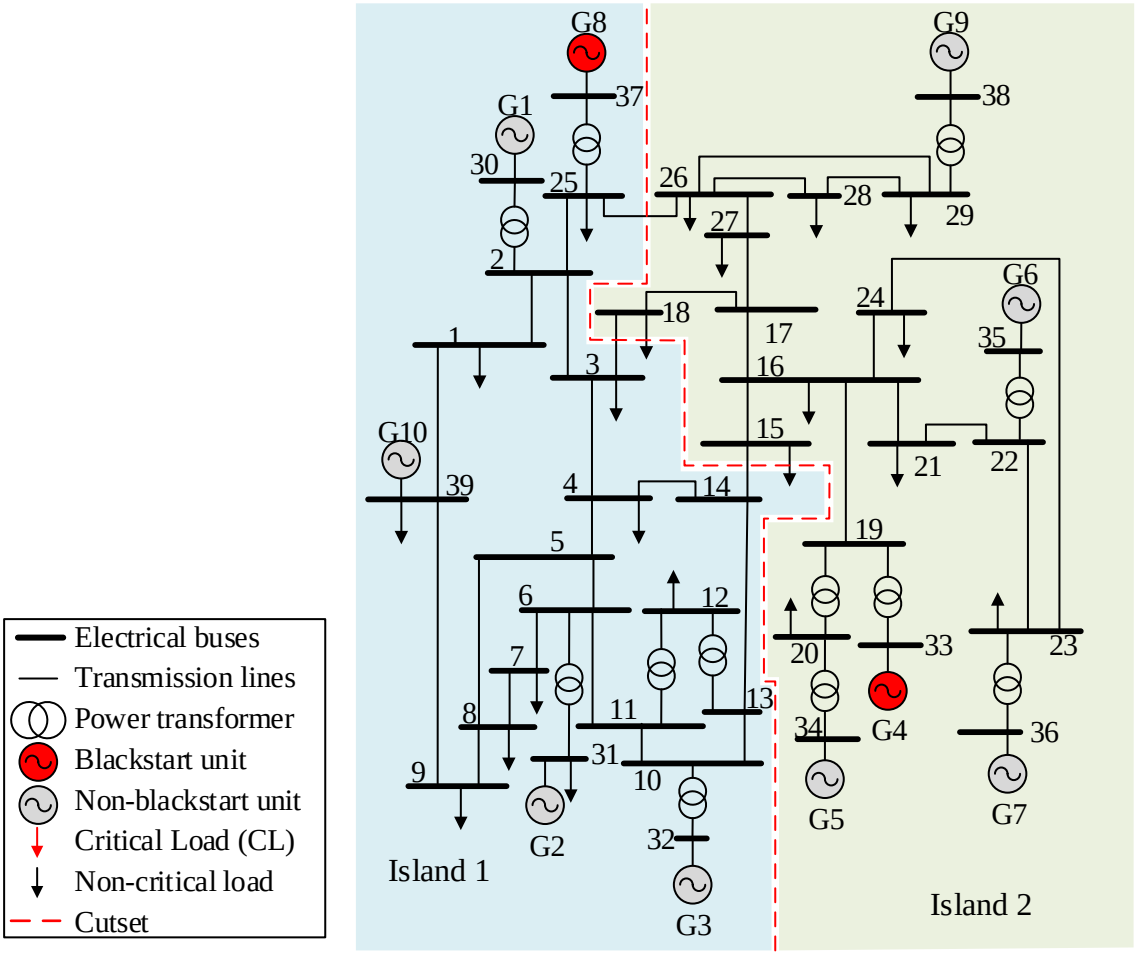

Figure 7.7: New England 39-bus test system sectionalised into two islands in case study 1 using the constrained spectral clustering-based methodology

It should be noted that Constraints 1, 2, 3 and 5 are all satisfied in this example. Furthermore, the methodology found a solution with only three tie-lines, which is significantly lower than the number of internal connections. Moreover, the solution has a quality index of 94.94%, which indicates that the ratio between the inter-island electrical distance and the intra-island electrical distance is smaller than 5.06% (100% – 94.94%), i.e., the islands defined by the sectionalising strategy determined by the proposed methodology will have strong internal connections and weak external connections, in terms of electrical distance. Finally, the methodology sectionalises the system across long

transmission lines. Indeed, the lines identified as tie-lines are those that separate the cranking groups with the largest reactance X_{ij} (see the impedance of the lines in Table B.4). Hence, the early stages of PPSR are protected from the high charging currents that may be produced by the reconnection of these long lines.

Table 7.2: Sectionalising results of the constrained spectral clustering-based methodology for the New England 39-bus system in case study 1

	Cutset	**Island No.**	**Cut**	**Volume**	$\eta(V_k)$ **(%)**	$wei(V_k)$ **(MW)**
Results using the proposed methodology	$e_{25,26}, e_{3,18}, e_{14,15}$	1	152	4610	96.70	1218.5
		2	152	3004	94.94	730.7

7.4.2.2 Case Study 2: Unavailability of System Assets

This second case study aims to demonstrate the adaptability of the methodology proposed in this chapter to any system condition. It is assumed that the generator at bus 35 (G6) is not available after the blackout. As explained in Section 6.4.2, G6 is selected as this is the largest machine in the cranking group V_{GN2}; hence, its unavailability creates larger imbalances. In addition, it is assumed that the line 3-18 (previously included in the sectionalising strategy) has lost monitoring ability, thus it cannot measure resynchronisation and the set E_C is extended to include the edge $e_{3,18}$. The cranking groups previously defined remain the same except the unavailability of the generator G6. Additionally, the new set of excluded-edges must also include the edge that represents the line 3-18. It is important to remember that this information is used to build the projection matrix **P** given by (7.5) and to change the edge weights using (7.6).

The implementation of Step 3 of the methodology considering this new post-blackout state determines initial sectionalising strategy shown in Figure 7.8.

Table 7.3 summarises the results of this scenario before implementing the refining algorithm in Step 4. As noticed, $wei(V_1) = 1540$ MW and $wei(V_2) = -278$ MW < 0. This indicates that there is more load than generation capability in Island 2. Since there is one island with negative generation-load difference, the refining stage must be used.

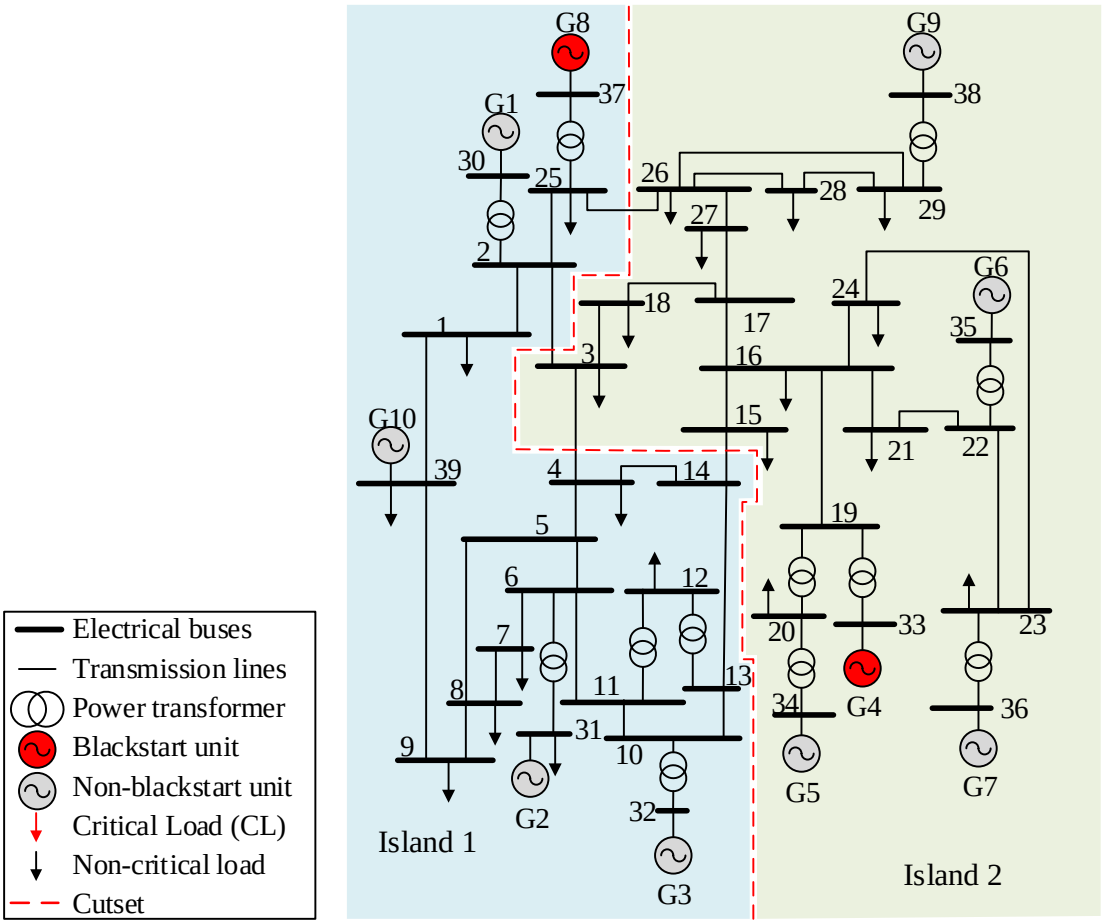

Figure 7.8: New England 39-bus test system sectionalised into two islands in case study 2 using the constrained spectral clustering-based methodology before refining algorithm

Table 7.3: Sectionalising results of the constrained spectral clustering-based methodology for the New England 39-bus system in case study 2

	Cutset	**Island No.**	**Cut**	**Volume**	$\eta(V_k)$ **(%)**	$wei(V_k)$ **(MW)**
Before refining algorithm	$e_{25,26}, e_{2,3}, e_{3,4}, e_{14,15}$	1	190	4439	95.72	1540
		2	190	3217	94.09	-278
After refining algorithm	$e_{25,26}, e_{17,18}, e_{14,15}$	1	199	4824	95.87	1108
		2	199	2831	92.97	154

For this purpose, the node set $N_L = \{v_3, v_4, v_{14}, v_{18}\}$ is defined using the nodes in the periphery of the islands. The methodology then exchanges the nodes $v_i \in N_L$ from one island to the other, and computes the quality index (7.4) and the total weight of the nodes (A.7) within each island. In this scenario, it was found that the optimal solution to ensure

$wei(V_k) \geq 0$ for both islands was achieved by moving load bus 3 from Island 2 to Island 1 (Figure 7.8). However, since line 3-18 was constrained to be excluded from the sectionalising strategy, the methodology moves both buses 3 and 18 from Island 2 to Island 1, excluding the line 3-18 from the final sectionalising strategy.

Figure 7.9 shows the final sectionalising strategy, and Table 7.3 summarises the results for this scenario. It should be noted that the refining process slightly reduces the quality of the sectionalising strategy from 94.05 % to 92.97 %. Nonetheless, this is necessary if Constraints 1, 2, 3 and 5 are all to be satisfied. Moreover, it should be noticed that the proposed methodology partitions, once again, the system in blackout across three tie-lines with high reactance X_{ij}.

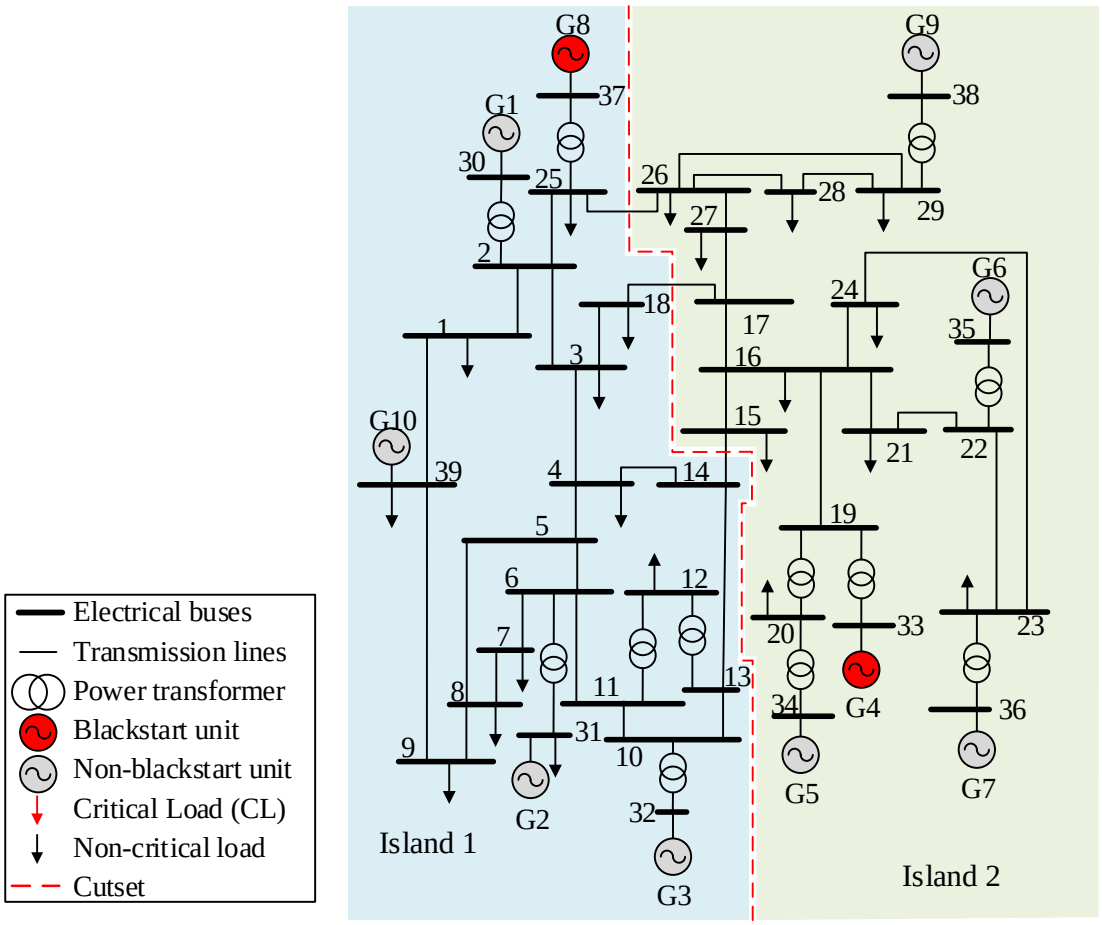

Figure 7.9: New England 39-bus test system sectionalised into two islands in case study 2 using the constrained spectral clustering-based methodology after refining algorithm

7.4.3. IEEE 118-Bus Test System

The methodology is now illustrated in a larger system, the IEEE 118-bus test system. It is considered in this case that every blackstart unit, non-blackstart unit, line and breaker is available after the blackout. The assumed critical loads are highlighted in Figure 7.10. It is assumed that the blackstart units are located at buses 31 and 87. The cranking groups are $V_{GN1} = \{v_{10}, v_{12}, v_{25}, v_{26}, v_{31}\}$ and $V_{GN2} = \{v_{46}, v_{49}, v_{54}, v_{59}, v_{61}, v_{65}, v_{66}, v_{69}, v_{80}, v_{87}, v_{89}, v_{100}, v_{103}, v_{111}\}$. The critical lines that maintain system voltage stability are found to be {5-8, 8-9, 9-10, 37-38, 38-65}. It is assumed, that every line can measure synchronisation with adjacent islands. However, edges that represent transformers are excluded from the sectionalising strategy by including the appropriate edges in the subset E_C. Thus, the subset of excluded-arcs $E_{EX} = E_{VS} \cup E_C$ is defined, and the applicable edge weights are changed using (7.6).

In Step 3, the initial sectionalising strategy is determined. Then, in Step 4, the methodology computes the difference between the available generation and the predicted load level, i.e., the generation-load difference, for each island. In this case, it was found that the initial sectionalising strategy also satisfies $wei(V_k) \geq 0$ for both islands. Hence, the final strategy, which corresponds to the initial sectionalising strategy, is shown in Figure 7.10.

Table 7.4 shows the value of the cut (A.5), the volume (A.6), the quality of each island (7.4) and the value of $wei(V_k)$ (A.7) for each island. As noticed, the quality of the sectionalising strategy is found to be 98.25%. It can also be observed that the quality index of the IEEE 118-bus test system is higher than that of the previous systems. In general, it is expected that the quality index of highly interconnected systems will be higher, as the number of tie-lines will be smaller compared to the number of internal connections.

Table 7.4: Sectionalising results of the constrained spectral clustering-based methodology for the IEEE 118-bus test system

	Island No.	**Cut**	**Volume**	$\eta(V_k)$ **(%)**	$wei(V_k)$ **(MW)**
Results using the proposed methodology	1	37	2124	98.25	747
	2	37	4951	99.25	2169

As noted, Constraints 1, 2, 3 and 5 are all satisfied, there are five tie-lines, which, as expected, is significantly lower than the number of internal connections. Finally, the created islands have strong internal connections (taking the electrical distance into account) and weak external connections. Indeed, the quality of the sectionalising strategy found by the methodology is 98.25%, meaning that the ratios between the inter-islands electrical distances and the intra-islands electrical distances are smaller than 1.75%.

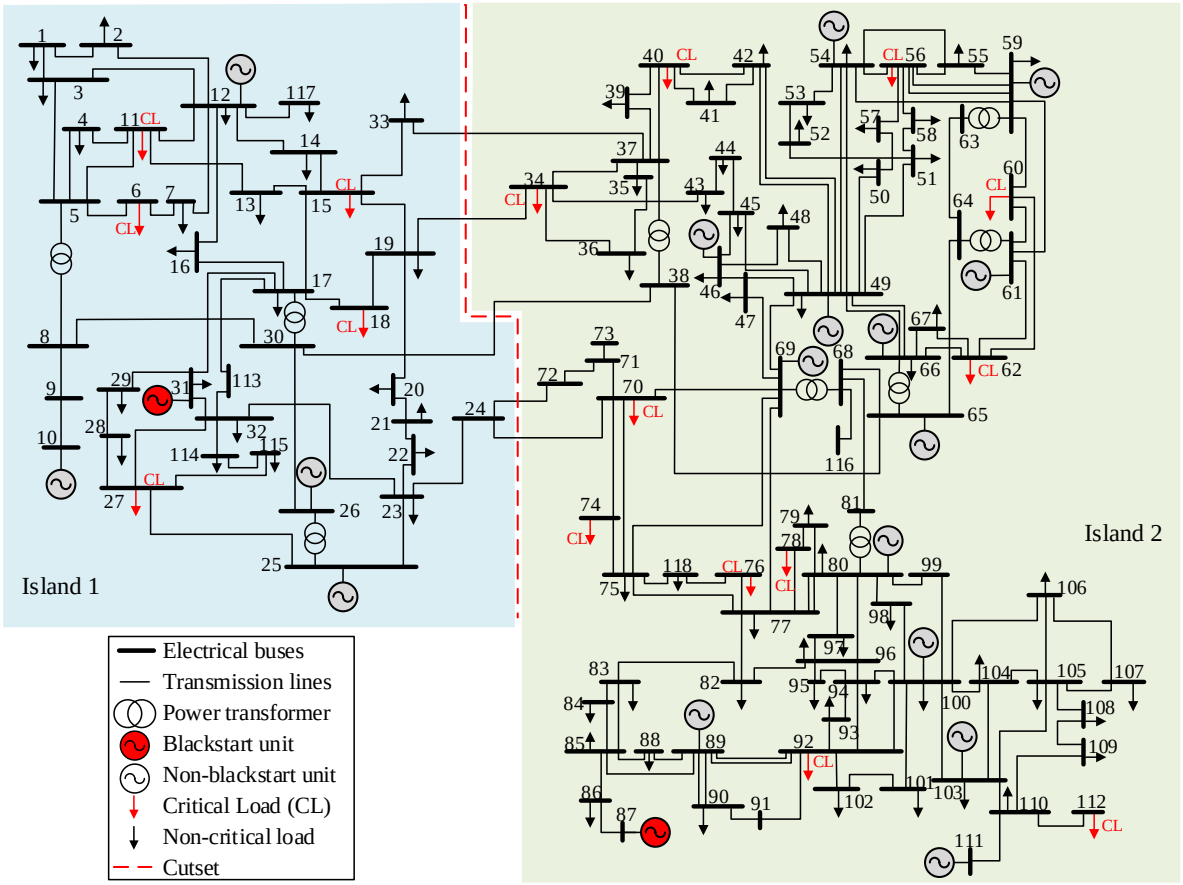

Figure 7.10: IEEE 118-bus test system sectionalised into two islands using the constrained spectral clustering-based methodology

7.4.4. Computational Efficiency of the Proposed Methodology

The eigendecomposition dominates the runtime of the methodology. The calculation of the eigenvectors of $\mathbf{L_N}$ represents approximately 80% of the total runtime of the methodology. Therefore, the computational complexity of the methodology is approximately $O\left(n^3\right)$ [74].

The mean runtime of the methodology for 100 trials of each test system are given in Table 7.5. The runtime for these systems is below a second, and is negligible in terms of the length of time necessary for the overall restoration process.

Table 7.5: Average runtime of the constrained spectral clustering-based methodology for sectionalising strategies

Test System	Runtime using the proposed methodology (s)
IEEE 9-bus	0.00008
New England 39-bus	Scenario 1: 0.009629 Scenario 2: 0.012629
IEEE 118-bus	0. 0218

7.4.5. Comparison

This section compares the constrained cutset matrix-based methodology presented in Chapter 6 referred to below as methodology-1, with the constrained spectral clustering-based methodology introduced in this chapter, referred to below as methodology-2.

Methodology-1 can determine numerous suitable sectionalising strategies, which all satisfy the critical constraints. Hence, these can all be used by operators for PPSR. On the other hand, methodology-2 can determine only one sectionalising strategy that, in addition to satisfying the critical constraints, ensures that the defined islands are electrically cohesive, i.e., the buses within the islands are strongly connected and they are weakly connected to buses in other islands. The solution obtained using methodology-2 is always included in the set of suitable sectionalising strategies obtained using methodology-1.

In terms of computation efficiency, methodology-2 is computationally more efficient than methodology-1. As shown in Table 6.4, methodology-1 requires about two minutes to find a set of 324 sectionalising strategies in the case of the IEEE 118-bus test system; whereas methodology-2 requires less than one second to determine a set of one sectionalising strategy. Although system operators commonly have several minutes during the preparation stage of PPSR to plan the most adequate sectionalising strategy, the computationally efficiency is always a factor to consider in any methodology, in particular when dealing with large-scale networks that require to be sectionalised for the purpose of PPSR.

7.5. Summary

This chapter has presented a methodology based on constrained spectral clustering that can rapidly determine a suitable sectionalising strategy for PPSR, which accelerates the restoration of a system in complete blackout. The methodology determines a suitable strategy to sectionalise the entire blackout area, whilst satisfying the constraint of blackstart availability within each island, preserving the integrity of the defined cranking groups, creating islands with more generation capacity than the predicted load level and excluding from the solution critical lines that maintain system voltage stability and those that cannot measure resynchronisation with adjacent islands.

The methodology uses the concept of electrical cohesiveness, as expressed by the electrical distances between buses, and formulates the sectionalising strategy problem to create islands that, in addition to satisfying the critical constraints, have strong internal connections – taking the electrical distance into account – and weak external connections. This approach could benefit PPSR as the number of tie-lines between islands is reduced whilst simultaneously increasing the number of internal connections. Furthermore, this approach sectionalises the system across electrically long and weak transmission lines, helping to reduce the effects of high charging currents, high overvoltages, and other voltage related issues that may arise when reconnecting these long and unloaded lines. The proposed methodology is intended for use during the preparation stage of PPSR, after updated post-blackout system information is provided, and it aims to create islands that would facilitate PPSR.

The proposed methodology has been illustrated using the IEEE 9-bus test system, New England 39- and IEEE 118-bus test systems. Simulation results have indicated that the methodology can determine in a few seconds sectionalising strategies that can provide guidance to operator on how the blackout area can be sectionalised. Numerous cases have been examined to demonstrate the adaptability of the methodology to any system condition, e.g., assets unavailability. Sectionalising strategies have been obtained with ratios between the electrical distance inter-clusters and the electrical distance intra-clusters smaller than 8% for small test systems and smaller than 2% for large test systems.

Chapter 8. Conclusions and Future Work

Chapter 8 summarises the work performed and the main conclusions that can be drawn from the results presented in this PhD thesis. Suggested areas of further research are also outlined.

This thesis has investigated the application of graph theory to Intentional Controlled Islanding (ICI) for blackout prevention and system sectionalising for Parallel Power System Restoration (PPSR). ICI is an effective corrective control action to minimise the impact of cascading outages leading to power system blackouts, and PPSR is the most effective strategy to restore isolated islands (subsystems) of the network in parallel after wide-area blackouts.

ICI seeks to split the system in a controlled manner after instabilities have been detected, but before the system becomes uncontrollable. ICI is a computationally demanding problem, and its complexity increases exponentially with the size of the system. Nonetheless, ICI methodologies must be computationally efficient and accurate, as this adaptive corrective control strategy must be undertaken in a very limited timeframe (of just a few seconds) and must ensure the creation of electrically separated and stable islands.

PPSR is commonly adopted as the restoration procedure in multiple power system utilities, as it considerably accelerates the restoration process of large-scale power systems affected by complete blackouts. PPSR sectionalises the entire blackout area into multiple islands and restores the created islands in parallel using their own cranking sources. To define the subsystems that will be restored in parallel, the system operators must identify a suitable sectionalising strategy during the preparation stage of PPSR that considers updated post-blackout system information. Hence, the determination of system sectionalising strategies for reliable restoration is a very important and critical task.

Therefore, this thesis has developed methodologies that can minimise the impact of large-area power system blackouts through adaptive corrective ICI schemes, and minimise the

duration of these catastrophic and expensive events through system sectionalising strategies for PPSR. In completing this research, different graph theoretic techniques have been used and methodologies developed, which can determine islanding and system sectionalising strategies. The development of methodologies for blackout prevention and faster restoration would lead to a more reliable operation of the interconnected power system.

This Chapter summarises the conclusions drawn from the research results, and present suggestions for future research that were not addressed in this research, as they are out of the scope of this thesis.

8.1. Discussion and Conclusions

The ICI methodology that has been presented in Chapter 2 determines islanding solutions for minimal dynamic coupling. In contrast to existing approaches, the new methodology is based on normalised spectral clustering, and it considers the dynamic coupling between the load buses and all of the generators that belong to a given coherent group. These two features have considerably increased the accuracy of the solution compared to an existing approach that also finds solutions for minimal dynamic coupling. The new methodology initially identifies the generators within each island, and then clusters together the strongest dynamically connected buses, determining thus an islanding solution that consists of the lines with the absolute weakest connections between the dynamically coherent groups of generators. This approach creates islands that are more likely to continue operating after islanding. The methodology proposed in this thesis avoids computationally demanding algorithms such as Gaussian elimination with complete pivoting, and this has considerably improved the computational efficiency of the proposed methodology compared to an existing approach. The application of the methodology in small, medium and large scale networks has shown that the new approach is faster and more accurate than the existing ICI method that also determines islanding solutions for minimal dynamic coupling.

The concept of weak connections has been extended in Chapter 3 to define the weak areas. The concept of the weak areas, which has been introduced for the first time in this thesis, defines the areas across the network where, based on the assessment of the dynamic

coupling between the system buses, multiple weak connections between the coherent groups of generators can be found. The weak areas contain the buses that are as strongly connected to buses in one island as they are to buses in another adjacent island. Hence, they could be used to determine islanding solutions using a second objective function, e.g., minimal power imbalance. Two new graph theory based techniques have been implemented in Chapter 3 to optimally place Phasor Measurement Units (PMUs) only across the weak areas and the boundary buses. The suggested optimal PMU placement seeks to provide support to ICI schemes, as real-time information would be available to compute the power flow in the lines, and thus the power balance in the future islands. This optimal PMU placement can also assist operators during PPSR, as the information of the electrical variables – voltage magnitudes and voltage phase angles – at the boundary buses can be constantly monitored during the resynchronisation of the islands independently restored.

The novel ICI methodology that has been presented in Chapter 4 can determine islanding solutions for minimal power imbalance, while ensuring that each island contains only coherent generators. Unlike existing approaches, the proposed ICI methodology can also constrain any branch to be excluded from the islanding solution, which can serve to exclude from the islanding solution any branch that operators deemed unsuitable for islanding, e.g., transformers and unavailable lines. The new methodology is based on the graph theoretic concept of a cutset matrix, which allows the possibility to explore the vast combinatorial space to always find the islanding solution with the minimum power imbalance. To considerably accelerate the determination of an islanding solution, whilst maintaining the level of accuracy, the determined weak areas have been utilised. Since the methodology takes into account the generator coherency when creating the islands, the transient stability of the future islands is significantly enhanced. The methodology presented in this thesis has been demonstrated using the IEEE 9-bus test system, New England 39- and IEEE 118-bus test systems. Simulation results have shown that the introduced approach is significantly faster than the conventional ICI methods for minimal power imbalance (OBDD-based methods) while maintaining the accuracy of the islanding solution.

The ICI methodology that has been presented in Chapter 5 determines better islanding solutions for minimal power flow disruption, while ensuring that each island contains only

coherent generators. Unlike the existing approaches, the ICI methodology also enables the exclusion of any branch from the islanding solution. A significant improvement over the existing approaches is that the new methodology uses the normalised Laplacian matrix associated with the graph, and this improves the quality of the islanding solutions compared to the existing SCCI algorithm. This methodology also has the significant advantage that it solves the associated eigenproblem only once, even if multiple islands are required. Moreover, the methodology avoids recursive bisection, and this considerably accelerates the determination of an islanding solution and simultaneously improves its quality. Finally, it reduces the order of a similarity matrix and avoids the use of iterative approaches (e.g., *k-means*), and these two features further contribute to accelerating the determination of an islanding solution. The methodology has been demonstrated using the IEEE 9-bus test system, New England 39- and IEEE 118-bus test systems and a model of the British network with 815 buses. Simulation results have demonstrated that the methodology proposed in this thesis determines better islanding solutions and that it is significantly faster than the existing SCCI algorithm. They also showed that the new approach can potentially be implemented in practical power systems to determine in a few seconds an islanding solution with minimal power flow disruption relative to the power in each island, for any given number of islands.

A new constrained cutset matrix-based methodology has been developed in Chapter 6 to determine suitable system sectionalising strategies that facilitate PPSR. The methodology introduced in this thesis satisfies the constraints of blackstart availability within each island, preserves the integrity of the defined cranking groups, creates islands with more generation capacity than the predicted load level, and excludes from the solution critical lines that maintain system voltage stability and those that cannot measure resynchronisation with adjacent islands. This technique has the advantage that it explores the vast combinatorial space to find in a few minutes a set of sectionalising strategies that satisfies the critical constraints for PPSR. These constraints seek to provide sufficient resources to maintain the steady-state stability of the created islands within acceptable limits during the actual restoration. The proposed methodology is intended for use during the preparation stage of PPSR after updated post-blackout system information is provided. Another advantage of the methodology over existing approaches is that it determines a set of feasible

sectionalising strategies that can ultimately be used by system operators to select, based upon their knowledge and experience, the most suitable sectionalising strategy for their system. The proposed methodology has been illustrated using the IEEE 9-bus test system, New England 39- and IEEE 118-bus test systems. The simulation results have indicated that the introduced approach is effective during the preparation stage of PPSR as it provides guidance to operators on how the blackout area can be sectionalised. Numerous cases have been examined to demonstrate the adaptability of the methodology to any system condition, e.g., assets unavailability. The solutions have been obtained in less than two minutes for the larger case with 118 buses. This indicates that the technique is computationally efficient enough to be used in the preparation stage of PPSR.

An innovative constrained spectral clustering-based methodology has been introduced in Chapter 7 to quickly determine a suitable sectionalising strategy for PPSR. This methodology is also intended for use during the preparation stage of PPSR. It also satisfies the critical constraints of blackstart availability within each island, preserves the integrity of the defined cranking groups, creates islands with more generation capacity than the predicted load level and excludes from the solution critical lines that maintain system voltage stability and those that cannot measure resynchronisation with adjacent islands. An important feature of this approach is that it uses the concept of electrical cohesiveness, as expressed by the electrical distances between buses. This concept is used to formulate the sectionalising strategy problem to create islands that, in addition to satisfying the critical constraints, have strong internal connections – taking the electrical distance into account – and weak external connections. This approach can potentially benefit PPSR as the number of tie-lines between islands is reduced whilst simultaneously increasing the number of internal connections. Furthermore, it sectionalises the power system across electrically long and weak transmission lines, which may help reduce the effects of high charging currents, high overvoltages, and other voltage related issues that may arise when reconnecting these long and unloaded lines. The proposed methodology has been illustrated using the IEEE 9-bus test system, New England 39- and IEEE 118-bus test systems considering the case of two islands. The simulation results have indicated that the methodology can effectively and quickly determine system sectionalising strategies with ratios between the electrical distance inter-clusters and the electrical distance intra-clusters smaller than 8% for small

test systems and smaller than 2% for large test systems. This has indicated that the larger the network, the smaller this ratio. Furthermore, these simulations have shown that the methodology proposed in Chapter 8 is very quick and that a solution can be obtained is less than one second for networks with up to 118 buses.

8.2. Applicability of the Proposed Methodologies

This section provides an outlook of the applicability of the proposed methodologies. On the one hand, the ICI methodologies that have been introduced in this thesis can cope with the increasing penetration of renewables, as in practice they will use real-time measurements from the installed PMUs or from the SCADA systems. By using real-time measurements, the actual power flows in the lines at the moment of islanding the system will be used as input variables to the methodologies. Additionally, since the proposed ICI methodologies avoid the use of reduced network approaches (i.e., it avoids reducing the size of the system for real-time analyses), the true topology of the network when splitting is considered. This ensures the determination of the best islanding solution. Finally, the ICI methodologies are capable of coping with complex future systems with high spatial variety in generation locations due to the proliferation of renewable energy resources installations.

On the other hand, the methodologies that can determine sectionalising strategies for PPSR can be used to create small areas that will contain as the main cranking source small distributed generators (DGs). As it is described in the literature, new restoration practices use small DGs to restore small areas of the distribution system, which are later reconnected to the transmission level. This not only accelerates the restoration process, but also provides local services to customers, reducing thus the cost of the blackout and improving the reliability of the power systems.

8.3. Future Work

The work presented within this thesis has fulfilled all of the research aims which were initially defined. This section suggests areas for further research based on the knowledge gained through the literature review, techniques and results included within this thesis.

Graph theory is a powerful technique that could be used to model and study any other partitioning problem in the context of power systems, as this mathematical technique is very robust, computationally efficient and accurate when splitting a graph. Hence, the application of these graph theoretic techniques, in particular spectral graph clustering, in areas such as the creation of zones for voltage control, Transmission Network Use of System (TNUoS) tariff, and generation zoning [129] would be very interesting. Graph theory may also be used to reveal the electrical and topological structure of the system, and thus, to systematically partition the power system into power network zones [125].

Spectral graph theory may be used to detect instabilities in the power system. During the normal operation of the electrical network, the spectrum (eigenvalues and associated eigenvectors) of the applicable graph that represents the power system should not change significantly. However, it is expected that this pattern will be affected by a major disturbance, thus changing the eigenvalues and the eigenvectors of the Laplacian matrix that is associated with the graph. In the spectral theory, the sudden change in the power system operation can be seen as an outlier, and can be detected using outliers detection algorithms [130]. Therefore, investigating the application of spectral graph clustering to evaluate the stability of the power system following major disturbances would be an interesting potential future work.

In the context of ICI, this thesis has focused on answering the questions "*where to split*". As explained in Chapter 1, the question "*when to split*" is associated with the early detection of instabilities. Therefore, investigating possible instability indicators that could provide, with a certain degree of confidence, information of future and potential instabilities in the power system, and thus, the proper timing for ICI is extremely important.

This thesis has presented in Chapter 2 a model-based methodology to determine dynamically coherent groups of generators. However, it is known that the system operating conditions and network configuration are constantly changing. Hence, the generators in each coherent group may vary in future networks. Furthermore, the accuracy of the system parameters (inertia constants, impedances and load levels) influences the efficacy of model-based techniques. Thus, it would be desirable to develop measurement-based coherency

identification approaches. In the measurement-based methods, all the system quantities and variables such as generator speed, generator rotor angle, output power and voltage at all system buses would be measured continuously and a snapshot would be utilised to find the coherent groups. These techniques would be benefited from Wide Area Measurement System (WAMS) technology, which could be used to obtain the real-time data across the whole network measured with time synchronous stamping. The development of measurement-based techniques to identify dynamically coherency groups of generators would also mean that methodologies to determine islanding solutions for minimal dynamic coupling using WAMS technology are necessary, as the determination of the minimal dynamic coupling between zones is entirely associated with the coherency identification problem. Therefore, the determination of measurement-based sensitivity factors between the voltage phase angles of the system buses and the rotor angle of the generators is also desirable, leading to a measurement-based methodology to determine islanding solutions for minimal dynamic coupling.

This thesis has presented in Chapter 3 a methodology to determine the weak areas, i.e., the areas where multiple weak connections and thus multiple islanding solutions can be determined. This methodology could be extended to study the impact of changes in the topology and the operating point of the electrical power system. This probabilistic study would provide a broader searching space and ensure the coverage of multiple scenarios (scenarios without certain elements) for the determination of islanding solutions.

The methodologies presented in Chapter 2, 4 and 5 to determine islanding solutions for minimal dynamic coupling, minimal power imbalance and minimal power flow disruption, respectively, have only been illustrated in this thesis using steady-state simulations, i.e., without perturbations. The proposed ICI methodologies require to be tested under transient studies to evaluate their efficiency and accuracy following major disturbance. Therefore, it is of major interest to extend the application of these methodologies under transients, and assess the dynamic response of the electrical power system after these events.

The methodologies presented in this thesis to split the power system and prevent blackouts have been illustrated assuming that all the information required (power flow in the

transmission lines) would be available and did not contain any noise. However, it is very important to investigate how the lack of certain measurements and noisy signals would affect the accuracy of ICI schemes in real power systems. To date, the existing methodologies to split the system and prevent blackouts have relied on the functionality of the elements involved in the controlled separation. However, the elements involved in the ICI schemes may fail, causing the probability of failure on demand to increase [131]. Therefore, it is of great interest for the reliable operation of the whole network to assess the reliability of existing islanding methods.

In the context of power system restoration, the investigation of the minimum number of blackstart units required to be online in order to accelerate the overall restoration process, i.e., to minimise the restoration time, is extremely important. Indeed, this investigation is vital as the operation cost of blackstart units is extremely high compared to the operation cost of the other machines [94]. Furthermore, it is important to develop methodologies to determine the optimal cranking groups, as this would serve to define the generators that will be included in each island for the purpose of parallel restoration.

This thesis has presented in Chapter 6 and 7 two different methodologies to determine system sectionalising strategies for PPSR. Therefore, it is now important to develop restoration strategies that could facilitate the actual restoration of the created islands. In this context, the application of graph theoretic algorithms to determine the shortest path from a cranking source (e.g., a blackstart unit) to an element in the system in blackout that requires restoration (e.g., a non-blackstart unit) would be desirable. These techniques can benefit the actual restoration process, as they are computationally efficient and could provide guidance to operators on how the element that requires restoration could be rapidly restored. Moreover, when developing the technique to restore the created islands, it is vital to consider that some load buses are more important and are required to be restored first; hence, taking into account certain weight factors that could be used in the restoration path selection is desirable. Finally, when determining a restoration path to send cranking power to non-blackstart units, it is also important to take into account the generator's status and availability.

References

[1] P. Kundur, *Power System Stability and Control*: McGrawHill, Inc., 1994.

[2] U.G. Knight, *Power System in Emergencies*. London, 2001.

[3] M. Vaiman, K. Bell, Y. Chen, B. Chowdhury, I. Dobson, P. Hines, *et al.*, "Risk assessment of cascading outages: Methodologies and challenges," *IEEE Transactions on Power Systems,* vol. 27, no. 2, pp. 631-641, May 2012.

[4] M. Panteli, "Impact of ICT Reliability and Situation Awareness on Power System Blackouts," PhD, Electrical Energy & Power Systems, The University of Manchester, Manchester, 2013.

[5] J. Machowski, J.W. Bialek, and J.R. Bumby, *Power System Dynamics Stability and Control*. West Sussex: John Wiley & Sons, 2008.

[6] P. Kundur, J. Paserba, V. Ajjarapu, G. Andersson, A. Bose, C. Canizares, *et al.*, "Definition and classification of power system stability IEEE/CIGRE joint task force on stability terms and definitions," *IEEE Transactions on Power Systems,* vol. 19, no. 3, pp. 1387-1401, Aug. 2004.

[7] P. Task Force on Understanding, Mitigation and Restoration of Cascading Failures of the IEEE Computing & Analytical Methods (CAMS) Subcommittee,, "Mitigation and prevention of cascading outages: Methodologies and practical applications," in *IEEE PES General Meeting*, 2013, pp. 1-5.

[8] T. Amraee and S. Ranjbar, "Transient instability prediction using decision tree technique," *IEEE Transactions on Power Systems,* vol. 28, no. 3, pp. 3028-3037, Aug. 2013.

[9] M. Abapour and M.R. Haghifam, "On-line assessment of the transient instability risk," *IET Generation, Transmission & Distribution,* vol. 7, no. 6, pp. 602-612, 2013.

[10] North American Electric Reliability Corporation, "High-Impact, Low-Frequency Event Risk to the North American Bulk Power System," Jun. 2010.

[11] G. Andersson, P. Donalek, R. Farmer, N. Hatziargyriou, I. Kamwa, P. Kundur, *et al.*, "Causes of the 2003 major grid blackouts in North America and Europe, and recommended means to improve system dynamic performance," *IEEE Transactions on Power Systems,* vol. 20, no. 4, p. 19221928, 2005.

[12] P. Kundur and C. Taylor, "Blackout experiences and lessons, best practices for system dynamic performance, and the role of new technologies," IEEE Task Force Report2007.

[13] H. You, V. Vittal, and Z. Yang, "Self-healing in power systems: an approach using islanding and rate of frequency decline-based load shedding," *IEEE Transactions on Power Systems*, vol. 18, no. 1, pp. 174-181, Feb. 2003.

[14] D. Hazarika and A.K. Sinha, "Power system restoration: Planning and simulation," *International Journal of Electrical Power & Energy Systems*, vol. 25, no. 3, pp. 209-218, March 2003.

[15] D. Lindenmeyer, H.W. Dommel, and M.M. Adibi, "Power system restoration — a bibliographical survey," *International Journal of Electrical Power & Energy Systems*, vol. 23, no. 3, pp. 219-227 March 2001.

[16] M.M. Adibi, *Power System Restoration, Methodologies and Implementation Strategies*. New York: IEEE Press Inc., 2000.

[17] D. Lindenmeyer, "A framework for power system restoration," Ph.D, Department of Electrical and Computer Engineering, The University of British Columbia, Vancouver, BC, Canada, 2000.

[18] Swiss Federal Office of Energy (SFOE), "Report on the blackout in Italy on 28 September 2003," Nov. 2003.

[19] U.S.-Canada Power System Outage Task Force, "Final report on the August 14, 2003 Blackout in the United States and Canada: Causes and recommendations," Apr. 2004.

[20] W. Lu, Y. Bésanger, E. Zamaï, and D. Radu, "Blackouts: Description, analysis and classification," in *6th WSEAS International Conference on Power Systems*, Lisbon, Portugal, 2006, pp. 429-434.

[21] P. Pourbeik, P. Kundur, and C.W. Taylor, "The anatomy of a power grid blackout - Root causes and dynamics of recent major blackouts," *IEEE Power & Energy Magazine,* vol. 4, no. 5, pp. 22-29, Sept.-Oct. 2006.

[22] UCTE, "Final Report System Disturbance on 4 November 2006," Jan. 2007.

[23] M. Bruch, V. Münch, M. Aichinger, M. Kuhn, M. Weymann, and G. Schmid. (Nov. 2011, Power Blackout Risks. *CRO Forum*.

[24] "Report of the enquiry committee on grid disturbance in the Northern region on 30th July 2012 and in Northern, Eastern & North-Eastern region on 31st July 2012," Ministry of Power, New Delhi16th August 2012.

[25] P. Hines, J. Apt, and S. Talukdar, "Large Blackouts in North America: Historical Trends and Policy Implications," *Energy Policy,* vol. 37, pp. 5249-5259, 2009.

[26] G. Liu and V. Venkatasubramanian, "Oscillation monitoring system based on wide area synchrophasors in power systems," in *IREP Symposium-Bulk Power System Dynamics and Control*, 2007.

[27] M.A.M. Ariff and B.C. Pal, "Coherency identification in interconnected power system — An independent component analysis approach," *IEEE Transactions on Power Systems*, vol. 28, no. 2, May 2013.

[28] A.G. Exposito, A. Bur, P. Rousseaux, A. de la Villa Jaen, and C. Gomez-Quiles, "On the use of PMUs in power system state estimation," in *17th Power Systems Computation Conference (PSCC)*, 2011.

[29] R. Franco, C. Sena, G.N. Taranto, and A. Giusto, "Using synchrophasors for controlled islanding—A prospective application for the Uruguayan power system," *IEEE Transactions on Power Systems*, vol. 28, no. 2, pp. 2016-2024, May 2013.

[30] S. Nourizadeh, M.J. Karimi, A.M. Ranjbar, and A. Shirani, "Power system stability assessment during restoration based on a wide area measurement system," *IET Generation, Transmission & Distribution*, vol. 6, no. 11, pp. 1171-1179 Nov. 2012.

[31] J. De La Ree, V. Centeno, J.S. Thorp, and A. G. Phadke, "Synchronized Phasor Measurement Applications in Power Systems," *IEEE Transactions on Smart Grid*, vol. 1, pp. 20-27, Jun. 2010.

[32] C. Juarez, A.R. Messina, R. Castellanos, and G. Espinosa-Perez, "Characterization of Multi-Machine System Behavior using a Hierarchical Trajectory Cluster Analysis," *IEEE Transactions on Power Systems*, vol. 26, no. 3, pp. 972-981, Aug. 2011.

[33] V. Terzija, G. Valverde, D. Cai, P. Regulski, V. Madani, L. Fitch, *et al.*, "Wide-area monitoring, protection, and control of future electric power networks," *Proceedings of the IEEE*, vol. 99, pp. 80-93, Jan. 2011.

[34] "IEEE Standard for Synchrophasor Measurements for Power Systems," in *IEEE Std C37.118.1-2011 (Revision of IEEE Std C37.118-2005)*, ed, 2011, pp. 1-61.

[35] D.M. Laverty, R.J. Best, P. Brogan, I. Al Khatib, L. Vanfretti, and D.J. Morrow, "The openPMU platform for open-source phasor measurements," *IEEE Transactions on Instrumentation and Measurement*, vol. 62, no. 4, pp. 701-709, Apr. 2013.

[36] S.C. Savulescu, *Real-Time Stability in Power Systems: Techniques for Early Detection of the Risk of Blackout*. New York, 2006.

[37] J. Yan, C.. Liu, and U. Vaidya, "PMU-based monitoring of rotor angle dynamics," *IEEE Transactions on Power Systems*, vol. 26, no. 4, pp. 2125-2133, Nov. 2011.

[38] F. Hashiesh, H.E. Mostafa, A.R. Khatib, I. Helal, and M.M. Mansour, "An intelligent wide area synchrophasor based system for predicting and mitigating transient instabilities," *IEEE Transactions on Smart Grid,* vol. 3, no. 2, pp. 645-652, Jun. 2012.

[39] D.T. Nguyen, Y. Shen, and M.T. Thai, "Detecting critical nodes in interdependent power networks for vulnerability assessment," *IEEE Transactions on Smart Grid,* vol. 4, no. 1, pp. 151-159, Mar. 2013.

[40] P. Wall, "Online Prediction of the Post-Disturbance Frequency Behaviour of a Power System," PhD, Electrical Energy & Power Systems, The University of Manchester, Manchester, 2013.

[41] N. Senroy and G.T. Heydt, "A conceptual framework for the controlled islanding of interconnected power systems," *IEEE Transactions on Power Systems,* vol. 2, no. 2, pp. 1005-1006, May 2006.

[42] N. Senroy, G.T. Heydt, and V. Vittal, "Decision tree assisted controlled islanding," *IEEE Transactions on Power Systems,* vol. 21, no. 4, pp. 1790-1797, Nov. 2006.

[43] M.M. Adibi, R.J. Kafka, S. Maram, and L.M. Mili, "On power system controlled separation," *IEEE Transactions on Power Systems,* vol. 21, no. 4, pp. 1894-1902, Nov. 2006.

[44] K. Sun, D. Zheng, and Q. Lu, "Splitting strategies for islanding operation of large-scale power systems using OBDD-based methods," *IEEE Transactions on Power Systems,* vol. 18, no. 2, pp. 912-923, May 2003.

[45] Q. Zhao, D. Zheng, J. Ma, and Q. Lu, "A study of system splitting strategies for island operation of power system: A two-phase method based on OBDDs," *IEEE Transactions on Power Systems,* vol. 18, no. 4, pp. 1556-1565, Nov. 2003.

[46] K. Sun, D. Zheng, and Q. Lu, "A simulation study of OBDD-based proper splitting strategies for power systems under consideration of transient stability," *IEEE Transactions on Power Systems,* vol. 20, no. 1, pp. 389-399, Feb. 2005.

[47] C. Wang, B.Zhang, Z. Hao, J. Shu, P. Li, and Z. Bo, "A novel real-time searching method for power system splitting boundary," *IEEE Transactions on Power Systems,* vol. 25, no. 4, pp. 1902-1909 Nov. 2010.

[48] L. Hao, G.W. Rosenwald, J. Jung, and C.C. Liu, "Strategic power infrastructure defense," *Proceedings of the IEEE,* vol. 93, no. 5, pp. 918-933, May 2005.

[49] L. Ding, F. Gonzalez-Longatt, P. Wall, and V. Terzija, "Two-step spectral clustering controlled islanding algorithm," *IEEE Transactions on Power Systems,* vol. 28, no. 1, pp. 75-84, Feb. 2013.

[50] H. You, V. Vittal, and X. Wang, "Slow coherency - Based islanding," *IEEE Transactions on Power Systems,* vol. 19, no. 1, pp. 483-491, Feb. 2004.

[51] B. Yang, V. Vittal, and G. Heydt, "Slow - coherency - based controlled islanding – A demostration of the approach on the August 14, 2003 blackout scenario," *IEEE Transactions on Power Systems,* vol. 21, no. 4, pp. 1840-1847, Aug. 2006.

[52] G. Xu and V. Vittal, "Slow coherency based cutset determination algorithm for large power systems," *IEEE Transactions on Power Systems,* vol. 25, no. 2, pp. 877-884, May. 2010.

[53] J.H. Chow, *Time-Scale Modeling of Dynamic Networks with Applications to Power Systems* vol. 46. NY: Springer-Verlag, 1982.

[54] S.S. Lamba and R. Nath, "Coherency identification by the method of weak coupling," *Electrical Power & Energy Systems,* vol. 7, no. 4, pp. 233-242, Oct. 1985.

[55] R.A. Date and J.H. Chow, "Aggregation properties of linearized two-time-scale power networks," *IEEE Transactions on Circuits and Systems,* vol. 38, no. 7, pp. 720-730, Jul. 1991.

[56] S.B. Yusof, G.J. Rogers, and R.T.H. Alden, "Slow coherency based network partitioning including load buses," *IEEE Transactions on Power Systems,* vol. 8, no. 3, pp. 1375-1382, Aug. 1993.

[57] P.A. Trodden, W.A. Bukhsh, A. Grothey, and K.I.M. McKinnon, "MILP formulation for controlled islanding of power networks," *International Journal of Electrical Power & Energy Systems,* vol. 45, no. 1, pp. 501-508, Feb. 2013.

[58] M.R. Aghamohammadi and A. Shahmohammadi, "Intentional islanding using a new algorithm based on ant search mechanism," *International Journal of Electrical Power & Energy Systems,* vol. 35, no. 1, pp. 138–147, Feb. 2012.

[59] L. Liu, W. Liu, D.A. Cartes, and I.Y. Chung, "Slow coherency and angle modulated particle swarm optimization based islanding of large-scale power systems," *Advanced Engineering Informatics,* vol. 23, pp. 45-56, 2009.

[60] X. Wang, "Slow coherency grouping based islanding using minimal cutsets and generator coherency index tracing using the continuation method," Ph.D., Iowa State University, Ames, , 2005.

[61] M.R. Irving and M.J.H. Sterling, "Optimal network tearing using simulated annealing," *IEE Proceedings Generation, Transmission and Distribution,* vol. 137, no. 1, pp. 69-72, Jan. 1990.

[62] A. Peiravi and R. Ildarabadi, "A fast algorithm for intentional islanding of power systems using the multilevel kernel *k-means* approach," *Journal of Applied Sciences,* vol. 9, no. 12, pp. 2247-2255, 2009.

[63] A. Peiravi and R. Ildarabadi, "Comparison of computational requirements for spectral and kernel k-means bisection of power system," *Australian J. of Basic and Applied Sciences,* vol. 3, no.3, pp. 2366-2388, 2009.

[64] M.R. Garey and D.S. Johnson, *Computers and Intractability: A Guide to the Theory of NP-Completeness*. San Francisco, CA: Freeman, 1979.

[65] R. Podmore, "Identification of coherent generators for dynamic equivalents," *IEEE Transactions Power Apparatus and Systems,* vol. PAS-97, no. 4, pp. 1344-1354, July/Aug 1978.

[66] A.J. Germond and R. Podmore, "Dynamic aggregation of generating unit models," *IEEE Transactions Power Apparatus and Systems,* vol. PAS-97, no. 4, pp. 1060-1069, July 1978.

[67] R. Podmore and A. Germond, "Development of dynamic equivalents for transient stability studies," Electric Power Reserach Intitute 763, May 1977.

[68] METIS Graph Partition Library. Available: http://glaros.dtc.umn.edu/gkhome/views/metis

[69] F.R. Chung, *Spectral Graph Theory*: ser. CBMS Regional Conference Series in Mathematics. American Mathematical Society, 1997, no. 92.

[70] A.Y. Ng, M.I. Jordan, and Y. Weiss, "On spectral clustering: Analysis and an algorithm," *Advances in Neural Information Processing Systems,* vol. 2, pp. 849-856, 2002.

[71] U. Von Luxburg, "A tutorial on spectral clustering," *Statistics and Computing,* vol. 17, no. 4, pp. 395-416, Dec. 2007.

[72] X. Wang and I. Davidson, "Flexible constrained spectral clustering," in *16th ACM SIGKDD International Conference on Knowledge Discovery and Data Mining (KDD 2010)*, Washington DC, USA, 2010, pp. 563-572.

[73] J.R. Lee, S.O. Gharan, and L. Trevisan, "Multi-way spectral partitioning and higher-order Cheeger inequalities," in *44th symposium on Theory of Computing*, 2012, pp. 1117-1130.

[74] X. Wang, B. Qian, and I. Davidson, "On constrained spectral clustering and its applications," *Data Mining and Knowledge Discovery,* pp. 1-29, Sep. 2012.

[75] J. Gutierrez, M. Staropolsky, and A. Garcia, "Policies for restoration of a power system," *IEEE Transactions on Power Systems,* vol. 2, no. 2, pp. 436-442, May 1987.

[76] M.M. Adibi, P. Clelland, L.H Fink, H. Happ, R.J. Kafka, J. Raine, *et al.*, "Power system restoration - A task force report," *IEEE Transactions on Power Systems,* vol. 2, no. 2, pp. 271-277, May 1987.

[77] M.M. Adibi and R.J. Kafka, "Power system restoration issues," *IEEE Computer Applications in Power,* vol. 4, no. 2, pp. 19-24, Apr. 1991.

[78] M.M. Adibi, L.H Fink, C.J. Andrews, F. Arsanjani, M.W. Lanier, J.M. Miller, *et al.*, "Special considerations in power system restoration," *IEEE Transactions on Power Systems,* vol. 7, no. 4, pp. 1419-1427, Nov. 1992.

[79] M.M. Adibi and L.H. Fink, "Power system restoration planning," *IEEE Transactions on Power Systems,* vol. 9, no. 1, pp. 22-28, Feb. 1994.

[80] J.J. Ancona, "A framework for power system restoration following a major power failure," *IEEE Transactions on Power Systems,* vol. 10, no. 3, pp. 1480-1485, Aug. 1995.

[81] L.H. Fink, K.L. Liou, and C.C. Liu, "From generic restoration actions to specific restoration strategies," *IEEE Transactions on Power Systems,* vol. 10, no. 2, pp. 745-751, May 1995.

[82] A. Borghetti, C. A. Nucci, and M. Paolone, "Chapter 14 - Restoration Processes after Blackouts," in *Handbook of Electrical Power System Dynamics: Modeling, Stability, and Control*, ed: John Wiley & Sons, Inc., 2013, pp. 864–899.

[83] W. Sun, C.C. Liu, and L. Zhang, "Optimal generator start-up strategy for bulk power system restoration," *IEEE Transactions on Power Systems,* vol. 26, no. 3, pp. 1357-1366, Aug. 2011.

[84] R. Podmore, "Smart grid restoration concepts," in *IEEE PES General Meeting*, Minneapolis, 2010, pp. 1-8.

[85] C. Wang, V. Vittal, and K. Sun, "OBDD-based sectionalizing strategies for parallel power system restoration," *IEEE Transactions on Power Systems,* vol. 26, no. 3, pp. 1426-1433, Aug. 2011.

[86] M.M. Adibi, R.W. Alexander, and B. Avramovk, "Overvoltage control during restoration," *IEEE Transactions on Power Systems,* vol. 7, no. 4, pp. 1464-1470, Nov. 1992.

[87] G.H. Cheng and Z. Xu, "A method for sustained overvoltage control during power system restoration," in *IEEE PES Power Systems Conference and Exposition*, 2004, pp. 473-477.

[88] A. Ketabi, A.M. Ranjbar, and R. Feuillet, "Analysis and control of temporary overvoltages for automated restoration planning," *IEEE Transactions on Power Delivery,* vol. 17, no. 4, pp. 1121-1127, Oct. 2002.

[89] M.M. Adibi, R.W. Alexander, and D.P. Milanicz, "Energizing high and extra-high voltage lines during restoration," *IEEE Transactions on Power Systems,* vol. 14, no. 3, pp. 1121-1126, Aug. 1999.

[90] M.M. Adibi, J.N. Borkoski, R.J. Kafka, and T.L. Volkmann, "Frequency response of prime movers during restoration," *IEEE Transactions on Power Systems,* vol. 14, no. 2, pp. 751-756, May 1999.

[91] S.A. Nezam Sarmadi, A.S. Dobakhshari, S. Azizi, and A.M. Ranjbar, "A sectionalizing method in power system restoration based on WAMS," *IEEE Transactions on Smart Grid,* vol. 2, no. 1, pp. 178-185, Mar. 2011.

[92] Z.Z. Lin, F.S. Wen, C.Y. Chung, K.P. Wong, and H. Zhou, "Division algorithm and interconnection strategy of restoration subsystems based on complex network theory," *IET Generation, Transmission & Distribution,* vol. 5, no. 6, pp. 674-683, Jun. 2011.

[93] PJM, "PJM Manual 36: System Restoration," Apr. 2013.

[94] National Grid Electricity Transmission, "The Grid Code," Dec. 2013.

[95] Y. Besanger, M. Eremia, and N. Voropai, "Chapter 13 - Major Grid Blackouts: Analysis, Classification, and Prevention," in *Handbook of Electrical Power System Dynamics: Modeling, Stability, and Control*, ed: John Wiley & Sons, Inc., 2013, pp. 789–863.

[96] S. Corsi and M. Pozzi, "A multivariable new control solution for increased long lines voltage restoration stability during black startup," *IEEE Transactions on Power Systems,* vol. 18, no. 3, pp. 1133–1141, Aug. 2003.

[97] Y. Liu and X. Gu, "Skeleton-network reconfiguration based on topological characteristics of scale-free networks and discrete particle swarm optimization," *IEEE Transactions on Power Systems,* vol. 22, no. 3, pp. 1267-1274, Aug. 2007.

[98] T.S. Sidhu, D.A. Tziouvaras, A.P. Apostolov, C.H. Castro, S.R. Chano, S.H. Horowitz, *et al.*, "Protection issues during system restoration," *IEEE Transactions on Power Delivery,* vol. 20, no. 1, pp. 47-56, Jan. 2005.

[99] PSERC, "Development and evaluation of system restoration strategies from a blackout," Arizona State University, ArizonaSep. 2009.

[100] IEEE PES Power System Engineering Committee, "Overvoltage control during restoration," *IEEE Transaction on Power Systems,* vol. 7, no. 4, pp. 1464-1470, Nov. 1992.

[101] M.M. Adibi, J. N. Borkoski, and R.J. Kafka, "Power system restoration - The second task force report," *IEEE Transactions on Power Systems*, vol. 2, no. 4, pp. 927-932, Nov. 1987.

[102] M.M. Adibi and N. Martins, "Power system restoration dynamic issues," presented at the IEEE Power and Energy Society General Meeting - Conversion and Delivery of Electrical Energy in the 21st Century, Pittsburgh, PA, 2008.

[103] M.M. Adibi and D.P. Milanicz, "Reactive capability limitation of synchronous machines," *IEEE Transactions on Power Systems*, vol. 9, no. 1, pp. 29-40, Feb. 1994.

[104] N. Deo, *Graph Theory with Applications to Engineering and Computer Science*: Prentice-Hall Inc., 1974.

[105] W.K. Chen, *Graph theory and its engineering applications* vol. Vol. 5,. Singapore: World Scientific Publishing, 1997.

[106] J.A. Bondy and U.S.R. Murty, *Graph Theory*, 2nd ed.: Springer, 2008.

[107] J. Zhu, *Power System Applications of Graph Theory*. New York: Nova Science Publishers, Inc., 2009.

[108] G. Kron, *Tensor Analysis of Networks*: New York: Wiley, 1939.

[109] F. Dörfler and F. Bullo, "Kron reduction of graphs with applications to electrical networks," *IEEE Transactions on Circuits and Systems - I: Regular Papers*, vol. 60, no. 1, Jan. 2013.

[110] P.M. Anderson and A.A. Fouad, *Power System Control and Stability*, 2nd ed. New York: IEEE Press, 2003.

[111] K.R. Padiyar, *Power System Dynamics Stability and Control*, 2nd ed.: BS Publications, 2008.

[112] R.W. Farebrother, *Linear Least Squares Computations*: Taylor & Francis, 1988.

[113] R.F. Nuqui and A.G. Phadke, "Phasor Measurement Unit placement techniques for complete and incomplete observability," *IEEE Transactions on Power Delivery*, vol. 20, no. 4, pp. 2381-2388, Oct. 2005.

[114] T.W. Haynes, S.M. Hedetniemi, S.T. Hedetniemi, and M. Henning, "Domination in graphs applied to electric power networks," *SIAM Journal on Discrete Mathematics*, vol. 15, no. 4, pp. 519–529, 2002.

[115] C. Moler, *Numerical Computing with MATLAB*: Society for Industrial and Applied Mathematics, 2004.

[116] J. Lind-Nielsen. (Jul.). *BuDDy package*. Available: http://sourceforge.net/projects/buddy/

[117] C. Perwass, *Geometric Algebra with Applications in Engineering*. Berlin Heidelberg: Springer-Verlag, 2009.

[118] A. Okabe, B. Boots, K. Sugihara, and S.N. Chiu, *Spatial Tessellations: Concepts and Applications of Voronoi Diagrams*, 2nd ed. England: John Wiley & Sons, 2000.

[119] IEEE PES PSDPC SCS. (2013, Oct.). *Power System Test Cases*. Available: http://www.sel.eesc.usp.br/ieee/

[120] DIgSILENT PowerFactory, ed. Heinrich-Hertz-Straße, Germany.

[121] M.M. Adibi, D.P. Milanicz, and T.L. Volkmann, "Asymmetry issues in power system restoration," *IEEE Transactions on Power Systems*, vol. 14, no. 3, pp. 1085-1091, Aug. 1999.

[122] M.M. Adibi, D.P. Milanicz, and T. L. Volkmann, "Remote cranking of steam electric stations," *IEEE Transactions on Power Systems*, vol. 11, no. 3, pp. 1613-1618, Aug. 1996.

[123] P. Lagonotte, J.C. Sabonnadiere, J.Y. Leost, and J.P. Paul, "Structural analysis of the electrical system: Application to secondary voltage control in France," *IEEE Transactions on Power Systems*, vol. 4, no. 2, pp. 479-486, May 1989.

[124] N. Müller and V. H. Quintana, "A sparse eigenvalue-based approach for partitioning power networks," *IEEE Transactions on Power Systems*, vol. 7, no. 2, pp. 520-527, May 1992.

[125] S. Blumsack, P. Hines, M. Patel, C. Barrows, and E. Cotilla-Sanchez, "Defining power network zones from measures of electrical distance," in *IEEE PES General Meeting*, 2009.

[126] E. Cotilla-Sanchez, P. Hines, C. Barrows, S. Blumsack, and M. Patel, "Multi-attribute partitioning of power networks based on electrical distance," *IEEE Transactions on Power Systems*, vol. in press, pp. 1-9, 2013.

[127] T.D. Bie, J. Suykens, and B.D. Moor, "Learning from general label constraints," in *IAPR International Workshop on Statistical Pattern Recognition*, Lisbon, 2004.

[128] G. Karypis and V. Kumar, "Multilevel *k*-way partitioning scheme for irregular graphs," *Journal of Parallel and Distributed Computing*, vol. 48, pp. 96-129, 1998.

[129] National Grid Electricity Transmission, "Initial view of TNUoS tariffs for 2013/14," April 2012.

[130] H. Kriegel, P. Kröger, and A. Zimek, "Outlier Detection Techniques," in *13th Pacific-Asia Confer-ence on Knowledge Discovery and Data Mining (PAKDD 2009)*, Bangkok, Thailand, 2009.

[131] J. Quirós-Tortós, M. Panteli, V. Terzija, and P. Crossley, "On evaluating the performance of intentional controlled islanding schemes," presented at the IEEE PES General Meeting, Vancouver, 2013.

[132] M. Stoer and F. Wagner, "A simple min-cut algorithm," *Journal of the ACM*, vol. 44, no. 4, pp. 585-591, Jul. 1997.

[133] R. Sánchez-García, M. Fennelly, S. Norris, G. Niblo, N. Wright, J. Brodzki, *et al.*, "Hierarchical clustering of power grids," *IEEE Transactions on Power Systems*, vol. in press, 2014.

[134] H. Lutkepohl, *Handbook of matrices*: Chichester: Wiley, 1997.

[135] W.E. Donath and A.J. Hoffman, "Lower bounds for the partitioning of graphs," *IBM Journal Res. Develop.*, vol. 17, pp. 420-425, Sept. 1973.

[136] M. Fiedler, "Algebraic connectivity of graphs," *Czechoslovak Mathematical Journal*, vol. 23, no. 98, pp. 298-305, 1973.

[137] B. Parlett, H. Simon, and L. Stringer, "Estimating the largest eigenvalues with the Lanczos algorithm," *Mathematics of Computation*, vol. 38, pp. 153-165, 1982.

[138] D.A. Spielman and S.H. Teng, "Spectral partitioning works: Planar graphs and nite element meshes," in *37th Annual Symposium on Foundations of Computer Science*, 1996, pp. 96-105.

[139] N. Alon, "Eigenvalues and expanders," *Combinatorica*, vol. 6, no. 2, pp. 83-86, 1986.

[140] A. Sinclar and M. Jerrum, "Approximate counting, uniform generation and rapidly mixing Markov chains," *Information and Computation*, vol. 82, no. 1, pp. 93-133, Jul. 1989.

[141] L. Hagen and A. Kahng, "New spectral methods for Ratio Cut partitioning and clustering," *IEEE Transactions on Computer-Aided Design*, vol. 11, no. 9, pp. 1074-1085, Sept. 1992.

[142] P.K. Chan, M.D.F. Schlag, and J.Y. Zien, "Spectral *k*-way Ratio-Cut partitioning and clustering," *IEEE Transactions on Computer-Aided Design of Integrated Circuits and Systems*, vol. 13, no. 9, pp. 1088-1096, Sept. 1994.

[143] J. Shi and J. Malik, "Normalized cuts and image segmentation," *IEEE Transactions on Pattern Analysis and Machine Intelligence*, vol. 22, no. 8,, pp. 888-905, Aug. 2000.

[144] C. Ding. (2004, May). *A tutorial on spectral clustering* [Talk presented at ICML]. Available: http://ranger.uta.edu/~chqding/Spectral/spectralA.pdf

[145] MATLAB and Statistics Toolbox Release 2012b, ed: The MathWorks Inc., Natick, Massachusetts, United States, 2010.

[146] T.W. Haynes, S.T. Hedetniemi, and P.J. Slater, *Fundamentals of Domination in Graphs*. New York: Marcel Dekke, Inc., 1998.

[147] F. Milano, "An open source power system analysis toolbox," *IEEE Transactions on Power Systems*, vol. 20, no. 3, pp. 1199-1206, Aug. 2005.

[148] R.D. Zimmerman, C.E. Murillo-Sánchez, and R.J. Thomas, "MATPOWER: Steady-state operations, planning, and analysis tools for power systems research and education," *IEEE Transactions on Power Systems*, vol. 26, no. 1, pp. 12-19, Feb. 2011.

[149] University of Washington. (2013, May). *Power system test case archive*. Available: http://www.ee.washington.edu/research/pstca/

[150] J.B. Ward, "Equivalent circuits for power-flow studies," *Transactions of the American Institute of Electrical Engineers*, vol. 68, no. 1, pp. 373-382, Jun. 2009.

[151] M. A. Pai, *Energy function analysis for power system stability*: Boston: Kluwer Academic Publishers, 1989.

[152] R.C. Degeneff, M.R. Gutierrez, S.J. Salon, D.W. Burow, and R.J. Nevins, "Kron's reduction method applied to the time stepping finite element analysis of induction machines," *IEEE Transactions on Energy Conversion*, vol. 10, no. 4, pp. 669-674, Aug. 2002.

[153] I. Dobson, "Voltages across an area of a network," *IEEE Transactions on Power Systems*, vol. 27, no. 2, pp. 993-1002, May. 2012.

[154] A.R. Griffing, B.R. Lynch, and E.A. Stone, "An eigenvector interlacing property of graphs that arise from trees by Schur complementation of the Laplacian," *Linear Algebra and its Applications*, vol. 438, no. 3, pp. 1078-1094, Feb. 2013.

[155] A. Rosen, "A new network theorem," *Journal of the Institution of Electrical Engineers*, vol. 62, no. 335, pp. 916-918, 1924.

[156] I. Wegener, *Branching Programs and Binary Decision Diagrams: Theory and Applications*. Philadelphia: Society for Industrial and Applied Mathematics, 2000.

Appendix A. Graph Theory and Electrical Power Systems

Appendix A presents an introduction to graph theory, and the way how this well-established theory can be used to study power systems. It also provides the definitions that are used in the chapters of this thesis. In particular, this appendix presents the power system represented through graphs for the purpose of Intentional Controlled Islanding (ICI) for blackout prevention and system sectionalising strategies for Parallel Power System Restoration (PPSR). The introduced definitions are exemplified throughout this appendix using the IEEE 9-bus test system and its different graph representations.

An interconnected power system with *n* buses, *m* generators and *l* branches (transmission lines and transformers) can be represented as a graph. A graph is a group of points (nodes) and lines called edges that connect them. A graph may be *undirected*, meaning that there is no distinction between the two points associated with each edge, or its edges may be *directed* from one point to another [106]. This chapter initially studies undirected graphs, and Appendix A.4 introduces the directed graph.

An undirected graph G is an *ordered pair* $\left(V(G), E(G)\right)$, consisting of a node set $V(G)$, and an edge set $E(G)$ disjoint from $V(G)$, i.e., they are mutually exclusive, together with an incidence function Ω_G that associates each edge of G with an unordered pair of nodes of G. Thus, if e_{ij} is an edge of G, and v_i and v_j are nodes such that $\Omega_G\left(e_{ij}\right)=\left\{v_i, v_j\right\}=\left\{v_j, v_i\right\}$, then e_{ij} is said to join v_i and v_j, and the nodes v_i and v_j are called the ends of the edge e_{ij} [106]. When there is no scope of ambiguity, the letter G from graph theoretic symbols is omitted, thus $V(G)$ and $E(G)$ are equivalently denoted by V and E, respectively.

Given a graph G, the elements $v_i \in V$, $i = 1,\ldots,n$, denote the nodes of the graph – also called vertices – and the elements $e_{ij} \in E \subset V \times V$, $i, j = 1,...,n$, denote its edges – also called links. It should be mentioned that the edge $e_{ij}=\left\{v_i, v_j\right\} \in E$ may also be denoted by e_k, $k = 1,\ldots,l$. Nevertheless, the first denotation is preferred over the second, as this provides an intuitive relationship between the edge e_{ij} and its end nodes v_i and v_j.

The sets V and E represent the buses and the branches of the network, respectively. In addition, the cardinality of the sets V and E, denoted by $|V|$ and $|E|$, are respectively equal to the number of buses n and branches l of the power system (see Example 1 below).

Graph theory allows various subsets of nodes and edges to be defined from the sets V and E, and this property is used in this thesis to represent particular features of the power system. For example, the subset $V_{GN} \subset V$, with elements $v_i^{GN} \in V_{GN}$ – called generation-nodes – can be defined to represent the m generation buses. Therefore, the subset $V_{LD} = V \setminus V_{GN}$ (where \ represents the set-theoretic difference and defines V_{LD} as the set of nodes in V that do not appear in V_{GN}), with elements $v_i^{LD} \in V_{LD}$ – called load-nodes – can be defined to represent the $n - m$ load buses (see Example 1). These two node subsets are used in this Appendix to provide examples of how graph theory can be used to represent different features of the power system. Other subsets are later introduced and explained in the subsequent sections of this appendix, and others are used in the main body of the thesis.

Graph theoretic techniques are used in this thesis to determine ICI strategies for blackout prevention and system sectionalising strategies for faster PPSR. Graph theoretic techniques are also used to optimally place monitoring equipment that can be used to gather real-time information during cascading outages and during the resynchronisation of the islands.

Example 1: Figure A.1 shows a single line diagram of the IEEE 9-bus test system [110]. This system data and parameters are given in the Appendix A.1. This system is used throughout this chapter to provide examples of the introduced concepts. Figure A.2 illustrates the corresponding graph representation $G = (V, E)$ of this power network, where

$$V = \{v_1, v_2, v_3, v_4, v_5, v_6, v_7, v_8, v_9\}, \tag{A.1}$$

$$E = \{e_{1,4}, e_{4,5}, e_{5,7}, e_{2,7}, e_{7,8}, e_{8,9}, e_{3,9}, e_{6,9}, e_{4,6}\}, \tag{A.2}$$

and the incidence function Ω_G is defined by

$$\begin{aligned}
&\Omega_G\left(e_{1,4}\right)=\left\{v_1,v_4\right\} \quad \Omega_G\left(e_{2,7}\right)=\left\{v_2,v_7\right\} \quad \Omega_G\left(e_{3,9}\right)=\left\{v_3,v_9\right\} \\
&\Omega_G\left(e_{4,5}\right)=\left\{v_4,v_5\right\} \quad \Omega_G\left(e_{7,8}\right)=\left\{v_7,v_8\right\} \quad \Omega_G\left(e_{6,9}\right)=\left\{v_6,v_9\right\}. \\
&\Omega_G\left(e_{5,7}\right)=\left\{v_5,v_7\right\} \quad \Omega_G\left(e_{8,9}\right)=\left\{v_8,v_9\right\} \quad \Omega_G\left(e_{4,6}\right)=\left\{v_4,v_6\right\}
\end{aligned} \tag{A.3}$$

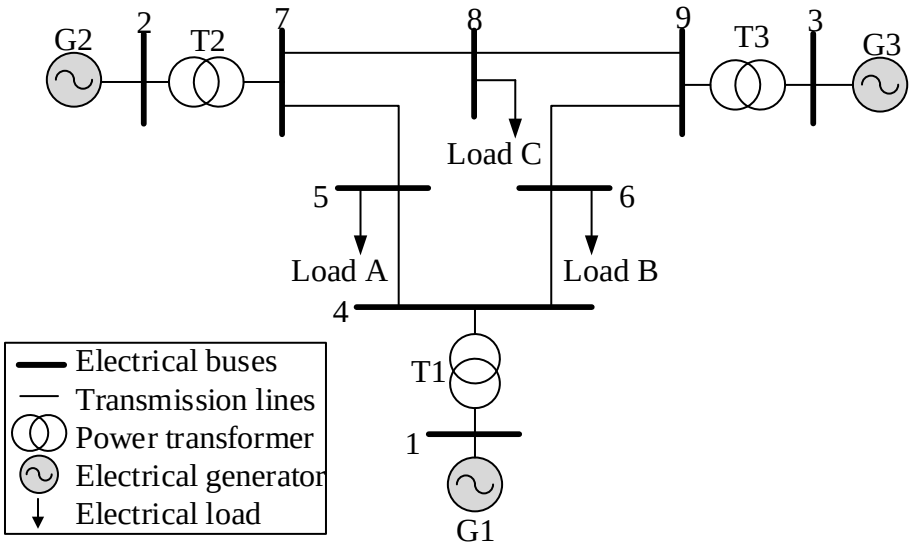

Figure A.1: Single line diagram of the IEEE 9-bus test system [110]

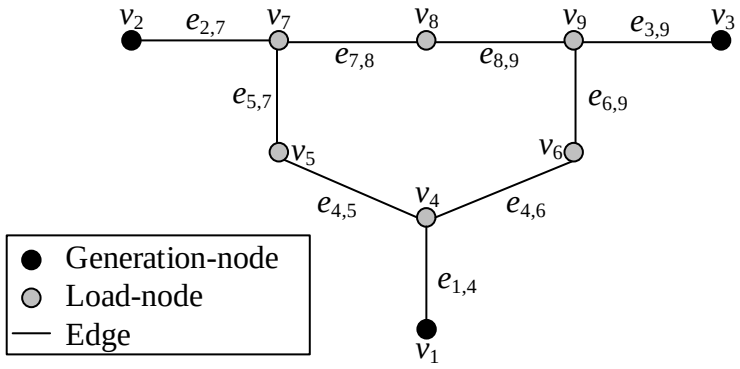

Figure A.2: Graph representation of the IEEE 9-bus test system

The analysis of the graph representation of the IEEE 9-bus test system shown in Figure A.2 provides the following two observations.

i. The number of nodes and edges in the graph *G* is equal to nine in both cases, i.e., $|V|=|E|=9$; and

ii. the generation-nodes V_{GN} and load-nodes V_{LD} are defined as $V_{GN} = \{v_1, v_2, v_3\}$ and $V_{LD} = \{v_4, v_5, v_6, v_7, v_8, v_9\}$, respectively.

As it is further explained in this thesis, graph theory can be used to represent multiple power system characteristics. For example, a three bus system can be represented as the graphs shown in Figure A.3 (a)-(c). As noticed, these graphs can be used to model different network properties, such as the susceptance Y_{ij} between buses (Figure A.3(a)), the active power P_{ij} between buses (Figure A.3(b)), and the dynamic coupling $\partial P_{ij} / \partial \delta_{ij}$ between buses and inertia constant H_i of machines connected at the buses (Figure A.3(c)).

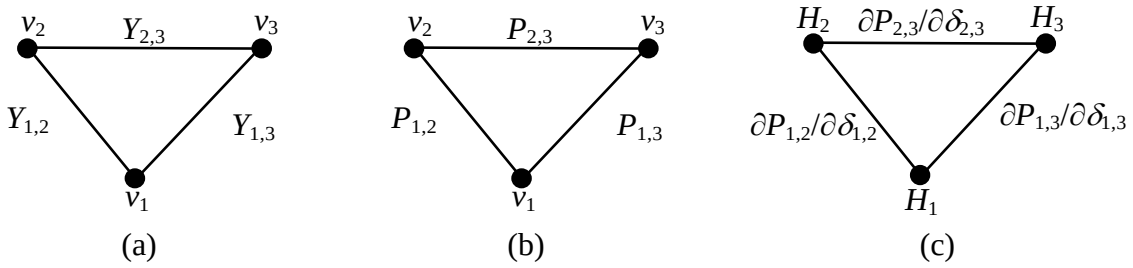

Figure A.3: Different graph representations of a 3-bus system

A.1. Drawing of Graphs

The drawing of a graph $G = (V, E)$ in the plane is the mapping of each node $v_i \in V$ to a distinct point – dot or circle – and each edge $e_{ij} = \{v_i, v_j\} \in E$ to a line (not necessarily straight) connecting the end nodes v_i and v_j according to the incidence function $\Omega_G(e_{ij})$ [106]. For example, the mapping of the graph G consisting of the sets V and E defined by (A.1) and (A.2), respectively, together with the incidence function defined by (A.3), is illustrated in Figure A.2. This mapping is referred to as the graph representation, and is used to illustrate the incidence between nodes and edges instead of the incidence function.

When drawing a graph in this thesis, two different node representations are used to distinguish the generation-nodes $(v_i^{GN} \in V_{GN})$ from the load-nodes $(v_i^{LD} \in V_{LD})$. While the

nodes representing the *m* generation buses are illustrated as black dots, the nodes representing the *n* – *m* load buses are shown as grey dots (see Figure A.2 for an example).

A.2. Weighted Graph

The graph above, commonly referred to as unweighted graph of the power system, only describes the topological structure of the corresponding electrical network [104, 105]. However, to capture the functional information of the power system weight factors associated with the nodes and edges must be used. A node weight is a positive or negative value assigned to the nodes through the function $\sigma : V \to \mathbb{R}$ such that $u_i = \sigma(v_i)$. Moreover, an edge weight is a positive value assigned to the edges through the function $\rho : E \to \mathbb{R}^+$ such that $w_{ij} = \rho(e_{ij})$. If weight factors are associated with *G*, it is called weighted graph and is denoted by $G = (V, E, \sigma, \rho)$. It should be noted that the unweighted case could be obtained from the weighted one, by defining $w_{ij} = 1$ for all $e_{ij} \in E$ and $u_i = 0$ for all $v_i \in V$.

In this thesis, the weight factors associated with the nodes and edges will be explicitly indicated. Node weights are used in the main chapters to represent the inertia constant of the machines connected at buses, or the total active power injections at the buses (see Table A.1 in the Example 2). Furthermore, the weight factors associated with the edges can represent the power flow in the branches of the power system (see Table A.2 in the Example 2), the synchronising coefficient between synchronous generators, information encountered in the *Jacobian* matrix of the static and dynamic power system, or the electrical distance between electrical buses. These weights factors are used to determine islanding solutions for blackout prevention and sectionalising strategies for PPSR.

Example 2: The power flow solution in the base case of the IEEE 9-bus test system is considered to compute the active power injection at the buses and the average power flow in the branches, accommodating network losses in both cases. The former is then used to define the node weights (Table A.1) and the latter to define the edge weights (Table A.2). These values are used throughout this chapter to exemplify the introduced concepts.

Table A.1: Node weights of the IEEE 9-bus test system

	Node weight (MW)
u_1	71.64
u_2	163.00
u_3	85.00
u_4	-0.21
u_5	-126.28
u_6	-90.76
u_7	-1.39
u_8	-100.28
u_9	-0.72

Table A.2: Edge weights of the IEEE 9-bus test system

	Edge Weight (MW)
$w_{1,4}$	71.64
$w_{4,5}$	40.95
$w_{5,7}$	86.61
$w_{2,7}$	163.00
$w_{7,8}$	76.39
$w_{8,9}$	24.17
$w_{3,9}$	85.00
$w_{6,9}$	60.83
$w_{4,6}$	30.69

A.3. Graph Theory Definitions

Within this section, the graph theory defitions used to describe and study graphs is presented. The definitions introduced in this section are followed by examples considering the graph representation of the IEEE 9-bus test system recently illustrated in Figure A.2 and the node weights and edge weights provided in Table A.1 and Table A.2, respectively.

A.3.1. Finite, Simple and Planar Graphs

A graph G is *finite*, if, and only if, the sets V and E contain a finite number of elements. The graph G is *simple* if, and only if, it has neither parallel edges between nodes nor loops. A loop is a special type of edge that connects a node to itself. Furthermore, a graph G is *planar* if, and only if, it can be drawn in such a way that edges only touch each other where they meet at nodes, in other words, if it can be embedded in the plane [106].

Due to the nature of power systems, its graph representation is always finite – there is no known network with infinite number of buses and transmission lines. Moreover, the power system can usually be simplified – parallel edges can be reduced to a single line equivalent using techniques available in the literature – and thus the graph can be considered as a simple graph. Finally, as none or only few transmission lines traverse each other, the graph representation of the power system can be planar or at least it is semi-planar [107]. The graph representation of the IEEE 9-bus test system is finite, simple, and planar. In this thesis, only finite, simple, and planar (or at least semi-planar) graphs are considered.

A.3.2. Order and Size of a Graph

The order and the size of the graph G refer to as the number of nodes and edges included in the node set V and the edge set E, respectively [106]. The order and the size of the graph shown in Figure A.2 are in both cases equal to nine. These values are associated with the number of elements in the electrical power system.

A.3.3. Incidence, Adjacent and Neighbours

Two nodes connected by an edge are said to be incident with the edge; two nodes that are incident with a common edge are adjacent; and two edges that are incident with a common node are adjacent. Finally, two distinct adjacent nodes are neighbours, and the neighbourhood of a node v_i is an induced subgraph formed by all nodes adjacent to v_i [106]. These definitions are essential to study the connectivity of the electrical network. To illustrate these definitions see Example 3.

Example 3: Consider the graph shown in Figure A.2. The nodes v_1 and v_4 are adjacent, and these are incident with the edge $e_{1,4}$. Likewise, the edges $e_{4,5}$ and $e_{5,7}$ are adjacent and these are incident with the node v_5. Finally, nodes v_8 and v_9 are neighbours, and the neighbourhood of the node v_6 is created by the nodes v_8 and v_9.

A.3.4. Paths, Walks and Cycles

Paths, *walks* and *cycles* are important concepts in the context of power system as they are used to study the connectivity of the network. The connectivity of the network is important to determine islanding solutions and sectionalising strategies.

A path from v_i to v_j in a graph G is a new graph $P = \left(V\left(P\right), E\left(P\right)\right)$ with $p + 1$ nodes and p edges starting with v_i and ending with v_j such that consecutive nodes are adjacent [106]. A path P must begin and end with nodes, such that each edge is incident with the nodes preceding and following it. Furthermore, the nodes and edges in a path P can appear only once, consequently, a path cannot contain repeated nodes or edges [104-106]. The length of a path is equal to the number of edges p. For example, there are two paths from v_1 to v_3 in the graph G shown in Figure A.2, and one of them is v_1, $e_{1,4}$, v_4, $e_{4,6}$, v_6, $e_{6,9}$, v_9, $e_{3,9}$, v_3. The length of this path is four (four edges).

A walk is a path in which nodes or edges may be repeated. A walk can be closed if the first and the last nodes are the same. If a walk is closed with no other repetitions of nodes or edges, than the repetition of the starting and ending node, then it is called a cycle [106].

A.3.5. Weighted-Degree and Degree of a Node

The weighted-degree of the node v_i, denoted by d_i, is defined as the total weight of the edges connected to that node, and is computed as follows [106].

$$d_i = \sum_{j=1}^{n} w_{ij} \tag{A.4}$$

When the edge weights represent the power flow in the transmission lines, the weighted-degree of a node corresponds to the total power at the corresponding system bus, and this can be seen as a degree of importance of the electrical bus [107]. When the edge weights represent the line susceptance, the weighted degree of a node represents the total susceptance connected to the corresponding bus, i.e., the elements in the main diagonal of the susceptance matrix **B**. This concept is further explained in Appendix A.6.3 and used in Chapter 7 to determine sectionalising strategies for PPSR.

Related to the weighted-degree, the degree of the node v_i indicates the total number of neighbours of that node, and this value can be calculated from (A.4) by defining $w_{ij}= 1$ for all $e_{ij} \in E$. The concept of degree of the node v_i can be used to identify leaf nodes, defined as nodes with degree one. The degree of the node can be used to determine the number of lines connected to a bus, and this is important to study the connectivity of the system. Example 4 presents the weighted degree and degree of the nodes of the graph representation of the IEEE 9-bus test system.

Example 4: Consider the graph representation of the IEEE 9-bus test system illustrated in Figure A.2, and the edge weights in Table A.2. The weighted-degree and the degree of the node v_i, $i = 1,\ldots,9$, are shown in Table A.3, where three leaf nodes can also be identified.

A.3.6. Subgraph of a Graph

A graph $G_1 = \left(V\left(G_1\right), E\left(G_1\right)\right)$ is called a subgraph of G, if, and only if, $V\left(G_1\right) \subset V\left(G\right)$, $E\left(G_1\right) \subset E\left(G\right)$, and Ω_{G1} is the restriction of Ω_G to $E\left(G_1\right)$ [106]. Subgraphs can be created after separating the original graph G into disjoint subgraphs. This separation can be achieved by removing certain edges (see Example 5), or by deleting certain nodes with the incident edges [106]. The nodes whose removals cause the separation of G into subgraphs are referred to as *cut* nodes or *separator* nodes. This definition is used in Appendix A.9 to create the *Depth First Search tree* of a graph, and define critical nodes of the graph. Critical nodes of a graph are used to determine the location of PMUs in Chapter 3.

The concept of a subgraph leads to the definition of the complement of the subgraph. Given a subgraph G_k, with node set V_k, the complement of the subgraph G_k, denoted by $\bar{G}_k$, is defined as the subgraph with node set $\bar{V}_k$, such that $V_k \cup \bar{V}_k = V$ (see Example 5) [106].

Table A.3: Weighted-degree and degree of the nodes of the IEEE 9-bus test system

Node	Weighted-degree	Degree
v_1	71.64	1
v_2	163.00	1
v_3	85.00	1
v_4	143.28	3
v_5	127.56	2
v_6	91.52	2
v_7	326.00	3
v_8	100.56	2
v_9	170.00	3

Example 5: The graph G shown in Figure A.2 is partitioned into two subgraphs by arbitrarily removing the edges $e_{4,5}$ and $e_{8,9}$. Consequently, the subgraphs $G_1 = (V_1, E_1)$ and $G_2 = (V_2, E_2)$ shown in Figure A.4 are obtained. The subgraph G_1 consists of the subsets $V_1 = \{v_2, v_5, v_7, v_8\}$ and $E_1 = \{e_{5,7}, e_{2,7}, e_{7,8}\}$, and the subgraph G_2 of the subsets $V_2 = \{v_1, v_3, v_4, v_6, v_9\}$ and $E_2 = \{e_{1,4}, e_{3,9}, e_{6,9}, e_{4,6}\}$. In this example, three cut nodes v_4, v_7 and v_9 can also be identified. Finally, the subgraph G_2 is the complement of G_1, as $V_1 \cup V_2 = V$.

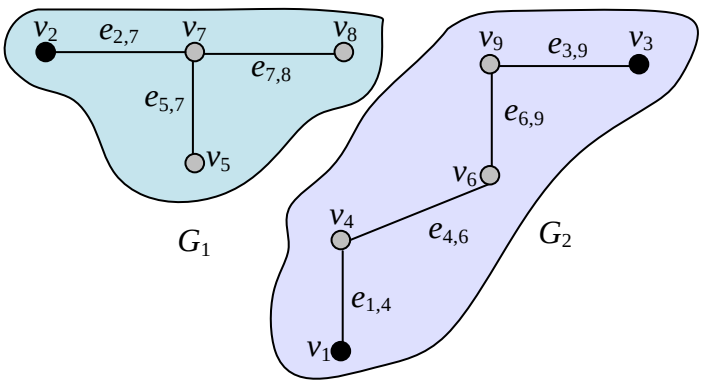

Figure A.4: Arbitrary partition of the IEEE 9-bus test system into two subgraphs

A.3.7. Boundary, Volume and Weight of a Subgraph

The boundary of a subgraph G_k, with node set V_k, denoted by *bou* (V_k), is the sum of the edge weights between nodes in V_k and nodes in $\bar{V}_k$, and is calculated as follows [71].

$$bou(V_k) = \sum_{v_i \in V_k, v_j \in \bar{V}_k} w_{ij} \tag{A.5}$$

As it can be noticed, the boundary of a subgraph (A.5) is the sum of edge weights of the tie-lines linking V_k with the rest of the graph (see Example 6). The volume of a subgraph G_k, denoted by *vol* (V_k), is defined as the sum of the weighted-degrees included in the node set, and is defined as follows [71].

$$vol(V_k) = \sum_{v_i \in V_k} d_i \tag{A.6}$$

The subgraph-weight, denoted by *wei* (V_k), is the sum of the node weights included in the subset V_k, and is calculated as follows [106].

$$wei(V_k) = \sum_{v_i \in V_k} u_i \tag{A.7}$$

As it is illustrated in Example 6, the boundary, the volume, and the weight of a subgraph can be used to represent the power exchange between one island and the system, the power flow within one island, and the power balance of the island, respectively. These definitions are used in this thesis to calculate the dynamic coupling between islands, the power flow disruption between islands, and the power imbalance within islands during the development of ICI strategies for blackout prevention. They are also used to define the load-generation balance within island during the determination of system sectionalising strategies for PPSR.

Example 6: The boundary, the volume and the weight of the subgraphs G_1 and G_2 illustrated in Figure A.4 are computed utilising the information provided in Table A.1 and Table A.2, and these are shown in Table A.4.

Table A.4: Boundary, volume and weight of the subgraphs after partitioning the IEEE 9-bus test system into two arbitrary clusters

Node set	Boundary (MW)	Volume (MW)	Subgraph-weight (MW)
V_1	65.12	717.12	-64.95
V_2	65.12	561.44	64.95

A.3.8. Cutset, Cut and Minimum-Cut Problem

A *cutset*, denoted by $E_S \subset E$, is a set of edges whose removal separates the connected graph into r $(r \geq 2)$ disjoint subgraphs [71]. As a results, the graph G is divided into subgraphs $G_1,\ldots,G_r$, with node sets $V_1,\ldots,V_r$ such that $V_1 \cup \ldots \cup V_r = V$ and $V_i \cap V_j = \varnothing$ for all $i \neq j$. The cutset E_S represents the branches that must be removed to partition the electrical power system. In this thesis, cutsets can represent ICI strategies for blackout prevention or system sectionalising strategies for faster PPSR.

Associated with the cutset of the graph G, the *cut* linked to E_S is by definition the sum of the edge weights included in E_S, and is computed as follows [71].

$$cut(V_1,\ldots,V_r) = \sum_{e_{ij} \in E_S} w_{ij} \tag{A.8}$$

The concepts of boundary (A.5) and cut (A.8) are related. While the boundary of G_k indicates the value of the cut required to separate that subgraph from the rest of the graph (A.9), the cut denotes the total sum of the edge weights required to separate the graph into r disjoint subgraphs. The equality (A.10) can be deduced from observing (A.5) and (A.8).

$$bou(V_k) = cut(V_k, \bar{V}_k) \tag{A.9}$$

$$cut\left(V_1,\ldots,V_r\right)=\frac{1}{2}\sum_{k=1}^{r}bou\left(V_k\right) \tag{A.10}$$

The right hand side of the equality (A.10) is divided by two as the boundaries are counted twice. For example, the value of the cut in Figure A.4 is 65.12 MW, and the sum of the boundaries (see Table A.4) is equal to double the value of the cut, i.e., 130.24 MW. When r = 2, the following relationship can be established between the cut and the boundary.

$$bou\left(V_1\right)=bou\left(V_2\right)=cut\left(V_1,V_2\right) \tag{A.11}$$

Given a connected graph G, the minimum-cut problem then consists in finding a cutset that splits the graph G with minimum cut, i.e., $\min\left\{cut\left(V_1,\ldots,V_r\right)\right\}$ [71]. Although the minimum-cut problem can efficiently be solved using minimum-cut algorithms (see Example 7) [132], the solution to the minimum cut problem without extra constraints usually gives spurious solutions – the node with the smallest weighted-degree may eventually be separated from the rest of the graph [71, 133]. Hence minimising the boundary of the subgraphs without additional constraints cannot be used in power systems [133]. Therefore, the concepts of *RatioCut* and normalised cut *Ncut* – introduced in Appendix A.7.4 – must be used instead to obtain an adequate partition of the graph G [71].

Example 7: The minimum-cut algorithm [132] is initially used to solve the minimum-cut problem for the graph shown in Figure A.2; and *spectral graph clustering* is used in Appendix A.7 to compare the solution. The graph is partitioned into two subgraphs (r = 2), and the cutset that induces the minimum cut (A.8) of 54.86 MW is $E_S=\left\{e_{4,6},e_{8,9}\right\}$ (see Figure A.5). Table A.5 shows the boundary and the volume of the created subgraphs. As r = 2, the boundary of each subgraph is equal to the value of the cut. A comparison between the results shown in Table A.4 and Table A.5 reveals that the cutset $E_S=\left\{e_{4,5},e_{8,9}\right\}$ shown in Figure A.4 produces higher cut, but the volume of the subgraphs is more balance.

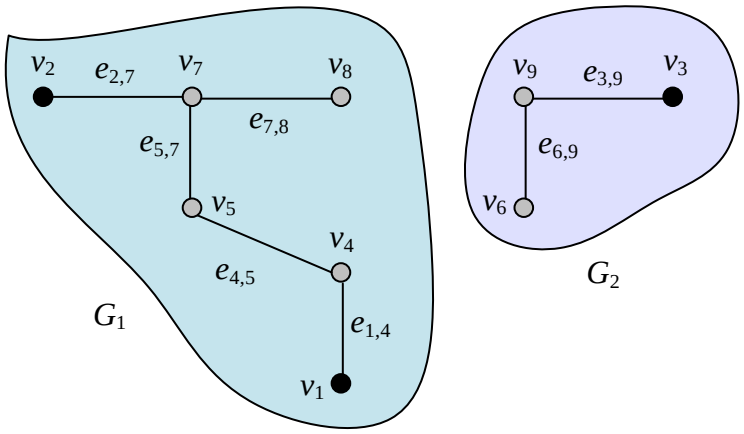

Figure A.5: Partition with minimum-cut for the IEEE 9-bus test system

Table A.5: Boundary, volume and weight of the subgraph after partitioning the IEEE 9-bus test system for minimum-cut

Node set	Boundary (MW)	Volume (MW)	Subgraph-weight (MW)
V_1	54.86	932.04	6.48
V_2	54.86	346.52	-6.48

A.3.9. Rank of a Graph

The *rank* of a graph is by definition the number of nodes *n* of *G* minus the number of *connected components c* of the graph *G*, and is calculated as follows [105].

$$rank\left(G\right)=n-c \tag{A.12}$$

The number of connected components of a graph *G* refers to the number of subgraphs included in that graph [106]. For example, the number of connected components of the graph shown in Figure A.2, which consists of nine nodes ($n = 9$), is one ($c = 1$). Thus, the rank of the graph shown in Figure A.2 is eight ($= 9 – 1$). Furthermore, the number of connected components of the graph shown in Figure A.4 is two; thus, the rank of the graph illustrated in Figure A.4, which indeed represents two subgraphs, is seven.

The rank of *G* represents the number of independent *cutsets* of the graph [106]. The determination of the rank of the graph *G* is useful to verify *connectivity* (see Appendix

A.5.3) [106]. A graph *G* is connected if, and only if, the rank of this graph is equal to the number of nodes minus one, i.e., the graph illustrated in Figure A.2 is connected.

A.4. Directed Graph

When dealing with certain power system challenges, for example, when solving the power flow problem [104, 105], the direction of the edges must be considered. If the edges have an associated direction, the graph is called directed graph, or simply *digraph*. Formally, a directed graph *H* is an ordered pair $\left(V\left(H\right),\bar{E}\left(H\right)\right)$, consisting of a node set $V:=V\left(H\right)$, and an arc set $\bar{E}:=\bar{E}\left(H\right)$ disjoint from $V\left(H\right)$, together with an incidence function Ω_H that associates each arc (an edge with defined direction) of *H* with an ordered pair of nodes of *H*. If $\bar{e}_{ij}$ is an arc and $\Omega_H\left(\bar{e}_{ij}\right)=\left\{v_i,v_j\right\}$, then $\bar{e}_{ij}$ is said to join v_i to v_j, and the node v_i is the tail of $\bar{e}_{ij}$ and v_j its head [106].

A digraph *H* can be obtained in two different ways. First, it can be constructed from a graph *G* by replacing each edge by two oppositely oriented arcs with the same ends. It may also be obtained from a graph *G* by replacing each edge by just one of the two possible arcs with the same ends. Such a digraph is called an orientation of *G* (see Example 8). Reciprocally, a graph *G* can be obtained from a digraph *H* by replacing each arc by an edge with the same ends. This graph is the underlying graph of *H*, denoted by $G\left(H\right)$.

Example 8: The power flow solution of the IEEE 9-bus test system is first considered. The power flow direction in each branch is then assigned to the corresponding edge of the graph *G* shown in Figure A.2. The resulting graph shown Figure A.6 in is now defined as the digraph representation of the IEEE 9-bus test system, in other words, the orientation of *G*. In this case, the node set remains the same as in (A.1), however the arc set $\bar{E}$ is defined as

$$\bar{E}=\left\{e_{1,4},e_{4,5},e_{7,5},e_{2,7},e_{7,8},e_{9,8},e_{3,9},e_{9,6},e_{4,6}\right\}, \tag{A.13}$$

and the incidence function Ω_H is defined by

$$\begin{aligned}
&\Omega_H\left(e_{1,4}\right)=\left\{v_1,v_4\right\} \quad \Omega_H\left(e_{2,7}\right)=\left\{v_2,v_7\right\} \quad \Omega_H\left(e_{3,9}\right)=\left\{v_3,v_9\right\} \\
&\Omega_H\left(e_{4,5}\right)=\left\{v_4,v_5\right\} \quad \Omega_H\left(e_{7,8}\right)=\left\{v_7,v_8\right\} \quad \Omega_H\left(e_{9,6}\right)=\left\{v_9,v_6\right\}. \\
&\Omega_H\left(e_{7,5}\right)=\left\{v_7,v_5\right\} \quad \Omega_H\left(e_{9,8}\right)=\left\{v_9,v_8\right\} \quad \Omega_H\left(e_{4,6}\right)=\left\{v_4,v_6\right\}
\end{aligned} \tag{A.14}$$

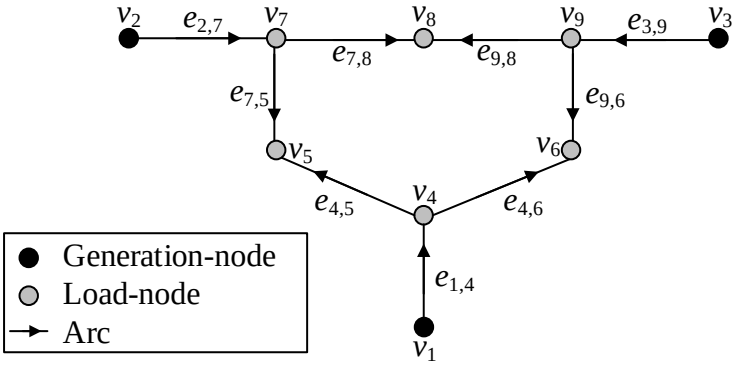

Figure A.6: Digraph representation of the IEEE 9-bus test system

A.4.1. Definitions for Directed Graphs

Although most of the definitions introduced in Appendix A.3 are still applicable for digraphs, this section introduces additional concepts that are exclusively related to digraphs.

A.4.1.1. Out-Degree and In-Degree

The concept of degree introduced in Appendix A.3.5 is extended to define the *out-degree* $\left(d_i^+\left(v_i\right)\right)$ and *in-degree* $\left(d_i^-\left(v_i\right)\right)$ of a node. While the former refers to the number of edges leaving the node, the latter denotes the number of edges entering the node [106]. The degree, the out-degree and the in-degree satisfy the equality (A.15).

$$d_i\left(v_i\right)=d_i^+\left(v_i\right)+d_i^-\left(v_i\right) \tag{A.15}$$

The concepts of out-degree and in-degree are used to define sources (generation buses) – nodes with zero in-degree – and sinks (load buses) – nodes with zero out-degree. In Figure A.6 nodes v_1, v_2 and v_3 are sources, and nodes v_5, v_6 and v_8 are sinks.

A.4.1.2. Cutset in a Digraph

A cutset in a digraph H produces a partitioning of the vertices of H into two disjoint subsets V_1 and V_2 such that the cutset consists of all those arcs that have one end node in V_1 and the other in V_2. All arcs in the cutset can be directed from V_1 to V_2, or from V_2 to V_1; or certain arcs can be directed from V_1 to V_2 and others from V_2 to V_1 (see Example 9). A cutset in which all arcs are oriented in the same direction is called a directed cutset [105].

Example 9: The digraph representation of the IEEE 9-bus test system is arbitrarily separated as shown in Figure A.7. The cutset is defined as being oriented from V_1 to V_2, and thus the arc $e_{9,6}$ is directed from V_1 to V_2 and the arc $e_{4,5}$ is oriented from V_2 to V_1.

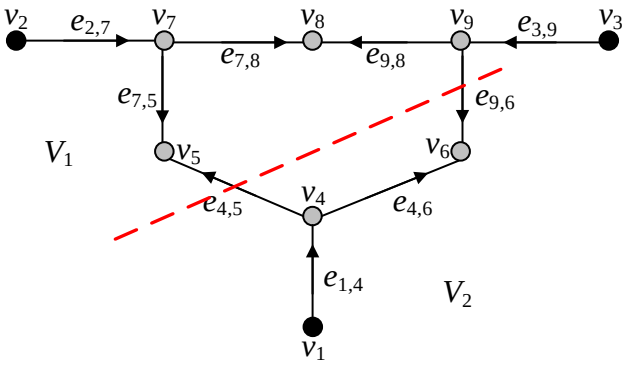

Figure A.7: Cutset in the digraph representation of the IEEE 9-bus test system

A.5. Structural Properties of a Graph

The position of the nodes and the shapes of the edges in graphs create different arrangements that can be described as follows.

A.5.1. Symmetry and Asymmetry

A graph is symmetrical if each pair of nodes linked in one direction is also linked in the other [106]. The graph G is always symmetrical (see Figure A.2 for an example), and the digraph H can be symmetrical if, and only if, there is a double directionality in all connected pair of nodes, in other words, if there is an arc in each direction between connected pair of nodes. A digraph is asymmetrical if at least one pair of nodes is

connected by only one arc (see Figure A.6 for an example). The symmetry of a graph is important to create the adjacency of the graph *G*, which is used to determine ICI strategies for blackout prevention and system sectionalising strategies for PPSR.

A.5.2. Complete Graph

A complete graph is a simple graph *G* with $|V| = n$ and $|E| = n(n-1)/2$ [106]. In a complete graph every pair of nodes $v_i, v_j \in V$ is connected through an edge $e_{ij} = (v_i, v_j) \in E$. Thus, the degree of every node in a complete graph is equal to $n - 1$. Complete graphs are used in Chapter 2 to study the dynamic coupling between generators and the coherency of generators. Figure A.8 shows two complete graphs with three and four nodes, respectively.

(a) (b)

Figure A.8: Complete graph with (a) three nodes (b) four nodes

A.5.3. Connectivity

Considering the concept of a path introduced in Appendix A.3.4, a graph *G* is connected, if, and only if, a path connects any two of its nodes [106]. Connectivity can also be expressed in terms of the rank. *G* is connected, if its rank is equal to $n - 1$ (see Appendix A.3.9) [107].

A.5.4. Tree

A tree is a connected graph $T = (V, E)$ in which any two vertices v_i and v_j are connected by only one simple path. In other words, any connected graph without simple cycles is a tree. The subgraphs shown in Figure A.4 are trees. Trees are used in Chapter 3 to optimally allocate PMUs for monitoring.

A.6. Matrices Associated with Graphs and Digraphs

Several matrices are used in graph theory to describe and study graphs [104-106], and this section introduces those used in this thesis. These matrices can represent the connectivity of the electrical network, the incidence between system buses and branches, the susceptance matrix of the electrical network and the power flow in the branches, as explained below.

A.6.1. Adjacency and Weighted Adjacency Matrices

The adjacency matrix shows the nodes of the graph which are adjacent to other nodes [106]. The weighted adjacency matrix displays the same relationship considering a certain level of strength defined by the edge weights. These matrices differ when considering undirected graphs and directed graphs as discussed below.

A.6.1.1. Undirected Graphs

The adjacency matrix $\mathbf{A} := \left(a_{ij}\right)$ of the graph G is the $n \times n$ matrix defined as follows [106].

$$\left[\mathbf{A}\right]_{ij} = \begin{cases} 1 & \text{if } i \neq j \text{ and } e_{ij} \in E; \\ 0 & \text{otherwise.} \end{cases} \tag{A.16}$$

The number of ones in the i^{th} column, or equally in the i^{th} row, of the matrix $\mathbf{A}$ is equal to the degree of the node v_i (see Example 10). The matrix $\mathbf{A}$ contains the connectivity of the electrical power systems. The weighted adjacency matrix $\mathbf{W} := \left(w_{ij}\right)$ of the graph G is the $n \times n$ matrix defined as follows [106].

$$\left[\mathbf{W}\right]_{ij} = \begin{cases} w_{ij} & \text{if } i \neq j \text{ and } e_{ij} \in E; \\ 0 & \text{otherwise.} \end{cases} \tag{A.17}$$

The sum of the values in the i^{th} row, or equally the i^{th} column, is equal to the weighted degree of the node v_i [71]. Similar to the matrix **A**, the matrix **W** contains the connectivity of the electrical network, with certain degree of strength (edge weights).

The matrices **A** and **W** are always symmetrical for an undirected graph, and they contain zeros in the diagonal, as the graphs considered are simple (see Example 10). The weighted adjacency matrix **W** can easily be constructed from the adjacency matrix **A**, by multiplying the *ij*-entry of **A** by the weight factor $w_{ij} = w_{ji}$ [115].

Example 10: The adjacency matrix **A** of the graph illustrated in Figure A.2 is shown in (A.18), and the weighted adjacency matrix **W** of the same graph, considering the edges weights provided in Table A.2, is illustrated in (A.19).

$$\mathbf{A} = \left[\begin{array}{c|ccccccccc} & v_1 & v_2 & v_3 & v_4 & v_5 & v_6 & v_7 & v_8 & v_9 \\ v_1 & 0 & 0 & 0 & 1 & 0 & 0 & 0 & 0 & 0 \\ v_2 & 0 & 0 & 0 & 0 & 0 & 0 & 1 & 0 & 0 \\ v_3 & 0 & 0 & 0 & 0 & 0 & 0 & 0 & 0 & 1 \\ v_4 & 1 & 0 & 0 & 0 & 1 & 1 & 0 & 0 & 0 \\ v_5 & 0 & 0 & 0 & 1 & 0 & 0 & 1 & 0 & 0 \\ v_6 & 0 & 0 & 0 & 1 & 0 & 0 & 0 & 0 & 1 \\ v_7 & 0 & 1 & 0 & 0 & 1 & 0 & 0 & 1 & 0 \\ v_8 & 0 & 0 & 0 & 0 & 0 & 0 & 1 & 0 & 1 \\ v_9 & 0 & 0 & 1 & 0 & 0 & 1 & 0 & 1 & 0 \end{array}\right] \tag{A.18}$$

$$\mathbf{W} = \left[\begin{array}{c|ccccccccc} & v_1 & v_2 & v_3 & v_4 & v_5 & v_6 & v_7 & v_8 & v_9 \\ v_1 & 0 & 0 & 0 & 71.64 & 0 & 0 & 0 & 0 & 0 \\ v_2 & 0 & 0 & 0 & 0 & 0 & 0 & 163.00 & 0 & 0 \\ v_3 & 0 & 0 & 0 & 0 & 0 & 0 & 0 & 0 & 85.00 \\ v_4 & 71.64 & 0 & 0 & 0 & 40.95 & 30.69 & 0 & 0 & 0 \\ v_5 & 0 & 0 & 0 & 40.95 & 0 & 0 & 86.61 & 0 & 0 \\ v_6 & 0 & 0 & 0 & 30.69 & 0 & 0 & 0 & 0 & 60.83 \\ v_7 & 0 & 163.00 & 0 & 0 & 86.61 & 0 & 0 & 76.39 & 0 \\ v_8 & 0 & 0 & 0 & 0 & 0 & 0 & 76.39 & 0 & 24.17 \\ v_9 & 0 & 0 & 85.00 & 0 & 0 & 60.83 & 0 & 24.17 & 0 \end{array}\right] \tag{A.19}$$

A.6.1.2. Directed Graphs

When using digraphs, the adjacency matrix $\mathbf{A_H}$ and the weighted adjacency matrix $\mathbf{W_H}$ are redefined as in (A.20) and (A.21), respectively, to consider the direction of the arcs [106].

$$\left[\mathbf{A_H}\right]_{ij} = \begin{cases} 1 & \text{if there is an arc } \underline{\text{from}}\ v_i\ \underline{\text{to}}\ v_j; \\ 0 & \text{otherwise.} \end{cases} \tag{A.20}$$

$$\left[\mathbf{W_H}\right]_{ij} = \begin{cases} w_{ij} & \text{if there is an arc } \underline{\text{from}}\ v_i\ \underline{\text{to}}\ v_j; \\ 0 & \text{otherwise.} \end{cases} \tag{A.21}$$

The matrices $\mathbf{A_H}$ and $\mathbf{W_H}$ also represent the connectivity between buses and the strength of this connection, respectively. However, this information is only represented from the tail of the edge to the head of the edge, i.e., from the sending-end to the receiving-end. The adjacency and the weighted adjacency matrices of digraphs can be symmetrical if, and only if, for each arc from v_i to v_j there also exists another arc from v_j to v_i [106]. Moreover, the number of ones in the i^{th} row and the number of ones in the i^{th} column of the matrix $\mathbf{A_H}$ are equal to the out-degree and the in-degree of the node v_i, respectively. Example 11 shows the matrix $\mathbf{A_H}$ of the digraph of the IEEE 9-bus test system, which is shown in Figure A.6.

Example 11: The matrix $\mathbf{A_H}$ of the digraph shown in Figure A.6 is shown in (A.22).

$$\mathbf{A_H} = \left[\begin{array}{c|ccccccccc} & v_1 & v_2 & v_3 & v_4 & v_5 & v_6 & v_7 & v_8 & v_9 \\ v_1 & 0 & 0 & 0 & 1 & 0 & 0 & 0 & 0 & 0 \\ v_2 & 0 & 0 & 0 & 0 & 0 & 0 & 1 & 0 & 0 \\ v_3 & 0 & 0 & 0 & 0 & 0 & 0 & 0 & 0 & 1 \\ v_4 & 0 & 0 & 0 & 0 & 1 & 1 & 0 & 0 & 0 \\ v_5 & 0 & 0 & 0 & 0 & 0 & 0 & 0 & 0 & 0 \\ v_6 & 0 & 0 & 0 & 0 & 0 & 0 & 0 & 0 & 0 \\ v_7 & 0 & 0 & 0 & 0 & 1 & 0 & 0 & 1 & 0 \\ v_8 & 0 & 0 & 0 & 0 & 0 & 0 & 0 & 0 & 0 \\ v_9 & 0 & 0 & 0 & 0 & 0 & 1 & 0 & 1 & 0 \end{array}\right] \tag{A.22}$$

A.6.2. Incidence Matrix

The incidence matrix shows the incidence between nodes and edges of a graph. This matrix is also called *node-edge* incidence matrix [106]. It is defined for undirected and directed graphs, as explained below. These matrices describe whether a branch in the system is incident to a particular bus or not. They are used in Chapter 4 and 6 to find islanding solutions for blackout prevention and sectionalising strategies for PPSR, respectively.

A.6.2.1. Undirected Graphs

The incidence matrix $\mathbf{M} := (m_{ik})$ of the graph G is the $n \times l$ matrix defined as follows [106].

$$[\mathbf{M}]_{ik} = \begin{cases} 1 & \text{if } v_i \in V \text{ is an end node of } e_k \in E; \\ 0 & \text{otherwise.} \end{cases} \tag{A.23}$$

Three important observations can be drawn from the incidence matrix **M**.

i. Each column of **M** has exactly two ones,

ii. The number of ones in each row equals the degree of the corresponding node; and

iii. If a graph is disconnected and consists of two components G_1 and G_2, the incidence matrix **M** (G) of the graph G can be written in a block diagonal form as (A.24)

$$\mathbf{M}(G) = \begin{bmatrix} \mathbf{M}(G_1) & 0 \\ 0 & \mathbf{M}(G_2) \end{bmatrix}, \tag{A.24}$$

where **M** (G_1) and **M** (G_2) are the incidence matrices of G_1 and G_2, respectively.

A.6.2.2. Directed Graphs

When considering digraphs, the incidence matrix is referred to as the oriented incidence matrix (see Example 12). This matrix $\mathbf{M_H}$ is defined as follows [106].

$$\left[\mathbf{M_H}\right]_{ik} = \begin{cases} 1 & \text{if arc } e_k \in \bar{E} \text{ is a link and node } v_i \text{ is the tail of } e_k; \\ -1 & \text{if arc } e_k \in \bar{E} \text{ is a link and node } v_i \text{ is the head of } e_k; \\ 0 & \text{otherwise.} \end{cases} \quad \text{(A.25)}$$

Three important observations about the oriented incidence matrix $\mathbf{M_H}$ are:

i. the sum of each column equals zero;

ii. the number of ones in each row equals the out-degree minus the in-degree of the corresponding node; and

iii. the rank of the matrix $\mathbf{M_H}$ corresponds to the rank of the associated graph (see Appendix A.3.9).

Example 12: The matrix $\mathbf{M_H}$ of the digraph shown in Figure A.6 is displayed in (A.26).

$$\mathbf{M_H} = \left[\begin{array}{c|ccccccccc} & e_1 & e_2 & e_3 & e_4 & e_5 & e_6 & e_7 & e_8 & e_9 \\ v_1 & 1 & 0 & 0 & 0 & 0 & 0 & 0 & 0 & 0 \\ v_2 & 0 & 0 & 0 & 1 & 0 & 0 & 0 & 0 & 0 \\ v_3 & 0 & 0 & 0 & 0 & 0 & 0 & 1 & 0 & 0 \\ v_4 & -1 & 1 & 0 & 0 & 0 & 0 & 0 & 0 & 1 \\ v_5 & 0 & -1 & -1 & 0 & 0 & 0 & 0 & 0 & 0 \\ v_6 & 0 & 0 & 0 & 0 & 0 & 0 & 0 & -1 & -1 \\ v_7 & 0 & 0 & 1 & -1 & 1 & 0 & 0 & 0 & 0 \\ v_8 & 0 & 0 & 0 & 0 & -1 & -1 & 0 & 0 & 0 \\ v_9 & 0 & 0 & 0 & 0 & 0 & 1 & -1 & 1 & 0 \end{array}\right] \quad \text{(A.26)}$$

A.6.3. Laplacian Matrices

Laplacian matrices are commonly defined for undirected simple graphs with positive weight factors only [71]. Two main types of Laplacian matrices exist: the unnormalised Laplacian matrix **L**, and the normalised Laplacian matrix $\mathbf{L_N}$. These matrices are widely used in graph theory, and have a clear power engineering interpretation, as presented below. Laplacian matrices also represent the main tools for *spectral clustering*.

This section presents basic definition and observations on the Laplacian matrices. The properties of these matrices, their eigenvalues, and the theoretical justification for using these matrices to partition graphs through *spectral clustering* are detailed in Appendix A.7.

A.6.3.1. Unnormalised Laplacian Matrix

The unnormalised Laplacian matrix **L** of a graph *G* is the $n \times n$ matrix defined as follows:

$$\left[\mathbf{L}\right]_{ij} = \begin{cases} d_i & \text{if } i = j; \\ -w_{ij} & \text{if } i \neq j \text{ and } e_{ij} \in E; \\ 0 & \text{otherwise.} \end{cases} \tag{A.27}$$

The matrix **L** can also be calculated in a matrix form as $\mathbf{L} = \mathbf{D} - \mathbf{W}$, where **D** is the $n \times n$ diagonal matrix with the weighted degrees d_i, defined by (2.4), in the main diagonal. The unnormalised Laplacian matrix **L** is symmetrical because of the symmetry of **W** and **D**; positive semi-definite; and the sum of each column (or row) is zero [71]. A matrix **L** is positive semi-definite if and only if $\mathbf{x}^T\mathbf{L}\mathbf{x} \geq 0$ for any vector $\mathbf{x} \in \mathbb{R}^n$ [134].

The unnormalised Laplacian matrix **L** has a strong power engineering use. For example, if the edge weights are equal to the line susceptance, then the unnormalised Laplacian is equal to the well-known susceptance matrix $\mathbf{B} = \mathrm{Im}\left(\mathbf{Y}_{\mathbf{BUS}}\right)$. There is no such established interpretation in power system when the edge weights are equal to the power flow [133].

A.6.3.2. Normalised Laplacian Matrix

The normalised Laplacian matrix $\mathbf{L_N}$ of a graph *G* is the $n \times n$ matrix defined as follows:

$$\left[\mathbf{L_N}\right]_{ij} = \begin{cases} 1 & \text{if } i = j; \\ -w_{ij} \Big/ \sqrt{d_i d_j} & \text{if } i \neq j \text{ and } e_{ij} \in E; \\ 0 & \text{otherwise.} \end{cases} \tag{A.28}$$

The matrix $\mathbf{L_N}$ of the graph *G* can also be expressed in a matrix form as follows:

$$\mathbf{L_N} = \mathbf{D}^{-1/2}\mathbf{L}\mathbf{D}^{-1/2} = \mathbf{I} - \mathbf{D}^{-1/2}\mathbf{W}\mathbf{D}^{-1/2} \tag{A.29}$$

where **I** is the identity $n \times n$ matrix.

The matrix $\mathbf{L_N}$ has the same power engineering use as the matrix **L**, but this is normalised with respect to the elements in the main diagonal. The normalised Laplacian matrix $\mathbf{L_N}$ is symmetrical because of the symmetry of **D** and **L**, positive semi-definite, i.e., $\mathbf{x}^T\mathbf{L_N}\mathbf{x} \geq 0$ for every $\mathbf{x} \in \mathbb{R}^n$. Furthermore, it has the advantage of being scale-independent, and it allows the comparison of graphs with different edge weights [70, 71, 73].

A.6.4. Cutset Matrices

A cutset matrix represents all the possible cutsets of a graph [105]. These matrices are useful to determine multiple cutsets to partition the graph that represents the electrical power system. Thus, they are used in this thesis to determine ICI strategies for minimal power imbalance in Chapter 5, and system sectionalising strategies for PPSR in Chapter 7.

Given a graph G with q cutsets, the cutset matrix $\mathbf{Q} := (q_{ik})$ of the graph is the $n \times q$ matrix defined as follows [106]:

$$[\mathbf{Q}]_{ik} = \begin{cases} 1 & \text{if } i^{\text{th}} \text{ cutset contains edge } e_k \in E; \\ 0 & \text{otherwise.} \end{cases} \tag{A.30}$$

The cutset matrix can also be defined for directed graphs as follows:

$$[\mathbf{Q_H}]_{ik} = \begin{cases} +1 & \text{if arc } e_k \text{ of cutset } Q_i \text{ has the same orientation as } Q_i; \\ -1 & \text{if arc } e_k \text{ of cutset } Q_i \text{ has the opposite orientation as } Q_i; \\ 0 & \text{otherwise.} \end{cases} \tag{A.31}$$

where Q_i is the i^{th} cutset of H, and it partitions the set V into two subsets V_1 and V_2. Moreover, it is assumed in (A.31) that the orientation of the cutset Q_i is from V_1 to V_2. Then the orientation of an arc e_k in the cutset Q_i is said to be the same as that of Q_i if e_k is of the form $\{v_i, v_j\}$, where $v_i \in V_1$ and $v_j \in V_2$, and opposite, otherwise. In Example 9 (Appendix A.4.1.2), the cutset labels are -1 for the arc $e_{4,5}$, 1 for the arc $e_{9,6}$, and zero for the others.

A.7. Spectral Graph Clustering

Spectral graph clustering studies how a graph $G=(V,E)$ can be optimally partitioned into r subgraphs using eigenvalues and eigenvectors of the associated Laplacian matrices described above. As further detailed in Appendix A.7.2, the eigenvalues, also called the spectrum of the graph, and eigenvectors of these matrices can be obtained by solving a classical algebraic eigenproblem [71]. Only undirected graphs can be split using spectral clustering, as this well-established technique ignores the direction of the edges [71].

In the sense of spectral graph clustering, an optimal partition means the creation of subgraphs such that the nodes in a cluster are highly connected among themselves (taking edge weights into consideration) but weakly connected to nodes in other clusters.

A.7.1. Brief History of Spectral Graph Clustering

The first works on spectral graph clustering date to 1973 when Donath and Hoffman [135] suggested using the eigenvectors of the adjacency matrix for clustering a graph. In the same year, Fiedler [136] associated the second smallest eigenvalue of the Laplacian matrix with the connectivity of the graph, and suggested clustering the nodes of the graph based on their value and the sign of this in the corresponding eigenvector. Because of his important contribution, the second smallest eigenvalue and associated eigenvector are called Fiedler value and Fiedler vector, respectively.

The most computationally demanding step in spectral clustering is the computation of the eigenvalues and eigenvectors associated with the matrices of the graph [71]. Fortunately, advances in algorithms for computing eigenvectors, such as the Lanczos algorithm [137],

made the computation of eigenvectors practical; and encouraged researches to develop further theoretical foundations on spectral clustering [138]. In the late 1980's, Alon [139] and Sinclair and Jerrum [140] demonstrated that if the Fiedler value is sufficiently small, then the partition of the graph based on the Fiedler vector will produce a cutset with small number of interconnections respect to the number of internal connections. Then, several works in the following years revealed that spectral clustering adequately works on graphs that commonly arise in practice, leading spectral clustering to become a standard tool for partitioning graph in many research areas. This standardisation was significantly improved by bounding the Fiedler values of the graphs of interest in scientific applications [138].

Spectral clustering was later modernised by the introduction of the *RatioCut* concept [141], the *multi-way RatioCut* [142], and more recently the normalised cut *Ncut* [143]. These significant improvements led to the use of the spectral clustering in several disciplines which have significantly contributed and developed new partitioning techniques based on spectral clustering (see [71, 144] for more details).

A.7.1.1. General Concept of Spectral Graph Clustering

Although spectral graph clustering has been significantly improved in the last decades, the general concept of this technique remains almost unchanged [71]. Spectral graph clustering uses the eigenvectors associated with the r smallest eigenvalues (after being ordered increasingly) of a Laplacian matrix to give geometric coordinates to the nodes $v_i \in V$ in Euclidean space $\mathbb{R}^r$, for some $2 \leq r \leq n$. The resulting data points are then clustered into r groups using some standard clustering algorithms developed for point clouds in $\mathbb{R}^r$ [133], i.e., for data points that are represented in a coordinate system. The general concept of spectral graph clustering and the fundamental justifications are described below.

The main advantage of spectral graph clustering compared to other clustering techniques such as such as *k-means* or single linkage [104, 105] is that it can find a good partition of the graph within polynomial time, as its complexity is dominated by that of the determination of the eigenvectors associated with the r smallest eigenvalues [71]. Spectral clustering is also simple to implement [133].

A.7.2. Eigenvalues and Eigenvectors of the Laplacian Matrices

A.7.2.1. Unnormalised Laplacian Matrix

The eigenvalues of the unnormalised Laplacian matrix **L** are given by the values of the scalar λ for which there are non-trivial solutions to (A.32) given below, where $\boldsymbol{\varphi}$ is an $n \times 1$ vector and $\boldsymbol{\varphi} \neq 0$. The n solutions of (A.32) form a set of eigenvalues (the spectrum of the Laplacian matrix) $\lambda = \lambda_1,\ldots,\lambda_n$.

$$\mathbf{L}\boldsymbol{\varphi} = \lambda\boldsymbol{\varphi} \tag{A.32}$$

The column vector $\boldsymbol{\varphi}_i$ which satisfies (A.32) for the i^{th} eigenvalue λ_i is referred to as the eigenvector of **L** associated with λ_i. In this thesis, it is assumed that the eigenvalues of **L** are always ordered increasingly and written as $\lambda_1 \leq \ldots \leq \lambda_n$. Thus, the smallest r eigenvectors refers to the eigenvectors associated with the smallest r eigenvalues.

A.7.2.2. Normalised Laplacian Matrix

The eigenvalues of the normalised Laplacian matrix $\mathbf{L_N}$ are given by the values of the scalar ν for which there are non-trivial solution to (A.33), where $\boldsymbol{\psi}$ is an $n \times 1$ vector and $\boldsymbol{\psi} \neq 0$. The n solutions to the eigenproblem (A.33) form the set of eigenvalues (the spectrum of the normalised Laplacian matrix) $\nu = \nu_1,\ldots,\nu_n$.

$$\mathbf{L_N}\boldsymbol{\psi} = \nu\boldsymbol{\psi} \tag{A.33}$$

The column vector $\boldsymbol{\psi}_i$ which satisfies (A.33) for the i^{th} eigenvalue ν_i is referred to as the eigenvector of $\mathbf{L_N}$ associated with ν_i. In what follows, it is assumed that the eigenvalues of $\mathbf{L_N}$ are always ordered increasingly and written as $\nu_1 \leq \ldots \leq \nu_n$. Thus, the smallest r eigenvectors refers to the eigenvectors associated with the smallest r eigenvalues.

A.7.2.3. A note about the Laplacian matrices

The Laplacian can be viewed as an operator on the space of non-zero functions $\mathbf{g}: V \to \mathbb{R}$ which satisfies (A.34) [71].

$$\mathbf{L_N g}(v_i) = \frac{1}{\sqrt{d_i}} \sum_{\substack{v_i \\ v_i \sim v_j}} \left(\frac{\mathbf{g}(v_j)}{\sqrt{d_j}} - \frac{\mathbf{g}(v_i)}{\sqrt{d_i}} \right). \tag{A.34}$$

Since $\mathbf{L_N}$ is symmetrical (see Appendix A.6.3.2), its eigenvalues are all real and nonnegative [71]. Thus, the variational characterisations of those eigenvalues in terms of the *Rayleigh quotient* $\mathcal{R}(\cdot)$ of $\mathbf{L_N}$ can be used. As $\mathbf{g}$ is an arbitrary function which assigns to each node of *G* a real value $\mathbf{g}(v_i)$, then

$$\begin{aligned} \frac{\langle \mathbf{g}, \mathbf{L_N g} \rangle}{\langle \mathbf{g}, \mathbf{g} \rangle} &= \frac{\langle \mathbf{g}, \mathbf{D}^{-1/2} \mathbf{L} \mathbf{D}^{-1/2} \mathbf{g} \rangle}{\langle \mathbf{g}, \mathbf{g} \rangle} = \frac{\langle \mathbf{f}, \mathbf{L f} \rangle}{\langle \mathbf{D}^{1/2} \mathbf{f}, \mathbf{D}^{1/2} \mathbf{f} \rangle} \\ &= \frac{\sum_{v_i \sim v_j} w_{ij} \left(\mathbf{f}(v_i) - \mathbf{f}(v_j) \right)^2}{\sum_{v_j \in V} \mathbf{f}(v_j)^2 d_j} := \mathcal{R}(\mathbf{f}) \end{aligned} . \tag{A.35}$$

where $\mathbf{g} = \mathbf{D}^{1/2} \mathbf{f}$ and $\sum_{v_i \sim v_j}$ denotes the sum over all unordered pairs for which v_i and v_j are adjacent. Here, $\langle \mathbf{f}, \mathbf{g} \rangle = \sum_{\mathbf{x}} \mathbf{f}(\mathbf{x}) \mathbf{g}(\mathbf{x})$ denotes the standard inner product in $\mathbb{R}^n$. The sum $\sum_{v_i \sim v_j} \left(\mathbf{f}(v_i) - \mathbf{f}(v_i) \right)^2$ is sometimes called the Dirichlet sum of *G* and the ratio on the left-hand side of (A.35) is often called the Rayleigh quotient of **f** (with respect to *G*) [73].

From equation (A.34), it can be noted that all eigenvalues are nonnegative [71]. Moreover, it can be deduced that zero is an eigenvalue of $\mathbf{L_N}$ and the associated eigenvector is $\mathbf{D}^{1/2}\mathbf{1}$, where **1** is the all-ones column vector. Therefore, the spectrum of the matrix $\mathbf{L_N}$ can be written as follows.

$$0 = \nu_1 \leq \nu_2 \leq \cdots \leq \nu_n \leq 2. \tag{A.36}$$

For a connected graph *G*, and considering standard variational principles [73], the following equality can be deduced.

$$\begin{aligned} \nu_k &= \min_{\mathbf{g}_1,\ldots,\mathbf{g}_k \in \mathbb{R}^2} \max_{\mathbf{g}\neq 0} \left\{ \frac{\langle \mathbf{g}, \mathbf{L}_\mathbf{N}\mathbf{g} \rangle}{\langle \mathbf{g}, \mathbf{g} \rangle} : g \in span\{\mathbf{g}_1,\ldots,\mathbf{g}_k\} \right\}. \\ &= \min_{\mathbf{f}_1,\ldots,\mathbf{f}_k \in \mathbb{R}^2} \max_{\mathbf{f}\neq 0} \left\{ \mathcal{R}(\mathbf{f}) : \mathbf{f} \in span\{\mathbf{f}_1,\ldots,\mathbf{f}_k\} \right\} \end{aligned} \tag{A.37}$$

where both minimums are over sets of *k* non-zero orthogonal functions in the Euclidean space $\mathbb{R}^2$.

A.7.2.4. Properties of the Laplacian Matrices and their Eigenvalues

The matrices **L** and $\mathbf{L_N}$ satisfy multiple properties [71], as described below.

1. For every vector $\mathbf{x} \in \mathbb{R}^n$, the equalities (A.38) and (A.39) are always satisfied.

$$\mathbf{x}^T\mathbf{L}\mathbf{x} = \frac{1}{2}\sum_{i,j=1}^{n} w_{ij}\left(\mathbf{x}_i - \mathbf{x}_j\right)^2 \tag{A.38}$$

$$\mathbf{x}^T\mathbf{L}_\mathbf{N}\mathbf{x} = \frac{1}{2}\sum_{i,j=1}^{n} w_{ij}\left(\frac{\mathbf{x}_i}{\sqrt{d_i}} - \frac{\mathbf{x}_j}{\sqrt{d_j}}\right)^2 \tag{A.39}$$

2. Equations (A.38)-(A.39) are used to express the actions defined by the Laplacian matrices. These help to visualise how the vectors of a Laplacian act as functions $\mathbf{x}=\left(\mathbf{x}(\nu_1),\mathbf{x}(\nu_2),\ldots,\mathbf{x}(\nu_n)\right)=\left(\mathbf{x}_1,\mathbf{x}_2,\ldots,\mathbf{x}_n\right)$ on the nodes, assigning a real number to each node [71]. The equality (A.38) is demonstrated in (A.40), and the equality (A.39) can be demonstrated following a similar analysis.

$$\begin{aligned}\mathbf{x}^T\mathbf{L}\mathbf{x} &= \mathbf{x}^T\mathbf{D}\mathbf{x} - \mathbf{x}^T\mathbf{W}\mathbf{x} = \sum_{i=1}^{n} d_i\mathbf{x}_i^2 - \sum_{i,j=1}^{n}\mathbf{x}_i\mathbf{x}_j w_{ij} \\ &= \frac{1}{2}\left(\sum_{i=1}^{n} d_i\mathbf{x}_i^2 - 2\sum_{i,j=1}^{n}\mathbf{x}_i\mathbf{x}_j w_{ij} + \sum_{j=1}^{n} d_j\mathbf{x}_j^2\right) = \frac{1}{2}\sum_{i,j=1}^{n} w_{ij}\left(\mathbf{x}_i - \mathbf{x}_j\right)^2\end{aligned} \tag{A.40}$$

3. The matrices **L** and $\mathbf{L_N}$ are both symmetrical because of the symmetry of **W** and **D**, and positive semi-definite as a consequence of the first property, which shows that $\mathbf{x}^T\mathbf{L}\mathbf{x} \geq 0$ and $\mathbf{x}^T\mathbf{L_N}\mathbf{x} \geq 0$ for all $\mathbf{x} \in \mathbb{R}^n$.

4. All the eigenvalues are nonnegative real numbers (see Example 13);

5. Zero is an eigenvalue with multiplicity equal to the number of connected components in the graph (see Example 13);

6. The graph accepts a good partition into *r* subgraphs if λ_r and ν_r are small (this is explained in more detail below using the Cheeger inequality); and

7. The eigenvalues of **L** are scale-dependent and have a priori no upper bound. However, the eigenvalues of $\mathbf{L_N}$ satisfy the inequality $0 \leq \nu_i \leq 2$ for all *i* (see Example 13).

From property (4) above, it is known that [71]:

i. $\lambda_1 = 0$ and $\boldsymbol{\varphi}_1 = \mathbf{1}$, where **1** is the all-ones column vector, thus $0 = \lambda_1 \leq \lambda_2 \leq \ldots \leq \lambda_n$;

ii. $\nu_1 = 0$ and $\boldsymbol{\psi}_1 = \mathbf{D}^{1/2}\mathbf{1} = \left[\sqrt{d_1}, \sqrt{d_2}, \ldots, \sqrt{d_n}\right]$, thus $0 = \nu_1 \leq \nu_2 \leq \ldots \leq \nu_n$; and

iii. $\lambda_2 > 0$ and $\nu_2 > 0$, as the graph *G* is connected, and the eigenvectors $\boldsymbol{\varphi}_2$ and $\boldsymbol{\psi}_2$ are referred to as the Fiedler vector [71] of the matrix **L** and $\mathbf{L_N}$, respectively.

Example 13: The eigenvalues of the unnormalised **L** and normalised $\mathbf{L_N}$ Laplacian matrices associated with the graph illustrated in Figure A.2 are shown in Table A.6. These values were calculated using built-in MATLAB function *eig* [145].

Table A.6: Eigenvalues of the Laplacian matrices of the IEEE 9-bus test system

Eigenvalue Number	Eigenvalues of the matrix L	Eigenvalues of the matrix L_N
1	0.0000	0.0000
2	20.4111	0.1428
3	26.7081	0.2522
4	87.5738	0.9999
5	106.0405	1.0000
6	130.9021	1.0001
7	205.3396	1.7478
8	245.2704	1.8571
9	456.3143	2.0000

A.7.3. Two Spectral Clustering Algorithms

There are three common spectral clustering algorithms: unnormalised spectral clustering, normalised spectral clustering according to Shi and Malik and normalised spectral clustering according to Ng, Jordan, and Weiss [71]. In this section, two of the most commonly used, and indeed implemented in power systems, are: unnormalised spectral clustering [71] and normalised spectral clustering according to Ng, Jordan, and Weiss [70].

A.7.3.1. Unnormalised Spectral Clustering

Input: Weighted adjacency matrix **W**, and number of clusters *r*.

1. Construct the matrix **L** (A.27) and compute the first *r* eigenvalues of the matrix by solving (A.32).

2. Place the eigenvectors $\boldsymbol{\varphi}_1,\ldots,\boldsymbol{\varphi}_r$ as column vectors, and create the matrix $\mathbf{X}\in\mathbb{R}^{n\times r}$ with rows $\mathbf{x}_i$, $i=1,\ldots,n$. Note that each vector $\mathbf{x}_i$ represents a data point in the *r*-dimensional Euclidean space $\mathbb{R}^r$.

3. Cluster the points $\mathbf{x}_i$ into clusters $C_1,\ldots,C_r$ using some standard clustering algorithm developed for points in Euclidean space (say *k-means*).

Output: Clusters $V_1,\ldots,V_r$ with $V_i=\{j \text{ such that } x_j\in C_i\}$.

A.7.3.2. Normalised Spectral Clustering According to Ng, Jordan, and Weiss

Input: Weighted adjacency matrix $\mathbf{W}$, and number of clusters r.

1. Construct the matrix $\mathbf{L_N}$ (A.28) (or (A.29)) and compute the first r eigenvalues of the matrix by solving (A.33).

2. Place the eigenvectors $\boldsymbol{\psi}_1,\ldots,\boldsymbol{\psi}_r$ as column vectors, and create the matrix $\mathbf{X}\in\mathbb{R}^{n\times r}$ with rows $\mathbf{x}_i$, $i=1,\ldots,n$. Note that each vector $\mathbf{x}_i$ represents a data point in the r-dimensional Euclidean space $\mathbb{R}^r$.

3. Normalise the vector $\mathbf{x}_i$ (A.61) to create the normalised vector $\mathbf{y}_i$ and the matrix $\mathbf{Y}\in\mathbb{R}^{n\times r}$.

4. Cluster the points $\mathbf{y}_i$ into clusters $C_1,\ldots,C_r$ using some standard clustering algorithm developed for points in Euclidean space (say *k-means*).

Output: Clusters $V_1,\ldots,V_r$ with $V_i=\{j \text{ such that } x_j\in C_i\}$.

Although the normalised spectral clustering looks similar to the unnormalised spectral clustering, the former commonly create better partitions [71].

A.7.4. RatioCut and Normalised Cut

Clustering refers to the partition of the graph G into a predefined number of r subgraphs, also called clusters. Clustering a graph means partitioning it such that the edges between different groups have very low weight (which means that nodes in different clusters are dissimilar from each other) and the edges within a group have high weight (which means that nodes within the same cluster are similar to each other) [71].

The concept of clustering is associated with the minimum-cut problem [132], which can be solved using a minimum-cut algorithm. However, this approach may eventually produce spurious solutions [71], as discussed in Appendix A.3.8.

Therefore, the *RatioCut* (A.41) [141] and the normalised *Ncut* (A.42) [143] approaches are introduced in this section to solve the problem associated with the minimum-cut algorithm. These approaches aim to normalise the boundary of the subgraphs [71]. While the *RatioCut* normalises the boundary of the subgraph with respect to the number of nodes $|V_k|$, the *Ncut* normalises the boundary with respect to the volume $vol(V_k)$ given by (A.6).

$$RatioCut(V_1,V_2,...,V_r) = \frac{1}{2}\sum_{k=1}^{r}\frac{bou(V_k)}{|V_k|} = \sum_{k=1}^{r}\frac{cut(V_k,\bar{V}_k)}{|V_k|} \tag{A.41}$$

$$Ncut(V_1,V_2,...,V_r) = \frac{1}{2}\sum_{k=1}^{r}\frac{bou(V_k)}{vol(V_k)} = \sum_{k=1}^{r}\frac{cut(V_k,\bar{V}_k)}{vol(V_k)} \tag{A.42}$$

The use of these approaches improves the quality of the clustering, as the created *r* partitions are relatively balanced [133]. Nevertheless, these normalisations make these cut problems to become *NP-hard*. Fortunately, spectral graph clustering is a computationally efficient algorithm that solves the relaxed version of those problems and approximates the optimal solution instead. As it is shown below, relaxing the *RatioCut* problem leads to unnormalised spectral clustering – spectral clustering using the matrix **L** – while relaxing the *Ncut* problem leads to normalised spectral clustering – spectral clustering using the matrix $\mathbf{L_N}$. Normalised spectral clustering performs better (see Appendix A.7.5) [71].

A.7.4.1. Approximating RatioCut [71]

The relaxation of the *RatioCut* minimisation problem to partition a set *V* into *r* sets $V_1,\ldots,V_r$ starts by defining *r* indicator vectors $\mathbf{h}_j = (h_{1,j},\ldots,h_{n,j})^T$.

$$h_{i,j} = \begin{cases} \dfrac{1}{\sqrt{|V_j|}} & \text{if } v_i \in V_j \\ 0 & \text{otherwise} \end{cases} \qquad (i = 1,\ldots,n;\ j = 1,\ldots r) \tag{A.43}$$

Then, the matrix $\mathbf{H} \in \mathbb{R}^{n \times r}$ is set to contain those *r* indicator vectors as columns. As detailed in [71], it can be further noticed that

$$\mathbf{h}_i^T \mathbf{L} \mathbf{h}_i = \frac{cut\left(V_i, \bar{V}_i\right)}{\left|V_i\right|}. \tag{A.44}$$

Moreover,

$$\mathbf{h}_i^T \mathbf{L} \mathbf{h}_i = \left(\mathbf{H}^T \mathbf{L} \mathbf{H}\right)_{ii}. \tag{A.45}$$

Thus,

$$RatioCut\left(V_1, V_2, ..., V_r\right) = \sum_{i=1}^{r} \mathbf{h}_i^T \mathbf{L} \mathbf{h}_i = \sum_{i=1}^{r} \left(\mathbf{H}^T \mathbf{L} \mathbf{H}\right)_{ii} = Tr\left(\mathbf{H}^T \mathbf{L} \mathbf{H}\right), \tag{A.46}$$

where $Tr(\cdot)$ denotes the trace of a matrix[3]. Thus, the problem of minimising $RatioCut\left(V_1, V_2, ..., V_r\right)$ can be rewritten as follows

$$\min_{V_1, V_2, ..., V_r} Tr\left(\mathbf{H}^T \mathbf{L} \mathbf{H}\right) \text{ subject to } \mathbf{H}^T \mathbf{H} = \mathbf{I}, \tag{A.47}$$

where **H** is as defined in (A.43). Then, to relax the problem, the entries of the matrix **H** can take arbitrary real values. Thus, the relaxed problem becomes

$$\min_{\mathbf{H} \in \mathbb{R}^{n \times r}} Tr\left(\mathbf{H}^T \mathbf{L} \mathbf{H}\right) \text{ subject to } \mathbf{H}^T \mathbf{H} = \mathbf{I}. \tag{A.48}$$

[3] The trace of an *n*-by-*n* square matrix **A** is defined to be the sum of the elements on the main diagonal.

This is the standard form of a trace minimisation problem, and a version of the Rayleigh-Ritz theorem [134] states that the solution is given by choosing **H** as the matrix which contains the eigenvectors associated with the *r* smallest eigenvalues of **L** as columns. Therefore, it can be noticed that the matrix **H** is in fact the matrix **X** used in the unnormalised spectral clustering algorithm as described in Appendix A.7.3.1. As the problem was relaxed to take arbitrary real values, the solution matrix needs to be re-converted to a discrete partition. As above, the standard way is to use the *k-means* algorithms on the rows of **X**. This obviously leads to the general unnormalized spectral clustering algorithm as presented in Appendix A.7.3.1.

A.7.4.2. Approximating Ncut [71]

A similar procedure can be followed to derive the normalised spectral clustering as a relaxation of minimal *Ncut*. Initially, the *r* indicator vectors $\mathbf{h}_j = \left(h_{1,j},\ldots,h_{n,j}\right)^T$ are defined.

$$h_{i,j} = \begin{cases} \dfrac{1}{\sqrt{vol\left(V_j\right)}} & \text{if } v_i \in V_j \\ 0 & \text{otherwise} \end{cases} \quad (i = 1,\ldots,n;\ j = 1,\ldots r) \tag{A.49}$$

The matrix $\mathbf{H} \in \mathbb{R}^{n\times r}$ is then set to contain those *r* indicator vectors as columns. Observe that $\mathbf{H}^T\mathbf{H} = \mathbf{I}$, $\mathbf{h}_i^T\mathbf{D} = 1$, and $\mathbf{h}_i^T\mathbf{L}\mathbf{h}_i = \dfrac{cut\left(V_i,\bar{V}_i\right)}{vol\left(V_i\right)}$. Thus, the problem of minimising *Ncut* can be written as

$$\min_{V_1,V_2,\ldots,V_r} Tr\left(\mathbf{H}^T\mathbf{L}\mathbf{H}\right) \text{ subject to } \mathbf{H}^T\mathbf{H} = \mathbf{I} \tag{A.50}$$

where **H** is now defined as in (A.49). Then, relaxing the discreteness and substituting $\mathbf{T} = \mathbf{D}^{1/2}\mathbf{H}$, the relaxed problem becomes

$$\min_{\mathbf{T}\in\mathbb{R}^{n\times r}} Tr\left(\mathbf{T}^T\mathbf{D}^{-1/2}\mathbf{L}\mathbf{D}^{-1/2}\mathbf{T}\right) \text{ subject to } \mathbf{T}^T\mathbf{T}=\mathbf{I}. \tag{A.51}$$

Again, this is the standard form of a trace minimisation problem which is solved by the matrix **T** which contains the eigenvectors associated with the *r* smallest eigenvalues of $\mathbf{L_N}$ as columns. This obviously leads to the general normalized spectral clustering algorithm presented in Appendix A.7.3.2.

A.7.5. Which Laplacian Matrix is Better?

A fundamental question related to spectral clustering is the choice of the Laplacian matrix to be used to compute the eigenvectors. When the degree of distribution of the weighted adjacency matrix is regular, the Laplacian matrices are very similar and both work well for clustering [71]. However, the inherent characteristics of the electrical power system commonly produce irregular graphs – graphs where the degree of distribution is not regular [133]. Therefore, the use of the normalised Laplacian matrix $\mathbf{L_N}$ for clustering is more advantageous, particularly for weighted graphs that evolve from power systems [69-74].

Since the normalised spectral clustering minimises the ratio between the boundary of the node set and the volume (minimises the value of the *Ncut* (A.42)), it groups nodes such that the nodes in a cluster are highly connected among themselves (taking edge weights into consideration) but weakly clusters connected to nodes in other. Due to the advantages that the use of the matrix $\mathbf{L_N}$ has over the use of the matrix **L**, the next sections focus on providing the fundamental results for the normalised Laplacian matrix $\mathbf{L_N}$. Indeed, Appendix A.7.7 shows how the use of the matrix $\mathbf{L_N}$ produces partitions with better quality.

A.7.6. Cheeger Inequality

The Cheeger inequality provides the main theoretical justifications for clustering algorithms that use the eigenvectors associated with the first *r* eigenvalues of the matrix $\mathbf{L_N}$ to embed the nodes into $\mathbb{R}^r$, and then apply geometric consideration to the embedding [71, 73]. The Cheeger inequality [73] is used to compare the quality between the approximate solution

(islanding or sectionalising strategy) obtained using spectral graph clustering and the optimal solution that cannot be computed in polynomial time, as this type of clustering problems are *NP-hard* [71, 73].

In order to define the Cheeger inequality, the *expansion* of the subgraph G_k, $k = 1,\ldots,r$, with node set V_k, denoted by $\phi(V_k)$, is defined as follows [71, 73].

$$\phi(V_k) = \frac{bou(V_k)}{vol(V_k)} = \frac{cut(V_k, \bar{V}_k)}{vol(V_k)} \tag{A.52}$$

Then, the quality of an r-partition can be defined as the maximum expansion among the subgraphs, which can be expressed as follows [71, 73].

$$\max_{k=1,\ldots,r} \phi(V_k) \tag{A.53}$$

The best r-partition overall (with respect to the expansion) is the minimum over all possible r-partitions of the graph, which is expressed as follows.

$$\phi_G(r) := \min_{V_1,\ldots,V_r} \max_{k=1,\ldots,r} \phi(V_k) \tag{A.54}$$

This quantity is called the *r-way expansion constant* of the graph G [71, 73]. Note that $\phi_G(r) = 0$ if and only if $\nu_r = 0$. Finding the best r-partition in the graph is generally *NP-hard* [64]. Fortunately, spectral clustering can determine an approximated solution through the use of the eigenvectors associated with the r smallest eigenvalues [133]. In order to measure how close this approximation is to the optimal solution and how adequate this optimal solution is overall, the Cheeger inequality is used. For the case of $r = 2$, the Cheeger inequality is defined as follows [69].

$$\frac{1}{2}\nu_2 \le \phi_G(2) \le \sqrt{2\nu_2} \tag{A.55}$$

This classical inequality has been recently generalised for the arbitrary case $r \ge 2$ following an asymptotic sense as follows [73].

$$\frac{1}{2}\nu_r \le \phi_G(r) \le O(r^2)\sqrt{\nu_r} \tag{A.56}$$

The right-hand side of both inequalities (A.55) and (A.56) are obtained by using spectral clustering with respect to the normalised Laplacian [73]. On the left-hand side, the value $1/2\nu_r$ represents the minimal value of the expansion of any *r*-partition of the graph. Therefore, the smaller ν_r is, the closer the approximate spectral clustering solution is to the optimal one, and the better this optimal solution is overall [71, 73].

A.7.7. Quality of a Partition

Using the concept of expansion of the subgraph (A.52), the quality of the subgraph G_k with node set V_k, denoted by $\eta(V_k)$, is defined in this thesis as follows.

$$\eta(V_k) = 1 - \phi(V_k) = 1 - \frac{cut(V_k, \bar{V}_k)}{vol(V_k)} \tag{A.57}$$

The value of $\eta(V_k)$ varies from zero to one. Since normalised spectral clustering aims to minimise the ratio between the boundary (A.5) and the volume (A.6) of a subgraph [71], the greater the value of $\eta(V_k)$, the better connected the node set V_k is considered to be in terms of clustering (see Example 14). Then, to determine the quality of a cutset, the worst (minimum) value of $\eta(V_k)$ among the node sets (A.58) is used.

$$\min_{k=1,\ldots r}\left(\eta\left(V_k\right)\right) \tag{A.58}$$

As detailed in the thesis, the graph partitioning problem can then be defined, in many cases, as finding the maximum of the worst quality as follows.

$$\max_{V_1,\ldots,V_r}\min_{k=1,\ldots,r}\left(\eta\left(V_k\right)\right) \tag{A.59}$$

Example 14: This example aims to demonstrate the improvements, in terms of the quality of the results, achieved with the use of the normalised Laplacian matrix $\mathbf{L_N}$. Consider the subgraphs shown in Figure A.4 and Figure A.5. These two partitions correspond to the solution of the normalised *Ncut* (A.42) and *RatioCut* (A.41) approaches, respectively. Table A.7 summarises the quality of these partitions. As noted, the best partition is obtained when the IEEE 9-bus test system is separated across the edges $e_{4,5}$ and $e_{8,9}$. In other words, the best partition (higher quality) is obtained using the normalised Laplacian matrix of the graph *G*. By comparing the quality of the results obtained using spectral clustering with the theoretical lower bound $\nu_2/2$: 0.0714, it can be observed that the optimal bipartition (which cannot be found in general in polynomial time) has a quality of at least 92.86%, in contrast to the approximation 88.40%, which was found avoiding an exponential search.

Table A.7: Comparison of the quality of two partitions for the IEEE-9 bus test system

	Nose set	Boundary (MW)	Volume (MW)	Quality (%)
Partition using $\mathbf{L_N}$ in Figure A.**4**	V_1	65.12	717.12	90.91
	V_2	65.12	561.44	**88.40**
Partition using **L** in Figure A.**5**	V_1	54.86	932.04	94.11
	V_2	54.86	346.52	84.17

A.7.8. Number of Clusters

The selection of the *r* number of subgraphs to be created is a general challenge in spectral clustering [71]. Fortunately, certain power system problems define this number based on system response or inherent characteristics of the network. For example, in the islanding

problem, the number of islands to create depends on the number of coherent groups of generators created after a disturbance [43]. Moreover, the number of islands for PPSR are commonly defined based on the number of blackstart units or system operators criteria [43].

In the cases when the number of clusters in uncertain, spectral clustering provides a theoretical formulation to determine the number of groups. Spectral clustering can utilise the eigengap heuristic [71] to choose the number *r* such that the eigenvalues $\nu_1,\ldots,\nu_r$ are very small, nevertheless ν_{r+1} is relatively large (see Example 15) [133]. In order to visualise the number of islands to be created, the concept of eigenvalue difference relative to their size, which is given by (A.60), is used to determine the value of *r*.

$$\varsigma_k = \frac{\nu_{k+1} - \nu_k}{\nu_k},\ (k \geq 2) \tag{A.60}$$

Example 15: The eigenvalues of the normalised Laplacian matrix shown in Table A.6 are used to compute the eigengaps (Figure A.9(a)) and their relative eigengaps (Figure A.9(b)). The graph accepts an adequate partition into three islands. However, to easily illustrate the next concepts, the remainder of this chapter considers only the case of two islands.

A.7.9. Spectral Embedding

Spectral embedding refers to as the representation of the graph *G* in Euclidean space using the eigenvectors associated with the matrices **L** or $\mathbf{L_N}$ [71]. As previously stated, this thesis uses the normalised Laplacian matrix $\mathbf{L_N}$ as this matrix generally performs better in the irregular graphs emerging from power system problems (see Appendix A.7.5). Therefore, the embedding of *G* is implemented using the eigenvectors $\boldsymbol{\psi}_1,\ldots,\boldsymbol{\psi}_r$. Ordering these eigenvectors as columns creates a matrix $\mathbf{X} \in \mathbb{R}^{n\times r}$ with rows $\mathbf{x}_i$, $i = 1,\ldots,n$. The vector $\mathbf{x}_i$ represents the coordinates of the node $v_i \in V$ in the *r*-dimensional Euclidean space $\mathbb{R}^r$.

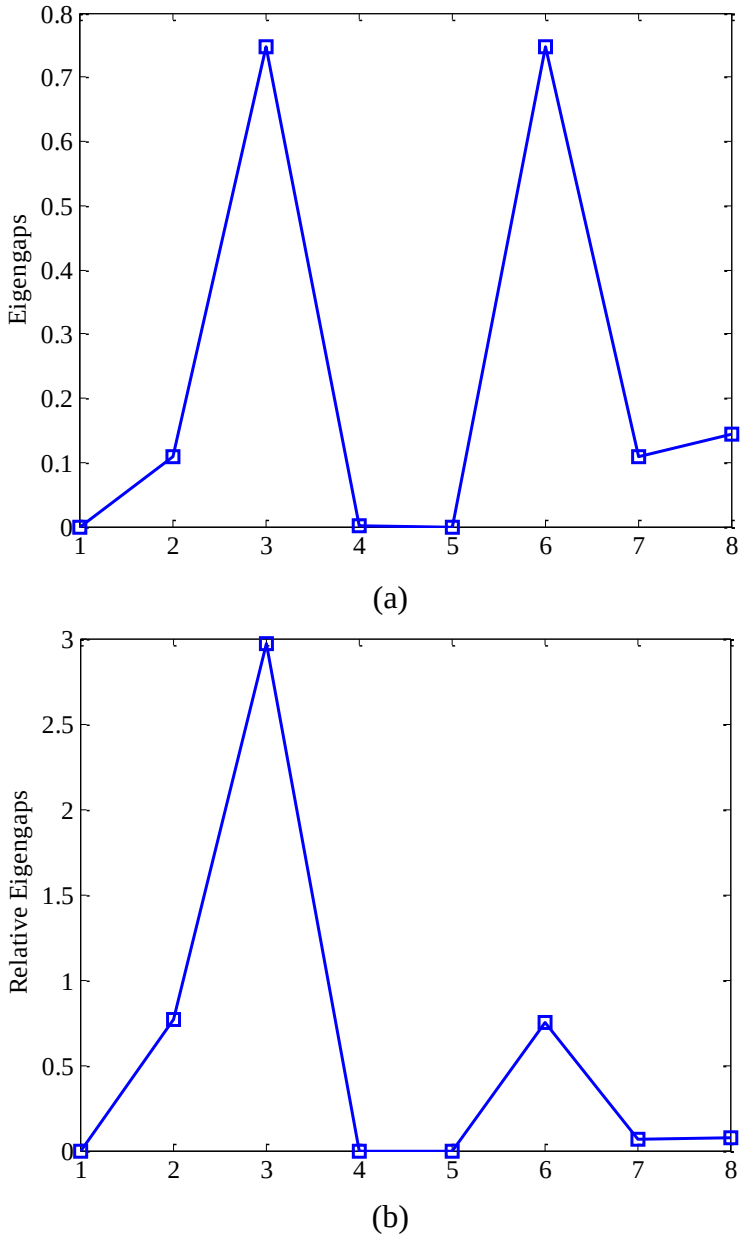

Figure A.9: (a) Eigengaps and (b) relative eigengaps between eigenvalues of the matrix $\mathbf{L_N}$ of the IEEE 9-bus test system

It has been demonstrated in [70, 73] that in order to improve the quality of the partition, the vectors $\mathbf{x}_i$ must be normalised to have length one before applying any clustering technique. Consequently, the normalised vectors are defined as follows.

$$\mathbf{y}_i := \frac{\mathbf{x}_i}{\|\mathbf{x}_i\|},\ i = 1,\ldots,n. \tag{A.61}$$

The normalisation performed in (A.61) projects the vectors $\mathbf{x}_i$ on the unit (r–1)-dimensional sphere $\mathbb{S}^{r-1} = \left\{ \mathbf{y}_i \in \mathbb{R}^r \text{ such that } \|\mathbf{y}_i\| = 1 \right\}$ and creates the matrix $\mathbf{Y} \in \mathbb{R}^{n \times r}$ with rows $\mathbf{y}_i$. Furthermore, it allows the visualisation of the clusters to be created in several cases (see Figure A.10(b) for an example). After computing the spectral embedding, the nodes $v_i \in V$ can be seen as data-points $\mathbf{x}_i$ in Euclidean space $\mathbb{R}^r$, or $\mathbf{y}_i$ on $\mathbb{S}^{r-1}$.

Example 16: The vectors $\mathbf{x}_i$ are plotted in (Figure A.10(a)) for the spectral embedding of the IEEE 9-bus test system when $r = 2$. The vectors $\mathbf{x}_i$ are then normalised to compute the vectors $\mathbf{y}_i$, which are represented on the unit circle shown in Figure A.10(b). The numbers on the diagrams correspond to node numbers. The normalisation of the eigenvectors $\mathbf{x}_i$ helps, in this case, visualise two clusters, i.e.,, $V_1 = \{v_2, v_5, v_7, v_8\}$ and $V_2 = \{v_1, v_3, v_4, v_6, v_9\}$. Comparing this solution with the best solution shown in Table A.7 and depicted in Figure A.4, it can be noted that normalised spectral clustering performs better. In other words, the normalised spectral clustering algorithm minimises the ratio between the cut and the volume, which is equivalent to create partitions with better quality index (A.57).

A.7.10. Similarity and Dissimilarity Measures

The spectral embedding of the graph *G* into Euclidean space $\mathbb{R}^r$ induces a new spectral distance between data points, which is also called a distance measure in Euclidean space [71]. Considering two data points $\mathbf{x}_i \in \mathbb{R}^r$ and $\mathbf{x}_j \in \mathbb{R}^r$, the spectral distance is used to create a similarity matrix **S** such that the *ij*-entry of **S**, denoted by $s(\mathbf{x}_i, \mathbf{x}_j)$, is equal to the spectral distance between these two points. Several methods to measure the spectral distance between points exist. The most common distance measures, as well as other measures preferred for solving power system problems due to their accuracy and efficiency are described below.

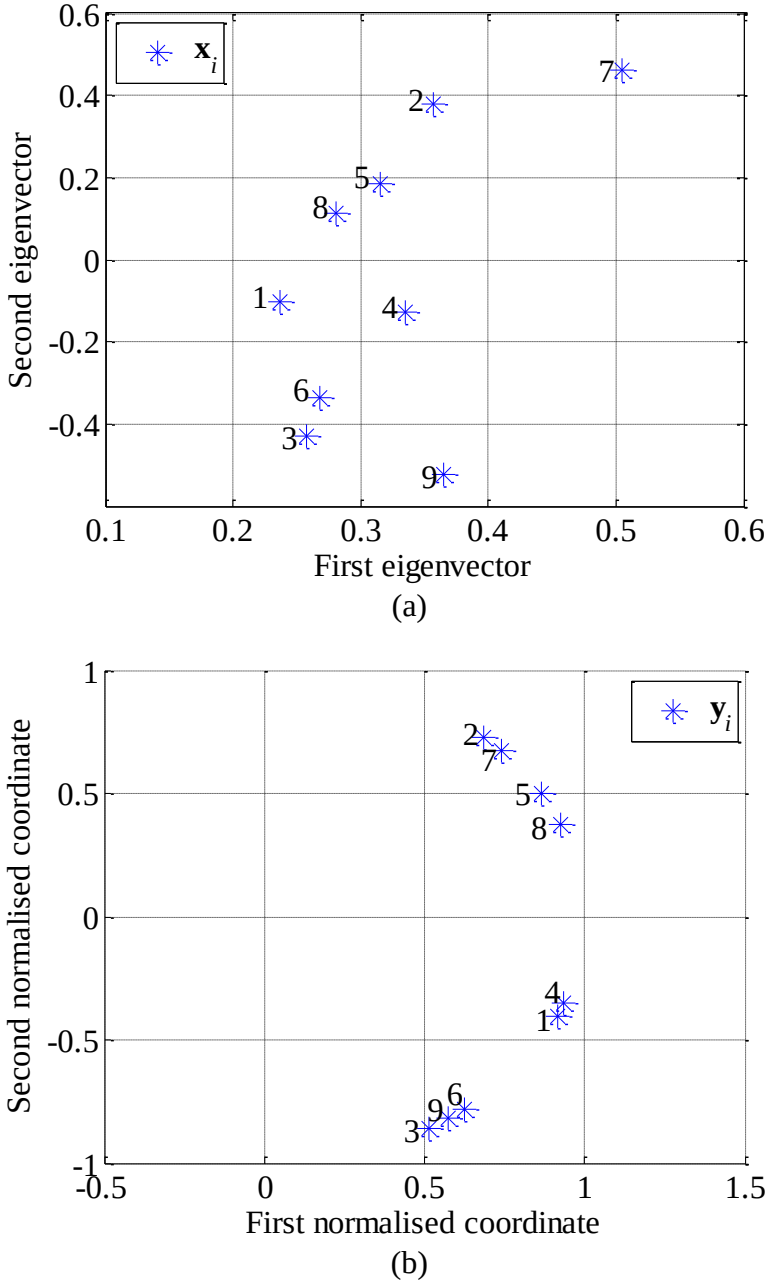

Figure A.10: Spectral embedding of the graph of the IEEE 9-bus test system (a) into Euclidean space $\mathbb{R}^2$ (b) onto the unit circle $\mathbb{S}^1$

A.7.10.1. Euclidean Distance

The Euclidean distance is the ordinary distance between two points $\mathbf{x}_i \in \mathbb{R}^r$ and $\mathbf{x}_j \in \mathbb{R}^r$ in Euclidean space possible to be measured with a ruler. The Euclidean distance between these two points can be calculated as in (A.62) [71].

$$s\left(\mathbf{x}_i,\mathbf{x}_j\right)=\sqrt{\sum_{k=1}^{r}\left(\mathbf{x}_i^k-\mathbf{x}_j^k\right)^2} \tag{A.62}$$

A.7.10.2. The Cosine Similarity

The cosine similarity measure can also be used to determine the similarity between vectors in Euclidean space. If $\mathbf{x}_i \in \mathbb{R}^r$ and $\mathbf{x}_j \in \mathbb{R}^r$ are represented in the *r*-dimensional Euclidean space, then, the cosine similarity between these points is given by (A.63) [106]

$$s\left(\mathbf{x}_i,\mathbf{x}_j\right)=\frac{\left\langle \mathbf{x}_i,\mathbf{x}_j \right\rangle}{\left\|\mathbf{x}_i\right\|\left\|\mathbf{x}_j\right\|}, \tag{A.63}$$

where $\left\langle \cdot,\cdot \right\rangle$ denotes the inner product and $\left\|\cdot\right\|$ denotes a vector norm.

A.7.10.3. Spherical Distance

The spherical distance measure is induced after projecting the vectors onto the unit sphere $\mathbb{S}^{r-1}$ [73, 117]. The spherical distance between two data points $\mathbf{y}_i \in \mathbb{S}^{r-1}$ and $\mathbf{y}_j \in \mathbb{S}^{r-1}$ can be approximated numerically by dividing the arc along the surface of the unit sphere into very small straight lines, and adding up the length of all of these small segments [117].

Although the spherical distance is commonly approximated [117], when *r* = 2 the spherical distance is the arc along the circumference of the unit circle (see Figure A.11 for an example). Therefore, the spherical distance for *r* = 2 can be calculated as in (A.64).

$$s\left(\mathbf{y}_i,\mathbf{y}_j\right)=\theta=\arccos\left(2-\frac{\sum_{k=1}^{2}\left(\mathbf{y}_i^k-\mathbf{y}_j^k\right)^2}{2}\right), \text{ if } r=2 \tag{A.64}$$

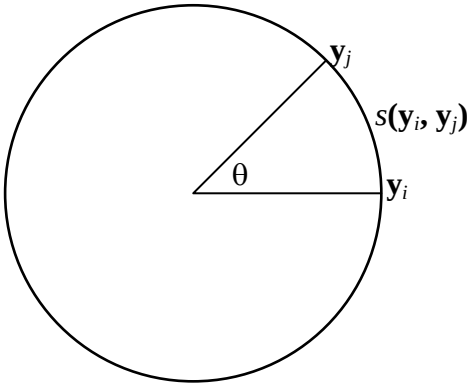

Figure A.11: Spherical distance on the unit circle

A direct calculation of the spherical distance can also be obtained when $r = 3$, as this value corresponds to the distance between points on the unit 2-dimensional sphere. As shown in (A.65), trigonometric functions can be used to find the spherical distance when $r = 3$ [117].

$$s\left(\mathbf{y}_i, \mathbf{y}_j\right) = \tan^{-1}\left(\frac{\left\|\mathbf{y}_i \times \mathbf{y}_j\right\|}{\mathbf{y}_i \cdot \mathbf{y}_j}\right), \text{ if } r = 3 \tag{A.65}$$

A.7.11. K-means Algorithm

The conventional *k*-means algorithm is one of the most commonly used clustering algorithms to partition data in Euclidean space. In this well-established algorithm, the number of clusters *k* is fixed [71]. Then, given the set of data points $\mathbf{X} = \left(\mathbf{x}_1, \mathbf{x}_2, \ldots, \mathbf{x}_n\right)^T$ in the *k*-dimensional Euclidean space $\mathbb{R}^k$, *k-means* aims to partition the points into *k* sets $V_1, \ldots, V_k$ so that the squared error function given by (A.66) is minimised.

$$error = \sum_{i=1}^{k} \sum_{\mathbf{x} \in V_i} s\left(\mathbf{x}, \boldsymbol{\mu}\left(V_i\right)\right) \tag{A.66}$$

In (A.66), $\boldsymbol{\mu}\left(V_i\right)$ is the centroid of the cluster V_i, and $s\left(\mathbf{x}, \boldsymbol{\mu}\left(V_i\right)\right)$ denotes the distance between **x** and the centre of the cluster.

The use of the *k-means* algorithm is sometimes not required, as the clustering structure emerges after the spectral embedding of the data points in Euclidean space, especially after the embedding onto the unit sphere. For example, Figure A.10 clearly shows that the clusters to be created are $V_1 = \{v_2, v_5, v_7, v_8\}$ and $V_2 = \{v_1, v_3, v_4, v_6, v_9\}$.

A.7.12. Voronoi Diagrams

A *Voronoi* diagram (*Voronoi* cell) is a region in Euclidean space created by a centroid and the points closer to that centroid than to any other [118]. Voronoi cells are used to represent the division of a space into a given number of regions. Figure A.12 shows two Voronoi diagrams for the points embedded in the unit circle in the case of the IEEE 9-bus system.

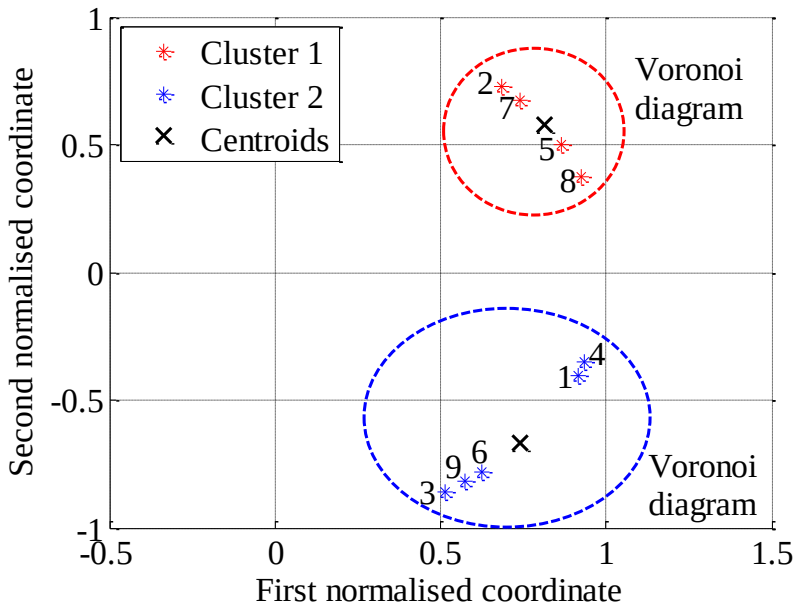

Figure A.12: Voronoi representation of the clusters

A.7.13. Constrained Spectral Clustering

Constrained spectral clustering is an extension of spectral clustering which allows two main types of constraints – Must-Link (ML-) and Cannot-Link (CL-) constraints – to be used [72, 74]. While a ML-constraint between two nodes indicates that the pair of nodes must be clustered together, a CL-constraint specifies that the pair of nodes cannot be assigned into the same cluster [72, 74].

There are two means of including ML- and CL-constraints. The first one is the modification of the weighted adjacency matrix; and the second one is the use a subspace trick [74]. These two approaches are briefly described below.

A.7.13.1. Modifying the Weighted Adjacency Matrix

When two nodes are required to be grouped in the same cluster, the weighted adjacency matrix **W** can be modified, and the edge weight between these two nodes can be modified to the greatest value in the matrix **W** [74]. Changing the edge weight of the constrained edge to the highest value significantly increases the possibility of the edge to be excluded from the cutset, and thus, cluster the nodes in the same group [72, 74]. This approach is used in Chapters 6 and 8 to exclude lines from the islanding and sectionalising strategies.

A.7.13.2. Subspace Trick

The subspace trick is used to map all the points belonging to the same class into a single point [72]. Thus, when performing clustering, the points which should be included in the same cluster are grouped together, whereas the points which should not be included in the same cluster are grouped separately. This approach is used in Chapter 8 to ensure that the machines within each cranking group are clustered together for preserving the integrity of the cranking groups during PPSR.

A.8. Dominating Set

A dominating set in a graph G is a set of nodes $S \subset V$ such that every node $v_i \in V$ is a neighbour of at least one node $v_j \in S$. In other words, a set S is called a dominating set if every node $v_i \in V$ is either an element of S or is adjacent to an element of S. The domination number $\gamma(G)$ of a graph equals the cardinality of a set S. Therefore, the Minimum Dominating Set (MDS) problem is to find the set $S \subset V$ such that $\gamma(G)$ is minimum [146]. The dominating set S in the graph shown in Figure A.2 is $S = \{v_4, v_7, v_9\}$. The concept of a dominating set is used in Chapter 3 to determine optimal PMU locations.

A.9. Tree Search Algorithm

Tree search algorithms, or tree traversal algorithms, refer to the process of searching in the graph through the progression of visiting nodes exactly once [106]. Such search is classified by the order in which the nodes are visited. These algorithms are used in unweighted graphs and utilise the spanning tree concept of graph [113]. A *spanning tree* is a connected graph using all nodes in which there are no cycles. Tree search algorithms are effective since they will always find the optimal solution, if such a solution exists [106]. However, the complexity of these algorithms is commonly bounded to applications with a reduced number of nodes or they must be used in offline applications, e.g., optimal PMU placements. Tree search algorithms are commonly related to Depth-First Search (DFS) algorithms and Breath-First Search (BFS) algorithms [106]. While the former may be used to find the cut nodes of a graph, the latter may be used to find the distances in a graph.

A.9.1. Depth-First Search Algorithm

Given a graph G with the corresponding adjacency matrix $\mathbf{A}$, the DFS algorithm creates a tree T, such that the node to be added to the tree T is a neighbour of the most recently included note to the tree, and it is not yet in T (see Example 17) [106]. A DFS algorithm initially defines a root node. It then scans the adjacency list of the most recently added node v_i for a neighbour not in T. If such neighbour exists, the algorithm then adds it to T. If not, the algorithm backtracks to the node which was added to T just before v_i and examines its neighbours. This step is repeated until all the nodes are visited. The resulting spanning tree is called a DFS-tree.

Example 17: Figure A.13 shows the DFS-tree of the graph shown in Figure A.2. The node v_1 is defined as the root. As the node v_4 is the neighbour of v_1, the DFS algorithm then adds the former to the tree T. It then scans the neighbours of v_4 and randomly selects v_5 (v_6 could have also been selected) as the next node to be added to the tree. The process is repeated until v_2 is reached. As the node v_2 has all its neighbours (v_7) in the tree T, the algorithm backtracks to v_7, and as node v_8 is neighbour of v_7, and it has not yet been added to the tree,

the DFS algorithm adds the node v_8 to the tree. The process is repeated and the final DFS-tree of the graph shown in Figure A.2 is illustrated in Figure A.13.

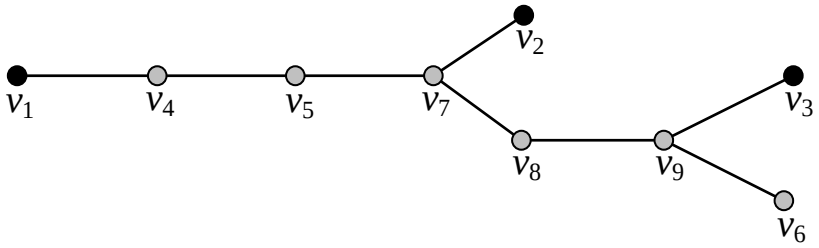

Figure A.13: DFS tree of the graph of the IEEE 9-bus test system

A.9.2. Breath-First Search Algorithm

A BFS algorithm follows a similar analogy of the DFS algorithms. However, the BFS algorithm selects a node to be added to *T* depending on the order in which the nodes already in the tree *T* were added. In other words, a BFS algorithm is a tree-search algorithm in which the adjacency lists of the vertices of *T* are considered on a first-come first-served basis – in increasing order of their time of incorporation into *T* (see Example 18) [106].

Example 18: Figure A.14 illustrates the final BFS-tree of the graph shown in Figure A.2. The node v_1 is defined as the root, and as v_4 is the only neighbour, and is then added to the BFS-tree. The neighbour nodes of v_4 (v_5 and v_6) are then added. The process is repeated until all the nodes are added to the tree.

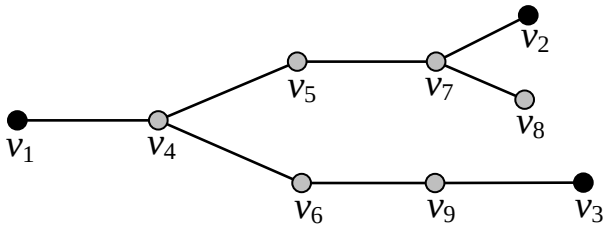

Figure A.14: BFS tree of the graph of the IEEE 9-bus test system

A.10. Test Networks and Their Graph

Throughout this thesis three standard test networks are used. All system details including line parameters, standard loading, and dynamic machine data is included in Appendix A. In all cases, simulations are performed in MATLAB [145], using modified PSAT functions [147] for the dynamic simulations, and modified MATPOWER functions [148] where only load flows are required. All times quoted throughout this thesis are based upon simulations performed on a PC with 2.93 GHz double core CPU and 4 GB RAM.

A.10.1. IEEE 9-Bus Test System

A small three-machine, nine-bus test system is introduced in [110] for the study of small dynamic systems. This system including the data shown in the Appendix A.1 is used throughout this thesis to initially test and explain the proposed methodologies in detail. The single line diagram of the system is shown in Figure A.1, and its undirected graph representation is illustrated in Figure A.2. A directed graph representation of this system is presented in Figure A.6.

A.10.2. New England 39-Bus Test System

A larger ten-machine, thirty-nine-bus test system is presented in [111] to study the dynamic behaviour and perform transient stability analysis of a larger system. This system including the data shown in the Appendix A2 is also used throughout this thesis to investigate the applications of graph theory to ICI for blackout prevention and system sectionalising for PPSR. The single line diagram of the network is shown in Figure A.15, and its undirected graph representation is illustrated in Figure A.16.

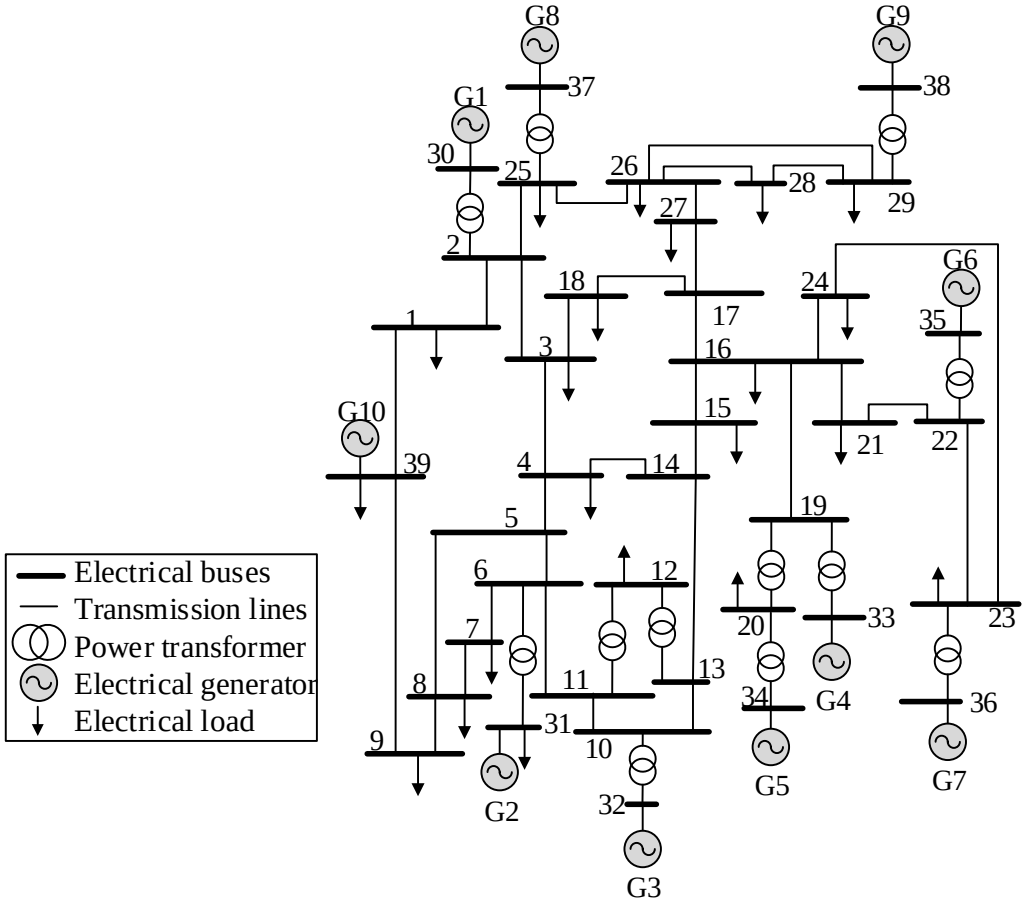

Figure A.15: Single line diagram of the New England 39-bus test system

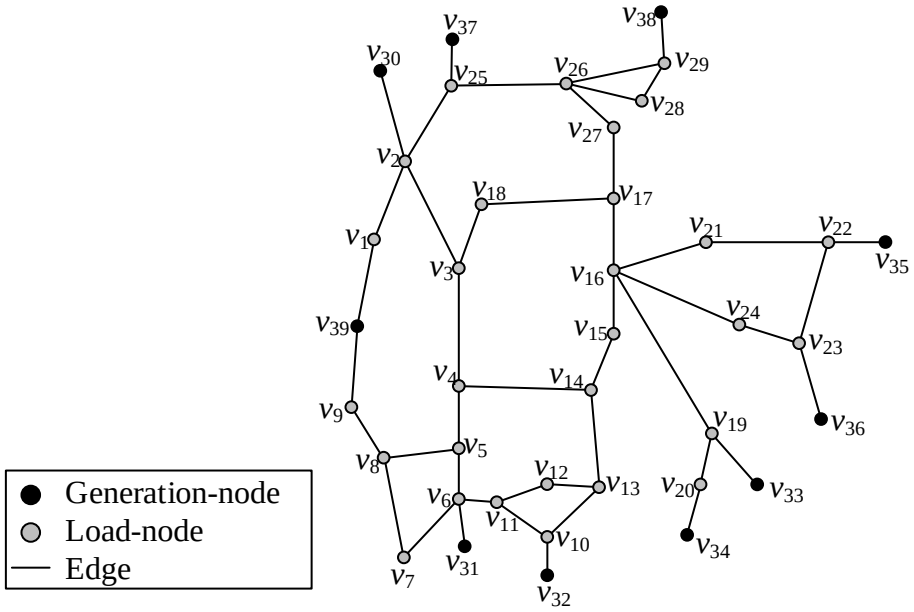

Figure A.16: Graph representation of the New England 39-bus test system

A.10.3. IEEE 118-Bus Test System

A much larger nineteen-machine, one-hundred-eighteen-bus test system is introduced in [149] to study the steady-state behaviour of a large system. This system is extended in [46] with the dynamic data of the classical 2nd order machine model to analyse the dynamic response of a large network. This system including the data shown in the Appendix A.3 is used throughout this thesis to demonstrate the applicability of the introduced methodologies for blackout prevention and power system restoration in large-scale power systems. The single line diagram of the network is shown in Figure A.17, and its undirected graph representation is illustrated in Figure A.18.

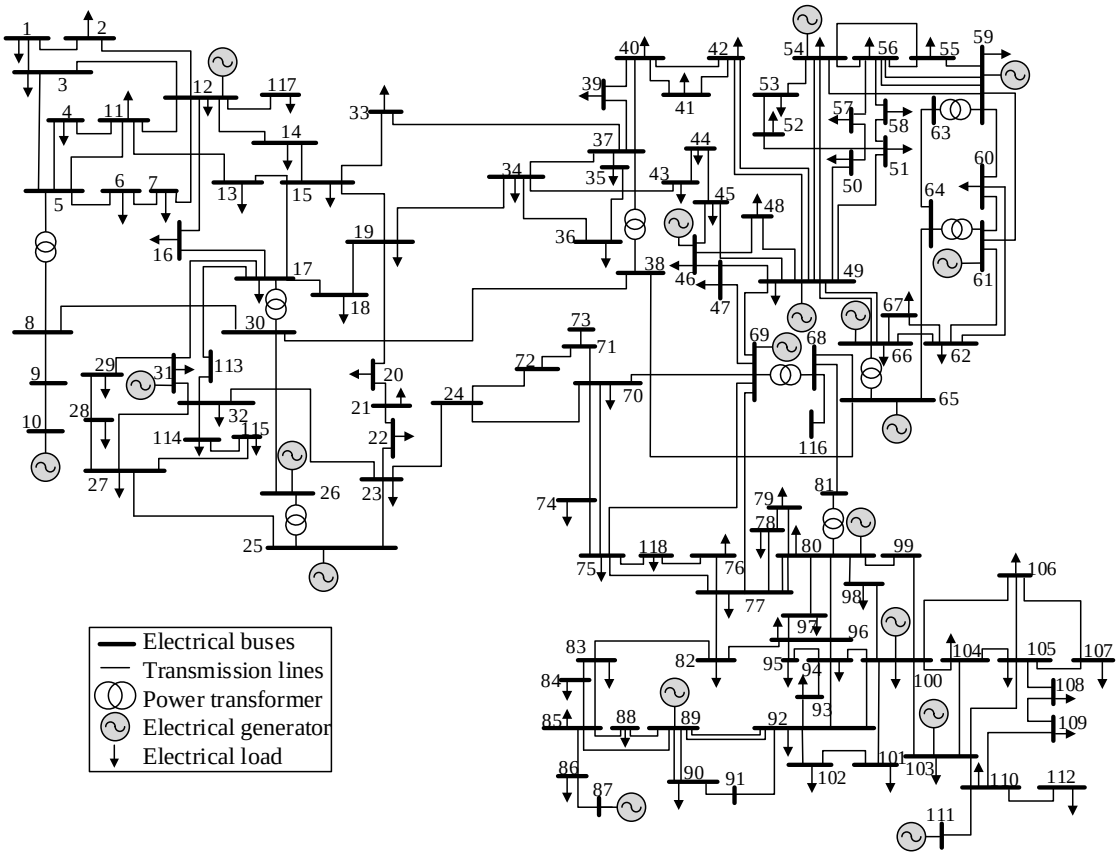

Figure A.17: Single line diagram of the IEEE 118-bus test system with 19 generators

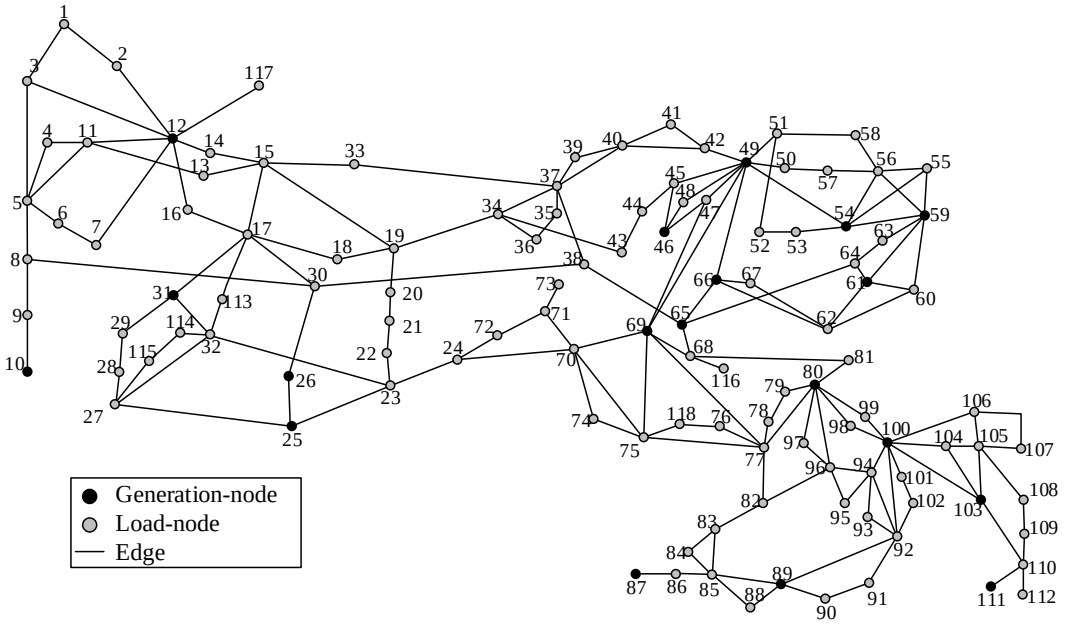

Figure A.18: Graph representation of the IEEE 118-bus test system

Appendix B. Network Data

This appendix provides the data required in order to perform static and dynamic studies on the test systems used throughout this thesis. In all cases a system base of 100 MVA is used.

B.1. IEEE 9-Bus Test System

All original data is adopted from [110]. The single line diagram is shown in Figure A.1.

B.1.1. Line Impedances

The line impedance data for the network is presented in Table B.1, including transformer off-nominal turns ratio (*TAP*) where applicable.

Table B.1: Line data for the IEEE 9-bus test system

From Bus	*To Bus*	*R (pu)*	*X (pu)*	*B (pu)*	*TAP*
1	4	0.0000	0.0576	0.0000	1
4	5	0.0100	0.0850	0.1760	0
5	7	0.0320	0.1610	0.3060	0
2	7	0.0000	0.0625	0.0000	1
7	8	0.0085	0.0720	0.1490	0
8	9	0.0119	0.1008	0.2090	0
3	9	0.0000	0.0586	0.0000	1
6	9	0.0390	0.1700	0.3580	0
4	6	0.0170	0.0920	0.1580	0

B.1.2. Load Flow Data

Data required to complete load flow is included in Table B.2, G1 connected to bus 1 is the slack bus.

Table B.2: Load flow data for the IEEE 9-bus test system

Bus	*V (pu)*	*Θ (deg)*	P_G *(pu)*	P_L *(pu)*	Q_L *(pu)*
1	1.040	0	-	-	-
2	1.025	-	163.00	-	-
3	1.026	-	85.00	-	-

4	-	-	-	-	-
5	-	-	-	125	50
6	-	-	-	90	30
7	-	-	-	-	-
8	-	-	-	100	35
9	-	-	-	-	-

B.1.3. Generator Dynamic Data

The generator dynamic data presented is given in Table B.3.

Table B.3: Generator dynamic data for the IEEE 9-bus test system

Gen	*Bus*	*M (s)*	*x'd (pu)*
G1	1	47.28	0.0608
G2	2	12.8	0.1198
G3	3	6.02	0.1813

B.2. New England 39-Bus Test System

All original data is adopted from [111]. The single line diagram is shown in Figure A.15.

B.2.1. Line Impedances

The line impedance data for the network is presented in Table B.4, including transformer off-nominal turns ratio (*TAP*) where applicable.

Table B.4: Line data for the New England 39-bus test system

From Bus	*To Bus*	*R (pu)*	*X (pu)*	*B (pu)*	*TAP*
1	2	0.0035	0.0411	0.6987	1.0000
1	39	0.0010	0.0250	0.7500	1.0000
2	3	0.0013	0.0151	0.2572	1.0000
2	25	0.0070	0.0086	0.1460	1.0000
2	30	0.0000	0.0181	0.0000	1.0250
3	4	0.0013	0.0213	0.2214	1.0000
3	18	0.0011	0.0133	0.2138	1.0000
4	5	0.0008	0.0128	0.1342	1.0000
4	14	0.0008	0.0129	0.1382	1.0000
5	8	0.0008	0.0112	0.1476	1.0000

6	5	0.0002	0.0026	0.0434	1.0000
6	7	0.0006	0.0092	0.1130	1.0000
6	11	0.0007	0.0082	0.1389	1.0000
6	31	0.0000	0.0250	0.0000	1.0700
7	8	0.0004	0.0046	0.0780	1.0000
8	9	0.0023	0.0363	0.3804	1.0000
9	39	0.0010	0.0250	1.2000	1.0000
10	11	0.0004	0.0043	0.0729	1.0000
10	13	0.0004	0.0043	0.0729	1.0000
10	32	0.0000	0.0200	0.0000	1.0700
12	11	0.0016	0.0435	0.0000	1.0060
12	13	0.0016	0.0435	0.0000	1.0060
13	14	0.0009	0.0101	0.1723	1.0000
14	15	0.0018	0.0217	0.3660	1.0000
15	16	0.0009	0.0094	0.1710	1.0000
16	17	0.0007	0.0089	0.1342	1.0000
16	19	0.0016	0.0195	0.3040	1.0000
16	21	0.0008	0.0135	0.2548	1.0000
16	24	0.0003	0.0059	0.0680	1.0000
17	18	0.0007	0.0082	0.1319	1.0000
17	27	0.0013	0.0173	0.3216	1.0000
19	33	0.0007	0.0142	0.0000	1.0700
19	20	0.0007	0.0138	0.0000	1.0600
20	34	0.0009	0.0180	0.0000	1.0090
21	22	0.0008	0.0140	0.2565	1.0000
22	23	0.0006	0.0096	0.1846	1.0000
22	35	0.0000	0.0143	0.0000	1.0250
23	24	0.0022	0.0350	0.3610	1.0000
23	36	0.0005	0.0272	0.0000	1.0000
25	26	0.0032	0.0323	0.5130	1.0000
25	37	0.0006	0.0232	0.0000	1.0250
26	27	0.0014	0.0147	0.2396	1.0000
26	28	0.0043	0.0474	0.7802	1.0000
26	29	0.0057	0.0625	1.0290	1.0000
28	29	0.0014	0.0151	0.2490	1.0000
29	38	0.0008	0.0156	0.0000	1.0250

B.2.2. Load Flow Data

Data required to complete load flow is included in Table B.5, G2 connected to bus 31 is the slack.

Table B.5: Load flow data for the New England 39-bus test system

Bus	*V (pu)*	*Θ (deg)*	P_G *(pu)*	P_L *(pu)*	Q_L *(pu)*
1	-	-	-	0.976	0.442
2	-	-	-	-	-
3	-	-	-	3.220	0.024
4	-	-	-	5.000	1.840
5	-	-	-	-	-
6	-	-	-	-	-
7	-	-	-	2.338	0.840
8	-	-	-	5.220	1.760
9	-	-	-	0.065	-0.666
10	-	-	-	-	-
11	-	-	-	-	-
12	-	-	-	0.085	0.880
13	-	-	-	-	-
14	-	-	-	-	-
15	-	-	-	3.200	1.530
16	-	-	-	3.290	0.323
17	-	-	-	-	-
18	-	-	-	1.580	0.300
19	-	-	-	-	-
20	-	-	-	6.280	1.030
21	-	-	-	2.740	1.150
22	-	-	-	-	-
23	-	-	-	2.475	0.846
24	-	-	-	3.086	-0.922
25	-	-	-	2.240	0.472
26	-	-	-	1.390	0.170
27	-	-	-	2.810	0.755
28	-	-	-	2.060	0.276
29	-	-	-	2.835	0.269
30	1.0475	-	2.500	-	-
31	0.9820	0	-	0.092	0.046
32	0.9831	-	6.500	-	-
33	0.9972	-	6.320	-	-
34	1.0123	-	5.080	-	-
35	1.0493	-	6.500	-	-
36	1.0635	-	5.600	-	-
37	1.0278	-	5.400	-	-
38	1.0265	-	8.300	-	-
39	1.0300	-	10.000	11.040	2.500

B.2.3. Generator Dynamic Data

The generator dynamic data presented is given in Table B.6.

Table B.6: Generator dynamic data for the New England 39-bus test system

Gen	*Bus*	*M (s)*	*x'd (pu)*
G1	30	84.0	0.0310
G2	31	60.6	0.0697
G3	32	70.6	0.0531
G4	33	57.2	0.0436
G5	34	52.0	0.1320
G6	35	69.6	0.0500
G7	36	52.8	0.0490
G8	37	48.6	0.0570
G9	38	69.0	0.0570
G10	39	1000.0	0.0060

B.3. IEEE 118-Bus Test System

All original data is adopted from [148]. The single line diagram is shown in Figure A.17.

B.3.1. Line Impedances

The line impedance data for the network is presented in Table B.7, including transformer off-nominal turns ratio (*TAP*) where applicable.

Table B.7: Line data for the IEEE 118-bus test system

From Bus	*To Bus*	*R (pu)*	*X (pu)*	*B (pu)*	*TAP*
1	2	0.03030	0.09990	0.02540	0.000
1	3	0.01290	0.04240	0.01082	0.000
4	5	0.00176	0.00798	0.00210	0.000
3	5	0.02410	0.10800	0.02840	0.000
5	6	0.01190	0.05400	0.01426	0.000
6	7	0.00459	0.02080	0.00550	0.000
8	9	0.00244	0.03050	1.16200	0.000
8	5	0.00000	0.02670	0.00000	0.985
9	10	0.00258	0.03220	1.23000	0.000
4	11	0.02090	0.06880	0.01748	0.000

5	11	0.02030	0.06820	0.01738	0.000
11	12	0.00595	0.01960	0.00502	0.000
2	12	0.01870	0.06160	0.01572	0.000
3	12	0.04840	0.16000	0.04060	0.000
7	12	0.00862	0.03400	0.00874	0.000
11	13	0.02225	0.07310	0.01876	0.000
12	14	0.02150	0.07070	0.01816	0.000
13	15	0.07440	0.24440	0.06268	0.000
14	15	0.05950	0.19500	0.05020	0.000
12	16	0.02120	0.08340	0.02140	0.000
15	17	0.01320	0.04370	0.04440	0.000
16	17	0.04540	0.18010	0.04660	0.000
17	18	0.01230	0.05050	0.01298	0.000
18	19	0.01119	0.04930	0.01142	0.000
19	20	0.02520	0.11700	0.02980	0.000
15	19	0.01200	0.03940	0.01010	0.000
20	21	0.01830	0.08490	0.02160	0.000
21	22	0.02090	0.09700	0.02460	0.000
22	23	0.03420	0.15900	0.04040	0.000
23	24	0.01350	0.04920	0.04980	0.000
23	25	0.01560	0.08000	0.08640	0.000
26	25	0.00000	0.03820	0.00000	0.960
25	27	0.03180	0.16300	0.17640	0.000
27	28	0.01913	0.08550	0.02160	0.000
28	29	0.02370	0.09430	0.02380	0.000
30	17	0.00000	0.03880	0.00000	0.960
8	30	0.00431	0.05040	0.51400	0.000
26	30	0.00799	0.08600	0.90800	0.000
17	31	0.04740	0.15630	0.03990	0.000
29	31	0.01080	0.03310	0.00830	0.000
23	32	0.03170	0.11530	0.11730	0.000
31	32	0.02980	0.09850	0.02510	0.000
27	32	0.02290	0.07550	0.01926	0.000
15	33	0.03800	0.12440	0.03194	0.000
19	34	0.07520	0.24700	0.06320	0.000
35	36	0.00224	0.01020	0.00268	0.000
35	37	0.01100	0.04970	0.01318	0.000
33	37	0.04150	0.14200	0.03660	0.000
34	36	0.00871	0.02680	0.00568	0.000
34	37	0.00256	0.00940	0.00984	0.000

38	37	0.00000	0.03750	0.00000	0.935
37	39	0.03210	0.10600	0.02700	0.000
37	40	0.05930	0.16800	0.04200	0.000
30	38	0.00464	0.05400	0.42200	0.000
39	40	0.01840	0.06050	0.01552	0.000
40	41	0.01450	0.04870	0.01222	0.000
40	42	0.05550	0.18300	0.04660	0.000
41	42	0.04100	0.13500	0.03440	0.000
43	44	0.06080	0.24540	0.06068	0.000
34	43	0.04130	0.16810	0.04226	0.000
44	45	0.02240	0.09010	0.02240	0.000
45	46	0.04000	0.13560	0.03320	0.000
46	47	0.03800	0.12700	0.03160	0.000
46	48	0.06010	0.18900	0.04720	0.000
47	49	0.01910	0.06250	0.01604	0.000
42	49	0.07150	0.32300	0.08600	0.000
42	49	0.07150	0.32300	0.08600	0.000
45	49	0.06840	0.18600	0.04440	0.000
48	49	0.01790	0.05050	0.01258	0.000
49	50	0.02670	0.07520	0.01874	0.000
49	51	0.04860	0.13700	0.03420	0.000
51	52	0.02030	0.05880	0.01396	0.000
52	53	0.04050	0.16350	0.04058	0.000
53	54	0.02630	0.12200	0.03100	0.000
49	54	0.07300	0.28900	0.07380	0.000
49	54	0.08690	0.29100	0.07300	0.000
54	55	0.01690	0.07070	0.02020	0.000
54	56	0.00275	0.00955	0.00732	0.000
55	56	0.00488	0.01510	0.00374	0.000
56	57	0.03430	0.09660	0.02420	0.000
50	57	0.04740	0.13400	0.03320	0.000
56	58	0.03430	0.09660	0.02420	0.000
51	58	0.02550	0.07190	0.01788	0.000
54	59	0.05030	0.22930	0.05980	0.000
56	59	0.08250	0.25100	0.05690	0.000
56	59	0.08030	0.23900	0.05360	0.000
55	59	0.04739	0.21580	0.05646	0.000
59	60	0.03170	0.14500	0.03760	0.000
59	61	0.03280	0.15000	0.03880	0.000
60	61	0.00264	0.01350	0.01456	0.000

60	62	0.01230	0.05610	0.01468	0.000
61	62	0.00824	0.03760	0.00980	0.000
63	59	0.00000	0.03860	0.00000	0.960
63	64	0.00172	0.02000	0.21600	0.000
64	61	0.00000	0.02680	0.00000	0.985
38	65	0.00901	0.09860	1.04600	0.000
64	65	0.00269	0.03020	0.38000	0.000
49	66	0.01800	0.09190	0.02480	0.000
49	66	0.01800	0.09190	0.02480	0.000
62	66	0.04820	0.21800	0.05780	0.000
62	67	0.02580	0.11700	0.03100	0.000
65	66	0.00000	0.03700	0.00000	0.935
66	67	0.02240	0.10150	0.02682	0.000
65	68	0.00138	0.01600	0.63800	0.000
47	69	0.08440	0.27780	0.07092	0.000
49	69	0.09850	0.32400	0.08280	0.000
68	69	0.00000	0.03700	0.00000	0.935
69	70	0.03000	0.12700	0.12200	0.000
24	70	0.00221	0.41150	0.10198	0.000
70	71	0.00882	0.03550	0.00878	0.000
24	72	0.04880	0.19600	0.04880	0.000
71	72	0.04460	0.18000	0.04444	0.000
71	73	0.00866	0.04540	0.01178	0.000
70	74	0.04010	0.13230	0.03368	0.000
70	75	0.04280	0.14100	0.03600	0.000
69	75	0.04050	0.12200	0.12400	0.000
74	75	0.01230	0.04060	0.01034	0.000
76	77	0.04440	0.14800	0.03680	0.000
69	77	0.03090	0.10100	0.10380	0.000
75	77	0.06010	0.19990	0.04978	0.000
77	78	0.00376	0.01240	0.01264	0.000
78	79	0.00546	0.02440	0.00648	0.000
77	80	0.01700	0.04850	0.04720	0.000
77	80	0.02940	0.10500	0.02280	0.000
79	80	0.01560	0.07040	0.01870	0.000
68	81	0.00175	0.02020	0.80800	0.000
81	80	0.00000	0.03700	0.00000	0.935
77	82	0.02980	0.08530	0.08174	0.000
82	83	0.01120	0.03665	0.03796	0.000
83	84	0.06250	0.13200	0.02580	0.000

83	85	0.04300	0.14800	0.03480	0.000
84	85	0.03020	0.06410	0.01234	0.000
85	86	0.03500	0.12300	0.02760	0.000
86	87	0.02828	0.20740	0.04450	0.000
85	88	0.02000	0.10200	0.02760	0.000
85	89	0.02390	0.17300	0.04700	0.000
88	89	0.01390	0.07120	0.01934	0.000
89	90	0.05180	0.18800	0.05280	0.000
89	90	0.02380	0.09970	0.10600	0.000
90	91	0.02540	0.08360	0.02140	0.000
89	92	0.00990	0.05050	0.05480	0.000
89	92	0.03930	0.15810	0.04140	0.000
91	92	0.03870	0.12720	0.03268	0.000
92	93	0.02580	0.08480	0.02180	0.000
92	94	0.04810	0.15800	0.04060	0.000
93	94	0.02230	0.07320	0.01876	0.000
94	95	0.01320	0.04340	0.01110	0.000
80	96	0.03560	0.18200	0.04940	0.000
82	96	0.01620	0.05300	0.05440	0.000
94	96	0.02690	0.08690	0.02300	0.000
80	97	0.01830	0.09340	0.02540	0.000
80	98	0.02380	0.10800	0.02860	0.000
80	99	0.04540	0.20600	0.05460	0.000
92	100	0.06480	0.29500	0.04720	0.000
94	100	0.01780	0.05800	0.06040	0.000
95	96	0.01710	0.05470	0.01474	0.000
96	97	0.01730	0.08850	0.02400	0.000
98	100	0.03970	0.17900	0.04760	0.000
99	100	0.01800	0.08130	0.02160	0.000
100	101	0.02770	0.12620	0.03280	0.000
92	102	0.01230	0.05590	0.01464	0.000
101	102	0.02460	0.11200	0.02940	0.000
100	103	0.01600	0.05250	0.05360	0.000
100	104	0.04510	0.20400	0.05410	0.000
103	104	0.04660	0.15840	0.04070	0.000
103	105	0.05350	0.16250	0.04080	0.000
100	106	0.06050	0.22900	0.06200	0.000
104	105	0.00994	0.03780	0.00986	0.000
105	106	0.01400	0.05470	0.01434	0.000
105	107	0.05300	0.18300	0.04720	0.000

105	108	0.02610	0.07030	0.01844	0.000
106	107	0.05300	0.18300	0.04720	0.000
108	109	0.01050	0.02880	0.00760	0.000
103	110	0.03906	0.18130	0.04610	0.000
109	110	0.02780	0.07620	0.02020	0.000
110	111	0.02200	0.07550	0.02000	0.000
110	112	0.02470	0.06400	0.06200	0.000
17	113	0.00913	0.03010	0.00768	0.000
32	113	0.06150	0.20300	0.05180	0.000
32	114	0.01350	0.06120	0.01628	0.000
27	115	0.01640	0.07410	0.01972	0.000
114	115	0.00230	0.01040	0.00276	0.000
68	116	0.00034	0.00405	0.16400	0.000
12	117	0.03290	0.14000	0.03580	0.000
75	118	0.01450	0.04810	0.01198	0.000
76	118	0.01640	0.05440	0.01356	0.000

B.3.2. Load Flow Data

Data required to complete load flow is included in Table B.8, G13 connected to bus 69 is the slack.

Table B.8: Load flow data for the IEEE 118-bus test system

Bus	*V (pu)*	*Θ (deg)*	P_G *(pu)*	P_L *(pu)*	Q_L *(pu)*
1	0.955	-	-	0.51	0.27
2	-	-	-	0.20	0.09
3	-	-	-	0.39	0.10
4	0.998	-	-	0.39	0.12
5	-	-	-	-	-
6	0.990	-	-	0.52	0.22
7	-	-	-	0.19	0.02
8	1.015	-	-	0.28	-
9	-	-	-	-	-
10	1.050	-	4.5	-	-
11	-	-	-	0.70	0.23
12	0.990	-	0.85	0.47	0.10
13	-	-	-	0.34	0.16
14	-	-	-	0.14	0.01

15	0.970	-	-	0.90	0.30
16	-	-	-	0.25	0.10
17	-	-	-	0.11	0.03
18	0.973	-	-	0.60	0.34
19	0.962	-	-	0.45	0.25
20	-	-	-	0.18	0.03
21	-	-	-	0.14	0.08
22	-	-	-	0.10	0.05
23	-	-	-	0.07	0.03
24	0.992	-	-	0.13	-
25	1.050	-	2.2	-	-
26	1.015	-	3.14	-	-
27	0.968	-	-	0.71	0.13
28	-	-	-	0.17	0.07
29	-	-	-	0.24	0.04
30	-	-	-	-	-
31	0.967	-	0.07	0.43	0.27
32	0.963	-	-	0.59	0.23
33	-	-	-	0.23	0.09
34	0.984	-	-	0.59	0.26
35	-	-	-	0.33	0.09
36	0.980	-	-	0.31	0.17
37	-	-	-	-	-
38	-	-	-	-	-
39	-	-	-	0.27	0.11
40	0.970	-	-	0.66	0.23
41	-	-	-	0.37	0.10
42	0.985	-	-	0.96	0.23
43	-	-	-	0.18	0.07
44	-	-	-	0.16	0.08
45	-	-	-	0.53	0.22
46	1.005	-	0.19	0.28	0.10
47	-	-	-	0.34	-
48	-	-	-	0.20	0.11
49	1.025	-	2.04	0.87	0.30
50	-	-	-	0.17	0.04
51	-	-	-	0.17	0.08
52	-	-	-	0.18	0.05

53	-	-	-	0.23	0.11
54	0.955	-	0.48	1.13	0.32
55	0.952	-	-	0.63	0.22
56	0.954	-	-	0.84	0.18
57	-	-	-	0.12	0.03
58	-	-	-	0.12	0.03
59	0.985	-	1.55	2.77	1.13
60	-	-	-	0.78	0.03
61	0.995	-	1.6	-	-
62	0.998	-	-	0.77	0.14
63	-	-	-	-	-
64	-	-	-	-	-
65	1.005	-	3.91	-	-
66	1.050	-	3.92	0.39	0.18
67	-	-	-	0.28	0.07
68	-	-	-	-	-
69	1.035	30	-	-	-
70	0.984	-	-	0.66	0.20
71	-	-	-	-	-
72	0.980	-	-	0.12	-
73	0.991	-	-	0.06	-
74	0.958	-	-	0.68	0.27
75	-	-	-	0.47	0.11
76	0.943	-	-	0.68	0.36
77	1.006	-	-	0.61	0.28
78	-	-	-	0.71	0.26
79	-	-	-	0.39	0.32
80	1.040	-	4.77	1.30	0.26
81	-	-	-	-	-
82	-	-	-	0.54	0.27
83	-	-	-	0.20	0.10
84	-	-	-	0.11	0.07
85	0.985	-	-	0.24	0.15
86	-	-	-	0.21	0.10
87	1.015	-	0.04	-	-
88	-	-	-	0.48	0.10
89	1.005	-	6.07	-	-
90	0.985	-	-	1.63	0.42

91	0.980	-	-	0.10	-
92	0.990	-	-	0.65	0.10
93	-	-	-	0.12	0.07
94	-	-	-	0.30	0.16
95	-	-	-	0.42	0.31
96	-	-	-	0.38	0.15
97	-	-	-	0.15	0.09
98	-	-	-	0.34	0.08
99	1.010	-	-	0.42	-
100	1.017	-	2.52	0.37	0.18
101	-	-	-	0.22	0.15
102	-	-	-	0.05	0.03
103	1.010	-	0.4	0.23	0.16
104	0.971	-	-	0.38	0.25
105	0.965	-	-	0.31	0.26
106	-	-	-	0.43	0.16
107	0.952	-	-	0.50	0.12
108	-	-	-	0.02	0.01
109	-	-	-	0.08	0.03
110	0.973	-	-	0.39	0.30
111	0.980	-	0.36	-	-
112	0.975	-	-	0.68	0.13
113	0.993	-	-	0.06	-
114	-	-	-	0.08	0.03
115	-	-	-	0.22	0.07
116	1.005	-	-	1.84	-
117	-	-	-	0.20	0.08
118	-	-	-	0.33	0.15

B.3.3. Generator Dynamic Data

The generator dynamic presented is given in Table B.9.

Table B.9: Generator dynamic data for the IEEE 118-bus test system

Gen	*Bus*	*M (s)*	*x'd (pu)*
G1	10	23.800	0.0592
G2	12	9.970	0.2200
G3	25	19.210	0.1391

G4	26	19.840	0.0961
G5	31	9.280	0.2467
G6	46	9.280	0.2467
G7	49	19.210	0.1391
G8	54	9.970	0.2200
G9	59	12.680	0.1531
G10	61	12.680	0.1531
G11	65	30.370	0.0668
G12	66	30.370	0.0668
G13	69	26.944	0.0527
G14	80	26.944	0.0527
G15	87	9.280	0.2467
G16	89	27.360	0.0475
G17	100	22.300	0.0948
G18	103	9.970	0.2200
G19	111	9.970	0.2200

Appendix C. Kron Reduction of Graphs

Kron reduction is a standard tool in the power systems community to obtain the so-called "network-reduced" or "Ward-equivalent" models for power flow studies [150], to reduce differential-algebraic power network models to purely dynamic models [151], and it is crucial for reduced order modelling, analysis, and efficient simulation of induction motors [152]. A recent application of *Kron* reduction is monitoring in smart power grids via synchronised PMUs [153]. *Kron* reduction has been recently studied in [109] from a graph theoretic point of view, i.e., using graphs.

As explained in Section 2.3.1.1, the application presented in this thesis of the *Kron* reduction aims to reduce the dynamic graph G_D to produce the reduced dynamic graph G_{DGN}. In this context, the dynamic graph G_D and its corresponding Laplacian matrix $\mathbf{L}$ should be considered. Furthermore, it is important to note that the Laplacian matrix $\mathbf{L}$ of the dynamic graph G_D can be written (partitioned in some sense) as follows,

$$\mathbf{L} = \begin{bmatrix} \mathbf{L}_{v_G v_G} & \mathbf{L}_{v_G v_L} \\ \mathbf{L}_{v_L v_G} & \mathbf{L}_{v_L v_L} \end{bmatrix} \tag{C.1}$$

where the submatrix $\mathbf{L}_{v_G v_G}$ represents the connections between internal-nodes only; the submatrices $\mathbf{L}_{v_G v_L}$ and $\mathbf{L}_{v_L v_G}$ represent the connections between internal-nodes and load-nodes and the connections between load-nodes and internal-nodes, respectively; and the submatrix $\mathbf{L}_{v_L v_L}$ represents the connection between load-nodes only. It should be noted that these connections can also represent certain level of strength, i.e., they can represent weight factors associated with the edges of the dynamic graph G_D.

Then, the Kron reduction of the dynamic graph G_D is the reduced dynamic graph G_{DGN} whose Laplacian matrix $\mathbf{L}_{\mathbf{red}}$ is obtained by the *Schur complement* [108] of the original Laplacian matrix $\mathbf{L}$ with respect to a specific subset of nodes. In the application presented

in this thesis, the aim has been to eliminate the subset of load-nodes $\mathbf{L}_{v_L v_L}$ and preserve only the internal-nodes $\mathbf{L}_{v_G v_G}$. It is important to mention that the information contained in the reduced dynamic graph will represent the information that was represented in the whole dynamic graph.

The reduced Laplacian matrix $\mathbf{L}_{\mathbf{red}}$ with respect to the internal-nodes, also called the *Schur complement* of $\mathbf{L}_{v_L v_L}$ in $\mathbf{L}$ [108, 154], can be calculated as in (C.2).

$$\mathbf{L}_{\mathbf{red}} = \mathbf{L}_{v_G v_G} - \mathbf{L}_{v_G v_L} \mathbf{L}_{v_L v_L}^{-1} \mathbf{L}_{v_L v_G} \tag{C.2}$$

The reduction of an electrical network via a *Schur complement* of the associated Laplacian matrix is known as Kron reduction [108]. It is important to note that in case of a star-like network without interior current injections and shunt conductances, the *Kron* reduction of a network reduces to the (generalized) star-triangle transformation [155].

In a particular application, the *Kron* reduction of the dynamic graph G_D whose Laplacian matrix $\mathbf{L}$ is constructed using as edges weights w_{ij} the susceptance between the system buses i.e., $w_{ij} = 1/X_{ij}$, would result in a reduced Laplacian matrix $\mathbf{L}_{\mathbf{red}}$ whose entries would correspond to the susceptance between the internal generator buses [109]. In other words, if the edge weights of the dynamic graph G_D represent the susceptance $1/X_{ij}$ between the system buses, the edge weights of the reduced dynamic graph G_{DGN} would then represent the susceptance between the internal generator buses.

As noticed, the *Kron* reduction is related to the well-known reduction of the extended power system to the internal generator buses [108].

Appendix D. Controlled Islanding Methods Used in the Comparisons

This appendix presents the basis of the slow coherency algorithm, the weak connections method, the OBDD-based method and the SCCI algorithm used throughout this thesis to compare the introduced approaches.

D.1. Slow Coherency Algorithm and Weak Connection Method

The slow coherency algorithm, which is used in Section 2.3 to compare the introduced approach, is based on the linearised second-order dynamic model of a power system with *m* machines that can be expressed as follows.

$$\begin{bmatrix} \Delta\ddot{\boldsymbol{\delta}} \\ 0 \end{bmatrix} = \begin{bmatrix} \mathbf{J_A} & \mathbf{J_B} \\ \mathbf{J_C} & \mathbf{J_D} \end{bmatrix} \begin{bmatrix} \Delta\boldsymbol{\delta} \\ \Delta\mathbf{V} \end{bmatrix} \tag{D.1}$$

The slow coherency algorithm then uses the classical system state matrix $\bar{\mathbf{A}} = \mathbf{J_A} - \mathbf{J_B}\mathbf{J_D}^{-1}\mathbf{J_C}$ and applies the following steps [53]:

1. Choose the number of coherent groups of generators *r*.

2. Compute the first *r* eigenvectors $\boldsymbol{\varphi}_1,\ldots,\boldsymbol{\varphi}_r$ associated with the *r* smallest eigenvalues of the eigenproblem (D.2), and use these eigenvectors as columns to create a matrix $\mathbf{X} \in \mathbb{R}^{m\times r}$.

$$\bar{\mathbf{A}}\boldsymbol{\varphi} = \lambda\boldsymbol{\varphi} \tag{D.2}$$

3. Apply Gaussian elimination to **X** to obtain the *r* reference generators.

4. Let $\mathbf{x}_i \in \mathbb{R}^r$ be the vector corresponding to the i^{th} row of the matrix **X**. Compute the matrix **S** using the (D.3) – cosine similarity – to describe the relationship that each non-reference generator has with the reference generators.

$$[\mathbf{S}]_{ij} = \frac{\mathbf{x}_i \cdot \mathbf{x}_j^T}{\|\mathbf{x}_i\|\|\mathbf{x}_j\|}, \; i = 1,\ldots,m; j = 1,\ldots,r \tag{D.3}$$

5. Use the matrix **S** to assign each bus to a reference generator according to the largest entry in each row of **S**, and then obtain the slowly coherent groups of generators [53].

The slow coherency algorithm has been recently extended to identify weak connections between coherent areas [56]. In the existing method [56], which has been used in Section 3.4 to compare methodology proposed in this thesis, the load buses are taken into account in the clustering problem by computing the eigenbasis matrix $\mathbf{X}_1 = \begin{bmatrix}\mathbf{X} & \mathbf{X}_\mathbf{V}\end{bmatrix}^T \in \mathbb{R}^{(m+n)\times r}$, where **X** is computed as above, and each vector $\mathbf{x}_{vi} \in \mathbf{X}_\mathbf{V}$ is computed as follows:

$$\mathbf{x}_{vi} = -\mathbf{J}_\mathbf{D}^{-1}\mathbf{J}_\mathbf{C}\mathbf{x}_i \tag{D.4}$$

Then, the weak connections method proceeds similar to the grouping algorithm of the slow coherency, but in Step 4, the matrix **S** is computed between the reference generators and all the other buses [56].

D.2. OBDD-based method

The OBDD-based method proposed in [44, 45], and used in Chapter 4 to compare the methodology proposed in this thesis, models the power system as a node-weighted graph $G_N = (V, E, \sigma)$. The OBDD-based methods aim to minimise the power imbalance within the islands while creating these with only coherent generators as shown in (D.5).

$$\min\left(\sum_{l=1}^{r}\left|P_G^l - P_L^l\right|\right) \tag{D.5}$$

subject to

$$V_{Gk} \subset V_k$$

In (D.5) P_G^l and P_L^l represent the active power generation and active power load of island *l*, and V_{Gk} represents the k^{th} coherent group of generators.

In order to solve this problem, the OBDD-based methods use Boolean algebra [156]. In this context, a Boolean variable $\bar{b}_{ij}$ is defined to represent the edge state between node *i* and node *j*. A set of these variables is used to form the adjacency matrix **A** of the graph G_N.

$$[\mathbf{A}]_{ij} = \begin{cases} \bar{b}_{ij} & if \;\; e_{ij} \in E \\ 0 & if \;\; e_{ij} \notin E \end{cases} \tag{D.6}$$

By using *AND* and *OR* as Boolean multiplication and addition operators, denoted $\otimes$ (often omitted) and $\oplus$, respectively, the reachability matrix $\mathbf{A}^*$ of the graph that represents all connection paths between nodes is defined as (D.7):

$$\mathbf{A}^* = \sum_{i=1,\ldots,n}^{\oplus} \mathbf{A}^i \tag{D.7}$$

To build the corresponding OBDD, the controlled islanding problem is expressed as a Boolean function F_1 that represents the requirements for stable islands [44, 45].

$$F_1 = SSC \otimes PBC \otimes MCC \tag{D.8}$$

The Separation and Synchronization Constraint (*SSC*) represents the requirement of generator coherency. As shown in (D.9), the *SSC* is comprised of three different components. The first term denotes that the generators of different coherent groups cannot be connected; the second term denotes that the generators in the same coherent group must be connected; and the third term denotes that every load must be connected to one and only one coherent generator group.

$$SSC = \left(\prod_{v_i \in V_G^l, v_j \in V_G^k, l \neq k}^{\otimes} \bar{\mathbf{A}}_{ij}^{*} \right) \cdot \left(\prod_{l=1,\ldots r}^{\otimes} \left(\prod_{v_i, v_j \in V_G^l}^{\otimes} \mathbf{A}^{*}{}_{ij} \right) \right) \cdot \left(\prod_{v_i \in V_L}^{\otimes} \left(\sum_{l=1,\ldots,r}^{\oplus} \sum_{v_j \in V_G^l}^{\oplus} \left(\mathbf{A}^{*}{}_{ij} \right) \right) \right) \tag{D.9}$$

In (D.9), V_G and V_L respectively represent the sets of generator nodes and the sets of load-nodes of G_N. V_G^l represents the coherent generator group in the island l.

The Power Balance Constraint (*PBC*) denotes that the active power imbalance of each island cannot exceed β. Here, β is a predefined threshold to indicate the power imbalance allowed with each island, usually very small.

$$PBC = \prod_{l=1,\ldots,r}^{\otimes} \left(\left| \sum_{v_i \in V_G^l} w_i + \sum_{v_j \in V_G^l, v_i \in V_L} \mathbf{A}^{*}{}_{ij} \cdot w_i \right| < \beta \right) \tag{D.10}$$

The Minimal Cutset Constraint (*MCC)* is used to reduce the number of islanding solutions by allowing only those edges that help to form islands to be disconnected:

$$MCC = \prod_{e_{ij} \in E}^{\otimes} \left(\mathbf{A}_{ij} \otimes \mathbf{A}^{*}{}_{ij} \oplus \bar{\mathbf{A}}_{ij} \otimes \bar{\mathbf{A}}_{ij}^{*} \right) \tag{D.11}$$

Using an OBDD software package, e.g., Buddy [116], every solution to the OBDD of the controlled islanding problem (D.8) can be found.

D.3. Spectral Clustering Controlled Islanding (SCCI) Algorithm

The SCCI algorithm introduced in [49] and used in Chapter 6 to compare the presented methodology based on constrained spectral clustering models the power system as an edge weighted graph $G=(V,E,\rho)$. The edge weights are computed as the absolute value of active power exchange between nodes. In this context, the problem that the SCCI algorithm seeks to solve is formulated as follows.

$$\min\left(\sum_{e_{ij}\in E_S}\frac{|P_{ij}|+|P_{ji}|}{2}\right) \tag{D.12}$$

subject to

$$V_{GNk}\subset V_k$$

As noted, the SCCI algorithm also minimises the power flow disruption, while creating islands with only coherent generators.

The SCCI algorithm uses an unnormalised Laplacian matrix **L**, which is built as follows.

$$[\mathbf{L}]_{ij}=\begin{cases}-\dfrac{|P_{ij}|+|P_{ji}|}{2} & \text{if } i\neq j\\ -\sum_{l=1,l\neq i}^{n}[\mathbf{L}]_{il} & \text{if } i=j\end{cases}. \tag{D.13}$$

Then, to determine an islanding solution that separates the system into *r* islands, the SCCI algorithm uses the following steps [49].

1. Construct a graph *G* of all nodes with the edge weights defined as $\left(|P_{ij}|+|P_{ji}|\right)/2$.

2. Construct the projection matrix **P** based on the generator grouping results:

$$\mathbf{P} = \begin{pmatrix} \mathbf{1}_{m_1} & \mathbf{1}_{m_1} & \mathbf{0}_{m_1 \times (n-m)} \\ \mathbf{1}_{m_2} & -\mathbf{1}_{m_2} & \mathbf{0}_{m_2 \times (n-m)} \\ \mathbf{1}_{n-m} & \mathbf{0}_{n-m} & \mathbf{I}_{(n-m)\times(n-m)} \end{pmatrix} \tag{D.14}$$

where the first m_1 nodes belong to the cluster C_1 and the next m_2 nodes belong to the cluster C_2. In (D.13), **I** is the identity matrix, **1** is the all-ones column vector, **0** is the zero matrix or zero column vector and $m = m_1 + m_2$.

3. Compute the first two eigenvectors $\boldsymbol{\varphi}_1$, $\boldsymbol{\varphi}_2$ of the generalised eigenproblem $\mathbf{P}^{\mathbf{T}}\mathbf{L}\mathbf{P}\boldsymbol{\varphi} = \lambda \mathbf{P}^{\mathbf{T}}\mathbf{P}\boldsymbol{\varphi}$.

4. Let $\mathbf{X} \in \mathbb{R}^{n \times r}$ be the matrix that contain the vectors $\mathbf{P}\boldsymbol{\varphi}_1$, $\mathbf{P}\boldsymbol{\varphi}_2$ as columns. Let $\mathbf{x}_i \in \mathbb{R}^2$ be the vector corresponding to the i^{th} row of **X**.

5. Cluster the nodes $\mathbf{x}_i \in \mathbb{R}^2$ into the clusters V_1 and V_2 using the *k*-means algorithm.

6. Select V_1 and V_2 as the node set of a new static graph and return to 1) until *r* clusters are created.

Appendix E. Publications from the Thesis

E.1. Patent Filed

[E.1] The University of Manchester (V. Terzija, **J. Quirós-Tortós** and P. Wall), "Method of Determining an Islanding Solution for an Electrical Power System," UK Patent GB1320858.2, Filed Jan. 2014.

E.2. Submitted International Journal Publications

[E.2] **J. Quirós-Tortós**, R. Sánchez-García, J. Brodzki, J. Bialek and V. Terzija, "Constrained Spectral Clustering Based Method for Intentional Controlled Islanding of Large-Scale Power Systems," submitted to IET Generation, Transmission & Distribution (under 2nd revision).

[E.3] **J. Quirós-Tortós**, P. Wall, L. Ding and V. Terzija, "Determination of sectionalising strategies for parallel power system restoration: A spectral clustering-based methodology," submitted to Elsevier: Electric Power System Research (under 2nd revision).

[E.4] **J. Quirós-Tortós**, P. Wall, L. Ding and V. Terzija, "Constrained spectral clustering-based sectionalising strategies for parallel power system restoration," submitted to IET Generation, Transmission & Distribution (under 1st revision).

[E.5] **J. Quirós-Tortós**, M. Panteli, P. Wall and V. Terzija, "A New Sectionalizing Methodology for Parallel System Restoration Based on Graph Theory," submitted to IEEE Transactions on Power Systems (under 1st revision).

E.3. In Preparation International Journal Publications

[E.6] **J. Quirós-Tortós**, P. Wall and V. Terzija, "Reducing excessive standing phase angle differences: A new approach based on OPF and wide area measurements," to be submitted to IET Generation, Transmission & Distribution.

[E.7] **J. Quirós-Tortós**, P. Wall and V. Terzija**,** "A New Methodology for Intentional Controlled Islanding Based on the Weak Areas Concept and Minimal Power Flow Disruption," to be submitted to IEEE Transactions on Power Systems.

[E.8] **J. Quirós-Tortós**, M. Panteli, P. Demetrio, E. Kyriakides and V. Terzija, "A Controlled Islanding Methodology and its Reliability Assessment: A Case Study in Cyprus," to be submitted to IEEE Transactions on Power Systems.

E.4. International Conference Publications

[E.9] **J. Quirós-Tortós** and V. Terzija, "A Power System Controlled Islanding Scheme for Emergency Control," 2nd International Conference on the Power Options for the Eastern Mediterranean Region (POEM 2013), Oct. 2013.

[E.10] **J. Quirós-Tortós**, M. Panteli, V. Terzija and P. Crossley, "On Evaluating the Performance of Intentional Controlled Islanding Schemes," IEEE-PES General Meeting 2013, Jul, 2013.

[E.11] **J. Quirós-Tortós** and V. Terzija, "A Graph Theory Based New Approach for Power System Restoration," IEEE-PES PowerTech 2013, Jun, 2013.

[E.12] P. Demetrio, **J. Quirós-Tortós**, E. Kyriakides and V. Terzija, "On Implementing a Spectral Clustering Controlled Islanding Algorithm in Real Power Systems," IEEE-PES PowerTech 2013, Jun, 2013.

[E.13] **J. Quirós-Tortós** and V. Terzija, "A Smart Power System Restoration Based on the Merger of Two Different Strategies," IEEE-PES ISGT Europe 2012, Oct. 2012.

[E.14] **J. Quirós-Tortós** and V. Terzija, "Controlled islanding strategy considering power system restoration constraints," IEEE-PES General Meeting 2012, Jul. 2012.

[E.15] G. Valverde, **J. Quirós-Tortós** and V. Terzija, "Comparison of Gaussian Mixture reductions for probabilistic studies in power systems," IEEE-PES GM 2012, Jul. 2012.

[E.16] **J. Quirós-Tortós**, L. Ding, G. Valverde and V. Terzija, "Optimal Placement of Phasor Measurement Units to Improve Parallel Power System Restoration," IEEE-PES ISGT Europe 2011, Dec. 2011.